Poly(Lactic Acid) Block Copolymers – Synthesis, Characterization, and Structure-Property Relationships

vorgelegt von

M. Sc.

Benjamín Rodríguez Hernández

an der Fakultät III – Prozesswissenschaften

der Technischen Universität Berlin

zur Erlangung des akademischen Grades

Doktor der Ingenieurwissenschaften

- Dr.-Ing. -

genehmigte Dissertation

Promotionsausschuss:

Vorsitzender: Prof. Dr. Peter Neubauer

Gutachter: Prof. Dr.-Ing. Dietmar Auhl

Gutachter: Prof. Dr. André Laschewsky

Tag der wissenschaftlichen Aussprache: 28.06.2022

Berlin 2022

Erklärung

Hiermit erkläre ich, dass die vorliegende Arbeit selbstständig und nur unter Zuhilfenahme der im Literaturverzeichnis genannten Quellen und Hilfsmittel angefertigt wurde. Alle Stellen der Arbeit, die anderen Werken dem Wortlaut oder dem Sinn nach entnommen wurden, sind kenntlich gemacht. Ich versichere, dass die Dissertation in der vorgelegten oder einer ähnlichen Fassung noch nicht zu einem früheren Zeitpunkt an einer anderen in - oder ausländischen Hochschule als Dissertation eingereicht worden ist.

Benjamín Rodríguez Hernández

Declaration

I hereby declare that the present work was prepared independently and only with the aid of the sources and aids mentioned in the bibliography. All parts of the work that have been taken from other works in terms of their wording or meaning are marked. I affirm that the dissertation in the version presented or a similar version has not been submitted as a dissertation to another domestic or foreign university at an earlier point in time.

Benjamín Rodríguez Hernández

Publications and Posters

Conference Poster:

Polydays Converence 2019, Berlin, September 11 – 13, 2019

Design of PLA block copolymer structures for film applications – first results

Benjamín Rodríguez Hernández, Antje Lieske, André Gomoll, Dietmar Auhl

Presentations:

6th PLA World Congress, Online, October 07 – 08, 2020

Design of PLA block copolymer structures for film applications

Benjamín Rodríguez Hernández, Antje Lieske

Biopolymehr 2022, Online, February 23 – 24, 2022

Design of PLA block copolymer structures for film applications – Winner Best Talk

Benjamín Rodríguez Hernández, Antje Lieske

Abstract

Poly(L-lactic acid) (PLLA) is currently the bio-based, biodegradable, and recyclable synthetic polymer with the highest installed production capacity in the world. The environmentally favorable characteristics of PLLA make it attractive for applications in which its biodegradability can prevent the leakage of plastics into the environment (organic waste collection films, agricultural mulch films) or where separation from organic material in direct contact makes recycling unfeasible (food packaging). The relatively high elastic modulus and low elongation at break of pure PLLA however, make for stiff and brittle films that cannot be used in many of the before-mentioned applications. At the same time, PLLA exhibits a relatively low melt strength and low melt viscosity when compared to conventional flexible film-grade materials, which makes processing of PLLA in conventional equipment difficult.

In the present work, the mechanical and rheological property profile of PLLA is modified through the synthesis of high molar mass PLLA-b-polyether-b-PLLA block copolymers in an industrially feasible synthesis method. To achieve this, high molar mass polyether diols are used as macroinitiators in the ring opening polymerization (ROP) of L-lactide under similar conditions to those used for the industrial synthesis of conventional PLLA homopolymers (bulk, tin(II) 2-ethylhexanoate [$Sn(Oct)_2$] catalyst, T ~ 180 °C). Different chemical structures of the polyether middle block are introduced into the copolymers by using polyether macroinitiators of different chemical structure (i.e. polyethylene glycol [PEG], polypropylene glycol [PPG], poly(ethylene-co-propylene glycol [PEPG]). The chemical structure of the outer PLLA blocks is modified by using other ring comonomers that are able to undergo copolymerization with the L-lactide monomer at the same reaction conditions (i.e. D-lactide, ε-caprolactone [CL]). Additionally, tetrafunctional PEPG macroinitiators are used to synthesize PLLA>b-polyether-b<PLLA block copolymers with a star topology. To obtain the highest possible block copolymer molar mass values (and thus higher melt viscosities), optimizations during the block copolymer synthesis are studied. Tris(nonylphenyl) phosphite (TNPP) is used to reduce the molar mass degradation reactions during synthesis, and the catalyst concentration is lowered to reduce the molar mass degradation reactions during subsequent processing of the block copolymers.

The effects of the different synthesized block copolymer chemical structures on the thermal, mechanical, and rheological properties are systematically investigated through the use of differential scanning calorimetry (DSC), tensile testing, melt flow index (MFI), and oscillatory rheometry to establish a series of structure-property relationships. Changes in the chemical structure of the block copolymers are found to cause changes in the glass transition temperature (Tg) and peak melting temperature (Tm). The changes in the thermal properties are found to significantly affect the mechanical and rheological properties of the block copolymers. The established structure-property relationships are used to design PLLA-b-polyether-b-PLLA block copolymer structures with the required mechanical and rheological properties for flexible blown film applications. The resulting block copolymers are successfully processed under stable conditions in a conventional blown film extrusion line. The obtained blown films have relatively low elastic moduli of around 140 MPa and elongation at break values above 400 %, which are comparable to commercial flexible film materials.

Zusammenfassung

Poly(L-Milchsäure) (PLLA) ist derzeit das biobasierte, biologisch abbaubare und recycelbare synthetische Polymer mit der weltweit höchsten installierten Produktionskapazität. Die umweltfreundlichen Eigenschaften von PLLA machen es attraktiv für Anwendungen, bei denen seine biologische Abbaubarkeit das Austreten von Kunststoffen in die Umwelt verhindern kann (Folien für die Sammlung organischer Abfälle, Mulchfolien für die Landwirtschaft) oder bei denen die Trennung von organischen Abfälle das Recycling unmöglich macht (Lebensmittelverpackungen). Der relativ hohe Elastizitätsmodul und die niedrige Bruchdehnung von reinem PLLA führen jedoch zu steifen und spröden Folien, die für viele der vorgenannten Anwendungen nicht geeignet sind. Gleichzeitig weist PLLA im Vergleich zu herkömmlichen flexiblen Folienmaterialien eine relativ geringe Schmelzfestigkeit und niedrige Schmelzviskosität auf, was die Verarbeitung von PLLA in herkömmlichen Anlagen erschwert.

In der vorliegenden Arbeit wird das mechanische und rheologische Eigenschaftsprofil von PLLA durch die Synthese von hochmolekularen PLLA-b-Polyether-b-PLLA-Blockcopolymeren in einem industriell durchführbaren Syntheseverfahren verändert. Dazu werden hochmolekulare Polyetherdiole als Makroinitiatoren in der Ringöffnungspolymerisation (ROP) von L-Lactid unter ähnlichen Bedingungen wie bei der industriellen Synthese herkömmlicher PLLA-Homopolymere verwendet (Bulk, Zinn(II)-2-Ethylhexanoat [$Sn(Oct)_2$]-Katalysator, T~180°C). Unterschiedliche chemische Strukturen des Polyether-Mittelblocks werden in die Copolymere eingeführt, indem Polyether-Makroinitiatoren unterschiedlicher chemischer Struktur verwendet werden (Polyethylenglykol [PEG], Polypropylenglykol [PPG], Poly(ethylen-co-propylenglykol [PEPG]). Die chemische Struktur der äußeren PLLA-Blöcke wird durch die Verwendung anderer Ringcomonomere modifiziert, die unter den gleichen Reaktionsbedingungen mit dem L-Lactid-Monomer copolymerisieren können (z.B. D-Lactid, ε-Caprolacton [CL]). Zusätzlich werden tetrafunktionelle PEPG-Makroinitiatoren verwendet, um PLLA>b-Polyether-b<PLLA-Blockcopolymere mit einer Sterntopologie zu synthetisieren. Um die höchstmöglichen Molmassenwerte der Blockcopolymere (und damit höhere Schmelzviskositäten) zu erreichen, werden Optimierungen während der Blockcopolymersynthese untersucht. Tris(nonylphenyl)phosphit (TNPP) wird verwendet, um die Molmassenabbaureaktionen während der Synthese zu reduzieren, und die Katalysatorkonzentration wird gesenkt, um die Molmassenabbaureaktionen während der anschließenden Verarbeitung der Blockcopolymere zu verringern.

Die Auswirkungen der verschiedenen chemischen Strukturen der synthetisierten Blockcopolymere auf die thermischen, mechanischen und rheologischen Eigenschaften werden systematisch mit Hilfe der Differential-Scanning-Kalorimetrie (DSC), der Zugprüfung, des Melt-Flow-Indexes (MFI) und der Oszillationsrheometrie untersucht, um eine Reihe von Struktur-Eigenschafts-Beziehungen zu definieren. Die Veränderungen in der chemischen Struktur der Blockcopolymere haben zu Veränderungen der Glasübergangstemperatur (Tg) und der Spitzenschmelztemperatur (Tm) geführt. Es wurde festgestellt, dass die Veränderungen der thermischen Eigenschaften (Tg, Tm) die mechanischen und rheologischen Eigenschaften der Blockcopolymere erheblich beeinflussen. Die

ermittelten Struktur-Eigenschafts-Beziehungen werden genutzt, um PLLA-b-Polyether-b-PLLA-Blockcopolymerstrukturen mit den erforderlichen mechanischen und rheologischen Eigenschaften für flexible Blasfolienanwendungen zu entwickeln. Die resultierenden Blockcopolymere werden erfolgreich unter stabilen Bedingungen in einer konventionellen Blasfolienextrusionsanlage verarbeitet. Die erhaltenen Blasfolien haben relativ niedrige Elastizitätsmodule von etwa 140 MPa und Bruchdehnungswerte von über 400 %, die mit kommerziellen flexiblen Folienmaterialien vergleichbar sind.

Table of Contents

1 Introduction

The industrial polymer material development process in the 20th century had two main constraints: cost and material performance. This led to the establishment of a wide range of polymeric materials with properties tailored for specific applications. Most of these polymers are made with relatively cheap, non-renewable fossil resources using highly optimized polymer manufacturing process technology to reduce costs. The obtained polymers are very chemically stable and can remain in the environment for long times. The mass production of these materials has contributed to the depletion of fossil resources, the emission of greenhouse gases, and to a growing global plastics pollution problem [1–9]. For these reasons, an additional constraint has been imposed on the modern industrial polymer material development process: sustainability.

Through developments in manufacturing technology, poly(lactic acid) (PLA) has emerged in the 21st century as the bio-based, biodegradable, and recyclable synthetic polymer with the largest installed production capacity in the world [11; 12]. Considering these environmentally favorable properties of PLA and its growing production capacity, PLA has the potential to satisfy the sustainability and cost constraints of the modern material development processes. The material performance of PLA in many applications, however, is restricted by its intrinsic properties. This thesis focuses on expanding the material properties of PLA-based materials through the synthesis of PLA block copolymers to enable the use of PLA in single-use applications (i.e. flexible films) were recyclability or biodegradability are desired.

The mainly-used material for flexible film applications is currently low-density polyethylene (LDPE) [4; 11; 13]. This polymer has a relatively low elastic modulus and a high elongation at break, which makes for soft and flexible films. At the same time, LDPE has a branched polymer chain structure, which gives it a high melt strength that allows production of uniform films in conventional cast or blown film extrusion equipment at a high throughput. Because LDPE is produced from non-renewable fossil raw materials and through optimized synthesis processes, it has a relatively low price of around 1.5 - 2 \$/kg [14]. Although mechanical recycling of LDPE is possible, the material must be downgraded after reprocessing due to thermal degradation of the polymer chains. Chemical recycling of LDPE is theoretically possible (to achieve virgin-quality resin after recycling), however, the high ceiling temperature (400 °C) of LDPE results in such processes being energy-intensive and expensive [6].

PLA can be chemically recycled through several routes and under much milder conditions than LDPE. Additionally, PLA is biodegradable under industrial composting conditions (EN 13432) [11]. This makes PLA attractive in applications were leakage of plastics into the environment is common (agricultural mulch films) or where the necessary collection, separation from organic waste, and subsequent recycling is laborious or economically unfeasible (food contact packaging, organic waste collection bags) [9; 15]. For these applications however, soft and flexible materials are required. PLA has a high elastic modulus, a low elongation at break, and a low melt strength, which makes for stiff and brittle films that are difficult to process in conventional blown or cast film extrusion processing equipment [11]. This restricts the use of PLA in such flexible film applications.

PLA currently has one of the more competitive prices (~ 2.5 – 2.9 $/kg) of the available bio-based, biodegradable and recyclable synthetic polymers. This has driven renowned polymer manufacturing companies to try to modify the mechanical properties of PLA to enable its use for flexible film applications. Commercial products such as Ecovio® from BASF [11] or Bio-Flex® from FKuR [16] currently available in the market have been developed to enable the use of PLA in flexible applications. These products are PLA-based blends with other biodegradable polyesters such as polybutylene adipate terephthalate (PBAT) in the Ecovio® material and polybutylene butylene succinate (PBS) in the Bio-Flex® material with relatively low PLA contents of around 40 %-wt [11; 16; 17].

In the scientific literature, polyethers such as polyethylene glycol (PEG), poly(ethylene-co-propylene glycol) (PEPG), and polypropylene glycol (PPG) have been used as plasticizers to improve the flexibility of PLA-based blends [18–24]. Similar mechanical properties to the ones obtained in commercial PLA-based blends (Ecovio® and Bio-Flex®) have been achieved in such polyether-plasticized systems at much higher PLA contents of around 80 %-wt [11; 24]. Changes in the morphology of polyether-plasticized PLA blends over longer storage times, however, were reported to cause migration of the polyether plasticizer to the material surface and changes in their mechanical properties [18; 19; 24]. Considering that polyethers such as PEG are widely commercially available, a lower cost than that of PBAT or PBS polyesters can be expected. Moreover, PEG has been found to be biodegradable in fresh water environments (Mn < 60 kDa) [11; 25], and is projected to be produced from renewable raw materials in the long term [26].

In the present work, the mechanical and rheological properties of PLA are modified through the synthesis of internally plasticized, high molar mass PLA-b-polyether-b-PLA block copolymers. The covalent bonds between the polyether plasticizer blocks and the PLA blocks are intended to reduce migration of the polyether plasticizer over time. The block copolymers are synthesized through an industrially feasible, ring-opening polymerization (ROP) synthesis method under common conditions encountered in established industrial PLA manufacturing processes (bulk, tin(II) 2-ethylhexanoate [Sn(Oct)$_2$] catalyst, T ~ 180 °C) [27]. Different polyether block chemical structures are introduced into the copolymers by using different polyether macroinitiators (i.e. PEG, PPG, PEPG). The chemical structure of the outer PLLA blocks is modified by using other ring comonomers that are able to undergo copolymerization with the L-lactide monomer at the same reaction conditions (i.e. D-lactide, ε-caprolactone [CL]). Additionally, tetrafunctional PEPG macroinitiators are used to synthesize PLLA>b-polyether-b<PLLA block copolymers with a star topology to improve the melt strength and processability of the block copolymers

Optimizations of the block copolymer synthesis are studied to achieve the highest possible block copolymer molar mass values (leading to higher melt viscosities). Tris(nonylphenyl) phosphite (TNPP) is studied as a chain extension agent in the ROP of lactide to counteract the molar mass degradation side reactions. Additionally, changes to the catalyst concentration are explored as a means to reduce the molar mass degradation rate during processing of the block copolymers. The variations in the chemical structure of the block copolymers are analyzed through thermal, mechanical, and rheological characterization methods to define a set of structure-property relationships. Based on said structure-property relationships, processing of an internally plasticized PLA-based block copolymer with the required mechanical properties for flexible film applications, is to be demonstrated on conventional semi-technical blown film extrusion equipment.

2 Theoretical Background

2.1 PLA Synthesis

PLA is the synthetic bio-based, biodegradable, and recyclable polymer that has enjoyed the biggest commercial growth and success until now. Carothers investigated the synthesis of PLA polymers from lactide (the cyclic dimer of lactic acid) as early as 1932 [27]. Due to its biocompatibility and degradation properties, PLA began being commercialized as a material for medical applications were the large margins outweighed its high production costs [28]. In the 1990's the joint venture Cargill - Dow LLC developed a low cost, continuous process for the production of PLA [27]. The largest industrial-scale PLA production plant in the world was built in Blair, Nebraska in the year 2002 by the company NatureWorks (formerly Cargill - Dow LLC) with an annual production capacity of 70 kTon [29]. The capacity of this production facility was expanded to 150 kTon/a in 2015. The higher production volumes and technological developments in the synthesis of PLA have allowed the price to be reduced from around 1,000 $/kg in the early 2000's when sold by DuPont for medical applications [2] to its current price of around 2.5 to 2.9 $/kg. This contributed to making PLA one of the most accessible bio-based, recyclable, and biodegradable synthetic polymers available currently in the market.

PLA production has been increasing over the last few years and further growth of the installed capacity is projected in the coming years. As of 2021, NatureWorks LLC (Jointly owned by Thailand's PTT Global Chemical and USA's Cargill, Inc.) and Total-Corbion (50/50 joint venture between French Total and Dutch Corbion) are the two main PLA producers with an installed capacity 150 kTon/a and 75 kTon/a (in operation since 2018) [30], respectively [11; 29]. Total-Corbion announced in September 2020 the construction of new production plant in Grandpuits, France to be in production by 2024 with an installed capacity of 100 kTon/a [31]. In August of 2021, NatureWorks LLC announced the construction of a second production plant in Nakhon Sawance Province, Thailand planned to start construction in the second quarter of 2022 and with an installed capacity of 75 kTon/a [32].

The current section describes the most commonly used two-step ring opening polymerization (ROP) process for the industrial synthesis of PLA [27]. The main reactions involved in the ROP as well as some of the challenges of synthesizing high molar mass PLA are introduced. Finally, some relevant material properties of PLA are discussed and compared with those of more established commodity polymers.

2.1.1 Lactic acid synthesis

Lactic acid is produced industrially by the anaerobic fermentation of sugars such as glucose, fructose, and sucrose into cellular energy and lactic acid [33]. These sugars are typically extracted from crops such as corn, sugar beets, or sugar cane depending on the geographic location. As the sugars are being fermented, the pH of the fermentation mixture starts decreasing quickly due to the increase of

the lactic acid concentration. To maintain the pH between 5.0 and 6.8, neutralizing agents such as calcium hydroxide ($Ca(OH)_2$) and calcium carbonate ($CaCO_3$) must be added to the fermentation mixture [27]. After fermentation of the sugars is complete, the mixture is acidified with sulfuric acid (H_2SO_4) to convert the neutralized lactate salts into lactic acid. The formed calcium sulfate ($CaSO_4$) crystallizes and can be filtered out from the mixture [27].

The fermentation microorganisms, nutrients and residual sugars are then removed from the mixture. Depending on the used microorganisms and their morphology, they can be directly filtered or must be flocculated and then filtered. Nutrients and residual sugars can be removed through solvent extraction or distillation [27]. Finally, the aqueous lactic acid solution is concentrated to a concentration of 60-90% further use [27]. Typical "analytical grade" lactic acid contains trace amounts of amino acids, carbohydrates, and parts per million of cations such as Na^+ that can lead to discoloration and/or racemization of the lactic acid during polycondensation [27]. For this reason, "polymerization grade" lactic acid of even higher purity is necessary for PLA production.

2.1.2 The direct polycondensation of lactic acid approach

PLA can be produced by the direct polycondensation of lactic acid with or without a catalyst through removal of the produced water in the equilibrium reaction shown in Figure 2.1. Product molecular weight however, is limited by several reasons explained below.
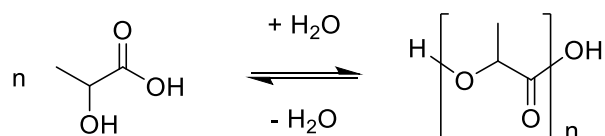
Figure 2.1: Polycondensation reaction of lactic acid

As the molecular weight of the product increases, the viscosity of the reaction mixture also begins to increase. Diffusion of the water byproduct molecules, which must be removed to push the equilibrium shown in Figure 2.1 towards further polymerization, becomes less favorable through the high viscosity melt and limits the achievable polymer molecular weight to a few ten thousand g/mol [33]. Removal of water from a viscous, high molecular weight PLA mass can only be achieved with expensive specialized reactors. High vacuum rotating disk reactors are an example of such a reactor that can generate a good surface renewal of the viscous polymer melt to enhance the mass transfer of the produced water [28].

Even if water can be efficiently removed, polycondensation of lactic acid to high molar mass PLA is additionally hindered due to the formation of a lactide byproduct as shown in Figure 2.5. As the lactide is usually volatile at the reaction temperature and pressure, removal of the ring structure from the reaction mixture leads to a decrease in yield and a limited maximum molar mass. Effectively refluxing lactide back into the reaction mixture (using a distillation column) while simultaneously

removing water efficiently from a highly viscous polymer melt is a technical challenge that has not allowed direct polycondensation of lactic acid to high molar mass PLA to be industrially feasible [34].

2.1.3   Lactide monomer synthesis

For the industrial synthesis of high molar mass PLA, normally a ring lactide monomer (Figure 2.2) is first synthesized. This ring lactide monomer can then undergo ring-opening polymerization (ROP) as further detailed in Section 2.1.4. ROP of lactide is preferred industrially because it does not require the removal of condensates (water byproduct) from the viscous polymer melt for the polymerization to take place. To produce the lactide monomer, oligomeric lactic acid chains of relatively low molar mass (~ 1 kDa) are first produced through polycondensation (Figure 2.1) of lactic acid. The lactic acid oligomers are heated under vacuum in the presence of a catalyst to higher temperatures (~ 230 °C) at which the backbiting depolymerization reaction (Figure 2.5) is favored. The lactide monomer is distilled from the oligomer and sublimated as a crystalline solid. This raw lactide distillate contains a mixture of the L-lactide, D-lactide, and meso-lactide stereoisomers (Figure 2.2).
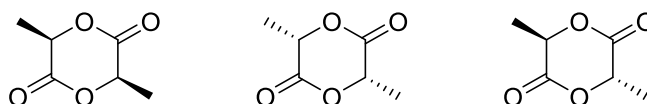
Figure 2.2: Lactide isomers present in the raw lactide mixture produced after depolymerization of lactic acid oligomers. From left to right: L-lactide, D-lactide, and meso-lactide

The composition of the raw lactide mixture depends on the stereopurity of the used raw lactic acid, the presence (or absence) of ions in the lactic acid, the chosen depolymerization temperature and the catalyst used. As it will be explained on Section 2.2, the stereopurity of the lactide monomer used for the ring opening polymerization can have an important effect of the thermal and mechanical properties of the produced PLA polymer. For these reasons, the raw lactide mixture is further purified through distillation and/or melt recrystallization to obtain stereopure (assay > 99.5 %) L-lactide, D-lactide, or meso-lactide monomers with a low acid content (AN) below 7meq_{-COOH}/kg [35]. These monomers must be handled under dry conditions to avoid their hydrolysis to lactoylactic acid dimers, which can cause undesired side reactions during ring opening polymerization as explained further in Section 2.1.4.

2.1.4   The ring-opening polymerization (ROP) approach

High molar mass PLA is industrially produced through ROP of lactide in the presence of tin(II) 2-ethyl hexanoate [tin octoate, $Sn(Oct)_2$] in the bulk and at temperatures of around 180 °C. The reaction is believed to occur through a coordination insertion mechanism [36; 37] as shown in Figure 2.3. One of the main advantages of the ROP mechanism is that no polycondensation byproduct must be

removed from the viscous melt during polymerization for the reaction to proceed. Although many other catalysts have been tested with some success, the Sn(Oct)$_2$ catalyst is preferred due to the high lactide monomer conversion, low monomer racemization, and its food contact approval in many countries [37; 38]. Depending on the temperature and reaction time, conversions above 90 % with less than 1 % racemization can be achieved while providing high product molar mass with the Sn(Oct)$_2$ catalyst [38]. A low degree of racemization is desired to gain control over the crystallinity of PLA and consequently, its material properties.
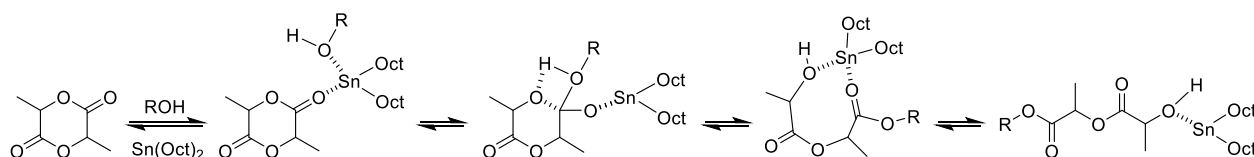

Figure 2.3: Proposed coordination-insertion mechanism modified from [38].

Impurities play an important role in the ring opening polymerization of lactide. Hydroxyl groups contained in high boiling alcohols (i.e. 1-undecanol) are typically used to control the molar mass of PLA as they have been found to act as a chain initiator in the ROP [38–45]. The theoretical degree of polymerization (DP$_{Theor}$) for a given reaction mixture can be estimated by considering the lactide monomer to –OH initiator molar ratio (Equation 2.1). The presence of hydroxyl groups in impurities that are difficult to avoid (i.e. water, hydrolyzed lactide), cause the experimental DP to be below the theoretical DP. If the DP of the polymer is known, the Mn can be calculated using Equation 2.2.

$$DP_{Theor} = \frac{[Lactide]}{[OH]}$$
Eq. 2.1

$$Mn = DP \cdot 144 \; g/mol$$
Eq. 2.2

Additionally, The presence of –COOH groups in the reaction melt (from hydrolyzed lactide) has been found to cause a reduction in the polymerization rate of lactide [39; 40; 47], while not affecting the conversion of the lactide monomer. The acid impurities are thought to coordinate with the tin catalyst and render it ineffective as an ROP site [38]. The obtained Mn of the PLA, however, does not change when increasing the –COOH concentration [39]. Hydrolysis of PLA chains or lactide monomer as well as initiation of the ROP by water molecules are known to produce –COOH groups during the ROP.

Side Reactions

Several undesired molar mass degradation reactions can occur both during and after the ROP of lactide. *During* the ROP, the undesired side reactions reduce the DP of the PLA chains to values below the ones expected by Equation 2.2. *After* the ROP, the undesired side reactions can still occur during storage of the synthesized PLA product or during subsequent exposure to high temperatures (processing). The main degradation reactions for PLA are shown in Table 2.1.

Table 2.1: Main PLA degradation reactions (Modified from [48])

	Hydrolysis	Depolymerization	Random thermal degradation
Dependence	- T - [Sn(Oct)$_2$] - [H$_2$O] - [-COOH] [49–51]	- T - [Sn(Oct)$_2$] - [Lactide] and lactide removal efficiency [a)]	- T - [Sn(Oct)$_2$]
Activation Energy [b)]	33.4 KJ/mol	94.2 KJ/mol	126 KJ/mol
Measures to reduce side reactions	- Lower active [Sn(Oct)$_2$] concentration - Dry reactants and PLA resin	- Lower active [Sn(Oct)$_2$] concentration - End-capping –OH end-groups	- Addition of heat stabilizers

[a)] Open system with high surface area to volume ratio (as for example the die exit of a blown film extrusion line) facilitates the removal of lactide from the PLA melt. The reduction of lactide concentration causes more depolymerization to occur to satisfy the equilibrium concentration.
[b)] Polymerization activation energy is 70.9 KJ/mol

Hydrolysis

The hydrolysis reaction has the lowest activation energy of the side reactions shown in Table 2.1 and can typically occur at lower temperatures than the other side reactions [48]. Hydrolysis requires the presence of water and is catalyzed by the Sn(Oct)$_2$ polymerization catalyst as well as by acidic –COOH groups [49–51]. Because the –COOH groups are generated during hydrolysis reactions (Figure 2.4), hydrolysis can be considered autocatalytic. The pKa of the carboxylic acid end-group of PLA and its oligomers has been found to be unusually low (~ 3) compared to most carboxylic acid groups (4.5 to 5) [52]. Both the ester bonds of the PLA polymer as well as the ester bonds of the lactide monomer are vulnerable to hydrolysis. Due to the higher mobility of the lactide monomer in the polymer melt however, it is expected to hydrolyze more readily than the PLA polymer [48]. Once the lactide monomer has been hydrolyzed, it can undergo transesterification with PLA chains causing a practically irreversible reduction of the polymer molar mass (if water is not actively removed from the mixture) [48].

a)
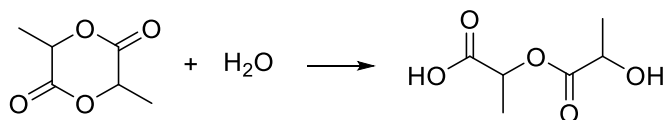
b)

Figure 2.4: Hydrolysis of a) lactide ester bond and b) polymer ester bond

Backbiting depolymerization reaction

In the backbiting depolymerization reaction (Figure 2.5), is an equilibrium reaction in which the –OH end-group of a PLA chain reacts intramolecularly with an ester-bond on the polymer backbone to form the lactide ring monomer. The equilibrium lactide concentration is defined by the temperature at which the reaction mixture is found and not by the catalyst concentration. The rate at which the lactide equilibrium concentration is reached depends on the catalyst concentration and the temperature.
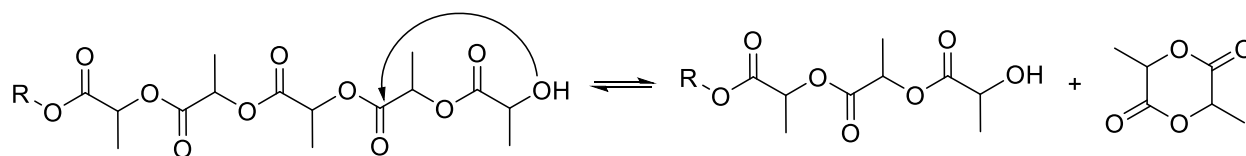
Figure 2.5: Backbiting depolymerization reaction

As the temperature of the reaction mixture is increased, the lactide equilibrium concentration is also increased as shown Figure 2.6. For this reason, the maximum ROP lactide conversion is reduced at higher reaction temperatures. Once the reaction mixture has been cooled after completion of the ROP, a given lactide concentration is present in the obtained PLA material. Although the equilibrium lactide concentration at room temperature is low (Figure 2.6), the low reaction rate of the lactide monomer at this temperature does not allow the lactide to polymerize (and reduce the lactide concentration). Thus, the equilibrium lactide concentration (achieved at the ROP temperature) remains in the PLA material.

Figure 2.6 shows the lactide equilibrium concentration at a wide range of temperatures as calculated with the depolymerization equilibrium model developed by Witzke [48]. At typical ROP reaction temperatures of around 180 °C, the lactide equilibrium is at values of around 3.5 %-wt as shown in Figure 2.6. Although lactide is non-toxic, its vulnerability to hydrolysis, its distinct smell, and the fact that it can cause equipment fouling during high temperature processing, require lactide to be

removed from the produced ROP mixture. According to Figure 2.6, cooling the ROP reaction mixture down to room temperature should bring the equilibrium lactide concentration to values around 0 %-wt. At these low temperatures however, the polymerization rate is very low and lactide is more likely to hydrolyze under atmospheric humidity before its concentration can be decreased through polymerization. Lactide is usually removed from the ROP product mixture through the demonomerization process further detailed in page 13.
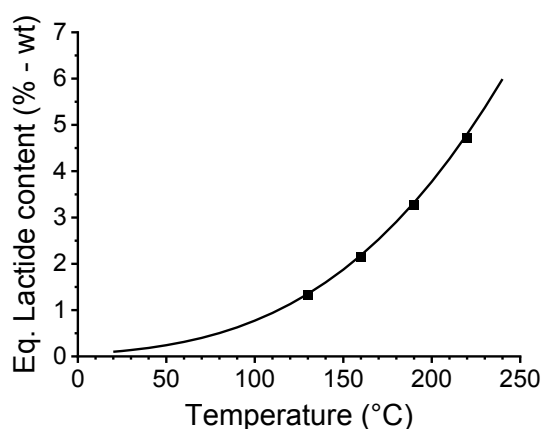
Figure 2.6: Equilibrium lactide concentration at different temperatures taken from experimental data by Witzke [48] (squares) and fitted data (continuous line) according to the model by Witzke [48].

Random thermal degradation

Several studies have been done to attempt to clarify the reactions behind the thermal degradation of PLA [48; 53–58]. However, studying the thermal degradation without the interference of the hydrolysis and the depolymerization mechanisms is difficult. McNeill and Leiper [55] proposed a backbiting ester interchange reaction mechanism at the chain ends or in the lactide ring monomer to explain the carbon monoxide and acetaldehyde degradation products observed through thermal volatilization analysis at temperatures above 230 °C. McNeill and Leiper [55] proposed an additional radical chain scission as a possible degradation mechanism for temperatures above 270 °C (not shown).
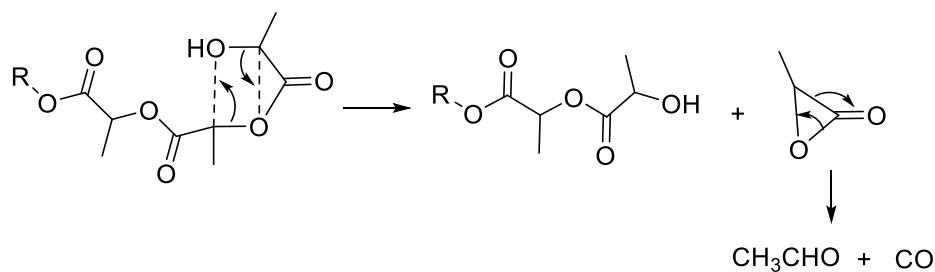
Figure 2.7: Backbiting ester interchange degradation reaction at PLA chain-ends proposed by McNeill and Leiper [55].

When comparing rheological measurements of PCL, PLA, and PHBV, Ramkumar et al. [59] observed significantly higher thermal degradation at similar measurement temperatures of PLA and PHBV than in PCL. The main difference between these polymers is the presence of a methyl side-group on the PLA and PHBV backbones which is absent in PCL. They concluded that the proton in the methyl side-group on the PLA and PHBV chains is labile, and that its proximity to the ester group affects the thermal stability of these polymers. A possible non radical random chain scission mechanism taking this into account was proposed by Yu et al. [58] (Figure 2.8) and was included in their PLA ROP kinetic model. The conjugated double bonds in one of the byproducts is proposed as an explanation to the observed discoloration in PLA after longer exposure to high temperatures. When considering the mechanism in Figure 2.8 in their kinetic model, they were able to fit the molar mass reduction of the reaction mixture after longer reaction times at temperatures between 130 °C and 180 °C [58] with good accuracy. Their experimental data shows that this reaction mechanism is catalyst dependent.
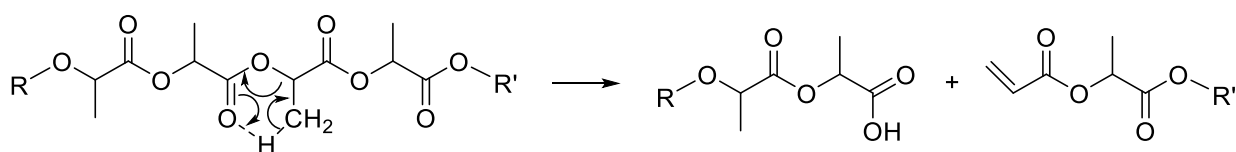
Figure 2.8: Non radical random chain scission of the labile methyl group of PLA [58; 59]

Although several different thermal random degradation mechanisms have been proposed, some conclusions on the characteristics of this type of degradation can be drawn. Relevant degradation through this mechanism occurs either at temperatures above 230 °C [38; 48; 55] and/or at longer times [58] due to its relatively high activation energy [48; 58]. A catalyst dependency was found by [55; 58] and the addition of radical stabilizers like 1,4-diaminoanthraquinone [55] has shown to hinder thermal degradation of PLA.

High molar mass, stable PLA

The development of the ROP catalyst technology allowed high Mn PLA with good stereoregularity to be a technically feasible material with a wider array of applications [38]. McNeill and Leiper wrote in 1984 however, that the ease of hydrolysis in PLA and PGA precluded the use of these polymers in any useful commercial application and limited them to surgical suture applications were polymer degradation is required [56].

Molar mass is an important parameter that defines many of the thermal, mechanical, and rheological properties of the material (Section 2.2). As explained in Section 2.1.4, the molar mass of PLA produced through ROP can in theory, be controlled by the monomer to initiator ratio. The molar mass degradation reactions shown in Section 2.1.4 however, make not only achieving this Mn during the synthesis of PLA a challenge, but also make maintaining the desired Mn during the subsequent demonomerization and processing steps difficult. The way in which these degradation side-reactions affect PLA polymers during synthesis and subsequent steps are described in this section. Some options found in the literature to avoid such Mn degradation are presented.

Bulk PLA synthesis through ROP

For the ROP of lactide to be done in bulk (in the absence of solvents), the reaction temperature must be above the melting temperature of PLA (Tm_{PLA} ~ 175 °C). Lower temperatures can lead to crystallization of the formed PLA chains as well as to high melt viscosities making stirring of the reaction mixture difficult. High temperatures increase the polymerization rate leading to lower ROP reaction times. Simultaneously however, the high temperatures also increase the reaction rate of the previously mentioned side reactions.

To reduce the molar mass degradation through hydrolysis, the ROP must be done under dry conditions. The increase in the viscosity of the reaction mixture during the ROP can be used to monitor the monomer conversion indirectly by measuring the mechanical stirrer torque. Monitoring the reaction helps avoid incomplete monomer conversion (too short reaction time) or thermal degradation reactions (unnecessarily long reaction time). The PLA product (containing an equilibrium lactide concentration) should be allowed to cool under dry conditions to avoid hydrolysis of the lactide. The PLA product should be kept under dry conditions until after the equilibrium lactide concentration is removed through demonomerization to avoid the formation of –COOH groups in the PLA ROP product, which can catalyze the hydrolysis of PLA.

Demonomerization

Several methods are described in the literature to remove the equilibrium lactide concentration from PLA after the ROP. Solvent extraction is not the preferred industrial method because of the large amount of toxic solvents necessary and the difficulties of recycling the removed lactide [48]. Bulk demonomerization methods without the need of a solvent are widely preferred. Some of these methods that can be found in the literature include vacuum devolatilization of crystallized pellets in a vacuum drying oven [48], nitrogen devolatilization of crystallized pellets [60], vacuum devolatilization of the melt in an twin-screw extruder [48; 61], or vacuum devolatilization in a falling thin-film evaporator [62] among others. The before-mentioned bulk demonomerization methods rely on the same general principles that are described in more detail below.

Two different equilibria are in competition during vacuum demonomerization of a PLA / lactide mixture (liquid or solid depending on the demonomerization method used). The first equilibrium is the chemical lactide equilibrium (Figure 2.5 and Figure 2.6), which is defined by the demonomerization temperature. The phase equilibrium (gas / liquid or gas / solid depending on the demonomerization conditions) is the second equilibrium and it is defined by the temperature and the partial pressure of lactide in the gaseous phase [48].

Each of these equilibria has its distinct kinetics that determine the rate at which the lactide concentration in the PLA / lactide mixture will change. The depolymerization equilibrium kinetics

depend on the temperature and the catalyst concentration in the PLA / lactide mixture. The phase equilibrium kinetics depend on the temperature, lactide partial pressure, surface area to volume ratio exposed to the gaseous phase, and viscosity of the PLA / lactide mixture. The final lactide concentration in the PLA / lactide mixture after demonomerization will be defined by the interplay between the kinetics of the chemical depolymerization equilibrium and the phase equilibrium.

Figure 2.9 shows the equilibrium lactide concentrations for both equilibria calculated independently from each other at different demonomerization conditions (temperature and pressure) through the models developed by Witzke [48]. At higher demonomerization temperatures and pressures, the %-wt lactide content defined by the phase equilibrium (red lines) is reduced. This dependency suggests that the demonomerization process should thus take place at higher temperatures and low pressures. The chemical depolymerization equilibrium (black line) however, shows that a higher %-wt lactide content is obtained as the demonomerization temperature is increased.
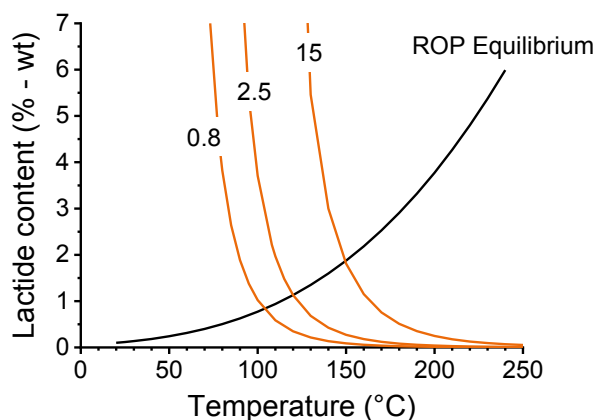
Figure 2.9: Phase equilibrium lactide concentrations (red lines) at different pressures (in mbar) according to Witzke model [48]. The ROP lactide equilibrium concentration (black solid line) also from Witzke [48] is added as a reference.

To give an example of a typical bulk demonomerization process, an ROP product produced at 180 °C with an equilibrium lactide concentration of around 3 %-wt is exposed to a given temperature and pressure to reduce the lactide concentration. At a temperature of 120 °C and a pressure of 2.5 mbar for example, both the phase equilibrium and the depolymerization equilibrium have an equilibrium lactide concentration of around 1 %-wt. If enough time is given for both the equilibria to be reached, the PLA / lactide mixture will reach a lactide content of 1 %-wt. The material can be maintained at these conditions for a long time and no further depolymerization should occur (although other types of degradation reactions can happen). If instead a temperature of 120 °C and a pressure of 15 mbar are chosen, the ROP product mixture would remain with a 3 %-wt lactide content as the phase equilibrium lactide concentration is significantly higher than 3 %-wt.

If a demonomerization temperature of 220 °C and a pressure of 2.5 mbar are chosen for the demonomerization of the PLA / 3 %-wt lactide mixture, the final lactide content will be defined by the kinetics of the phase and the chemical equilibria together with the demonomerization time. The faster the kinetics of the phase equilibrium are in comparison to the depolymerization equilibrium

kinetics, the closer the final lactide content will be to the phase equilibrium lactide concentration. This will lead to a very low lactide content after demonomerization (close to 0 %-wt). Inversely, if the depolymerization equilibrium kinetics are much faster than the phase equilibrium kinetics, the final lactide concentration will be closer to the depolymerization equilibrium concentration of 4.8 %-wt. If the kinetics of both equilibria are similar, the lactide concentration will be somewhere in between both equilibrium concentrations. In the latter case, significant depolymerization at longer demonomerization times can be expected because the demonomerization equilibrium will produce additional lactide to make up for the lactide lost to the gas phase.

To reduce the lactide %-wt content after demonomerization of the ROP PLA product, the chemical depolymerization kinetics should be as slow as possible and the phase equilibrium kinetics should be as fast as possible. The depolymerization rate can be reduced by lowering the catalyst concentration in the polymer. Adding catalyst deactivators before the demonomerization process, or end-capping the –OH PLA chain ends can alternatively be used to reduce the depolymerization rate [63]. The phase equilibrium kinetics can be increased in several ways depending on the demonomerization method. If demonomerization is done in the solid state, reducing the particle size of the solid PLA / lactide mixture can increase the surface area to volume ratio and improve mass transfer. In the case of working in the melt state in an extruder, increasing the RPM and reducing the mass flow rate as well as using an inert gas vapor sweep can help increase the lactide mass transfer rate [48]. Using falling thin film evaporators with continuous surface renewal will increase the surface area to volume ratio [62].

Additives and Stabilizers

Several stabilization additives have been proposed to improve the melt stability of PLA. Carbodiimide water scavengers such as Stabaxol® have been found to reduce hydrolytic degradation during melt processing when blended into the PLA resin after demonomerization [64]. At the same time, the use of peroxides was found by Södergård to reduce the Mn loss during processing through crosslinking and catalyst deactivation mechanisms [65]. Catalyst deactivation through the addition of acidic chelating agents such as tartaric acid [61; 63], poly(acrylic acid) [61; 66], acid phosphates [63], and others [67] has been widely reported in the literature. Addition of molecules containing multiple epoxide groups such as Joncryl® [68–71] or epoxidized vegetable oils [61; 72; 73] were shown to cause branching in the material and reduce Mn degradation during processing. Finally, the reduction of catalyst concentration has been widely proven to reduce the Mn degradation during processing [48; 74–76]. It is important to mention that most of the mentioned stabilization additives were characterized on materials with varying catalyst concentrations, lactide concentrations, humidity conditions, and sometimes on commercial PLA materials with unknown additives. Comparison of the efficiency of each of the before-mentioned stabilizing systems based on the available literature is thus difficult.

The addition of organophosphites such as tris(nonyl phenyl) phosphite (TNPP), tris(2,4-di-tert-butylphenyl) (TDBP), or triphenyl phosphite (TPP) into PLA as melt stabilizers has been widely reported

in the scientific literature. Organophosphites have been shown to lead to chain extension of PLA chains and consequently dampening the Mn degradation of PLA during processing [74; 75; 77–79; 80; 81–83]. The before mentioned phosphites (TNPP, TDBP, TPP) are thought to react with the hydroxyl end-groups of PLA as shown below in Figure 2.10.
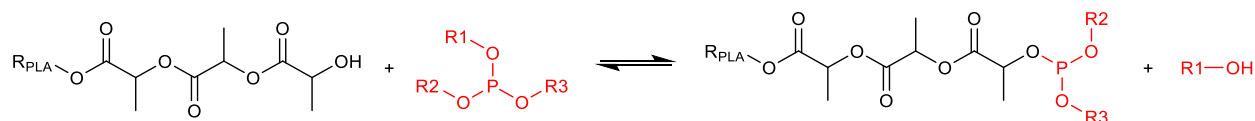
Figure 2.10: Reaction between PLA -OH end-group and organophosphite

The product of the previously shown reaction in Figure 2.10 consisting of a PLA chain with a phosphite chain-end can further react with additional hydroxyl end-groups from other PLA chain as shown in Figure 2.11 and Figure 2.12. These reactions result in the formation of a chain-extended PLA polymer chain held together by a relatively labile and hydrolysis prone (when compared to the PLA ester bonds) phosphorous bond [83].
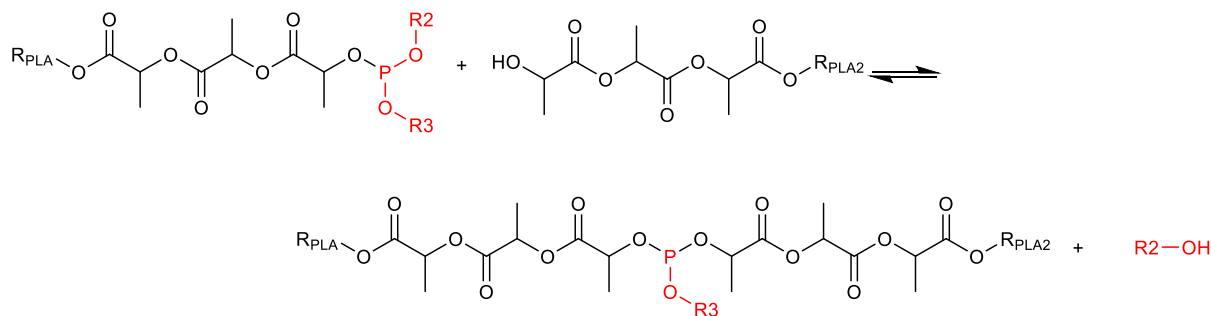
Figure 2.11: Reaction of the phosphited PLA chain-end with a second PLA hydroxyl end-group
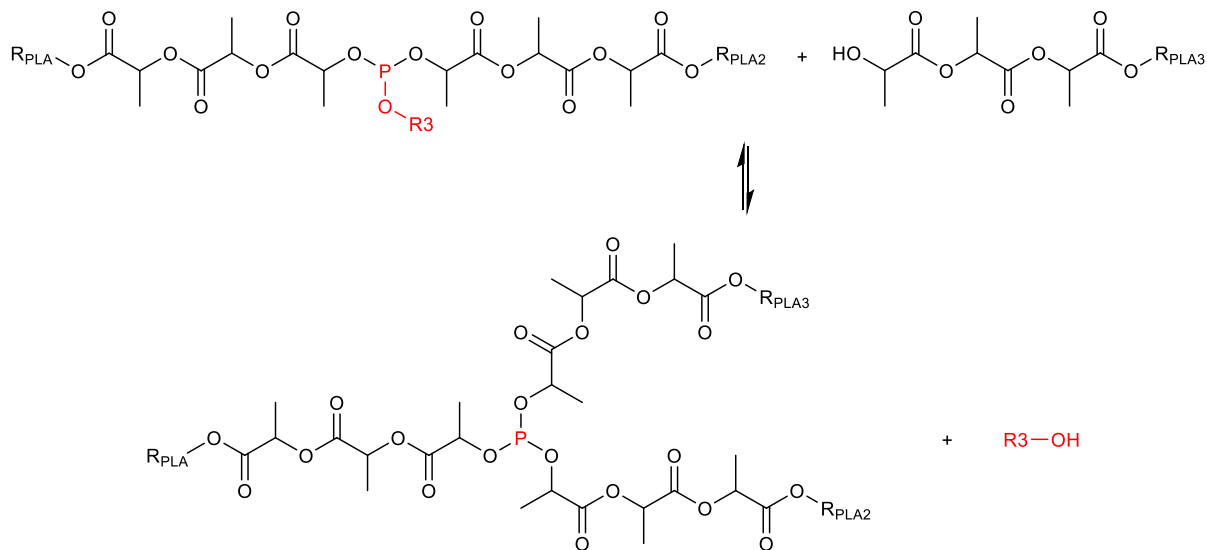
Figure 2.12: Reaction of the chain-extended PLA chain with a third PLA hydroxyl end-group

These reactions are equilibrium driven, so the presence or the absence of the R-OH byproduct in the reaction medium is thought to determine the ability of such phosphorous bonds to continue to be produced [83]. The phosphite chain ends are believed to be able to undergo transesterification with carbonyl groups present in the PLA material. This reaction should theoretically produce a PLA ester bond (more stable than the phosphorous bond) and a phosphite byproduct as shown in Figure 2.13.
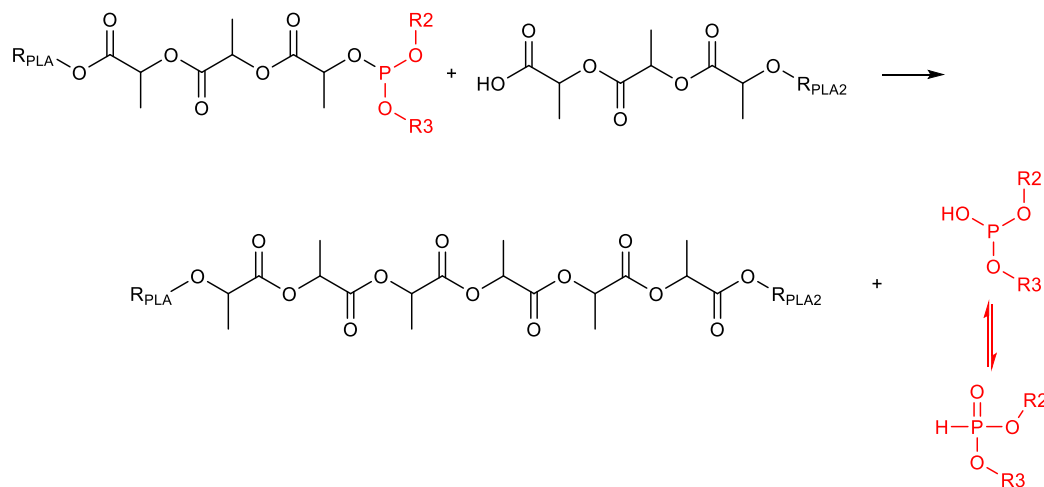
Figure 2.13: Transesterification reaction of a phosphited PLA chain-end and a carbonyl (-COOH) PLA chain-end

The bis(nonylphenyl) phosphite byproduct shown in Figure 2.13 is thought to cause an equilibrium displacement resulting in scission of the labile phosphorous chain extending bonds found in other PLA chains and consequently in Mn decrease [83] as shown in Figure 2.14.
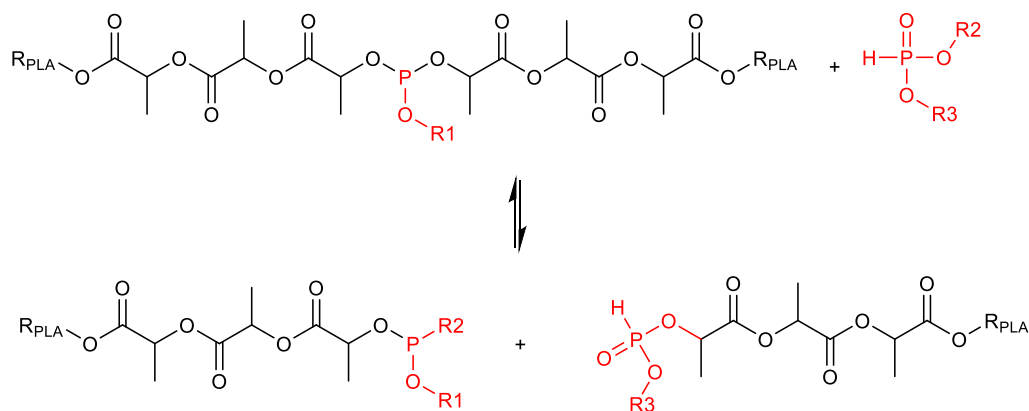
Figure 2.14: Phosphorous bond scission due to the presence of the bis(nonylphenyl) phosphite byproduct causing equilibrium displacement

In many studies, addition of small amounts of organophosphites (TNPP, TDBP, TPP) led to an increase in the molar mass of the polyesters likely due to a chain extension mechanism [77–79; 81; 83; 84]. Further increase of organophosphite above a given concentration however, has been observed to cause no further increase of the molar mass. This observation was explained by Jacques et al. [83] through the reduction of the hydroxyl end-group concentration in the reaction mixture by the reaction

shown in Figure 2.10 and its effects on the polycondensation equilibrium. Considering the chemical equilibrium shown below in Figure 2.15, the equilibrium constant can be calculated as shown on Equation 2.3 below.

$$[\text{-OH}] \ + \ [\text{-COOH}] \ \rightleftharpoons \ [\text{-COO-}] \ + \ [\text{H}_2\text{O}]$$
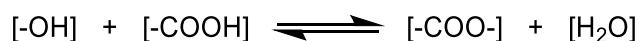
Figure 2.15: Polycondensation equilibrium

$$K_{eq} = \frac{[-COO-][H_2O]}{[-COOH][-OH]} \qquad \text{Eq. 2.3}$$

To satisfy the equilibrium constant, a given concentration of –COOH and –OH end-groups must be present in the material for a given –COO– and H_2O concentration. If the –OH end-group concentration is reduced in the polymer melt (through the reaction in Figure 2.10), the system re-equilibrates by producing –COOH and –OH end-groups through the hydrolysis of ester bonds in the polymer backbone [83]. The molar mass degradation caused by this hydrolysis reaction is believed to offset the molar mass increase caused by the TNPP chain extension reactions (Figure 2.11 and 2.13) [83].

2.1.5 Physical properties of PLA homopolymer and main fields of application

As a solid, PLA can be found as an amorphous glass or a semicrystalline polymer depending on its stereochemistry and its thermal history [27]. High molar mass, amorphous PLA is typically found as a glassy solid at room temperature due to its glass transition temperature (Tg) of around 58 °C [27]. Semicrystalline PLA can have a melting temperature (Tm) between 140 °C and 175 °C depending on the stereoregularity and thermal history [11]. Highly stereoregular PLLA with a melting point close to 175 °C can be produced by using a stereopure L-lactide monomer (Figure 2.2), a low racemization catalyst [such as Sn(Oct)$_2$], and the appropriate reaction conditions.

High molar mass PLA shows a relatively high stiffness and a high transparency (in its amorphous state) [11] making it suitable for applications such as rigid packaging or cold drink cups. The low heat deflection temperature of PLA (especially in its amorphous state) however, limit its use in high temperature applications (coffee cups). The poor barrier properties of PLA and its low impact strength when compared with PET (Table 2.2) limit its use in plastic bottle applications [11].

When considering PLA as a possible material for flexible blown film applications, several limitations can be recognized. Currently, flexible films are mainly produced using low-density polyethylene (LDPE) as a raw material due to its appropriate mechanical and rheological properties. LDPE's high elongation at break and moderate to low elastic modulus (Table 2.2) make for soft and flexible films, while its

branched structure give it the high melt strength necessary for efficient blown film processing. The high elastic modulus and low elongation at break of PLA (Table 2.2) make for stiff and brittle films. At the same time, the low melt strength of PLA caused by its linear polymer chain topology can make processing PLA in conventional blown film processing equipment difficult [71].

Table 2.2: Selected mechanical [11; 85] and barrier properties [28] of PLA, PET, and LDPE

Test	Reference	Standard	PLA	PET	LDPE
Transparency	[11]		transparent	transparent	transparent
Density (g/cm3)	[11]	ISO 1183	1.25	1.35	0.92
Melting Point (°C)	[11]	DSC	140-175	245	105 - 115
Glass transition temperature (°C)	[11]	DSC	58	75	-100
Biodegradability	[11]	EN 13432	yes	no	no
Modulus of elasticity (MPa)*		ISO 527	3,600	3,100	250
Elongation at break (%)*		ISO 527	3	50	500
Notched Izod impact resistance (J/m)	[28; 85]	ASTM D256	12 [28]	90 [85]	-
O_2 transmission rate T = 30 °C (10^{-17} kg m m^{-2} s^{-1} Pa^{-1})	[28]		0.495	0.033	8.250
CO_2 transmission T = 30 °C (10^{-17} kg m m^{-2} s^{-1} Pa^{-1})	[28]		1.52	0.02	52.82

* Mechanical properties measured on 4 mm injection molded tensile test specimens

2.2 Structure-property relationships of polymers

The general chemical structure of PLA and the ways in which the degree of polymerization and the stereochemistry can be controlled were described in the previous sections. The changes in the chemical and molecular structure of PLA can have important effects in the thermal, mechanical and rheological properties. In the present section, the theoretical dependencies of the material properties on the molecular structure of polymers found in the literature are described. These structure-property relationships are later used to interpret the obtained experimental results in Section 5.
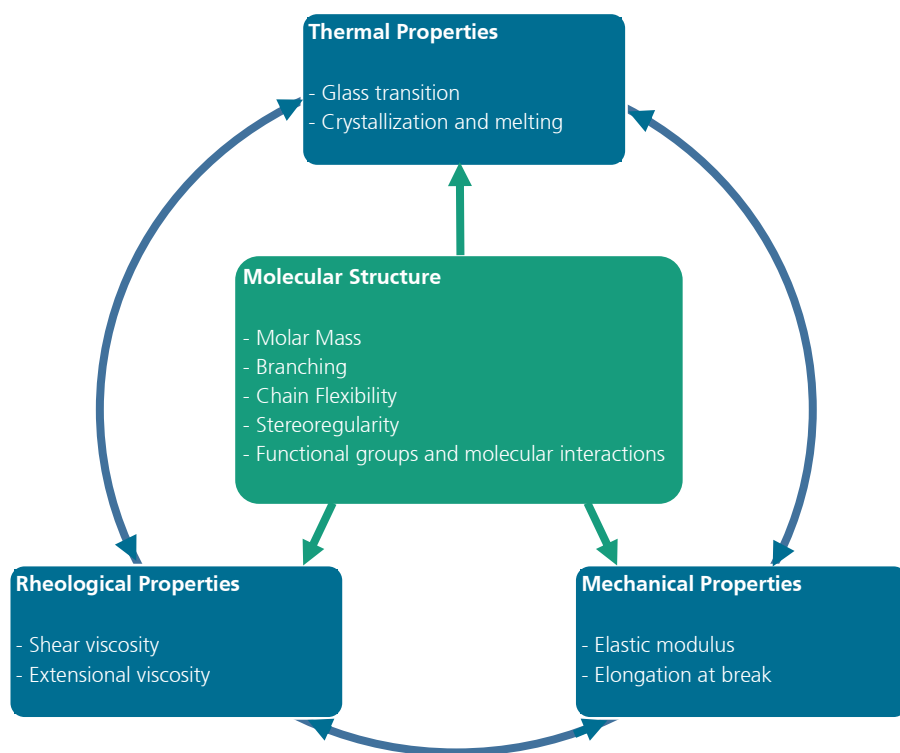
Figure 2.16: Relevant chemical structure variables and resulting material properties

Figure 2.16 shows the different changes in molecular structure that can be controlled within the synthetic limitations of PLA and its copolymers. The molecular structure can have a direct effect on the thermal, rheological, and mechanical properties as shown in Figure 2.16. The rheological and mechanical properties however, vary significantly depending on the temperature at which they are measured and on the presence (or absence) of crystal structures. For this reason, the glass transition and the crystallization behavior of polymers were chosen as the starting point to describe the structure-property relationships of polymers relevant to this thesis. The effects of the molecular structure on the glass transition are introduced and the changes of the mechanical and rheological properties with respect to the glass transition temperature are described. The same analysis is then repeated for the crystallization and melting phenomena. Finally, the remaining direct dependencies of mechanical and rheological properties to the molecular structure are covered.

2.2.1 Properties of pure homopolymers

Thermal properties

The glass transition

The glass transition temperature (Tg) is the temperature range above which the polymer chain segments can undergo long-range translational motion and below which only local motion is active [86]. When a polymer melt is cooled below its Tg, the density of the material and its molecular relaxation times begin to increase. Over a given temperature range, the molecular motion will become so slow that an equilibrium packing of the molecules cannot be achieved during relevant experimental times. When this occurs, it is said that the material has undergone the glass transition to form an amorphous solid or glass [87]. The glass transition is not considered to be a true second-order phase transition because the amorphous solid is not in an equilibrium state, but a kinetically defined state that, although very slowly, is changing over time. In the amorphous state, the polymer molecules in the material are found in a disordered arrangement similar to what would be expected in the liquid state. In the glass state however, the material is not able to flow (in relevant time scales) and will have mechanical properties more similar to those of a brittle solid [87].

Although both low molecular weight compounds and polymers can undergo glass transition, it is not equally likely [87]. For most low molecular weight materials, special effort must be made to suppress crystallization and achieve glass formation. With polymers the glassy state is always obtained, whether a particular polymer is crystallizable or not, due to the long-chain structure of polymers. Even very regular polymer structures that allow the possibility of crystal formation do not ensure that crystallization will occur rapidly or completely even during very slow cooling rates. Depending on the experimental conditions, the polymer domain may be anywhere from almost 100% crystalline to 100% amorphous (or glass). However, a small fraction of amorphous, glassy domains will always be present in polymeric materials [87].
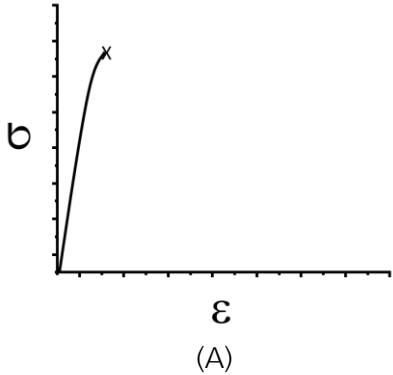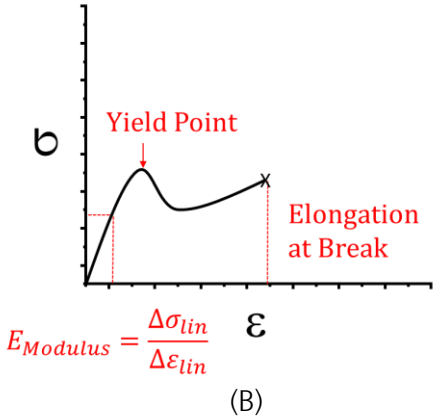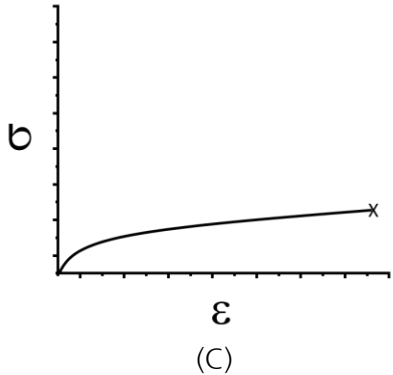
In the current section, the effects of the Tg on the mechanical and rheological properties of amorphous polymers will be discussed. This will be followed by some general correlations between the chemical structure of a homopolymer and its Tg. The section will end with some possible options to modify the Tg of a polymer.

Mechanical properties at and around Tg

Uniaxial tensile tests are typically used to observe the response of materials to mechanical deformation. In this type of test, a standardized tensile test specimen is clamped on both sides to a universal tensile testing machine. The clamps begin moving apart from each other causing the

specimen to be deformed at a given elongation rate (ΔL/t) and temperature. The machine measures the force necessary to cause the prescribed deformation of the sample, which when divided by the initial cross-sectional area of the tensile test specimen gives the engineering stress. From this type of tests, a stress (σ) - strain (ε) curve can be obtained with which relevant mechanical properties such as elastic modulus (MPa) and elongation at break (%) values can be determined (Table 2.3 graph B).

Table 2.3: Schematic of expected stress-strain curves at and around the glass transition [88]

Relative position of Tg for the amorphous phase	Typical shape of stress-strain curve measured at room temperature (RT)	Examples of polymers in this class
Tg > RT	(A)	PS PMMA PLA
Tg ≈ RT	(B)	PP PBT
Tg < RT	(C)	LDPE

Materials with a Tg significantly above the measurement temperature, usually have high strength but are relatively brittle (Table 2.3, graph A). Polystyrene (PS), poly(methyl methacrylate) (PMMA), and PLA have Tg values of 100, 100, and 58 °C respectively. Their high Tg, cause them to have a relatively high elastic modulus and a low elongation at break when their mechanical properties are measured at room temperature. These materials are relatively hard to deform, however they exhibit brittle fracture at low deformation (strain values) once this energetic barrier is overcome.

Polymers with Tg close to room temperature (Table 2.3, graph B), show both a relatively high elastic modulus and a ductile behavior after a given strain. Such materials reach a yield point after which the molecules begin to "flow" under the applied load and start to align themselves in the direction of the deformation [87]. The macroscopic thinning of the test specimen at the points were the molecules begin to align is called necking. The aligned molecules in the necking regions of the test specimen make deformations in these areas more difficult. For this reason, stretching continues in the un-necked portions of the specimen and further elongation is possible with a slightly drop in stress. When necking has expanded to most of the test specimen, further deformation continues now in the regions with aligned polymer chains, showing some strain hardening effects before failure [87]. Materials with Tg close to 25 °C (0 - 50 °C) like polypropylene (PP) and polybutylene terephthalate (PBT) usually exhibit this kind of behavior at room temperature. These materials are difficult to deform and they show ductile behavior instead of brittle failure. These materials are generally described as "tough" but relatively stiff materials.

Materials with Tg well below the measurement temperature exhibit a relatively low elastic modulus, ductile behavior, and uniform necking. In this case, the material can start to realign its molecules at much lower applied stresses and necking occurs more uniformly throughout the complete length of the test specimen. This reduces the concentration of stress at local points throughout the sample and brings a significant increase in the elongation at break of the material. LDPE (Tg ~ -100 °C) is an example of a soft and flexible material (Table 2.3 graph C), with ideal tensile properties for flexible film applications.

The before mentioned examples highlight the dependency of the Tg of polymers and their mechanical properties at room temperature. However, since the glass transition is a kinetically defined state, it is important to discuss the effect of time on the mechanical properties. A sufficiently slow deformation rate can also give the molecules in a brittle material enough time to begin to "flow" under the mechanical load. Under such slow strain rates, a brittle material could potentially go from behaving as shown in graph (A) in Table 2.3, to behaving as shown on graph (B). Such slow deformations are typically too slow to be relevant in many applications. This is because it has been found that a logarithmic increase in the strain rate affects the brittle-ductile transition equivalently to a linear decrease in temperature [89]. The opposite however, is quite relevant as very fast deformation rates can be experienced by materials when it is subjected to sudden impacts. In this case, a ductile material can behave like a brittle material. Depending on the intended application for a polymeric material, the appropriate tensile test (or impact testing) conditions must be chosen to adequately select a material.

Tg and the rheological properties

The viscosity of a polymer melt is closely linked to the glass transition temperature of a polymer to a much higher degree than in low molar mass liquids [87]. To illustrate this, the typical Arrhenius temperature dependence of viscosity (η) for low molar mass liquids (Equation 2.4) can be analyzed.

$$\eta(T) = A_R exp\left(\frac{E_a}{RT}\right)$$
<div align="right">Eq. 2.4</div>

The value of A_R in Equation 2.4 is an empirical pre-factor with units of viscosity, E_a is the activation energy and R is the ideal gas constant. Equation 2.4 suggests that the only thing limiting flow is an energetic barrier to the molecules sliding past each other, which can be more easily overcome at higher temperatures. In the case of amorphous high molar mass polymers, experimental data shows an asymptotically high increase in viscosity at temperatures close to Tg (Figure 2.17).
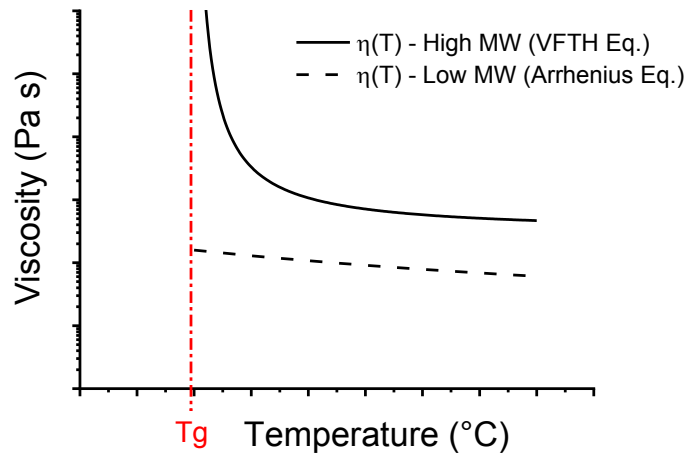
Figure 2.17: Schematic dependency of viscosity (log$_{10}$) with respect to temperature (linear) for high molar mass polymers (solid line) and low molar mass molecules (dashed line) above Tg.

This behavior has been explained by postulating that flow in glass-forming liquids is impeded primarily by a lack of free volume, rather than by an energy barrier (although such barriers should still contribute) [87]. A mathematical description for this was formulated by Doolittle [90] through Equation 2.5:

$$\eta = A'exp\left(\frac{B'V_{occ}}{V_f}\right)$$
<div align="right">Eq. 2.5</div>

where A' and B' are empirical constants, V_{occ} refers to the volume occupied by the polymer chains and V_f refers to the free volume or "elbow room" between the molecules required for them to undergo rotation and translational motion. Doolittle's equation reformulated in terms of the temperature and the Tg is known as the Vogel-Fulcher-Tammann-Hesse (VFTH) equation and is shown below in Equation 2.6.

$$\eta = A_{VFTH} \, exp\left(\frac{B}{T - T_0}\right)$$

<div align="right">Eq. 2.6</div>

$$B = \frac{B'}{\alpha_f}$$

<div align="right">Eq. 2.7</div>

$$T_0 = Tg - \frac{f_g}{\alpha_f}$$

<div align="right">Eq. 2.8</div>
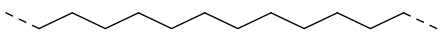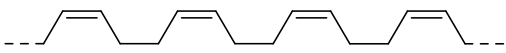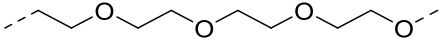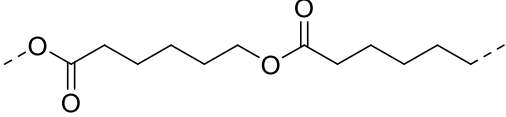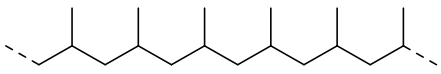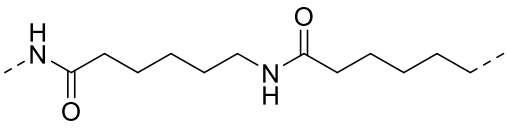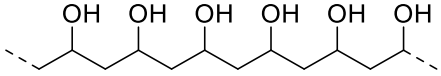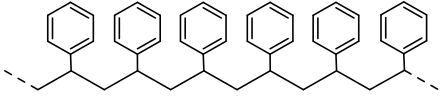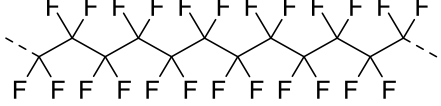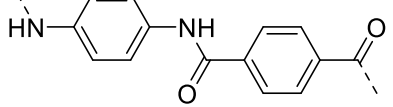
In Equation 2.6, Equation 2.7, and Equation 2.8, α_f is the coefficient of expansion of the free volume only, f_g is the fractional free volume at temperatures below the Tg, and T_0 is referred to as the Vogel temperature. The main take-away from Equation 2.6, is that the viscosity increases asymptotically as the measurement temperature (T) is reduced to a value of T_0 (which is some f_g / α_f degrees below Tg) [87]. Depending on the values of f_g and α_f for the given polymer, the viscosity increases quite strongly already at temperatures around Tg. The widely used VFTH equation (Equation 2.6) has been found to appropriately describe the dependency of viscosity on measurement temperature (T) and Tg.

As in the case of the mechanical properties, the rheological properties of polymers (viscosity) also depend strongly on the measurement temperature and its proximity to Tg. This dependency can be used to obtain the necessary rheological properties for certain processing methods as further described in Section 5.2 of this thesis.

Chemical structure and Tg

The previous two sections highlighted the importance of Tg on the mechanical and rheological properties of the materials. In the current section, the influence of the chemical structure of polymers on defining or anchoring Tg to a specific region on the temperature scale is discussed. Although it is difficult to define strict relationships between the chemical structures and Tg, general correlations can be extracted based on the bond flexibility, the presence of side-groups, and molecular interactions present in the polymer chains [87]. The different features of the chemical structure can work synergistically or competitively to cause different effects on the Tg of the polymer. The net effects caused by the different molecular structure features of a polymer yield a single Tg value, which is practically constant for polymers of high molar mass. Typical Tg values of selected (high molar mass) polymers with a wide range of molecular structures are shown in Table 2.4.

Table 2.4: Representative values of Tg and Tm (for stereoregular forms, where applicable) for some common polymers [87].

Polymer name	Abbreviation	Schematic diagram of polymer chain segment	Tg (°C)	Tm (°C)
Polyethylene	PE		-120[a]	135
cis-1,4-Polybutadiene	Butadiene rubber		-112	12
Poly(ethylene oxide)	PEG		-70[a]	65
Polycaprolactone	PCL		-72[b]	58[b]
Polypropylene	PP		-10	188
Polycaprolactam	PA 6		47[b]	220[b]
Poly(vinyl alcohol)	PVA		90	240
Polystyrene	PS		100	240
Poly(tetrafluoroethylene)	PTFE		130	330
Poly(p-phenylene terephthalamide)	Kevlar®		240	325

a) Values are difficult to measure due to the fast crystallization kinetics. b) values obtained from a different source: [85]

a) Backbone flexibility

The Tg usually lowers as the backbone flexibility is increased. This can be observed when comparing the Tg values of PE and Kevlar®. The Tg of Kevlar® is significantly higher than that of PE due to the presence of stiff aromatic rings on Kevlar®. A notable exception to this correlation is the Tg of PEG. Although the C–O bonds in PEG are more flexible than the C–C bonds in PE, the Tg of PEG is significantly higher [87]. In this case, the molecular interactions likely play a more important role in defining the Tg of the polymer.
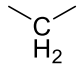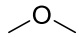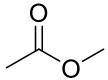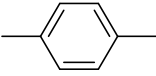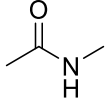
b) Side-groups

The effect of the side-groups on the Tg of polymers can be analyzed by comparing the structures of PE and PP (Table 2.4) and their respective Tg values. The structures of these polymers is practically the same except for the presence of the methyl side-group on PP. The significantly different Tg values of PE and PP (Tg_{PE} ~ -120 °C, Tg_{PP} ~ -10 °C), highlight the impact of the methyl side-group on Tg. If additionally, a polar –OH group is added to the methyl side-group (as in the case of PVA) an additional increase of the Tg is observed. Bulky side-groups like aromatic rings in PS and/or flour substituents on the backbone carbons of PTFE impede backbone rearrangements and further increase Tg to 100 °C and 130 °C respectively.

c) Molecular interactions

Polymers that have weak molecular interactions, such as the purely dispersive interactions in the case of polyolefins, generally have lower Tg values than more strongly interacting polymer chains such as PVA with its polar –OH side groups [87]. Such polar groups cannot only be found as side-groups, but also directly in the polymer backbone. This is the case of polyethers, polyesters, and polyamides (among other examples). The effect of such polar groups on the polymer backbone can be analyzed by comparing their molar cohesive energies listed in Table 2.5.

Table 2.5: Molar cohesive energies of functional groups found in polyesters and polyethers [91]

Structure	Name of group	Cohesive energy (kcal/mol)
	hydrocarbon	0.68
	ether	1.00
	ester	2.90
	aromatic	3.80
	amide	8.50

The differences in the cohesive energies of the different backbone functional groups is especially clear when comparing PCL and PA6. Both of these polymers have practically the same structure except for the ester bonds found in PCL and the amide bonds found in PA6. The large difference in Tg (ΔTg = 119 °C) between these two polymers must be due to the equally large differences in cohesive energies of the ester and the amide bonds ($\Delta E_{Cohesive}$ = 5.60 kcal/mol). Similarly, when comparing the chemical structures of PE and PEG (Table 2.4), the presence of the ether bond in the PEG backbone can be recognized as the main difference. The interactions of the ether bonds in PEG (Table 2.5) likely lead to its higher Tg (ΔTg = 50 °C), even with the higher flexibility of the C–O bonds in PEG (which theoretically should reduce Tg).

Additionally to the presence of polar groups on the polymer backbone, the spacing between these polar groups also has an important effect on Tg. To contextualize the effects of the molecular structure of PLA on its Tg, a comparison with other aliphatic polyesters is shown in Figure 2.18.
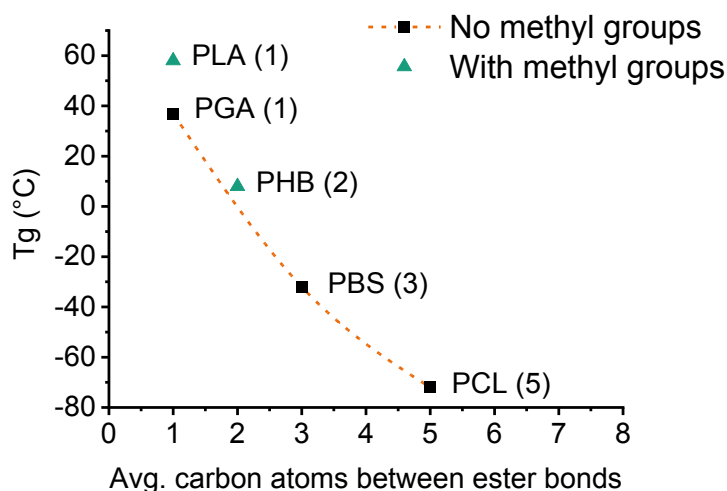
Figure 2.18: Tg of various aliphatic polyesters with different average carbon atoms between ester bonds. Tg values of polyglycolide (PGA), polycaprolactone (PCL), and polyhydroxybutyrate (PHB) taken from [85]. Tg values of polylactide (PLA) and polybutylene succinate (PBS) taken from [11]

The Tg of aliphatic polyesters decreases as the average amount of carbon atoms between the ester bonds is increased as shown in Figure 2.18. PCL has a backbone with a relatively high flexibility and rotation due to the five carbon atoms between each of its ester bonds, resulting in a relatively low Tg of -72 °C. When the average amount of carbon atoms between ester bonds is reduced to three as in the case of polybutylene succinate (PBS), an increase of the Tg to a value of around -32 °C can be observed. Further reduction to the number of carbon atoms between ester bonds to one, results in a Tg of 37 °C for poly(glycolic acid) (PGA). Added to the increased backbone stiffness, the concentration of ester bonds in PGA is much higher than in PCL so that the molecular interactions are significantly higher in PGA.

PLA has a very similar structure to PGA with the exception of a methyl side-group on the backbone carbon atom between the ester bonds in the polymer chain. The increase of the Tg from 37 °C for PGA to 58 °C for PLA is likely due to the reduced flexibility and rotation caused by the presence of the methyl group (similarly to the case of PE and PP). Similar observations have been made by [92] in polyamides containing such short chain side-groups.

Although Tg data for an aliphatic polyester with 2 carbon atoms between ester bonds and without methyl groups is not available, Figure 2.18 shows that the Tg of PHB is slightly higher to the expected Tg when performing a polynomial fitting of the Tg values of PGA, PBS, and PCL. Although the comparison is not ideal, the same tendency is found as in the case of the addition of a methyl group to the polyesters with one carbon atom between ester bonds (PGA, PLA). It is expected that the effect would be reduced in the case of PHB because the methyl group is only present in one out of two carbon atoms between the ester bonds.

The shown examples demonstrate some of the general tendencies of the effects that certain features in the molecular structure of a polymer can have on the Tg of a polymer. As revealed in the case of PEG and PE, different effects may work simultaneously both synergistically or competitively to different degrees. For this reason, a prediction of the net results of the different molecular features on Tg is often difficult. The previously described molecular effects however, can be used as general guidelines when speculating on the effects of different chemical structures on the Tg of a given copolymer.

Plasticization to modify Tg

Plasticization refers to the modification of the properties of a material by blending it with a low molar mass component, another polymer of low Tg, and/or copolymerizing it with a comonomer that increases chain flexibility and/or reduces crystallinity [93]. When a copolymer is synthesized and the plasticizing agent (or comonomer) is covalently bonded to the polymer, the system is said to be "internally" plasticized [94]. When a plasticizer is simply blended into a polymer matrix, the system is said to be "externally" plasticized [94].

Several mathematical equations have been formulated that allow the prediction of the effect of a plasticizer on the Tg of the final material with different levels of accuracy [87; 95]. Due to its simplicity and acceptable accuracy, the most popularly used equation is the Fox equation [87].

$$\frac{1}{Tg} = \frac{w_1}{Tg_1} + \frac{w_2}{Tg_2}$$
<div align="right">Eq. 2.9</div>

In the Fox equation above, the weight fraction of each component (w_n) together with their corresponding Tg_n values (as absolute temperatures) must be input to obtain the Tg of the mixture of the two components. The Fox equation has a generally good agreement with experimental data in the case of both miscible blends and copolymers.

Molar mass and Tg

The effect of Mn on Tg has been found to be adequately described by Equation 2.10 proposed by Fox and Flory [96] with an empirical parameter "A" specific for each polymer and a value of the Tg at infinite molar mass $T_g(M \to \infty)$. Equation 2.10 treats the polymer chain ends as impurities that introduce free volume into the system causing a reduction of the Tg at higher Mn values. The free volume is increased because the distance between covalently bonded atoms is shorter than intermolecular nearest neighbor distances found at the chain ends [87].

$$Tg(Mn) = Tg(M \to \infty) - \frac{A}{Mn}$$

Eq. 2.10

Although Tg varies significantly with Mn, usually only a single Tg is reported for polymers of high molar mass as seen on Table 2.4. This is common because Tg reaches a plateau at higher Mn values as shown below for PS and PLLA (Figure 2.19). Tg seems to reach a plateau above Mn values of 60 kDa at Tg = 100 °C for PS and Tg = 56 °C for PLLA (Figure 2.19).
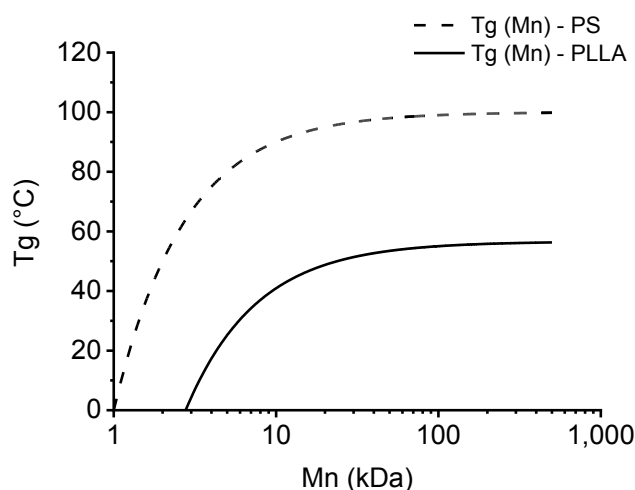
Figure 2.19: Dependence of Tg (linear) with respect to Mn ($\log_{10}$) calculated from Equation 2.8. Used equation parameters are: A_{PS} = 100 kg · K / mol, $T_g(M \to \infty)_{PS}$ = 373 K [87]; A_{PLLA} = 157 kg · K / mol, $T_g(M \to \infty)_{PLLA}$ = 329.6 K [48]

Although Tg can be varied quite significantly by changing the molar mass of the polymeric materials, significant reductions in Tg occur only when the molar mass is reduced to relatively low values. Figure 2.19 shows this "threshold" Mn value to be around 4 kDa for PS [87] and around 10 kDa for PLA [48]. At these low molar mass values however, the required mechanical properties for many applications as well as the rheological properties required for adequate processing are usually insufficient. For these reasons, modifying the Tg by changing the Mn of the material is not common practice.

Crystallization and melting

Crystallization is considered a thermodynamic first order phase transition from a liquid to an ordered crystalline phase. In low molar mass substances, crystallization occurs at such high rates that freezing and melting occur practically at a single temperature [87]. Because of this, achieving the glassy state in a low molar mass substance requires very high cooling rates to be able to bypass crystallization.

In polymers, the transition from liquid to crystal is overshadowed by kinetic factors [87], causing the crystallization temperature (Tc) to be different than the melting temperature (Tm) of crystallizable polymers. The ability of polymers to form crystalline structures depends on their chemical structure and those polymers that *can* form crystalline structures always have a fraction of amorphous, disordered molecules in the material. Due to the existence of this non-equilibrium mixture of amorphous and crystalline regions, such polymers are more adequately called semicrystalline polymers. Crystallinity in polymers normally conveys enhanced mechanical strength, greater resistance to degradation and better barrier properties [87] in comparison to the same materials in their amorphous states.

Effects of crystallization on the mechanical properties

Crystallinity in polymers normally causes the elastic modulus of polymers to increase with a corresponding reduction in the elongation at break when compared to their amorphous counterparts. Additionally, higher degrees of crystallinity can be used as a way to provide a material with mechanical stability at temperatures well above the Tg (as in the case of LDPE). As shown before in Table 2.3, amorphous materials show a strong reduction in their elastic modulus when the material is deformed at a temperature above Tg. A material with a high enough degree of crystallinity however, can keep a relatively high elastic modulus at temperatures well above the Tg because the cohesive forces in the crystalline regions of the material can only be destroyed by increasing the temperature above the melting temperature [97].

A classic example of the importance of crystallinity for low Tg materials is commercial isotactic PP (iPP) with a Tg of around -10 °C and a Tm of around 188 °C (Table 2.4). iPP can be used in injection molded articles with service temperatures of up to around 140 °C while maintaining an acceptable mechanical strength due to the high degree of crystallinity that can be achieved in relatively short times [98]. PLLA's slow crystallization kinetics, make it commercially unattractive for applications were mechanical stability at higher temperatures are necessary [98]. Although the Tm of PLLA's crystallites can reach temperatures of around 170 °C, relatively long annealing times at temperatures close to 100 °C are necessary to achieve a high enough degree of crystallinity to provide mechanical stability at higher temperatures [98; 99].

Rheological properties and crystallization

In the case of semicrystalline polymers, the temperature at which crystallization starts to occur represents a lower processing temperature boundary for the given polymer inside the extruder. Pogodina and Winter [100] proposed a "physical gelation" mechanism in which the crystalline structures restrict the movement of the polymer chains and increase the connectivity between the different crystalline regions in the material. This results in a drastic increase of relaxation times after a given physical gel-point is reached. Relatively low degrees of crystallization of 2-15% are enough to cause physical gelation [100; 101]. Physical gelation occurs at temperatures below the melting point of the polymer and it is controlled by the crystallization kinetics. Due to the residence time distribution of the polymer in the extruder, processing materials at temperatures below the Tm can put the extrusion equipment at risk if physical gelation occurs. For this reason, it is common practice to process semicrystalline materials at temperatures significantly above Tm.

Chemical structure and crystal melting temperature

Molecular flexibility and molecular interactions play an important role on crystallization and the melting temperature of the produced crystals. This is better illustrated by analyzing the changes of thermodynamic values during melting (Equation 2.11). At the melting temperature (Tm), the Gibbs free energy change of the melting process (ΔG_M) is zero (Equation 2.12) [102]. Tm can then be related to the enthalpy change (ΔH_M) and entropy change (ΔS_M) during melting as shown on Equation 2.13.

$$\Delta G_M = \Delta H_M - Tm\Delta S_M \qquad\qquad \text{Eq. 2.11}$$

$$0 = \Delta H_M - Tm\Delta S_M \qquad\qquad \text{Eq. 2.12}$$

$$Tm = \frac{\Delta H_M}{\Delta S_M} \qquad\qquad \text{Eq. 2.13}$$

ΔH_M is related to the strength of the intermolecular interactions present in the polymer chains. If intermolecular interactions are strong, a high ΔH_M is required to break these physical interactions. ΔS_M is related to the polymer chain flexibility. Stiff chains are expected to experience a low reduction in entropy during melting (low ΔS_M) from the ordered crystalline state [102]. Keeping Equation 2.13 in mind, the effects of the chemical structure of common aliphatic polyesters on the crystallization can be analyzed using Figure 2.20 below.
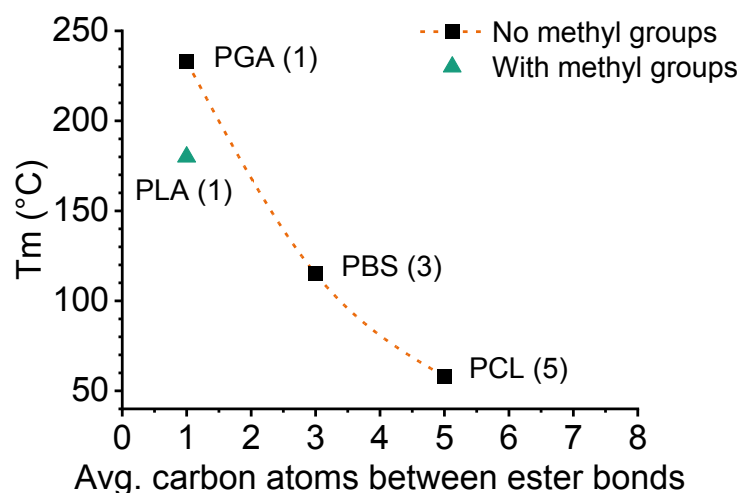
Figure 2.20: Tm of various aliphatic polyesters with varying average carbon units between the ester bonds. Tm values of PGA and PCL from [85]. Tm values of PLA and PBS from [11]

PCL is the polymer on Figure 2.20 with the lowest concentration of ester bonds on the polymer backbone (low ΔH_M value) and with the highest concentration of relatively flexible C–C bonds (high ΔS_M value), resulting in a relatively low Tm as suggested by Equation 2.13. As the concentration of ester bonds in the polymers is increased and the concentration of flexible C–C bonds is decreased, the Tm values of the shown aliphatic polyesters on Figure 2.20 increase.

Due to the methyl side-group present in PLA, a significantly lower Tm is observed when compared to the PGA polyester that does not contain a methyl side-group. The presence of the side-group likely causes steric hindrance to the ester-ester interactions between the polymer chains (reducing ΔH_M) in the unit cell crystal arrangement. At the same time, the methyl side-group should theoretically cause the rigidity of the polymer chain to increase (reducing ΔS_M). Although these effects are contradicting, it seems that the steric hindrance effect dominates over the increase of the chain stiffness caused by the methyl side-group, resulting a net Tm reduction.

In this context, the example of stereocomplex PLA (sc-PLA) becomes relevant. In sc-PLA, a tighter packing of the PLA chains is achieved by using PLLA and PDLA preferably at 1:1 ratio [103]. The Tm of the sc-PLA crystals is at around 230 °C, which is quite similar to the Tm of PGA. This supports the theory that the steric hindrance of the methyl side-group could be the reason behind the net reduction of the Tm of PLA even though the stiffness of the chain is increased.

Tacticity and crystal melting temperature

The introduction of non-crystallizable comonomer into the polymer backbone reduces Tm of the produced crystals and can even completely hinder crystallization. A non-crystallizable repeating unit can have a completely different chemical structure as the main polymer repeating unit or it can be an isomer of the backbone repeating unit with a side-group pointed in a different direction (i.e. different stereochemistry). These non-crystallizable repeating units reduce the regularity in the chain structure and lead to interruption of the crystalline arrangements. In the case of PLA, the degree of stereoregularity can be quite well controlled during the synthesis by using an appropriate catalyst and the desired ratio of L-lactide, D-lactide and/or meso-lactide stereoisomer monomer ratio. The melting temperature depression of the polymer can be calculated using Equation 2.14 developed by Flory [104; 34] if the content of non-crystallizable comonomer (1 - x_A) is known.

$$\frac{1}{Tm} - \frac{1}{T_m^*} = -\frac{R}{\Delta H_u} ln(x_A)$$

Eq. 2.14

In Equation 2.14, Tm is the modified melting point, T^*_m is the equilibrium melting point in the absence of non-crystallizable comonomer, R is the ideal gas constant, ΔH_u is the heat of melting per mole of repeat unit, and X_A is the mole fraction of the crystallizable monomer [34; 104]. This rather simple equation, is based on the consideration that non-crystallizable monomer acts as an "impurity" which, as in the case of low molar mass substances, causes a melting point depression. A plot of Equation 2.14 for PLA containing different D-lactide contents using values from [105] is shown in Figure 2.21.
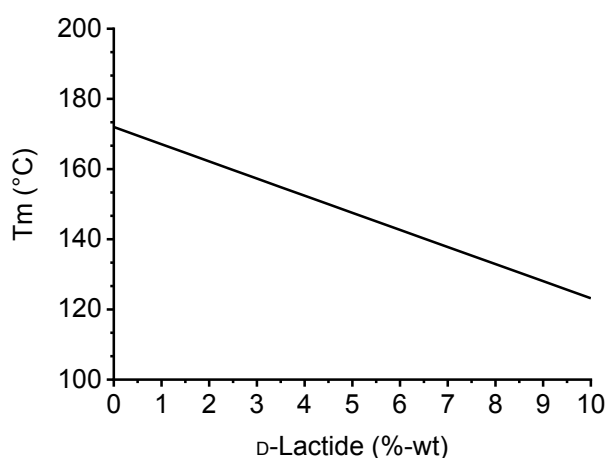
Figure 2.21: Plot of the dependency of Tm on the D-lactide content in PLA according to Equation 2.14. A ΔH_u value of 93 J/g (6,700 J/mol$_{RU}$) [105] and a T_m^* value of 172 °C were used.

The negative slope of the line in Figure 2.21 translates into a Tm reduction of around 10 °C for every 2 %-wt D-lactide content which is in reasonable agreement with what is presented experimentally in the literature by [105–107].

At the same time, the crystallization rate and the maximum attainable degree of crystallinity have been found to be reduced with an increase of non-crystallizable comonomer [106; 107]. Kolstad [106]

found that the crystallization half-time increases by 40 % for every 1 %-wt of meso-lactide content in the PLA polymerization mixture. At the same time, D-lactide contents of around 7 %-wt or above practically prevent any crystallization from occurring without significantly long annealing times [107].

Molar mass and crystal melting temperature

Analogously to changes of Tg with respect to the Mn (Equation 2.8), the increase in chain-end concentration brought about by a reduction of the Mn, can also be thought of as an "impurity" that interrupts the growth of crystal structures. Equation 2.15 was postulated by Flory [34] and shows a dependency of Tm with respect to the DP, its functionality (f), and the heat of melting per mole of repeating unit (ΔH_u). Equation 2.13 is displayed graphically on Figure 2.22 with parameters specific for PLLA found in the literature [105; 108].

$$\frac{1}{Tm} - \frac{1}{T_m^{\circ}} = \frac{R}{\Delta H_u}\left(\frac{f}{DP}\right)$$

Eq. 2.15
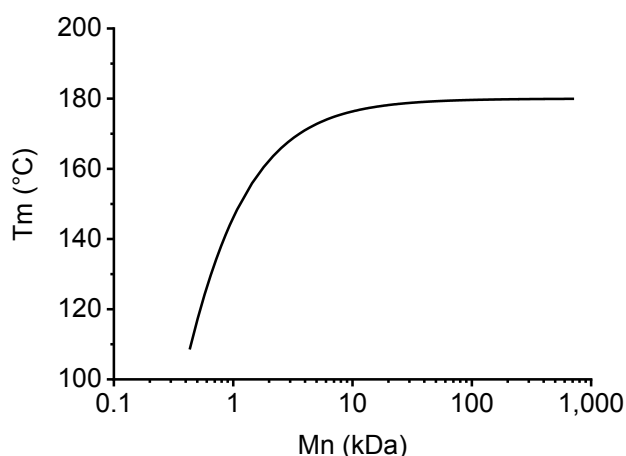
Figure 2.22: Plot of the dependency of Tm on the Mn of PLA according to Equation 2.13. An ΔH_u value of 93 J/g (6,700 J/mol$_{RU}$) [105] and a T_m^0 value of 180 °C [108] were used.

Similarly to the case of Tg, the value of Tm increases quite significantly as the Mn of the polymer increases at relatively low Mn values for the polymer. When the Mn reaches a threshold value, the dependency of Tm on Mn becomes relatively weak and the function plateaus to an almost constant Tm value. The shape of the curve is similar to what is reported in the literature for PLLA, however the reduction of the Tm happens at different Mn values depending on the experimental data [109]. The graph in Figure 2.22 should be considered only schematically to have an idea of the general dependence of Tm on Mn of PLA.

Crystallization kinetics

The effect of Mn and crystallization temperature on the crystallization kinetics can be analyzed with the theory of polymer crystallization kinetics formulated by Hoffman and Lauritzen [110]. It describes the rate of radial or lateral crystal growth with respect to the degree of undercooling below Tm [111]. Lateral crystal growth rate can be studied through polarized light optical microscopy (PLOM) in which the spherulite radius size can be tracked over time. In general, the Hoffman-Lauritzen theory postulates that the nucleus formation depends on a term considering the energy of activation for nucleus formation and a transport term that takes into consideration the diffusion of polymer chains to the nucleation site. This is mathematically described through Equation 2.16 [112] shown below.

$$G(T_C) = G_0 \cdot exp\left(-\frac{U^*}{R(Tc - T_\infty)}\right) \cdot exp\left(-\frac{K_g}{Tc \cdot \Delta T \cdot f_F}\right) \qquad \text{Eq. 2.16}$$

In Equation 2.16, G_0 is a pre-exponential empirical factor with units of length over time. On the first exponential term, U^* is the activation energy for transport of chain segments to the crystallization site, R is the ideal gas constant, Tc is the isothermal crystallization temperature, and T_∞ is the hypothetical temperature below Tg at which viscous flow ceases (for PLA T_∞ = Tg - 30 K [112]). On the second exponential term, K_g is the nucleation constant, ΔT is the degree of undercooling (T_m° – Tc), and f_F is a factor that accounts for the large change in heat of fusion, ΔH_f as the temperature is decreased below T_m° [f_F = 2·T_c/ (T_m° + Tc)] [112].

The first exponential term accounts for the viscous transport of stems to the nucleation sites. This term is highly dependent on the free volume and consequently on the Tg value contained within T_∞ (note the mathematical similarity of the term and the VTFH equation). As the isothermal crystallization temperature (Tc) is reduced (i.e. Tc approaches T_∞), the molecular movement in the material is reduced and the value of the first exponential becomes smaller to account for this.

The second exponential term accounts for the energy barrier that must be overcome to allow nuclei formation. As isothermal crystallization temperature (Tc) is reduced (i.e. degree of undercooling ΔT is increased), the thermodynamic driving force for crystallization to occur is increased and nuclei are easier to form [87]. The value of the second exponential term increases at lower Tc values.

Because the transport term finds its maximum at high Tc values (near Tm) and the nucleation energy barrier term finds its maximum at low Tc values (near Tg), the maximum overall radial crystal growth rate is found between Tg and Tm where both terms contribute to the crystal growth rate. Vasanthakumari and Pennings [112] measured the crystal radial growth rate at different isothermal crystallization temperatures of PLA with different viscosity average molar masses (Mv). The dependency of crystal growth rate with respect to the isothermal crystallization temperature expressed by Equation 2.16 is graphed below on Figure 2.23 using the fitted parameters for PLA of different Mv obtained by Vasanthakumari and Pennings [112].
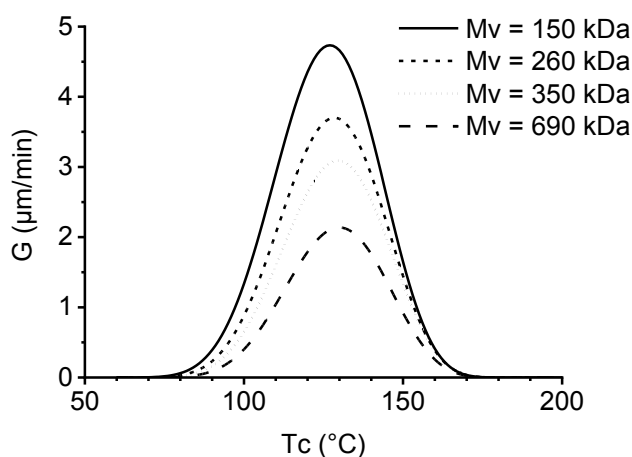
Figure 2.23: Spherulite radius growth rate, G at different crystallization temperatures, Tc calculated with Equation 2.16 using the empirical values obtained by Vasanthakumari et al. [112] for PLA of various molar masses

As seen on Figure 2.23, the temperature (Tc) at which the crystal growth rate is the highest is not significantly influenced by the molar mass of the PLA polymer and remains practically fixed at a temperature of around 130 °C for pure PLLA. The crystal growth rate can be seen to significantly decrease as the molar mass of the polymer is increased because of more restricted chain mobility [109]. It is important to mention that the dependency of crystal growth rate on molar mass has been found to be reduced above a threshold molar mass [87].

Rheological properties

Due to the wide range of material properties that can be accessed with synthetic polymers, they are industrially processed into many different shapes (bottles, films, tubes, filaments). Polymer manufacturing companies normally offer a vast portfolio of chemically identical products that have been engineered and optimized for specific processing methods. As an example, NatureWorks offers PLA grades optimized for extrusion, thermoforming, injection molding, fiber/nonwovens, films and sheets, injection stretch blow molding, foams and binders, and adhesive applications [113]. All of these products have the most appropriate mechanical properties for the intended applications. Equally as important however, these materials have the most appropriate rheological properties for the processing operations that are expected for the intended applications.

As an example, one can compare the melt flow index (MFI) (measured at 210 °C under a 2.16 kg load) of 22 g/10min of the Ingeo® 3001D grade designed for injection molding applications and the MFI (210 °C - 2.16 kg) of 7 g/10 min of the Ingeo® 4032D grade designed for general purpose film applications [113]. Both products have a Tg of 55 °C – 60 °C and a Tm of 155 °C – 170 °C suggesting that the stereochemical purity of both PLA materials is similar. The difference of the MFI values

however, reveals a big difference in the flow properties of both materials. The higher MFI values of the Ingeo® 3001D grade should not only help improve mold filling and reduce the cycle times of the injection molding operations, but also make more complex moldings possible [114]. Moreover, the Ingeo® 4032D grade has a significantly lower MFI, which one could expect translates into more stable operation in blown film extrusion lines.

Although practical, the MFI value only gives a narrow picture of the rheological profile of a polymer melt. Non-Newtonian shear thinning behavior typical in viscoelastic polymer melts, can lead to big differences in flow behavior under different shear rates as further explained in the following sections. Among other techniques, oscillatory rheometry can be used to characterize the rheological properties of polymer melts and even gain some further knowledge of its molecular structure and topology. This technique is further discussed in the coming sections together with the relationships of molecular structure and rheological properties relevant to the current work.

Oscillatory rheology

A step strain experiment can be performed on a polymer viscoelastic melt by using a drag flow rheometer. Although several types of such drag-flow rheometers exist, rotary cone and plate and rotating parallel disks rheometers are preferred for highly viscous polymer melts. A typical parallel disks geometry is shown below on Figure 2.24.
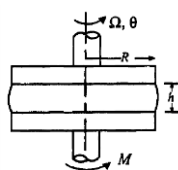
Figure 2.24: Schematic description of a parallel plate rheometer. Taken from [115]

On this type of experiment, a strain (γ) can be imposed on the polymer melt by rotating the top disk with a given angular velocity (Ω) to a given angle (θ) while keeping the bottom disk in place. The value of the torque (M) measured at the bottom plate can be used to calculate the stress (σ) response of the polymer melt.

Oscillatory rheometry is a more common experimental approach for characterizing the viscoelastic response of polymer melts than the single step strain experiment. Although a complete stress relaxation curve can be obtained from a step strain test, the precision at longer relaxation times is limited due to physical limits of the instrument [116]. Oscillatory rheometry does not only allow the measured signals to be in a more convenient and measurable range, but also allows the relaxation phenomena to be analyzed at different frequencies [87; 116].

In oscillatory rheometry, a time varying, oscillating strain γ(t) (Equation 2.17) with a defined frequency (ω) is applied to a viscoelastic polymer melt. A time-varying oscillating stress response σ(t) (Equation

2.18) with the same frequency (ω) but shifted by a phase angle (δ) is measured by the instrument. An example of how the input and output signals could look in such an experiment is shown on Figure 2.25.

$$\gamma(t) = \gamma_0 sin(\omega t) \qquad \text{Eq. 2.17}$$

$$\sigma(t) = \sigma_0 sin(\omega t + \delta) \qquad \text{Eq. 2.18}$$
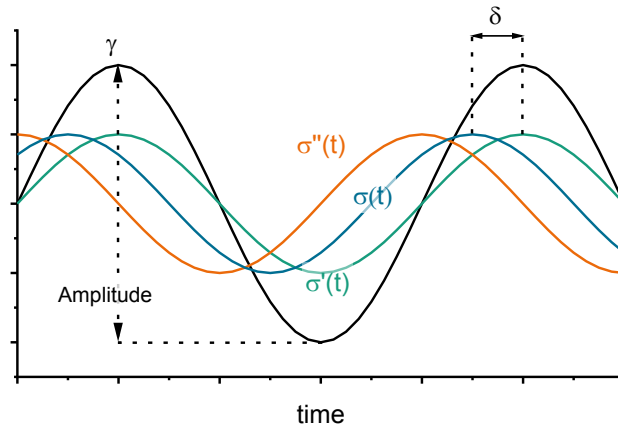
Figure 2.25: Viscous [$\sigma''(t)$], elastic [$\sigma'(t)$], and viscoelastic [$\sigma(t)$] stress response to an oscillating strain (γ) input in a typical oscillating rheological measurement.

In an oscillating strain experiment, the stress response of a completely viscous liquid to the oscillating strain input would be out-of-phase with the input strain by a phase angle of $\delta = 90°$ as shown by $\sigma''(t)$ in Figure 2.25. The stress response of an elastic solid would be exactly in phase with the input oscillating strain ($\delta = 0°$) as shown by $\sigma'(t)$ in Figure 2.25. The response of a viscoelastic polymer melt can be expected to be out-of-phase with the input strain oscillation by a phase angle between 0° and 90°.

By remembering the trigonometric identity $sin(\alpha \pm \beta) = sin(\alpha)cos(\beta) \pm sin(\beta)cos(\alpha)$, the shear stress response (Equation 2.18) can be expanded as shown below.

$$\sigma(t) = \sigma_0[sin(\omega t)\,cos(\delta) + sin(\delta)\,cos(\omega t)] \qquad \text{Eq. 2.19}$$

$$\sigma(t) = \sigma_0\,cos(\delta) \cdot sin(\omega t) + \sigma_0 sin(\delta) \cdot cos(\omega t) \qquad \text{Eq. 2.20}$$

Dividing Equation 2.20 by the amplitude (γ_0) of the imposed oscillating strain wave results in Equation 2.21 below.

$$\frac{\sigma(t)}{\gamma_0} = \frac{\sigma_0}{\gamma_0}cos(\delta) \cdot sin(\omega t) + \frac{\sigma_0}{\gamma_0}sin(\delta) \cdot cos(\omega t) \qquad \text{Eq. 2.21}$$

The storage modulus G' and loss modulus G'' can thus be defined as shown in Equation 2.22 and Equation 2.23.

$$G' = \frac{\sigma_0}{\gamma_0} cos(\delta)$$

Eq. 2.22

$$G'' = \frac{\sigma_0}{\gamma_0} sin(\delta)$$

Eq. 2.23

The newly defined G' and G'' terms can be substituted into Equation 2.21 to yield Equation 2.24.

$$\frac{\sigma(t)}{\gamma_0} = G' \cdot sin(\omega t) + G'' \cdot cos(\omega t)$$

Eq. 2.24

Remembering that cos(ωt) is the same wave as sin(ωt) just phase-shifted by a factor of 90°, a parallelism of Equation 2.24 and the waves of σ' and σ'' from Figure 2.25 can be found. The term containing G' can thus be interpreted as the component of σ(t) / γ_0 that is in-phase with the imposed oscillating strain having a behavior typical of an elastic solid. Analogously, the term containing G'' can be interpreted as the component of σ(t) / γ_0 that is 90° out-of-phase with the imposed oscillating strain as would be expected from a viscous liquid. The sum of both components results in the experimental shear stress of the viscoelastic polymer melt indirectly measured in the oscillating strain experiment.

By finding the derivative of the imposed oscillating strain γ(t) from Equation 2.17, we can find the strain rate γ̇(t) as shown in Equation 2.25.

$$\dot{\gamma} = \frac{d\gamma}{dt} = \gamma_0 \frac{d}{dt} sin(\omega t) = \gamma_0 \omega \cdot cos(\omega t)$$

Eq. 2.25

From Equation 2.17 and Equation 2.23, we can find that the applied oscillating strain (γ) is a function of sin(ωt) and that the applied oscillating strain rate (γ̇) is a function of cos(ωt). Hooke's law shows that the stress response of a solid is a function of the strain (γ) while Newton's law equates the shear stress as a function of strain rate (γ̇). The same dependencies can be found for the storage and loss moduli in Equation 2.22 and Equation 2.23.

Utilizing complex notation to describe the dynamic modulus in terms of the complex stress γ* = $\gamma_0 \cdot$ exp(iωt) and complex strain σ* = $\sigma_0 \cdot$ exp(i(ωt+δ)), yields Equation 2.26 where the term containing the imaginary number "i = (-1)$^{1/2}$" represents the out-of-phase imaginary component of G*.

$$G^*(w) = \frac{\sigma^*}{\gamma^*} = G' + iG''$$

Eq. 2.26

The complex modulus G*(ω) can be represented as a vector with magnitude |G*| and an angle δ with a component in the real plane (G') and a component in the imaginary plane (G''), yielding the relationships shown below in Equation 2.27 and Equation 2.28.

$$|G^*| = \sqrt{G'(\omega)^2 + G''(\omega)^2}$$
Eq. 2.27

$$tan(\delta) = \frac{G''}{G'}$$
Eq. 2.28

The tangent of the phase angle tan(δ) is commonly referred to as the loss tangent and describes the ratio of the viscous and elastic components of the polymer melt's viscoelastic response. When the material is behaving like a liquid, tan(δ) >> 1, and when the material behaves like a solid, tan(δ) << 1 [87]. Additionally, the complex viscosity can be defined as shown below in Equation 2.29.

$$\eta^* = \frac{\sigma^*}{\dot{\gamma}^*}$$
Eq. 2.29

Taking into account that $\dot{\gamma}^* = d\gamma / dt = i\omega\gamma^*$, the relation shown in Equation 2.30 can be found.

$$G^* = i\omega\eta^*$$
Eq. 2.30

The magnitude of the complex viscosity can thus be expressed as shown below in Equation 2.31.

$$|\eta^*| = \frac{\sqrt{G'(\omega)^2 + G''(\omega)^2}}{\omega}$$
Eq. 2.31

One of the most common experimental methodologies used in oscillatory rheometry is the so-called frequency sweep. In this experiment, an oscillating strain with a constant amplitude (γ_0) within the linear viscoelastic regime of the polymer is applied on the polymer melt sample over a wide range of frequencies (ω) as schematically shown in Figure 2.26. Typical ranges go from 1,000 rad/s down to values of around 0.01 rad/s.
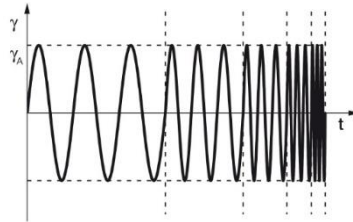
Figure 2.26: Typical oscillating strain profile of a frequency sweep experiment with a constant amplitude (γ_0) and five different frequencies. Taken from [117]

The previously defined material functions described by Equations 2.20, 2.27, 2.28 and 2.31 are calculated from the phase angle (δ) and shear stress amplitude (σ_0) measured at each frequency, and the obtained values are graphed as a function of frequency as shown below on Figure 2.27.
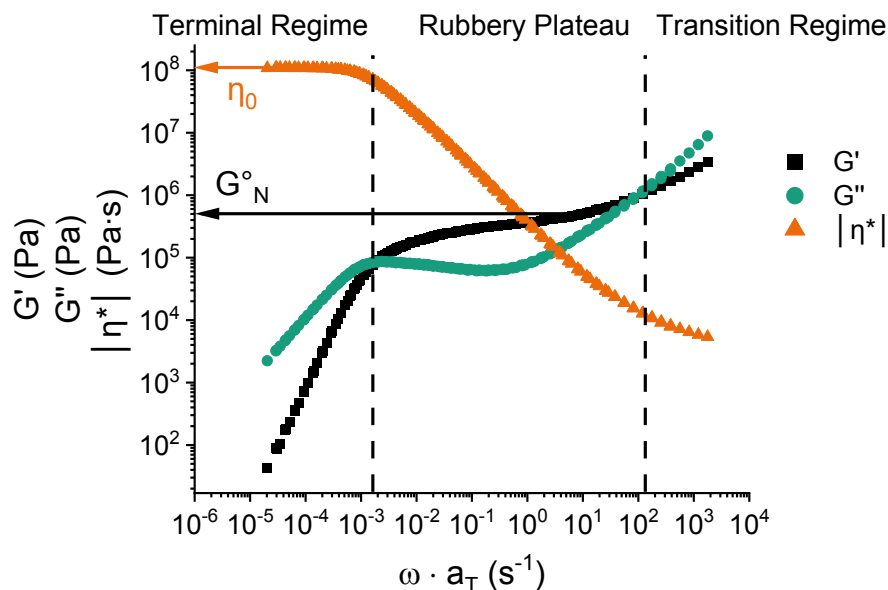
Figure 2.27: Oscillatory rheometry frequency sweep of poly-(cis 1,4 isoprene) with Mw = 94.9 kDa, PDI = 1.03. Data from Auhl et al. [118]

Three similar regimes to the ones described in Figure A1 appear in such a frequency sweep oscillatory rheometry measurement. At low frequencies, a higher value of the loss modulus G'' in comparison to the storage modulus G' describes a viscous relaxation regime analogous to the terminal regime observed at higher relaxation times on Figure A 1. This regime corresponds to the motion of large subsections or in some cases, of entire molecules in the polymer melt. As the frequencies approach zero, the viscosity reaches a plateau and becomes independent of frequency (as in the case of Newtonian fluids). The value of the viscosity at this plateau is termed the zero-shear viscosity, and is highly sensitive to the molar mass of the polymer (as further explained in in the following section).

At a frequency above 10^{-3} rad/s in Figure 2.27, the storage modulus G' becomes larger than the loss modulus G'' and reaches a plateau at a value of G°_N. The relaxation event in the terminal regime (at lower frequencies) is interrupted, and the polymer melt adopts a solid-like behavior as also observed in the stress relaxation data on Figure A 1. As the frequency is increased, the full polymer chains can no longer follow the rate of deformation and begin to become obstacles to each other forming so-called "molecular entanglements" [119]. Once the entanglements are formed according to the reptation theory, the polymer chain segments (with a molar mass M_e) between these entanglements are the only parts of the polymer that can follow the applied oscillatory deformation. For a range of frequencies (within the rubber plateau regime), the entanglements are present and the polymer melt behaves as an elastic solid [120]. The shearing forces introduced by the higher frequencies assists the segments of molar mass M_e that can follow the deformation to "reptate" or creep out of the entanglements. This reduces the entanglement density at high enough frequencies [115], resulting in the relaxation event observed in the transition regime in Figure 2.27.

The plateau modulus G°_N shown in Figure 2.27, has a similar value to the solid modulus of the same polymer if it were to be lightly cross-linked (as in a rubber band) [87]. The molecular weight between entanglements (M_e) can be calculated analogously to the modulus of a lightly cross-linked rubber (G

= ρRT/M$_x$. where ρ is the density and M$_x$ is the molecular weight between crosslinks), if the entanglements are considered to be "temporary crosslinks" as shown below on Equation 2.30 [87].

$$M_e = \frac{\rho RT}{G_N^\circ}$$

Eq. 2.32

Effects of the molar mass and chemical structure on the viscoelastic properties of polymer melts

The shear viscosity of polymers depends heavily on the molar mass of the polymer. It has been experimentally found that the zero shear viscosity (η_0) depends on the Mw of a monodisperse polymer as shown on the data plotted below on Figure 2.28.
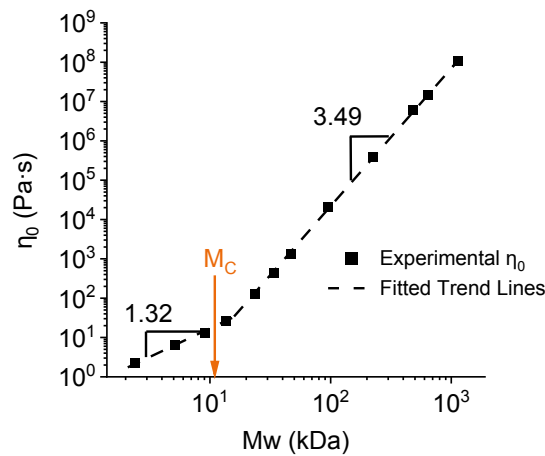
Figure 2.28: log-log plot of zero-shear viscosity (measured by oscillatory rheometry) vs Mw (measured by GPC) of poly-(cis 1,4 isoprene) samples with a wide range of Mw and a practically constant PDI of 1.04 (±0.05). Data taken from Auhl et al. [118; 121]. M$_c$ refers to the critical molar mass.

Figure 2.28 shows a changing dependency of the zero shear viscosity on the Mw of the polymer samples around a critical molar mass (M$_c$). The slope of 1.32 of the η_0 values of the samples with Mw values below M$_c$ on the log-log scale show to a dependence of $\eta_0 \sim Mw^{1.32}$. The samples with Mw > Mc in turn, show a dependency of $\eta_0 \sim Mw^{3.49}$. Both of these values are similar to what is widely accepted as the experimental dependence of Mw on η_0 [120; 122] shown on Equation 2.31.

$$\eta_0 \sim \begin{cases} Mw, & if\ Mw < M_C \\ K \cdot Mw^{3.4}, & if\ Mw > M_C \end{cases}$$

Eq. 2.33

M$_C$ has been found to be proportional to the molar mass between entanglements (M$_e$) of the polymer chains [122] by approximately M$_C \approx$ 2-3 · M$_e$ [87]. As previously stated, the value of M$_e$ is related to the plateau modulus (G$^\circ_N$) as shown on Equation 2.30. The oscillatory rheometry data [118; 121] of some of similar samples to the one shown on Figure 2.27 but with different Mw values are presented below on Figure 2.29, to help illustrate the relationship between η_0, Mw, and ultimately G$^\circ_N$.
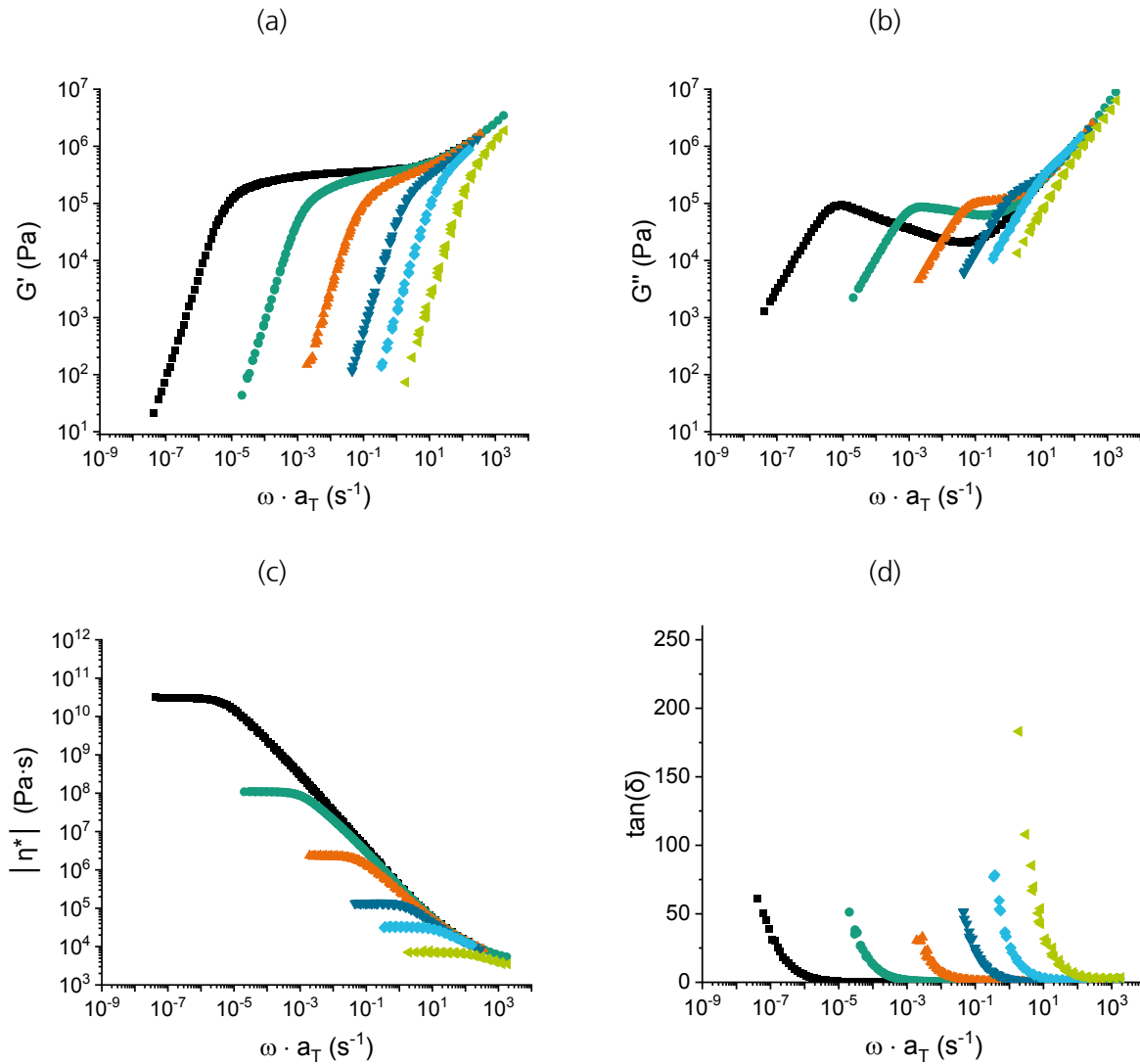
Figure 2.29: Comparison of the a) storage modulus (G'), b) loss modulus (G''), c) complex viscosity $|\eta_0|$, d) tan(δ) as a function of frequency (ω) for various polyisoprene melts with Mw values of (■) 483, (●) 95, (▲) 34, (▼) 14, (◆) 5, and (◄) 2.4 kDa, shifted to a temperature of 25 °C. Data taken from [118] and [121].

A clear $G°_N$ can be observed on Figure 2.29 (a) for all the samples with a Mw higher than the Mc (~ 10 kDa) above which a η_0 dependency of $Mw^{3.49}$ is observed on Figure 2.28. As the Mw of the polymers is reduced however, the range of frequencies over which the $G°_N$ can be recognized is also reduced until, for polymers of Mw < 10 kDa, $G°_N$ practically vanishes. These relationships suggests that when the polymer chains have an Mw > Mc, the chains are able to produce entanglements (as suggested by the appearance of a $G°_N$ in the G' flow curve). Furthermore, the presence of these entanglements seems to cause the dependency of the η_0 on Mw to increase from the close to linear Mw^1 dependency up to the exponential $Mw^{3.4}$ dependency.

The molar mass between entanglements (M_e) varies for each polymer depending on the chemical structure [87]. It ranges from around 1 to 50 kDa or from 50 to 200 monomer units [87]. The difference in the ability of chains to form entanglements has been correlated to the packing length

(p*) shown on Equation 2.34. The packing length (p*) refers to the ratio of volume occupied by a chain with respect to its mean square end-to-end distance $\langle h^2 \rangle$.

$$p^* = \frac{M}{\rho N_{av}} \frac{1}{\langle h^2 \rangle} = \frac{M}{\rho N_{av} 6 \cdot R_g^2}$$

Eq. 2.34

In Equation 2.34, N_{av} refers to the average number of bonds on the polymer backbone, M_{bond} = molar mass per backbone bond, ρ = density of the polymer melt, $\langle h^2 \rangle$ = the mean square end-to-tend distance, and R_g = the radius of gyration. Chains with bulky side-groups such as polystyrene have a higher packing length in comparison to thinner chains such as PE or PEG, as shown below on Table 2.6. A lower packing length translates into a lower M_e, which in turn means that the given polymer can more easily form entanglements [87]. Other factors such as bond stiffness, which plays a role in the R_g of the polymer, will also affect the polymer's ability to form entanglements [87].

Table 2.6: Recompilation of entanglement data for polymers relevant to the present work taken from the scientific literature measured at different temperatures (T_{meas}).

Polymer		T_{meas}	M_e	G°_N	ρ	p*
		[°C]	[kDa]	[MPa]	[g/mL]	[Å]
Polyethylene	PE [123]	140	0,84	2.6	0.784	1.69
Poly(ethylene oxide)	PEG [124]	140	1.97	1.8	1.034	1.99
Poly(propylene oxide)	PPG [123]	25	2.80	0.7	1.000	2.77
Poly(lactic acid)	PLA [124; 125]	140	3.96[1] 8.70[2]	1.0[1]	1.152[1]	2.51[1]
1,4 – Polyisoprene	1,4 – PI [123]	25	5.10	0.35	0.900	3.10
Polystyrene	PS [123]	140	13	0.20	1.040	3.95

G°_N has been found to correlate quite well with the packing length and the temperature as described by Equation 2.35 [87] for a wide range of polymers. This equation shows that the plateau modulus of a given polymer is only related to the measurement temperature and the chemical structure and is independent of the molar mass of the given polymer (as long as Mw > Mc and the G°_N actually occurs). As observed on Figure 2.29 (a) for the G' flow curve of the PI samples, all of the polymers (with equal chemical structure) showed the same plateau modulus value independent of their molar mass.

$$G^\circ_N = \frac{k_B T}{443 \cdot (p^*)^3}$$

Eq. 2.35

---

[1] PLA with a 20 %-wt D-Lactide [125].
[2] For PLA with 2 %-wt D-lactide content [124].

As defined by Equation 2.28, loss tangent or tan(δ) describes the ratio of G'' to G'. On Figure 2.29 (d), the values of the loss tangent are graphed for various frequencies for each of the polymers with varying Mw. The polymers with high Mw values show an exponential increase of tan(δ) to values higher than one at lower frequency values. This means that the higher Mw polymers exhibit a predominantly elastic or solid-like behavior over a longer range of frequencies than the low Mw polymers.

Effect of long chain branching (LCB) on rheological properties

Long chain branching (LCB) is said to occur when the molar mass of the branches (M_B) of the branched polymer structure is larger than the M_e defined by the chemical structure of the polymer. The viscosity of such LCB polymers are typically higher than the viscosity of linear polymers of equal chemical structure and molar mass [115]. This is due to the increase in the relaxation times caused by the branches which hinder motion along the backbone of the polymer [126]. The relaxation mode thus changes from a simple "reptation" mode typical in linear entangled polymers to a slow "arm retraction" mode for LCB polymers [127]. Depending on the synthesis method, several type of LCB topologies such as random branched, star, H-molecule, combs and dendrimers can be obtained [122; 128]. The random branched topology commonly found in LDPE has found commercial application in processes with a highly elongational character such as film blowing where LCB increases the extension thickening behavior [126]. An example of the elongational viscosity and shear viscosity at various constant elongational strain rates (Hencky strains) and shear strain rates for a LCB polymer are shown below on Figure 2.30.
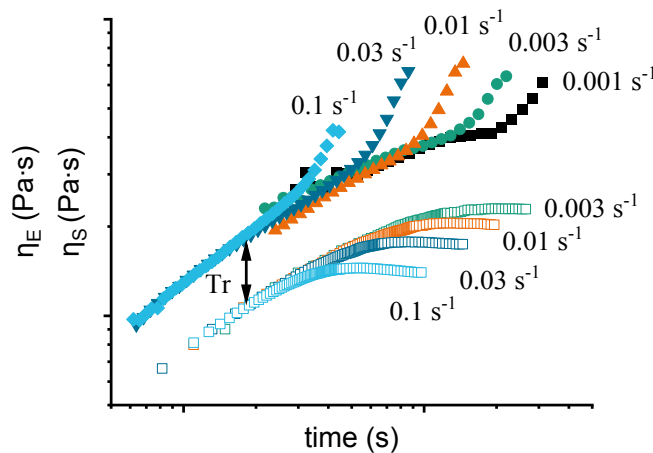
Figure 2.30: Example of uniaxial elongational (solid symbols) and shear (open symbols) viscosity measurements for a typical LCB polymer melt at different Hencky strains and shear strain rates. Tr refers to the Trouton ratio which is defined as Tr = $\eta_E/3\cdot\eta_S$. Data taken from [121].

At low strains (i.e. in the linear viscoelastic regime) shown in Figure 2.30, the elongational viscosity and the shear viscosity differ by the Trouton ratio (Tr = η_E / 3$\cdot\eta_S$) [115; 129]. At higher strains, the shear viscosity drops below the Trouton ratio and the elongational viscosity increases above it. This

increase of the elongational viscosity above the Trouton ratio at strains outside of the linear viscoelastic regime are not typically observed for linear polymers [115]. As suggested by the Trouton ratio, a linear polymer with a high shear viscosity should have an accordingly high elongational viscosity (at least 3 times as high as the shear viscosity) which means a linear material can also exhibit a high melt strength. LCB polymer melts which exhibit extension-thickening behavior however, can have a high melt strength with a lower shear viscosity, which is advantageous to reduce extruder power consumption in processing operations.

Considering the difficulties related with extensional measurements such as sagging of the polymer melt, the decrease of the sample thickness during elongation [122], or the difficulties clamping or gripping the polymer melt (without inducing shearing effects), can make a systematic comparison of materials through reliable extensional rheology experimental data difficult [130]. Some correlations between oscillatory rheometry data and the polymer chain topology have been made in the scientific literature. Some examples of these methods are presented in the following sections.

Phase angle (δ) vs complex modulus |G| plots*

Trinkle et al. [128; 131] systematically studied oscillatory rheological data of polymers with different molar masses, PDI, and topologies using phase angle (δ) vs complex modulus plots |G*| which are sometimes referred to as the van Gurp – Palmen plot (vGP-plot). These plots can be constructed by graphing the phase angle (δ) on a linear y-axis and the complex modulus |G*| on the x-axis in the logarithmic scale. Figure 2.31 shows the effects of varying either the Mw, the PDI, or the star topology on the δ vs |G*| plots. A reduction of δ to lower values as the Mw is increased from 55 kDa to 644 kDa is observed in Figure 2.31 (a). A similar shift is observed in Figure 2.31 (b) as the PDI of the polymers is increased from 1.04 up to 9.7. Figure 2.31 (c) shows the effects of the symmetric star topology on the δ vs |G*| plot as the arm molar mass (M_{arm}) was increased. At low M_{arm} values, almost no deviation from the δ vs |G*| plot behavior of the linear polymer can be recognized. As the M_{arm} is increased, a bump at higher |G*| values is observed with a slower ascent to δ values close to 90 ° due to a shift in balance between two different relaxation processes [128].

(a)

(b)

(c)
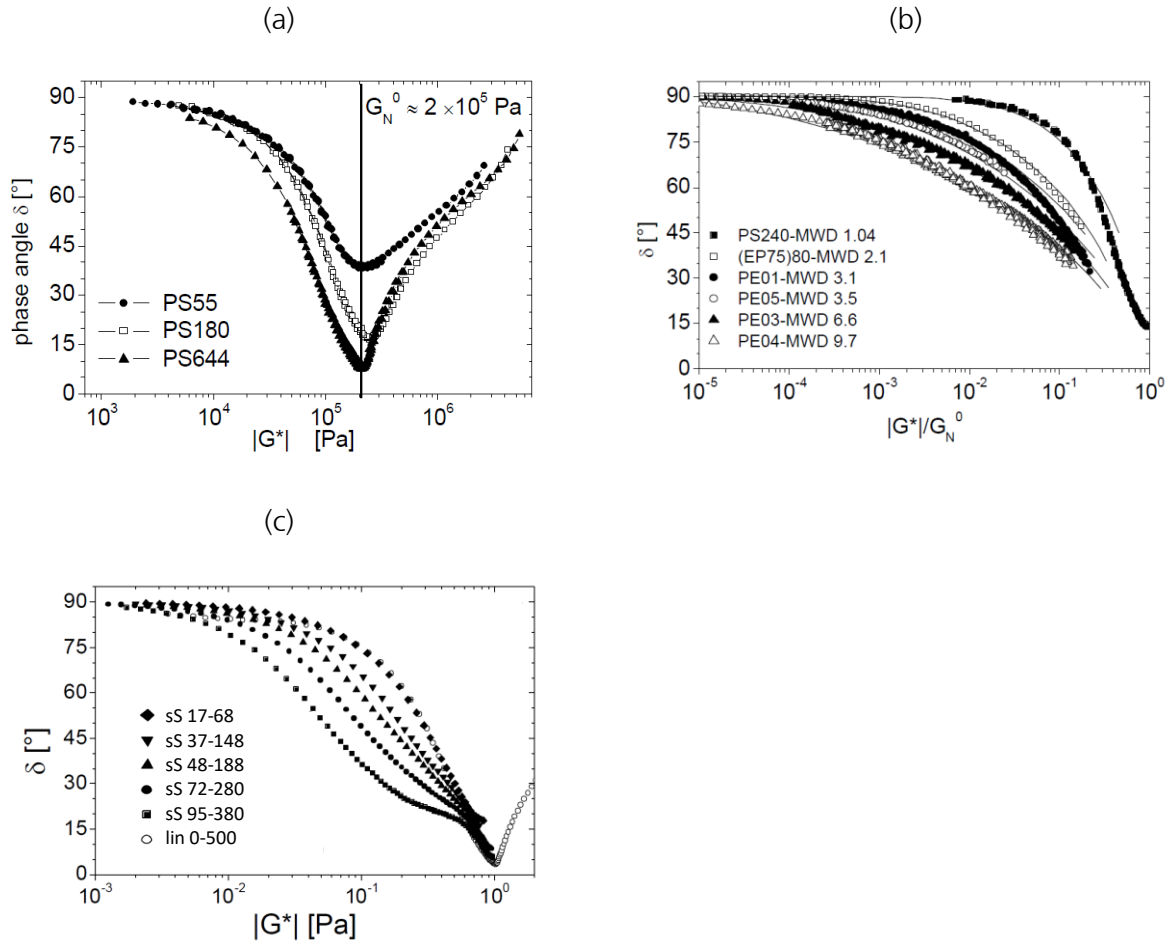
Figure 2.31: δ vs |G*| plots for (a) three linear polystyrene samples of similar PDI but different Mn. The suffix after "PS" on the legend gives the sample Mw in kDa. Taken from [131], (b) linear polymers with the same Mw of 250 kDa but with varying PDI value (given after the letters "MWD" for each sample). Taken from [131], and (c) of symmetric 4-arm star poly(isoprene) polymers (sS) with different total molar masses (Mw). As an example, sS 17-68 in the legend refers to a symmetric star with a Mw_{arm} of 17 kDa and a Mw_{total} of 68 kDa. Graph modified from [128].

Loss tangent [tan(δ)] and melt strength

As previously mentioned, the tan(δ) can be measured relatively easily through oscillatory rheology experiments and is defined as the ratio between the G'' and G'. Keeping this in mind, values of tan(δ) < 1 suggest that the behavior is predominantly elastic (G' is higher than G'') at the given frequency while tan(δ) > 1 suggest the opposite. As shown in Figure 2.29 (d), linear polymer melts have an exponential growth of the tan(δ) value at lower frequencies. The observed increase of the tan(δ) at lower frequencies is shifted to lower frequencies as the molar mass of the linear polymer melt is increased. Other works [116; 127; 132; 133] have shown that the tan(δ) value also responds to the chain topology. The works by Kruse [116] and Xu et al. [127] show that as the degree of branching was increased in PET and PLA polymer melts, the expected extensional thickening effect was observed

in elongational viscosity measurements and a simultaneous reduction of the tan(δ) values at low frequencies (measured by oscillatory rheometry) were observed. Other works in the literature have also observed a reduction in the tan(δ) values at low frequencies measured by oscillatory rheometry as the branching agent was increased [132; 133]. Regardless of whether a decrease of the tan(δ) values at lower frequencies is caused by an increased Mn value or by LCB, such data can give a useful insight into the melt strength of polymer melts.

Star topology in PLA

Although as mentioned in Section 2.3.6, several options exist for introducing branching into PLA, perhaps the simplest way is by using multifunctional initiators in the ROP of lactide. Given the chain-growth polymerization mechanism occurring in ROP, such multifunctional initiators lead to star topologies in the synthesized PLA polymers [125; 134; 135]. PLA polymers with star topologies have higher viscosities than PLA polymers of equal total Mw but with linear topologies [125; 134] as expected for LCB polymers. Dorgan et al. [125] also found a dependency of $\eta_0 \sim Mw^{4.6}$ for the star PLA polymers which contrasts with the expected $\eta_0 \sim Mw^{3.4}$ relationship for linear polymers. Such an increase of the dependency of η_0 on Mw is expected for LCB polymers [122]. Additionally, Kim et al. [134] found an increased temperature dependency of the shear viscosity for star PLA polymer melts when compared to linear polymer melts of the same Mw.

Mechanical properties

As previously explained, the measurement temperature (with respect to Tg) and the thermal history (crystallinity) have important effects on the mechanical properties of polymers. Keeping these external factors aside however, the mechanical properties are known to depend on the molar mass of the polymer. The molar mass dependency of the mechanical properties is strong at low molar mass values and plateaus at higher molar mass values (similarly to the dependency of Tg on Mn) as described by Flory [136] through Equation 2.36.

$$MP = a_0 + \frac{a_1}{Mn}$$
Eq. 2.36

In Equation 2.36, MP refers to a given material property (elastic modulus, elongation at break, tensile strength) [136; 137] while a_0 and a_1 are empirical constants. The constant a_1 usually takes negative values for tensile properties [137]. Molecular entanglements are believed to play an important role on the observed plateau of the mechanical properties at higher molar mass. When the molar mass is close to M_e of the material, the polymer chains can slip out of the bulk material at the craze interface during tensile fracture. On the contrary, polymers with a much higher molar mass than M_e, generate a higher amount of entanglements which are believed to anchor polymer chains to the bulk material during fracture [87].

2.2.2 Blending and copolymerization

Theoretical aspects

The phase equilibrium of polymer-polymer system is controlled largely by the degree of polymerization, the blend composition, and the types of monomer used. These effects can be quite well conceptualized through thermodynamic theories of polymer solutions by Flory [138] and Huggins [139]. The phase state is governed by the balance between enthalpic (ΔH_{Mix}) and entropic (ΔS_{Mix}) contributions to the systems' Gibbs free energy of mixing [140] as shown below.

$$\Delta G_{Mix} = \Delta H_{Mix} - T\Delta S_{Mix}$$

Eq. 2.37

The statistical models by Flory [138] and Huggins [139] for the combinational entropy of mixing (ΔS_{Mix}) and the enthalpy of mixing (ΔH_{Mix}) are defined as shown below,

$$-\Delta S_{Mix} = k_B T \left[\frac{\phi_1}{N_1} ln(\phi_1) + \frac{\phi_2}{N_2} ln(\phi_2) \right]$$

Eq. 2.38

$$\Delta H_{Mix} = \phi_1 \phi_2 \chi$$

Eq. 2.39

where k_B is the Boltzmann constant, the subscripts "1" and "2" refer to the components in the binary polymer blend, ϕ refers to the volume fraction of the given component in the polymer mixture, and N refers to the number of segments per polymer molecule. The term "χ" is known as the Flory-Huggins segment-segment interaction parameter and has a reciprocal dependence on temperature ($\chi \sim 1/T$). The term χ establishes the magnitude and sign of the energy of mixing and can be roughly estimated using Equation 2.40 below [140].

$$\chi = \frac{1}{k_B T} \left[\epsilon_{12} + \frac{1}{2}(\epsilon_{11} + \epsilon_{22}) \right]$$

Eq. 2.40

The terms ϵ_{ij} refer to the contact energy between segments i and j. If 1-2 segment contacts have a lower contact energy than half of the sum of 1-1 and 2-2 segment contacts, a negative value of χ will be obtained. A negative χ value results from a favorable energy of mixing and can be encountered for certain types of interaction such as hydrogen bonding [140]. Hydrogen bonding requires a hydrogen atom covalently bonded to an electron-withdrawing atom and a structure that can donate electrons situated at about 180° from the bond containing the hydrogen atom [141]. Figure 2.32 shows two possible hydrogen bonding interaction schemes of known miscible polymer blends.
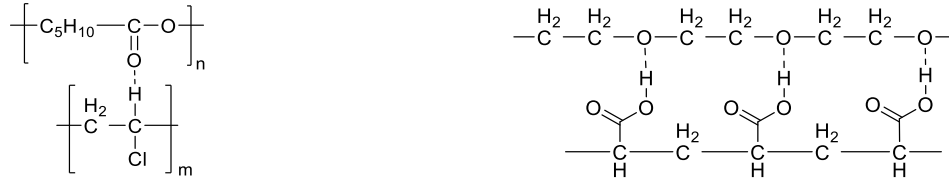
Figure 2.32: Proposed weak hydrogen bonds in miscible PCL/PVC[3] (left) and in a PAA[4]/PEG (right) blends. Modified from [141].

To calculate the Gibbs free energy per segment (ΔG_{Mix}) associated with mixing two random walk (Guassian) polymer chains on an incompressible ($\phi_1 + \phi_2 = 1$) lattice, Equation 2.38 and Equation 2.39 are introduced into Equation 2.37 to produce the relation shown below.

$$\frac{\Delta G_{Mix}}{k_B T} = \frac{\phi_1}{N_1} ln(\phi_1) + \frac{1 - \phi_1}{N_2} ln(1 - \phi_1) + \phi_1(1 - \phi_1)\chi$$

Eq. 2.41

Equation 2.41 shows the influence of the before mentioned factors that control the phase equilibrium behavior in polymer-polymer systems. The entropic contribution to the Gibbs free energy of mixing is inversely proportional to the degree of polymerization of the polymer chains in the system. Because longer chains can assume fewer configurations in an incompressible mixture lattice, ΔS_{Mix} decreases with increasing N. The effect of the composition of the blend is determined by the values of ϕ and the effect of the types of monomer used is determined by the value of χ. The phase behavior can be predicted with Equation 2.41 based on the standard criteria for equilibrium at constant temperature and pressure also applicable for low molar mass solutions [140]. For the symmetrical case where $N_1 = N_2$ and $N_1 + N_2 = N$, the equations for the binodal, spinodal, and the critical point are simplified to the ones shown below in Equation 2.42, Equation 2.43, and Equation 2.44 respectively.

$$\chi = \frac{1}{N(2\phi_1 - 1)} ln\left(\frac{\phi_1}{1 - \phi_1}\right)$$

Eq. 2.42

$$\chi = \frac{1}{2N\phi_1(1 - \phi_1)}$$

Eq. 2.43

$$\chi_c = \frac{2}{N} \ and \ \phi_c = \frac{1}{2}$$

Eq. 2.44

A plot of χ at equilibrium (binodal) and at the stability line (spinodal) with respect to the ϕ_1 composition, can be obtained using Equation 2.42 and Equation 2.43 for a given N. The equilibrium plot for a mixture of polymer 1 and 2 both having N = 1,400 (which accounts for an approximate Mn ~ 100 kDa for PLA) is shown in Figure 2.33.

---

[3] PVC = poly(vinyl chloride)
[4] PAA = Poly(acrylic acid)
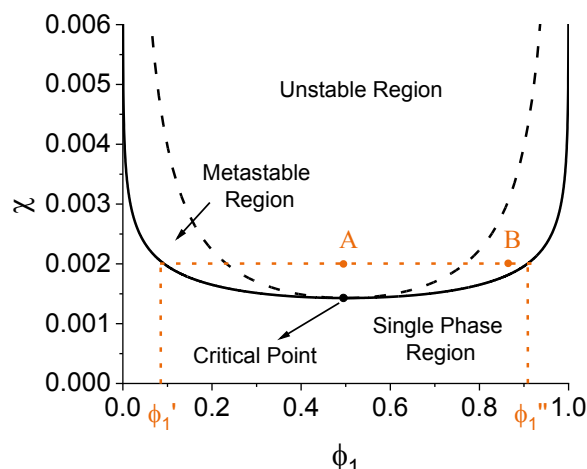
Figure 2.33: Theoretical phase diagram for a binary polymer blend with both components having N = 1,400. The spinodal (dashed line) and binodal (continuous line) are shown.

Several regions can be recognized in Figure 2.33. If the χ value of the polymer-polymer blend at the given composition is below the binodal line, the polymer mixture will exists as a stable single phase. If the value of χ for the given polymer pair is below $\chi_c = 2 / N$ the polymer mixture will be stable over the complete composition range. Point A on Figure 2.33 shows a point (ϕ, χ) in which the polymer blend is located in the unstable region of the equilibrium plot. In this case, the given blend will spontaneously phase separate into a phase poor in component 1 (ϕ_1') and a phase rich in component 1 (ϕ_1'') through the spinodal decomposition mechanism illustrated in Figure 2.34. Although spinodal decomposition in polymer melts is spontaneous, it is around N^2 slower than in low molar mass mixtures under comparable conditions [140]. Point B shows a blend that is located in the metastable region. In this case, the polymer blend is stable against small fluctuations but not globally stable against separation [87]. The blend in point B requires the free energy barrier to be overcome for phase separation to occur. This can happen through a nucleation mechanism in which a small droplet with a $\phi_1 > \phi_1''$ is formed. Further increase of droplet size occurs via droplet coalescence or Ostwald ripening [140] as shown in Figure 2.34.
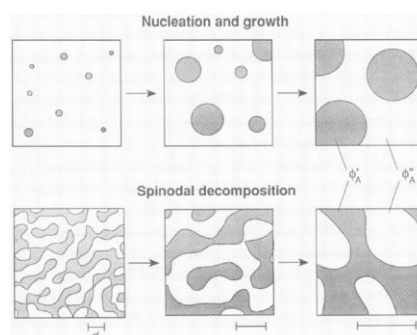
Figure 2.34: Time evolution of phase separation in binary homopolymer mixtures, taken from [140].

The equilibrium chart changes quite strongly depending on the molar masses of the components in the polymer blend as defined by Equation 2.40. Figure 2.35 (a) shows the effect of increasing the molar mass of both components simultaneously on the binodal and the spinodal curves. The blends

with lower molar mass components allow for miscibility of polymer pairs with higher values of the Flory-Huggins interaction parameter because the binodal is shifted to higher values of χ as the molar mass is reduced. The widths of the binodal and spinodal curves are also reduced when the molar mass of the components are reduced. This allows stable blends to be formed at higher ϕ_1 values even when the χ parameter is above χ_c.

Figure 2.35 (b) shows the changes in the spinodal line as the degree of polymerization of component 1 (N_1) is reduced. N values of 50, 253, and 430 are roughly equivalent to Mn of 1.3, 12, and 20 kDa, respectively for PEG. The critical point is skewed to higher values of ϕ_1 and the area of the unstable region is reduced as N_1 is reduced. Note that the scale of the y-axis in Figure 2.35 (b) is significantly increased [compared to Figure 2.35 (a)] to accommodate the changes in the values of N_1. As the value of N_1 approaches 1, the case of a solvent is reached in which very high solvent fractions can be introduced into the mixture.
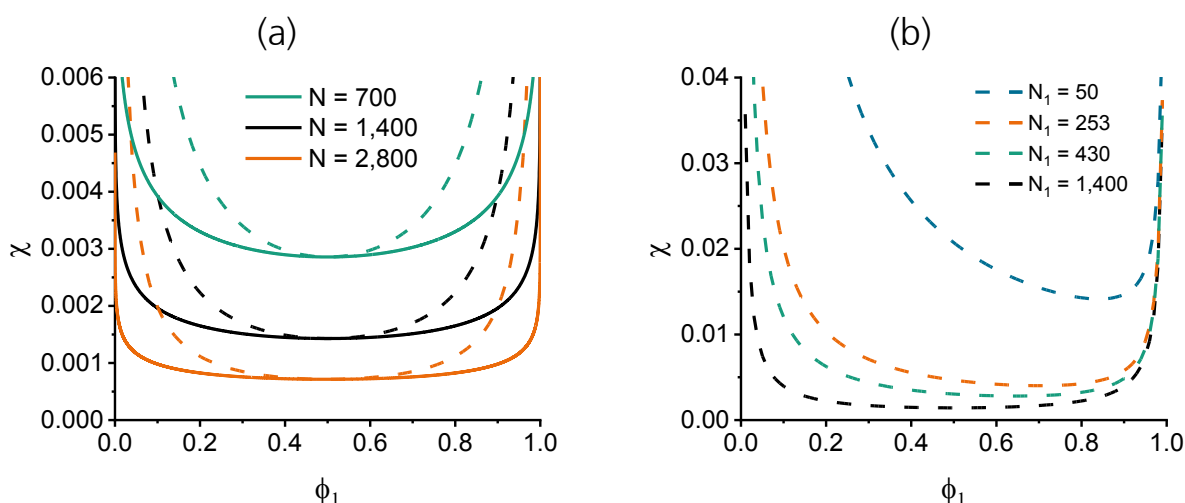
Figure 2.35: Effect of changing the number of segments "N" in the polymer molecules of both components in the blend simultaneously on the spinodal and binodal (a). Effect of keeping N_2 constant at 1,400 and reducing N_1 to lower values (b)

Theoretical aspects of microphase separation in block copolymers

Block copolymers consist of two or more chemically distinct homopolymer subunits or blocks that are covalently linked in the same polymer chain. As an example, an A-B-A triblock copolymer has two outer blocks with the monomeric unit "A" covalently bonded to a middle block with the monomeric unit "B".

The covalent bonds linking chemically distinct structures (having high χ values) found in block copolymers restrict the macroscopic separation of the different blocks. Instead, phase separation of block copolymers in the bulk leads to the formation of microscopic heterogeneities of molecular dimensions (diam. ~ 50 to 1,000 Å) [140] that go on to form well-defined physical networks [141].

These phase-separated physical networks give the material improved recovery properties that can be similar to the ones found in chemically crosslinked rubber.

Although many other aspects play a role in achieving elastomer-like properties, this type of micro phase separated block copolymers are generally known as thermoplastic elastomers. Additionally, the different chemistries of the blocks in the copolymers give them surfactant-like behavior which can be used for compatibilizing polymer blends or as surfactants in low molar mass dispersions [141]. Some of the more common commercially used block copolymers are listed in Table 2.7.

Table 2.7: Commercially relevant block copolymers [141]

Category	Types	Commercial materials
Thermoplastic Elastomers	• Styrene-diene A-B-A triblock copolymers • Ester-ether (A-B)$_n$ multiblock copolymers (TPE-E) • Polyurethane-ether (A-B)$_n$ multiblock copolymers (TPU) • Polyamide-ether (A-B)$_n$ multiblock copolymers	• Kraton (Shell), Solprene (Dynasol) • Hytrel (DuPont) • Desmopan (Covestro), Elastollan (BASF) • Pebax (Arkema)
Surfactants	• Polyethylene oxide – polypropylene oxide A-B / A-B-A di-/tri-block copolymers	• Pluronics (BASF)
Blend Compatibilizers	• Depend on the blend to stabilize	

The more widely used theories on the equilibrium behavior of block copolymers are those from Krause [142] and Meier [143] although others exist [141]. The theory of Meier [143] focuses on the factors influencing the types of microstructures that are created when phase separation occurs in block copolymers. Because in the present project the aim is to use block copolymers as internally plasticized polymers where phase separation is not desired, the theory of Meier will not be discussed in detail.

The theory of Krause [142] is able to adequately describe the conditions necessary for microphase separation in a block copolymer system of monomers A and B as a function of block copolymer composition, molecular mass, number of blocks per molecule, and the interaction parameter between the corresponding homopolymers. This theory predicts that the surface free energies necessary for microphase separation make it more difficult than would otherwise be expected for a homopolymer blend [142]. The effects of the different parameters are summarized in Table 2.8 and have been observed experimentally in PLA/PCL block copolymers by [144] and [145].

Table 2.8: Effect of the different block copolymer structures on the phase behavior.

	χ_c	Phase separation becomes
Higher number of blocks / constant copolymer molar mass & A to B ratio	increases	more difficult
Higher A-block content / constant number of blocks & copolymer molar mass	decreases	less difficult
Higher copolymer molar mass / constant A to B ratio & number of blocks	decreases	less difficult

2.3 PLA property modification concepts

There have been several efforts in the scientific literature to alter PLA's properties based on the previously described structure-property relationships (Section 2.2) in order to enable its use for flexible film applications. Lower elastic moduli and higher elongation at break values have been obtained by blending PLA with other biodegradable polymers, by introducing biodegradable plasticizers, and/or by copolymerizing lactide with other biodegradable components. Almost none of these studies have considered the effects of these modifications on the rheological properties of the materials. On the other hand, improvements of PLA's rheological properties and processability have been widely studied. Improved processability has been achieved mainly by introducing long chain branching into the PLA polymer structure. The mechanical properties however, have not been the main focus in these studies. A general summary of the state of the art of the modification of the mechanical and rheological properties of PLA is outlined below.

2.3.1 Blends with other biodegradable polymers

Many efforts have been made to reduce PLA's elastic modulus and increase its elongation at break to make it suitable for flexible film applications. PLA blends with more flexible biodegradable polyesters such as polybutylene adipate terephthalate (PBAT) [11], [146], polybutylene succinate (PBS) [147], [148], [149], [17] and polycaprolactone (PCL) [150], [151] have been documented in the scientific literature. However, the current low commercial availability of these polyesters [11] and the high contents of these polyesters necessary to achieve the required properties (at least 60% for flexible film applications [11], [17]) could make such compounds unattractive.

2.3.2 Blends with low molar mass plasticizers

Many different biodegradable low molar mass plasticizers such as glycerol, citrate ester, and oligomeric lactic acid (OLA) were tested in the study by Martin and Avérous [152] with varying success. Of the studied plasticizers, 10 %-wt and 20 %-wt OLA reduced the Tg of PLLA from 58 °C to 37 °C and 18 °C, respectively. The elongation at break of these plasticized blends was increased from 9 % (± 2) for pure PLLA to 32 % (± 4) and 200 % (± 24) for the 10 %-wt and 20 %-wt plasticized blends, respectively. Little information was given about the molar mass of the used OLA. Loomis [153] and Sinclair [154] also found that lactide and OLA can effectively improve the elongation at break when blended with PLA. Loomis recognized that excessive levels of lactide or OLA can cause reduced uniformity in the films due to the separation and deposition of lactide and/or OLA on the cooling roll surfaces of the cast film extrusion lines leading to uneven heat transfer [153].

Ljunberg and Wesslen [155] worked with triacetine [156], tributyl citrate (TbC) [155], and diethyl bishydroxymethyl malonate (DBM) [155] as low molar mass biocompatible plasticizers. When producing blends containing 15 %-wt of each of these plasticizers, they found reductions of the Tg of the blends from 58 °C to around 25 °C. Over longer periods of storage however, cold crystallization of the PLLA caused by the reduced Tg led to plasticizer migration and changes in the material properties. To get around this problem, Ljungberg and Wesslen [155] synthesized DBM oligomers with a Mn of 1.6 kDa equipped with an amide functionality (DBMATA) that could undergo hydrogen bonding with the PLLA. The plasticized PLLA with 15 %-wt DBMATA had a Tg of 39 °C and an elongation at break of around 200 % which was stable after 6 weeks of storage [155].

2.3.3 Blends with polyether plasticizers

Plasticization of PLA through the addition of commercially available polyethers such as polyethylene glycol (PEG) [18], [20], [21], [157], [158] polypropylene glycol (PPG) [22], and statistical copolymers of ethylene and propylene oxide [poly(ethylene glycol-co-propylene glycol)] (PEPG) [159], [23], [24], [160] has been studied extensively in the literature. Hu et al. [20] demonstrated the miscibility of up to 30 %-wt of PEG (Mn 8 kDa) in a PLA matrix with low stereoregularity (13%-wt D-lactide content). Elongation at break values of up to 500 % for a 30 %-wt PEG content and 200 % for a 10 %-wt PEG content were measured at an elongation rate of 11.5 mm/min (used for the tensile testing). The quenched blends (likely amorphous) with a PEG content above 20 %-wt showed spontaneous crystallization of PEG over longer storage times at ambient conditions. This translated into a reduction of elongation at break and an increase of the elastic modulus during storage. A later study by Hu et al. [19] showed a reduction of the miscibility of PEG with an increase in the stereoregularity of PLA.

Kulinski et al. used low molar mass (Mn 0.4 – 1 kDa), amorphous PPG as macromolecular plasticizers in a PLA matrix (6 %-wt D-lactide) in an attempt to avoid crystallization of the plasticizer during storage time in ambient conditions [22]. They were able to show miscibility of the 0.4 kDa PPG up to at least 12.5 %-wt contents with similar results on the mechanical properties as homologous PEG

blends. Phase separation was observed for the higher molar mass PPG (1 kDa) at the same 12.5 %-wt fraction.

Jia et al. prepared blends of up to 20 %-wt PEPG (Mn 12 kDa, Tm = -2 °C) content in highly stereoregular PLA (2 % D-lactide) and compared them to similar PEG/PLA blends [24]. They observed that PEPG and PEG had similar miscibilities and effects on the mechanical properties of the freshly produced tensile test samples. Although PEPG did not crystallize out of the PLA matrix at ambient conditions, a similar reduction of the elongation at break values was observed with both plasticizers. Further investigations showed that in the annealed blends with a high PEPG content, the PLA matrix was able to cold crystallize pushing the PEPG out of the crystalline regions and causing phase separation.

2.3.4 Block copolymers of polyethers and PLA

PLA-b-polyether-b-PLA triblock copolymer structures have been investigated mainly as biodegradable amphiphilic micelles, particles, and gels for biomedical applications [161], [162]. PLA-b-polyether-b-PLA block copolymers of relatively low Mn (20 -30 kDa) have been studied as compatibilizers to allow blending of plasticizers [161] or other polyesters [163] into PLA to improve its toughness. The molar mass of the PLA-b-polyether-b-PLA triblock copolymers used in these studies however, was limited by the relatively low molar mass polyether macroinitiators used for the ROP of lactide.

Two works [164; 165] were found in which high molar mass PLA-b-PEG-b-PLA triblock copolymers were synthesized. Baimark et al. [164] used PEG macroinitiators of 20 – 35 kDa to synthesize triblock copolymers and reported Mn values of around 120 kDa (measured by ^{1}H-NMR). It was mentioned in this study however, that the MFI values of the obtained block copolymers (190 °C, 2.16 kg) were too low to be measured which makes the reported Mn value of 120 kDa questionable. Elongation at break values below 25 % (ΔL/t = 55 mm/min) for the block copolymer containing 20 %-wt PEG block content were reported in this study. Yun et al. [165] used a PEG macroinitiator of 20 kDa to obtain PLA-b-PEG-b-PLA triblock copolymers with a reported Mn of 93 kDa (^{1}H-NMR) and an elongation at break of 381 % (ΔL/t = 55 mm/min). The rheological properties of the synthesized block copolymers however, were not mentioned in this study.

2.3.5 Random copolymers of lactide and ε-caprolactone

Random ring-opening copolymerization of ε-caprolactone (CL) and lactide has been studied extensively in the literature [166–172] due to the bio-degradable nature of PCL and its low Tg. The difference in the reactivities of CL and lactide causes longer sequences of homopolymerized monomer to be formed in the polymer chain giving the copolymers a semi-block or gradient structure. Variation of the polymerization temperatures yielded copolymers with different average sequence lengths of homopolymerized monomer, which had a big effect on the thermal and mechanical properties of the

copolymer [166]. A more statistical distribution of the CL comonomer can be promoted by increasing the ROP temperature (to increase CL reaction rate) or increasing the ROP time (to promote transesterification).

The effects of the gradient nature of the CL / lactide copolymers were observed by Grijpma and Pennings [166]. The elongation at break of a 50 / 50 CL / lactide copolymer changed from 880 % to 480 % by changing the synthesis temperature from 110 °C to 80 °C as a result of the changes in the distribution of the CL comonomer in the copolymers. Additionally, the gradient copolymer structure reduced the elongation at break and increased the elastic modulus over longer periods of storage time [168]. Spontaneous crystallization at room temperature of the PLA segments in these 50 / 50 CL / lactide copolymers even with relatively low average lactide continuous monomer sequence lengths (synthesized at 190 °C) [168] was observed. The use of antimony trioxide [173] or bismuth(III) *n*-hexanoate [174] catalysts for the copolymerization gave a more statistical comonomer distribution in the copolymers at a cost of significantly slower reaction kinetics.

2.3.6 Rheological modifications of PLA

PLA is known for having relatively poor shear and elongation properties in the melt [71]. The linear structure of PLA causes it to have a relatively low extensional viscosity, which leads to poor melt strength and necking or bubble instabilities during film processing [71; 72]. Ideally, materials for blown film applications should have a relatively low shear viscosity to reduce the amount of power necessary to extrude the polymers, while having a high elongational viscosity to avoid sagging of the melt when being stretched in the blown film extrusion process.

A way to increase the extensional viscosity of PLA is to increase its molecular mass. According to the Trouton ratio (Figure 2.30), the extensional viscosity is three times higher than the shear viscosity in the low strain linear viscoelastic regime [115]. If the extensional viscosity of a polymer melt is increased by increasing its molar mass, the shear viscosity will be simultaneously increased. If the molar mass (and thus the extensional viscosity) of PLA is increased to values where necking or bubble instabilities are avoided, the shear viscosity will be proportionally higher and will require high extruder motor power to be successfully processed [72]. Although the motor power requirement can be reduced by increasing the melt temperature (thus reducing η_S), the onset of degradation reactions at higher temperatures and the resulting loss of product quality must be kept in mind [72].

As discussed in Section 2.2.1, the extensional viscosity of a polymer can be increased through long chain branching (LCB) on the polymer backbone. Long chain branching in polymers induces strain hardening, which significantly increases the extensional viscosity of the melt when reaching the nonlinear viscoelastic regime at higher strain rates during extensional flow [115; 122]. This effect is present to a much lower extent or, in the case of PLA, absent in linear polymers [69–71; 127]. Gruber et al. [72] copolymerized multifunctional epoxidized vegetable oils with lactide to obtain branched PLA polymers with reduced necking and extruder power consumption compared to linear PLA polymers with similar Mn. Several other groups have obtained branched PLA through reactive extrusion of commercial PLA with relatively expensive commercial multi-epoxide oligomeric chain

extenders like Joncryl® (BASF®) or CESA® (Clariant®) [68–71]. Mallet et al. [71] observed an increase in the blown film processing window (wider range of BUR's and TUR's) of commercial Ingeo® 4043D PLA when blended with Joncryl®, PEG, and nucleating agents.

As mentioned in Section 2.2.1, PLA polymers with star topologies have been synthesized in the literature by Kim et al. [134; 135] and Dorgan et al. [124]. Compared to linear PLA polymers, star PLA polymers of equal molar mass have a higher shear viscosity and a higher temperature dependency of shear viscosity.

Latent AB_2 comonomers like glycidol [175] or mevalonolactone [176] and others [177] have been reported in the scientific literature, however most of these comonomers are not commercially available at industrial scale and their branching capabilities have not been proven to come with the desired rheological advantages for film applications.

2.4 Blown film extrusion processing

Blown film extrusion is one of the most significant processing methods for flexible plastic films for commodity, single-use applications with relatively low profit margins such as flexible packaging, general-purpose bags, and waste disposal bags. Consequently, very sophisticated processing technology as well as polymeric materials have been developed to produce films at high output rates with consistent product properties [13]. Not only do currently used polymeric materials for blown film applications have adequate mechanical properties for their specific end-uses, but their rheological properties have been optimized to allow stable processing over a wide range of processing conditions. To simplify their introduction into the market, new sustainable materials must be designed as a drop-in solution that allows processing of the materials in standard blown film extrusion equipment. A general overview of the state of the art for blown film extrusion processes as well as the desired property profile of the most commonly used materials for blown film extrusion is given below.

Blown film extrusion begins by producing a homogeneous polymer melt in an extruder. The polymer melt then flows through an annular die that produces a molten polymer tube (Figure 2.36). An air cooling ring located at the exit of the die provides a high-speed air stream that helps remove and solidify the polymer melt at a given frost-line height. Once the polymer tube is solidified, a set of nip-rolls shut the tube hermetically, flatten it, and pull the film through into a winding device. The polymer tube is inflated by injecting a pulse of air through a duct placed in the middle of the annular die, into the inside of the polymer tube.
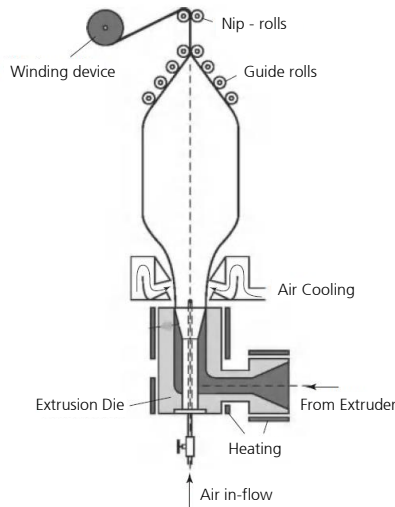
Figure 2.36: Post-extruder section of a typical blown film extrusion line. Modified from [178]

The film thickness and film diameter can be controlled within equipment and material limitations through a series of processing variables (Table 2.9). This can be done in-line without the need of modifying the die geometry or the auxiliary equipment specifications.

Table 2.9: Effect of increasing processing parameters on the film thickness, bubble diameter, and frost line height [13].

Variable to increase	Film thickness	Bubble Diameter	Frost line height
Nip-roll speed	↓	↑	↑
Screw speed	↑	↑	↑
Cooling speed	↑	↓	↓
Bubble volume	↓	↑	↓

Changing the processing parameters also affects the molecular orientation of the polymer chains. The degree of molecular orientation in a blown film is described by the draw ratio (DR) defined by Equation 2.43 and the blow-up ratio (BUR) defined by Equation 2.44. By changing DR and BUR, different levels of orientation in both the machine direction (MD) and the transverse direction (TD) can be achieved in blown film extrusion. This results in films with a more uniform strength in both MD and TD without the need of expensive, biaxial orientation process equipment necessary for achieving this through flat cast film extrusion [14]. Materials that can be processed at a wide range of DR and BUR values are preferred as this allows a wide range of film geometries and levels of molecular orientation to be obtained with a single material in the same processing equipment.

$$DR = \frac{Nip-roll\ velocity}{Extrusion\ throughput\ velocity} = \frac{V_N}{V_0} \qquad \text{Eq. 2.45}$$

$$BUR = \frac{Radius\ of\ the\ final\ film}{Radius\ at\ the\ die\ exit} = \frac{r_f}{r_0} \qquad \text{Eq. 2.46}$$

2.4.1 Desired material property profile for blown film extrusion

Low density polyethylene (LDPE) is the most widely used material for blown film applications due to its appropriate mechanical properties, wide processing window and low cost [13]. LDPE is a lightweight material with a good balance of strength and flexibility, water resistance, and a good degree of clarity for many applications [13]. Development of the LDPE manufacturing technology allows it to be produced at a relatively low cost and its branched molecular structure gives it a high melt stability resulting in a wide processing window. Although LDPE can be produced from renewable ethanol, most of the LDPE is produced from non-renewable fossil-based resources. Regardless of the raw materials used, both the renewable and the non-renewable LDPE have the same material properties including LDPE's high chemical stability resulting in a low biodegradability [11].

LDPE has a high elongation at break and a relatively low elastic modulus, which make for soft and flexible films with a high tear resistance. At the same time, LDPE has a relatively low melting temperature (135 °C) allowing the material to be processed at moderate temperatures and with a low extruder motor power consumption [13]. The long chain branched (LCB) structure of the polymer chains has been shown to induce a strain hardening effect in which the extensional viscosity of the material increases during stretching of the melt [179]. A high extensional viscosity provides the necessary melt stability to the polymer tube during blown film extrusion. If a material has a low melt stability, the air bubble inside the blown film tube is free to move around under certain processing conditions due to the ductility of the polymer melt. This low bubble stability can cause film thickness variation during processing, resulting in variations of the mechanical properties at different regions within the film.

3   High molar mass PLLA-b-PEG-b-PLLA block copolymer approach

As discussed in the previous section, several possibilities have been explored to modify the mechanical properties of PLA to allow its use in applications like flexible films in which softer and more flexible materials than PLA are typically used. Of the different approaches mentioned in Section 2.3, the use of polyethers as plasticizers in PLA are attractive for several reasons. One main reason is the lower polyether plasticizer %-wt contents required to bring similar changes to the mechanical properties of PLA when compared to inhomogeneous blends with other biodegradable polyesters such as PBAT, PBS, and PCL. Only a 15 – 20 %-wt PEG must be blended with PLA to increase the elongation at break from 5 % (pure PLA) to 400 % (blend) [24], while a PBAT content of around 55 %-wt is necessary to achieve the same elongation at break [11]. Differently to PBAT, PBS, and PCL, polyethers like PEG and PPG are commercially available and relatively low-cost polymers. Additionally, polyethers like PEG are reported to be degradable in fresh water at molar masses of up to 60 kDa [25] and are projected to be produced from renewable raw materials in the long term [25]. A joint venture between Clariant and India Glycols for the production of ethylene oxide derivatives from renewable resources was announced in 2022 [26].

Unfortunately, polyether plasticized PLA blends produced in our laboratories have shown migration of the polyether plasticizers after about 2 weeks of storage under nitrogen atmosphere causing sticky surfaces in the produces films. The migration of the polyether plasticizer is thought to lead to changes in the mechanical properties. Additional morphological changes driven by crystallization of the PEG plasticizer [18–20] or of the PLA matrix itself [23] during storage have reportedly led to changes in the mechanical properties of the plasticized blends.

In the present work, it is attempted to avoid migration of the polyether plasticizer by covalently bonding it to the PLA polymer chains. To do this, triblock copolymer structures with an inner polyether block and two outer PLA blocks were synthesized through a straightforward method. The produced block copolymers should have the necessary polyether plasticizing block content to obtain the necessary mechanical properties for flexible film applications, while having a high enough molar mass so as to allow adequate processing of the block copolymers in standard processing equipment. The chosen synthesis method and the challenges associated to the synthesis of such block copolymers are described in the following sections.

3.1   PLLA-b-PEG-b-PLLA block copolymer synthesis concept

Similarly to the current industrial synthesis process of commercial PLA homopolymers [27], the block copolymers were to be synthesized through the ROP of L-lactide in the bulk, using $Sn(Oct)_2$ as a catalyst and at a temperature of 190 °C. The classical high-boiling alcohol initiators (typically used industrially to control the molar mass of PLA) are substituted by polyether diol or tetraol macroinitiators such as PEG to synthesize PLLA-b-PEG-b-PLLA triblock copolymers (Figure 3.1).
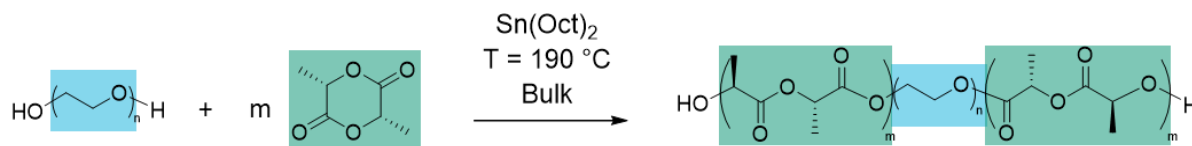
Figure 3.1: ROP of lactide using a difunctional PEG polymer as a macronitiator.

The Mn of the block copolymers can be controlled by modifying the lactide monomer to –OH end-group (in the polyether macroinitiator) molar ratio present in the reaction mixture as expressed by Equation 2.2. If the functionality and the Mn of the polyether are known, the theoretical Mn of the PLLA blocks in a reaction like the one shown in Figure 3.1 can be calculated for a given polyether diol %-wt content in the reaction mixture. Figure 3.2 shows the calculated theoretical Mn of PLLA block copolymers initiated with PEG macroinitiators of different Mn values (6, 8, 12, 20 kDa) at varying %-wt PEG macroinitiator contents.
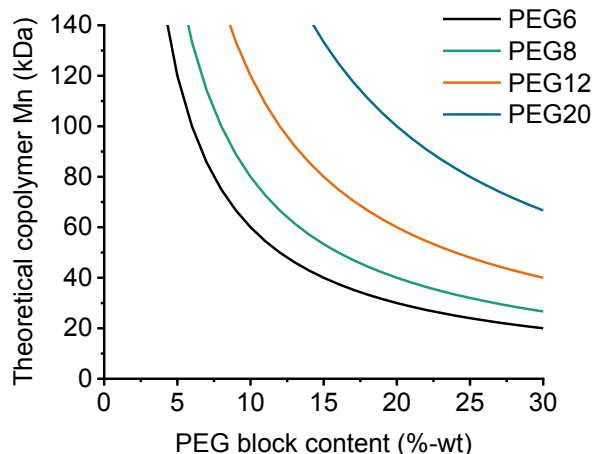
Figure 3.2: Theoretical copolymer Mn of PLLA-b-PEG-b-PLLA block copolymers initiated with PEG macroinitiators of different Mn values (6, 8, 12, 20 kDa) of varying PEG macroinitiator %-wt contents.

Figure 3.2 clarifies the effect of using higher-Mn macroinitiators in the ROP of L-lactide to synthesize the PLLA-b-PEG-b-PLLA block copolymers. PEG20 (Mn = 20 kDa) contains only few –OH end-groups per gram of PEG20 introduced into the reaction mixture. This helps maintain the L-lactide monomer to –OH initiator ratio high even for elevated %-wt PEG20 plasticizing block contents.

A ROP reaction mixture made up of 20 %-wt PEG20 macroinitiator and 80 %-wt L-lactide monomer for example, would theoretically lead to a block copolymer with a total Mn of around 100 kDa (Figure 3.2). If the same reaction mixture was prepared using the PEG6 macroinitiator (Mn = 6 kDa) instead of with PEG20, a much lower theoretical block copolymer Mn of 30 kDa would be expected.

The Ingeo® 4043D film-grade commercial PLA homopolymer has a Mn of 110 kDa (measured by ^{1}H-NMR), which gives it the required rheological properties to allow stable processing in conventional processing equipment. Keeping this in mind, the calculations in Figure 3.2 highlight the importance of using high molar mass macroinitiators in the synthesis of the PLLA-b-PEG-b-PLLA block copolymers to implement the necessary amount of plasticizing polyether block %-wt content in the block

copolymers, while still maintaining a high enough block copolymer molar mass (~ 100 kDa) to allow adequate processing.

The PLLA-b-polyether-b-PLLA block copolymer synthesis concept additionally allows variation of the chemical structure of the polyether block as long as the polyether is soluble in the L-lactide monomer during the ROP synthesis. The effects of modifying the chemical structure of the polyether block on the material properties of the block copolymers by using different polyether macroinitiators (Table 3.1) are studied in this work.

Several polyether chemical structures (poly(THF), PEG, PPG, PEG-b-PPG block copolymers, PEPG statistical copolymers) are commercially available, however their molar mass values are typically relatively low (~ 3 -10 kDa) [91]. The main field of application for such polyethers is as building blocks for the synthesis of commercial polyurethane multi-block copolymers. Given the step-growth reaction mechanism of such polyurethane multi-block copolymers, their total molar mass is not limited by the Mn of the polyether building blocks. Thus, high molar mass polyethers as polyurethane building blocks are relatively rare commercial products. Actually, polyether polymers of higher molar mass (Mn ~ 10 – 35 kDa) are typically commercialized as binders, adhesives, thickeners, or solubilizing agents [180; 181]. The high molar mass polyether polyols used in the present work and their general characteristics are summarized in Table 3.1.

Table 3.1: Plasticizing polyether macroinitiators used for the synthesis of the different PLLA-b-polyether-b-PLLA block copolymers in this work.

Polyether	Mn	-OH functionality	EO:PO[a]	Tg[b]	Tm[b]
	[kDa]	[mol_{OH}/$mol_{Polyether}$]	[mol_{EO}:mol_{PO}]	[°C]	[°C]
PEG6	6	2	1:0	-66[c]	63
PEG8	8	2	1:0	-66[c]	63
PEG12	12	2	1:0	-66[c]	64
PEG35	35	2	1:0	-66[c]	67
PEPG5.6[d]	5.6	2	2:1	-70	amorphous
PEPG12[d]	12	2	3:1	-70	0
PEPG20[d]	20	4	4:1	-66	2
PPG8	8	2	0:1	-66	amorphous
PPG12	12	2	0:1	-66	amorphous

[a] EO refers to the ethylene oxide and PO to the propylene oxide monomer content in the macroinitiator [b] Measured by DSC [c] The Tg could not be measured due to the high crystallization rate, the shown value was taken from the literature [20] [d] PEPG: statistical copolymers of ethylene oxide (EO) and propylene oxide (PO) - poly(ethylene glycol-co-propylene glycol).

The available polyether polymers range from molar masses of 5.6 kDa to 35 kDa and are composed of ethylene oxide (EO) and/or propylene oxide (PO) repeat units. The PEG polymers are semicrystalline, while the PPG polymers are completely amorphous. Crystallinity in the statistical copolymers of EO and PO (PEPG) varies depending on the EO content. The PEPG12 and PEPG20 copolymers containing 75 %-mol and 80 %-mol EO repeat units, respectively, can undergo crystallization at temperatures

below 0 °C, but are liquids at room temperature. The PEPG5.6 copolymer with only a 66 %-mol EO content does not show crystallization at the measurement conditions.

The chemical structure of the PLLA blocks of the PLLA-b-polyether-b-PLLA triblock copolymers can be varied by introducing comonomers that are able to undergo ROP at the same conditions as the L-lactide monomer. In this work, the effects on the material properties of the block copolymers are investigated when using D-lactide and ε-caprolactone as comonomers.

To quickly identify the different chemical structures that were synthesized for this work, a systematic nomenclature system for the PLLA-b-polyether-b-PLLA block copolymers had to be defined. The nomenclature first informs the topology block copolymer by using the "lin-" or "star-" prefixes. This is followed by the chemical structure and molar mass (i.e. PEPG12) of the polyether (according to Table 3.1) with the polyether %-wt block content as a subscript. Finally, if a comonomer was incorporated into the PLLA blocks, it is specified using the abbreviation "DLac" for D-lactide or "CL" for ε-caprolactone followed by the comonomer %-mol content (with respect only to the PLLA block[5]) as a subscript. If no comonomer is specified, the block copolymer was synthesized using only L-lactide as a monomer. For example, a lin-PEPG12$_{13\%}$DLac$_{4\%}$ block copolymer is linear, has a 13%-wt PEPG block content with a 12 kDa block Mn, and two PLLA blocks containing 4 %-mol D-lactide units.

3.2 Technical challenges of the block copolymer synthesis

As mentioned in Section 2.1.4, moisture can reduce the molar mass of the PLLA blocks obtained through ROP of L-lactide due to the reactive –OH group present in the water molecule. Polyethers with high contents of the hydrophilic EO repeat units, are capable of absorbing significant amounts of water at ambient humidity. The water %-wt content of PEPG12 (Table 3.1) was measured before and after drying for 4 h at 150 °C under strong nitrogen bubbling by Karl-Fischer titration. The water content in the PEPG12 could be reduced from around 0.2 %-wt before drying to 0.02 %-wt after drying. The effect of the presence of water in the PEG macroinitiator on the theoretical Mn of the synthesized block copolymer is presented in Figure 3.3.

---

[5] The polyether is not taken into consideration for this %-mol content. The number of comonomer repeat unit moles is compared to the total number of repeat unit moles in the PLLA blocks
(i.e. %-mol$_{CL-R.U.}$ = mol$_{CL-R.U.}$ / (mol$_{L-lactide-R.U.}$ + mol$_{CL-R.U.}$) · 100%)
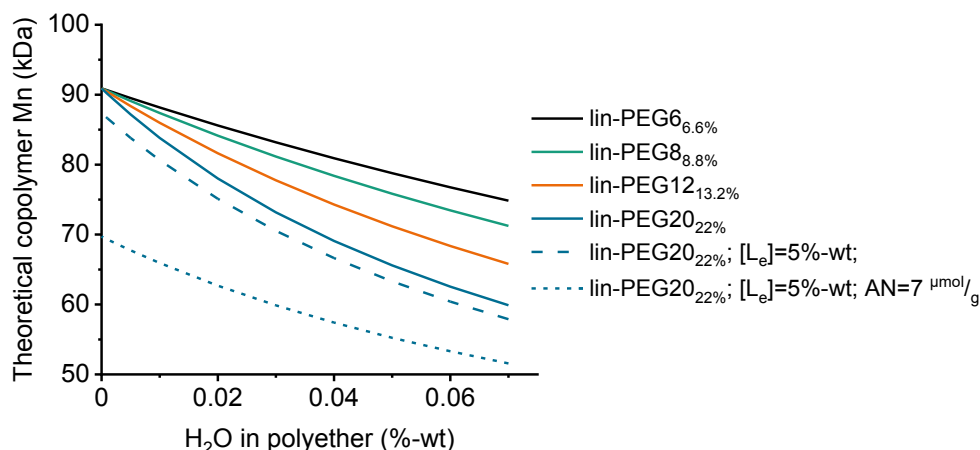
Figure 3.3: Theoretical block copolymer Mn as a function of water content in the polyether macroinitiator used. Block copolymers with varying %-wt polyether block contents and with different polyether block Mn are compared. Additionally, (– –) shows the effect of incomplete lactide conversion caused by a lactide equilibrium concentration [L_e] of 5 %-wt and (---) the effect of a slightly hydrolyzed L-lactide monomer with an acid number (AN) of 7 μmol$_{COOH}$/g$_{Lactide}$.

Figure 3.3 highlights the more pronounced reduction of the block copolymer Mn as the moisture-containing PEG content is increased. For example, Mn of a lin-PEG6$_{6.6\%}$ block copolymer would be reduced from 91 kDa down to around 86 kDa if the water content in the polyether before the ROP were to be increased from 0 %-wt to 0.02 %-wt. If instead, a 22 %-wt PEG20 content were to be introduced into the reaction mixture with the same 0.02 %-wt water content in the polyether, Mn of the resulting lin-PEG20$_{22\%}$ block copolymer would be reduced to a value of 78 kDa.

In praxis, incomplete lactide conversion (due to the lactide equilibrium – Section 2.1.4) causes further reduction the block copolymer Mn. If an equilibrium L-lactide [L_e] concentration of 5 %-wt is considered after the ROP of a mixture with 22 %-wt PEG20 content (containing 0.02 %-wt water), the block copolymer Mn would be reduced to 75 kDa (Figure 3.3).

When L-lactide is exposed to environmental humidity, it is known to hydrolyze to lactoyllactic acid and/or lactic acid, which contain –OH end-groups that can initiate the ROP (Section 2.1.4). Polymer-grade L-lactide monomer typically lists a maximum free acid (acid number – AN) content of 7 μmol$_{COOH}$/g$_{Lactide}$ [35]. If this AN is considered together with the 22 %-wt PEG20 content (containing 0.02%-wt water) and the [L_e] = 5 %-wt, a Mn value of 63 kDa can be expected for the resulting lin-PEG20$_{22\%}$ block copolymer. Thus, Figure 3.3 shows that the presence of humidity in the PEG macroinitiator, the incomplete L-lactide conversion, and the presence of hydrolyzed L-lactide monomer can significantly reduce the Mn of a lin-PEG20$_{22\%}$ block copolymer by close to 30 kDa when considering these realistic experimental values.

4 Experimental

4.1 Materials

Purified L-lactide and D-lactide were purchased from Corbion Purac (Netherlands) stored under nitrogen atmosphere in sealed aluminium bags at -30°C until use without further purification. ε-Caprolactone was purchased from Fluka, dried over calcium hydride (CaH_2) for 24 h at room temperature, distilled at reduced pressure and stored under molecular sieves and in a desiccator under phosphorus pentoxide (P_2O_5) until use. The polyethers described in Table 3.1 were obtained from TechnoCompound (Germany) and dried at 150 °C under strong nitrogen bubbling for 4 h directly before use. Tin(II)-2-ethylhexanoate ($Sn(Oct)_2$, ≥ 95 %), dry toluene (≤ 30ppm H_2O), and tris-nonyl phenyl phosphite (TNPP) were purchased from Sigma-Aldrich and were used as received.

4.2 Block Copolymer synthesis

Block copolymers could be synthesized in batch operation at both the laboratory (30 g batches) and the semi-technical scale (3 kg batches). In both cases, the torque required to maintain a defined stirrer RPM could be monitored during the ROP. As the ROP progressed, the viscosity of the reaction mixture increased and an increase of the stirrer torque was observed. The ROP was ended when the measured stirrer torque reached a stable plateau.

The 30 g of material that could be recovered from the ROP performed at the laboratory scale allowed the general characterization of the materials (MFI, oscillatory rheology, ^{1}H-NMR, DSC, tensile testing). The ROP had to be performed in the semi-technical scale (3 kg) to allow blown film extrusion experiments (Section 5.3) in a semi-technical blown film extrusion line (Section 4.3.1). The experimental procedures for the laboratory and semi-technical scale ROP experiments are detailed in the following sections.

4.2.1 Laboratory scale: ROP of lactide

Copolymers were prepared in the bulk through ring opening polymerization (ROP) of lactide catalyzed by $Sn(Oct)_2$ using different polyether diols as macromolecular hydroxyl initiators under a nitrogen atmosphere. The reaction melt was mechanically stirred and the torque measured at the stirrer head was recorded during the reaction. The product was removed from the reactor 5 min after stable plateau in the torque profile was reached (usually 20 min after the first torque increase). As an example, PEPG20 (7.9 g, 3.97 · 10^{-4} mol) was introduced into a 70 mL three-neck glass reactor and nitrogen was bubbled through the PEPG20 melt for 4 h at 150 °C through a long glass tube to dry

the polyether. $Sn(Oct)_2$ (0.015 g, $4 \cdot 10^{-4}$ mol) in a 1 %-wt toluene solution (1.50 g) was introduced through a syringe over the PEPG20 melt under nitrogen flow. L-lactide, D-lactide or a mixture thereof (53.1 g, 0.368 mol) were added into the reaction mixture. For some reactions, TNPP (0.21 g, $3.1 \cdot 10^{-4}$ mol) was introduced at this moment (before the ROP) into the reaction mixture. The flask was inserted into an oil bath at 200 °C (T_{melt} = 190 °C) for around 30 s to allow the lactide to melt. A mechanical glass screw stirrer was then attached through the middle neck of the flask and the stirring speed was set at 200 RPM to ensure complete mixture of the reactants. After the torque reached 20 N·cm, the stirring speed was reduced to 50 RPM and the reaction was allowed to continue. When a plateau in the torque profile was reached, the product was mechanically removed from the flask under nitrogen flow and allowed to cool in a closed container under strong nitrogen flow. For some reactions, TNPP (0.21 g, $3.1 \cdot 10^{-4}$ mol) was added to the melt (after the ROP), and the mixture was stirred for an additional 10 min before releasing it from the reactor. Once cooled, the product was pelletized into particles of 1-5 mm (minimizing moisture contact) and introduced into a vacuum oven at 2 mbar for demonomerization. The temperature program used for demonomerization in the vacuum oven consisted of an initial 4 h period at 70 °C, followed by a heating ramp from 70 °C to 120 °C over 2 h to allow crystallization. The block copolymer pellets were then maintained at 120 °C for 10 h to remove the unreacted monomer and volatiles. The pellets were then allowed to cool to RT under vacuum and stored under nitrogen atmosphere in a desiccator (in the presence of P_2O_5).

4.2.2   Semi-technical scale: ROP of lactide in 7.5 L reactor

To produce enough material for blown film extrusion processing experiments, the ROP was upscaled to a 7.5 L Büchi stainless-steel reactor equipped with an anchor stirrer. The polyol was dried separately in a three-neck round bottom flask under heavy nitrogen bubbling at 150°C over 4 h directly before the reaction. The reactor was dried by toluene distillation under vacuum and cooled to room temperature before adding lactide (4,120 g, 28.59 mol), PEPG20 (529.6 g, 0.0265 mol), and a 10 %-wt solution of $Sn(Oct)_2$ in toluene (9.95 $g_{solution}$, $2.46 \cdot 10^{-3}$ $mol_{Sn(Oct)2}$). For some reactions, TNPP (14.8 g, $2.15 \cdot 10^{-2}$ mol) was added into the reaction mixture at this point (before the ROP). The mixture was then stirred while the reactor temperature was increased to 180 °C. The reaction progress was monitored via the measured torque at the stirrer shaft. When a plateau in the torque was reached, TNPP (14.8 g, $2.15 \cdot 10^{-2}$ mol) was added to the polymer melt and the mixture was stirred for 10 min at 180 °C. The copolymer was released through a die and allowed to cool under nitrogen flow before being pelletized. The polymer pellets were demonomerized in a vacuum oven as previously described for the lab scale ROP procedure.

Note that the removal of the synthesized block copolymers required 2 to 3 h. During this time, the material was maintained at T = 180 °C to avoid crystallization of the material. Because of this wide "residence time distribution" of the block copolymer in the reactor, the Mn measurements done by ^{1}H-NMR were found to have a variability of around ± 20 kDa.

4.3 Processing

4.3.1 Blown Film Processing

The copolymer pellets were dried in a GTT 101 hot-air dryer (Gerco, Germany) for 4 h at 70 °C prior to blown film extrusion. The material was then fed into the nitrogen-flushed hopper of a Collin E 25P single-screw extruder (Germany) equipped with a 50 mm annular die (8 mm slit thickness) connected to a Collin BL180/400E blown film line (Germany). The extruder has 8 heating zones (including the die). The feeding zones were cooled to 25 °C and the temperature set-point was gradually increased to equal the die temperature within the first 5 heating zones. The die temperature was 190 °C for the pure L-lactide copolymer formulation and 160 °C for the formulations containing comonomers in the PLLA blocks (D-lactide, or ε-caprolactone). Screw RPM and nip-roll speed were varied as explained in Section 5.3.4 to achieve different levels of molecular orientation.

4.4 Block copolymer characterization

4.4.1 Proton nuclear magnetic resonance

Proton nuclear magnetic resonance (^{1}H-NMR) spectra were measured using a Varian Unity INOVA 500 (Varian Inc.) spectrometer operating at a frequency of 499.8 MHz at 23°C. A 10 mg sample of the block copolymer in question was dissolved in 0.5 mL of deuterated chloroform for each measurement. Examples of the peaks assigned to the protons in the different block copolymer structures are shown in Figure A 5, Figure A 6, Figure A 7, Figure A 8, Figure A 9, and Figure A 10.

In theory, the integrals of both the signal at 5.2 ppm (–C$\underline{H}$O- proton in the PLA main chain) and the signal at 1.6 ppm (–C$\underline{H}_3$ protons of the PLA methyl side-group) could be used in combination with the signal at 4.35 ppm (–C$\underline{H}$OH proton of the PLA end-group) to calculate the Mn of the block copolymers through end-group analysis. The signal at 1.6 ppm (–C$\underline{H}_3$ protons of the PLA methyl side-group) however, overlaps with the signal at 1.7 ppm (–C$\underline{H}_3$ protons of the lactide monomer methyl group). Such overlap is not observed for the signal at 5.2 ppm (–C$\underline{H}$O– proton in the PLA main chain) and the signal at 5.0 ppm (–C$\underline{H}$O– proton in lactide). For this reason, the Mn values shown throughout this work are calculated with the integrals of the 5.2 ppm ($I_{5.2ppm}$) and 4.35 ppm ($I_{4.35ppm}$) signals together with the functionality of the used initiator (f) as shown below in Equation 4.1.

$$Mn_{Block\ Copolymer} = \frac{I_{5.2ppm}}{I_{4.35ppm}} \cdot f \cdot 72 \frac{g}{mol} + Mn_{Polyether} \qquad \text{Eq. 4.1}$$

The small end-group signal (4.35 ppm) used to calculate the Mn is at the measurable limit, however it had a generally good accordance with MFI and rheological measurements. The effects of changing

the integration limits of the signal at 4.35 ppm on the same ^{1}H-NMR spectrum of an expected high molar mass star-PEPG20$_{10\%}$ block copolymer (given the high [lactide] / [-OH] ratio) was analyzed and is shown on Figure A 4. The analysis showed that a variation of around ± 8.5 kDa can be expected for the calculated Mn value.

The %-wt content of unreacted lactide with respect to the total PLA chain content in the block copolymers could also be calculated using the integrals of the signals at 5.2 ($I_{5.2ppm}$) and 5 ppm (I_{5ppm}) for the –C$\underline{H}$OH proton in the PLA chains, and in the unreacted lactide monomer, respectively. For this calculation, the integral of the satellite peak of the 5.2 ppm signal at 5.3 ppm ($I_{5.3ppm}$) was substracted from the I_{5ppm} as shown below in Equation 4.2.

$$\% - wt\ Lactide = \frac{I_{5ppm} - I_{5.3ppm}}{I_{5ppm} - I_{5.3ppm} + I_{5.2ppm}} \cdot 100 \qquad \text{Eq. 4.2}$$

4.4.2 Differential scanning calorimetry

Differential scanning calorimetry (DSC) measurements were performed on a Q1000 DSC instrument (TA Instruments) under nitrogen flow with a sample size of 4 - 5 mg. For Tg measurements, the material was heated to 20 °C above Tm and allowed to stay at this temperature for 2 min. The material was then cooled at 20 °C/min (unless stated otherwise) to obtain a mostly amorphous material (no clear crystallization peak observed during cooling). The subsequent heating cycle at 10 °C/min was used to determine the Tg, Tc, and Tm. The temperature at the middle of the inclined region in the DSC curve was used to determine the Tg. Peak temperatures of the exothermic crystallization peak and endothermic melting peak were used for Tc and Tm respectively. Degree of crystallinity was calculated using Equation 4.3 shown below and a value of ΔH$_{m100\%}$ of 93 J/g as estimated by Fischer et al. [105].

$$X_C = \frac{\Delta H_m - \Delta H_c}{\Delta H_{m100\%}} \qquad \text{Eq. 4.3}$$

For isothermal DSC experiments, the materials were first heated 20°C above the Tm and allowed to stay at this temperature for 2 min. The materials were then cooled at 50 °C/min to the desired isothermal crystallization temperature and allowed to stay at this temperature for at least 30 min. The crystallization half-time values shown in Figure 5.12 were calculated using the polynomial extrapolation methodology described in [182] to extend the experimental data to the baseline and allow integration of the isothermal crystallization curve. The crystallization half-time values shown in Figures 5.40, 5.41, and 5.49 were calculated from the isothermal crystallization experiments shown in Figures A 16 – A 22 following the baseline substraction methodology described in [183; 184].

4.4.3 Tensile testing

Tensile tests of injection molded and blown film samples were performed using a Zwick/Roell Z010 universal testing machine. According to DIN EN ISO 527, the samples were conditioned at 23°C and 50% relative humidity for 24 h before each testing.

DIN EN ISO 527-2 type 5A samples were produced using a HAAKE MiniJet injection molding system (ThermoFischer Scientific). All materials were dried at 70 °C for 4 h at 5 mbar vacuum before molding. Melting cylinder temperature was set 20 °C above the Tm as measured by DSC and the mold was kept at room temperature to obtain practically amorphous samples. The tensile tests of injection-molded samples were performed with a load of 10 kN and at a crosshead rate of 19 mm/min (2 mm/min for determination of the E-modulus). All resulting data is an average of 5 tensile tests.

Blown Films were extruded as previously described. The films were cut into strips according to DIN EN ISO 527-3 type 2 (10 mm width, >120 mm length). Tensile tests were done with the strips elongated in both machine direction (MD) and transversal direction (TD).

4.4.4 Melt flow index

The melt flow index (MFI) was measured using a MPX 62.92 melt flow indexter (Göttfert) with a standardized die and weight of 2.16 kg (DIN EN ISO 1133). Polymer pellets were dried for 4 h at 70 °C before measurement to minimize hydrolytic degradation of the PLA-based polymers. Around 4 g of material were introduced into the temperature-controlled barrel and allowed to melt under 10 kg load for 1:30 min to press air bubbles out as much as possible (pressurized melting step). After the pressurized melting step, the material was allowed to stabilize at the measurement temperature in the absence of a load for 100 s (temperature stabilization step). After the temperature stabilization step, the 2.16 kg load was applied on the melt and the piston height was recorded over time. Forty piston height measurements were done from which the MVR (melt volumetric flow rate) could be calculated. A constant melt density of 1.24 g/cm^3 was used to calculate the MFI of all the materials. For the measurements shown in Figure 5.38, the temperature stabilization time was varied from 100 s to 200 s and to 300 s. The 40-recorded MFI measurements are shown for each temperature stabilization time in Figure 5.38.

4.4.5 Shear dynamic rheometry

Oscillatory rheology experiments were performed using an ARES rheometer (TA Instruments) with a parallel plate geometry with plate radii of 25 mm and a plate gap of 1 mm (± 0.1 mm). The measured

samples were dried for at least 4 h at 80 °C in a vacuum drying oven and stored in 1 g portions under dry nitrogen in sealed aluminium bags until directly before the measurement. The samples were allowed to melt at the specified measurement temperature under a nitrogen atmosphere for 7 min before the measurement was started. A strain sweep was done with a relatively low viscous block copolymer and a relatively high viscous block copolymer to determine a strain at which both materials were within the viscoelastic regime and the obtained signal was within the instrument sensitivity. A strain of 2 % was chosen for the frequency sweep experiments. The frequency sweep experiments were done from high frequencies of 500 rad/s down to low frequencies of 0.5 rad/s with 5 points per decade.
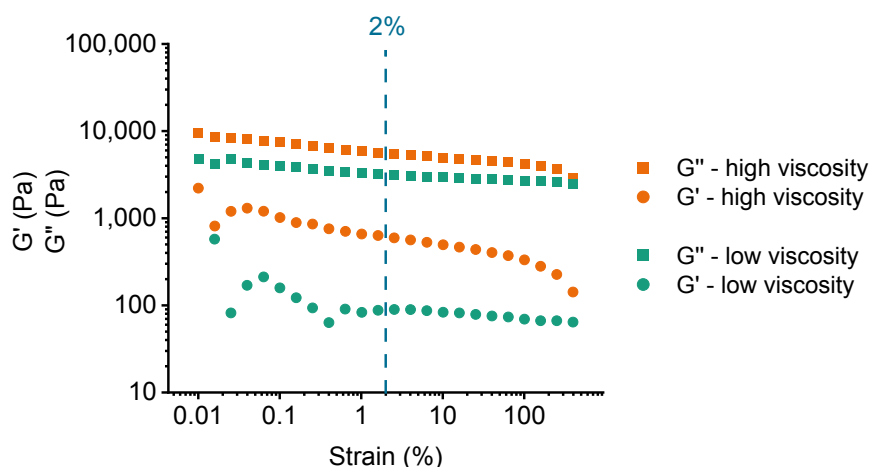
Figure 4.1: Amplitude sweep of a relatively high viscosity (star-PEPG20$_{11\%}$) and a relatively low viscosity (lin-PEPG13$_{12\%}$) block copolymer.

Measurements of the copolymers synthesized at the laboratory scale (30 g batches) were done directly with the obtained granulate. The copolymers synthesized at the semi-technical scale (3 kg batches) had to be injection molded into 1.2 mm disks prior to oscillatory rheological measurements due to the presence of nitrogen bubbles in the obtained pellets (which affected the oscillatory rheometry measurements). The nitrogen bubbles diffused into the pellets during removal of the polymer from the reactor. Nitrogen had to be injected at the top of the reactor to create pressure and push the viscous polymer melt through the die located at the bottom of the reactor. Some of the nitrogen, however, diffused into the polymer melt and formed bubbles in the pellets.

4.4.6 Gel permeation chromatography

Gel permeation chromatography (GPC) was performed on a WGE Dr. Bures system with a SEC 3010 pump, an autosampler with a column oven 3010, a refractive index (RI) detector 3010, two columns (PL HFIPgel). The measurements were done in a hexafluoroisopropanol (HFIP) solution with a 0.05 mmol/L sodium trifluoroacetate content at a flow rate of 0.8 mL/min at a temperature of 40 °C. Calibration was performed using PMMA-standards over a molecular weight range of 875 – 981,000 g/mol.

5 Results and Discussion

5.1 Mechanical and thermal property matrix at the laboratory scale

5.1.1 Linear PEG–initiated triblock copolymers

Three linear tri-block copolymers of roughly equal Mn as measured by ^{1}H-NMR containing a middle PEG block and two outer stereoregular PLLA blocks were synthesized at the laboratory scale according to the procedure described in Section 4.2.1. The PEG block content was varied while maintaining the copolymer Mn practically constant by using PEG macroinitiators of different molar masses (Table 3.1) in the ROP of lactide and appropriately varying the lactide to –OH molar ratio according to Equation 2.2. All copolymers were synthesized using a $1 \cdot 10^{-4}$ $mol_{Sn(Oct)2}/mol_{Lactide}$ catalyst content and lactide monomer to –OH initiator molar ratio resulting in a theoretical Mn of around 91 kDa (including the Mn of the PEG block). The expected chemical structure of the PLLA-b-PEG-b-PLLA block copolymers is shown in Figure 5.1, and the descriptions of the produced copolymers and their measured Mn (^{1}H-NMR) are listed in Table 5.1.
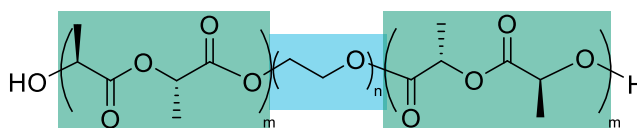
Figure 5.1: Expected chemical structure for the PLLA-b-PEG-b-PLLA block copolymers.

Table 5.1: Measured Mn values of the linear PLLA-b-PEG-b-PLLA block copolymers synthesized in the laboratory scale with different PEG block lengths and %-wt PEG block contents.

Initiator	Expected block copolymer structure	PEG block content[a] [%-wt]	Copolymer name	Theoretical Mn [kDa]	Mn (^{1}H-NMR) [kDa]
Undecanol	PLLA	0	lin-PLA	91	[b]
PEG6	PLLA-b-PEG6-b-PLLA	6.6	lin-PEG6$_{6.6\%}$	91	60
PEG8	PLLA-b-PEG8-b-PLLA	8.7	lin-PEG8$_{8.7\%}$	92	65
PEG12	PLLA-b-PEG12-b-PLLA	13	lin-PEG12$_{13\%}$	92	52

[a] Confirmed by ^{1}H-NMR measurement. [b] No end-group signal found, stoichiometrical lactide to hydroxyl ratio was the same as for the PEG initiated ROP's. Lactide content of all copolymers is around 3 %-wt.

Although the measured Mn is considerably lower than the expected theoretical Mn for the given lactide monomer to –OH initiator molar ratio as defined by Equation 2.2, quite similar block copolymer Mn values of around 58 kDa (± 7 kDa) were measured by ^{1}H-NMR (Table 5.1). The low experimental Mn values are likely caused by the moisture content in the highly hydrophilic PEG polyether, the

incomplete lactide conversion (to the lactide equilibrium of around 5 %-wt), and the hydrolyzed lactide (lactoyllactic acid, lactic acid) present in the used monomer as explained in Section 3.2.

The obtained PEG-containing block copolymer structures behaved similarly to the homologous PEG/PLA blends produced by Hu et al. [18–20]. As shown below in Figure 5.2 (a), increasing PEG block content reduced Tg and peak Tc as measured by DSC, while the peak Tm stayed practically constant. The reduction of Tg follows the trend prescribed by the Fox equation quite closely as shown in Figure 5.2 (b) suggesting a good miscibility of the PEG blocks with the PLLA blocks in the amorphous fraction of the copolymer. The reduced Tc with increasing PEG block content is likely due to an increase in crystallization rate likely caused by the improvement of chain segment transport to the crystallization sites due to the plasticizing effect of PEG. The practically constant Tm values observed in Figure 5.2 (a), suggest that the crystal unit cells are composed almost exclusively of PLLA chains and that the PEG blocks are excluded to the upper and lower lamellar surfaces were chain folding occurs and amorphous domains are located.
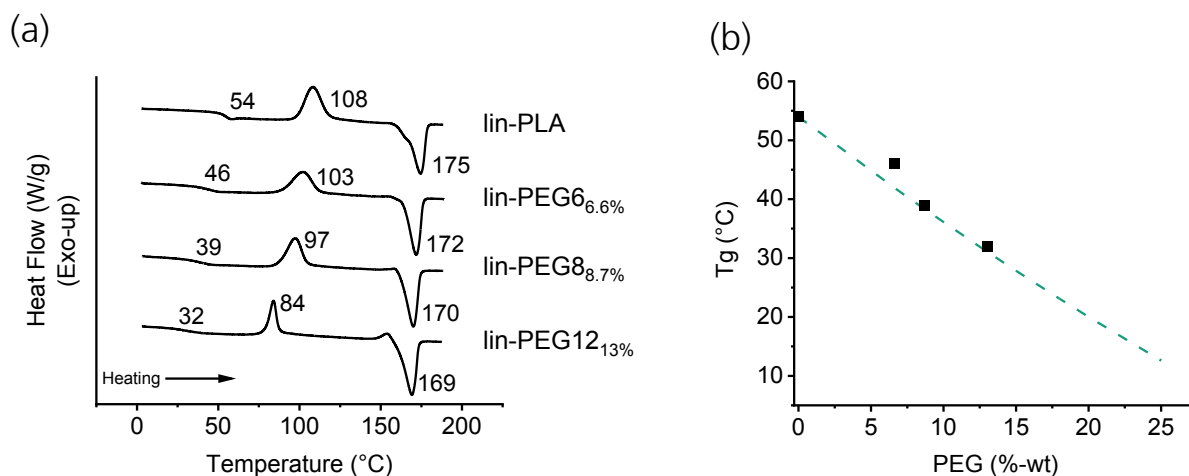
Figure 5.2: (a) Non-isothermal DSC thermograms (second heating cycle) of the lin-PLA reference and the synthesized PLLA-b-PEG-b-PLLA block copolymers. (b) (■) Experimental and (-----) theoretical Tg values for different %-wt PEG contents in the block copolymers. The theoretical block copolymer Tg values were calculated using the Fox equation (Equation 2.9) and Tg_{PEG} = - 66 °C as done in [20].

The successful reduction of Tg significantly changed the mechanical behavior of injection molded tensile test specimens of the block copolymers, as shown on the tensile stress-strain diagram in Figure 5.4. The linear PLA homopolymer with a Tg of 54 °C had a relatively high elastic modulus, a low elongation at break value, and exhibited brittle failure. As the Tg of the copolymers was reduced, a more ductile behavior was observed. The lin-PEG6$_{6.6\%}$ block copolymer (Tg = 46 °C) exhibited a distinct yield point beyond which the polymer chains began to "flow" under the applied stress until failure. The lin-PEG8$_{8.7\%}$ block copolymer (Tg = 39 °C) also exhibited yielding behavior and a slight strain hardening effect just before failure. The lin-PEG12$_{13\%}$ block copolymer (Tg = 32 °C) exhibited yielding at significantly lower stress followed by a clear strain hardening effect at strain values above 100 %. The initially transparent lin-PEG12$_{13\%}$ samples became opaque during tensile testing suggesting that some strain induced crystallization due to the alignment of polymer chains could have occurred.
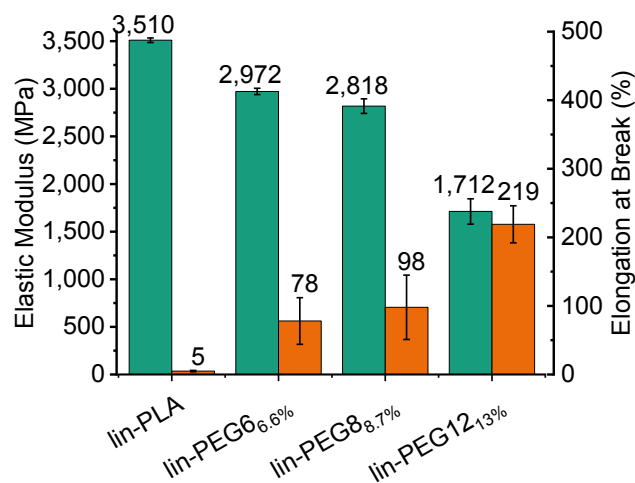
Figure 5.3: (■) Elastic modulus and (■) elongation at break of the PLLA-b-PEG-b-PLLA block copolymer injection molded samples with different PEG block length and %-wt content.
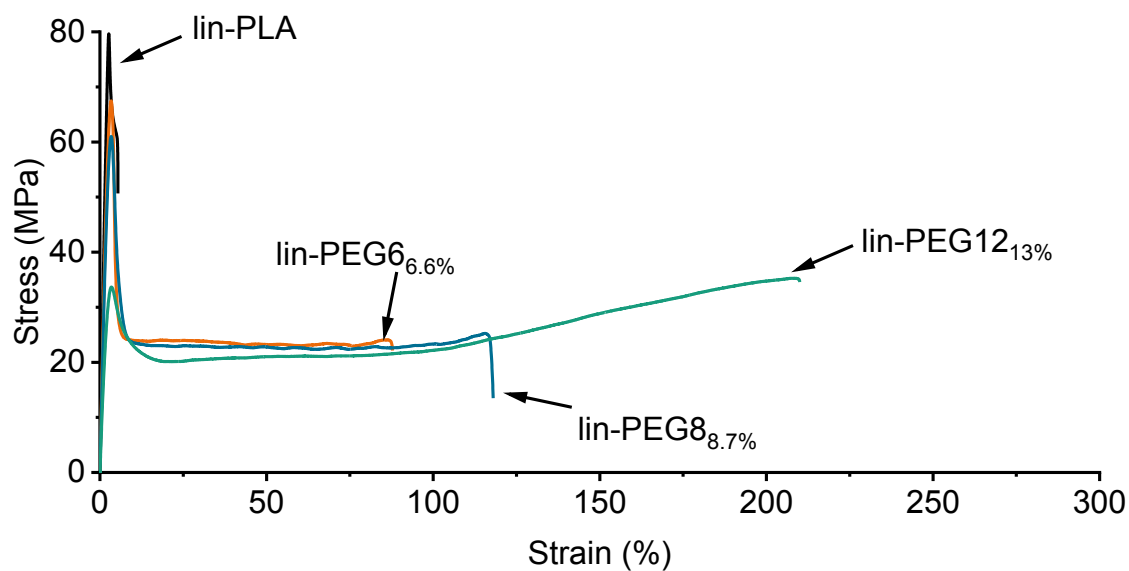
Figure 5.4: Stress strain curves of the performed PLLA-b-PEG-b-PLLA block copolymer tensile tests

5.1.2 Linear PPG–initiated triblock copolymers

Two linear stereoregular PLLA-co-PPG-co-PLLA triblock copolymers were synthesized in bulk at the laboratory scale using PPG8 and PPG12 as macromolecular initiators (Table 3.1). A catalyst to monomer ratio of $1 \cdot 10^{-4}$ $mol_{cat}/mol_{Lactide}$ and a monomer to initiator ratio of 640 $mol_{Lactide}/mol_{PPG}$ were used for both syntheses to obtain copolymers with a theoretical total Mn of close to 91 kDa. The given monomer to initiator molar ratio equates to an 8.7 %-wt PPG8 and a 13 %-wt PPG12 content in the copolymers. The PLLA homopolymer shown in the previous section is also used here as a reference because of the equal lactide monomer to 1-undecanol hydroxyl initiator ratio used for the block copolymers.
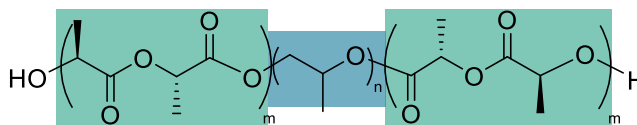
Figure 5.5: Expected chemical structure for the synthesized linear PLLA-b-PPG-b-PLLA block copolymers.

Table 5.2: Measured Mn values of the synthesized linear PLLA-b-PPG-b-PLLA block copolymers with different PPG block lengths and %-wt PPG block contents.

Initiator	Expected block copolymer structure	PPG block content[a] [%-wt]	Copolymer name	Theoretical Mn [kDa]	Mn (^{1}H-NMR) [kDa]
Undecanol	PLLA	0	lin-PLA	91	[b]
PPG8	PLLA-b-PPG8-b-PLLA	8.7	lin-PPG8$_{8.7\%}$	92	81
PPG12	PLLA-b-PPG12-b-PLLA	13	lin-PPG12$_{13\%}$(1)	92	75
PPG12	PLLA-b-PPG12-b-PLLA	13	lin-PPG12$_{13\%}$(2)	92	64

[a] Confirmed by ^{1}H-NMR measurement. [b] No end-group signal found, stoichiometrical lactide to hydroxyl ratio was the same as for the PPG initiated ROP's. Lactide content of all copolymers is around 3%-wt

The PPG containing block copolymers shown on Table 5.2 caused a significantly higher torque increase during the ROP than the PEG initiated copolymers. As shown in Figure A 11, the high measured torques were more similar to the measured torques during the ROP for the lin-PLA homopolymer. One possible explanation could be the higher Mn (measured by ^{1}H-NMR) of the PLLA-b-PPG-b-PLLA block copolymers than that of the PLLA-b-PEG-b-PLLA ones. Such a higher Mn could be caused by inadequate initiation of the ROP due to the low miscibility of the PPG macronitiators in the L-lactide monomer (increasing [lactide] / [-OH]). This inadequate initiation however, should lead to a bimodal molar mass distribution curve with one peak around the Mn of the pure PPG12 macroinitiator (12 kDa) and a second peak around the Mn value of the lin-PPG12$_{13\%}$(1) block copolymer (~ 64 kDa). The measured GPC curve in Figure 5.6 (a) however, does not show such a bimodal distribution for the lin-PPG12$_{13\%}$(1) block copolymer suggesting that most of the block copolymer chains were successfully initiated by PPG12.

Additionally, ^{1}H-NMR spectra of the similarly produced lin-PPG12$_{13\%}$(2) block copolymer were measured before and after dissolution of the lin-PPG12$_{13\%}$(2) block copolymer in chloroform followed by precipitation in isopropanol (non-solvent of PLA and a solvent of PPG). The results in Figure 5.6 (b) show the removal of low molar mass PLA fractions and of unreacted lactide, while in both ^{1}H-NMR spectra the PPG12 %-wt content remained constant at 13.2 %-wt. Both the GPC and ^{1}H-NMR dissolution test results confirm that the PPG blocks were successfully bonded to the PLA blocks.

(a)

(b)

	Mn$_{H-NMR}$ [kDa]	PPG content [%-wt]	Unreacted Lactide [%-wt]
Directly after ROP	64	13.2	6.6
After repreciptation	73	13.2	1.0
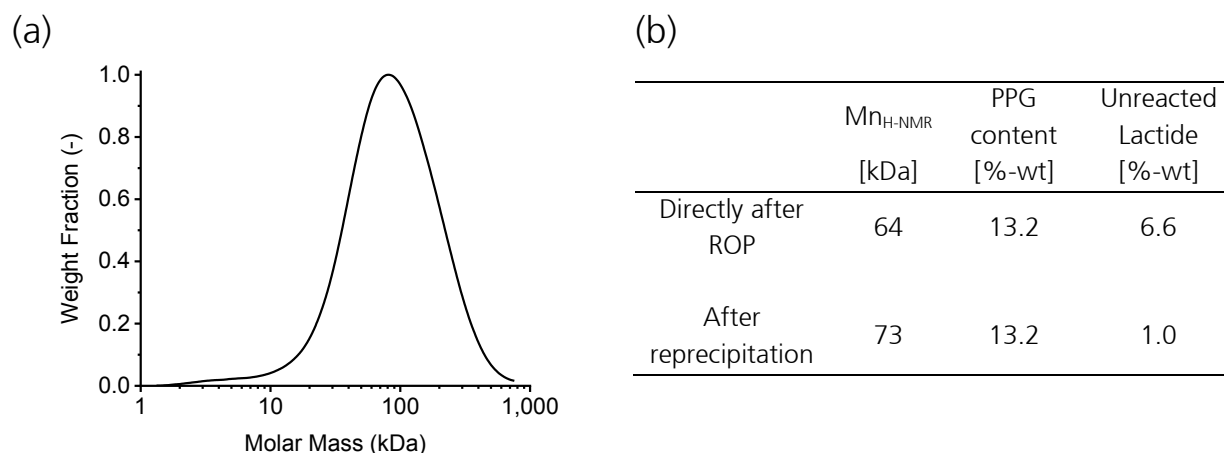
Figure 5.6: (a) GPC measurement of the lin-PPG12$_{13\%}$(1) block copolymer, measured Mn = 54.2 kDa, PDI = 2.131 and (b) ^{1}H-NMR measurement of the lin-PPG12$_{13\%}$(2) block copolymer before and after repreciptation of the dissolved lin-PPG12$_{13\%}$ block copolymer in CHCl$_3$ into cold isopropanol.

The GPC measurement of the lin-PPG12$_{13\%}$(1) block copolymer additionally shows a lower Mn value 54.2 kDa than the Mn value measured by ^{1}H-NMR for the same lin-PPG12$_{13\%}$(1) block copolymer of 75 kDa. This difference is likely due to the relative nature of the GPC measurement given that PMMA standards were used. The GPC measurements depend on the hydrodynamic radius of the polymer chains being analyzed, which is then compared to that of the calibration standard (in this case PMMA). Because the hydrodynamic radius of the block copolymers can be influenced by the more flexible polyether blocks and the different polyether block %-wt contents used in this thesis, ^{1}H-NMR measurements were preferred. Although no information of the molar mass distribution is obtained using the end-group analysis by ^{1}H-NMR measurements, they give equivalent (not relative to a standard of different chemical structure) Mn values that can be compared for block copolymers of different chemical and molecular structures (with their expected different hydrodynamic radii).

Figure 5.7 (a) shows the non-isothermal DSC measurements of the two synthesized PLLA-b-PPG-b-PLLA block copolymers. Both the lin-PPG8$_{8.7\%}$ and the lin-PPG12$_{13\%}$ block copolymers show a Tg slightly above the Tg of the PLA homopolymer. When comparing the measured Tg values to the expected Tg values predicted by the Fox equation [Figure 5.7 (b)], the miscibility of the PPG's can be questioned. Such immiscibility of PPG in PLA can be expected when comparing the results from [22] with the results of [18; 20; 24]. Kulinski et al. [22] found good miscibility of PPG of 0.4 kDa at a 12.5 %-wt content in PLA, but a reduced miscibility of PPG of 1 kDa at a 12.5 %-wt content. In contrast, Hu et al. [20] and Jia et al. [24] found good miscibility at a similar concentration (13 %-wt) of PEG with a much lower entropic contribution to the Gibbs' free energy of mixing (Equation 2.39) due to the higher Mn of the PEG (~ 12 kDa) used for their blends. This comparison thus suggests that

the Flory-Huggins segment-segment interaction parameter "χ" is significantly higher for PPG in PLA than for PEG in PLA. So much so, that slightly increasing the Mn of PPG (and with it, decreasing the entropic contribution to the Gibbs' free energy of mixing) from 0.4 to 1 kDa places the blend in the unstable region of the polymer blend phase diagram (see Figure 2.33). Because in the synthesized block copolymers, the PPG blocks have significantly higher Mn values of 8 and 12 kDa, immiscibility of the PPG blocks could explain the lack of change in the Tg. It seems that even with the reduction of the PLLA block length, the miscibility of the PPG blocks could not be promoted, even for the PPG8 blocks of lower Mn. To further confirm the immiscibility of the PPG blocks, the Tg of the PPG blocks was searched using non-isothermal DSC at low enough temperatures (-70 °C). No Tg of the PPG blocks could be found on DSC. However, this could be due to the low PPG content in the material and the limited sensitivity of the instrument.

The immiscibility of the PPG blocks could also explain the relatively high torque measured during the PPG-initiated ROP of lactide. In the case of the PEG initiated block copolymers, the presence of the plasticizing PEG polymers should also reduce the viscosity of the reaction melt as proposed by the VFTH equation (Equation 2.6). This plasticization effect is absent during the ROP of the PPG-initiated copolymers [as suggested by the higher Tg values in Figure 5.7 (a)] causing the reaction viscosity and hence the torque during the ROP to be higher. The absence of the plasticization effect seems to be a more plausible explanation to the higher observed torque during the ROP than the possibility of the higher Mn of the PPG-initiated block copolymers than that of the PEG-initiated ones causing the higher torque. This is further supported by the low torque measured during the synthesis of the PEPG-initiated block copolymers (which will be discussed in Section 5.1.3) even with their similar Mn (^{1}H-NMR) values (~70 kDa) to those of the PPG-initiated ones (~70 kDa).
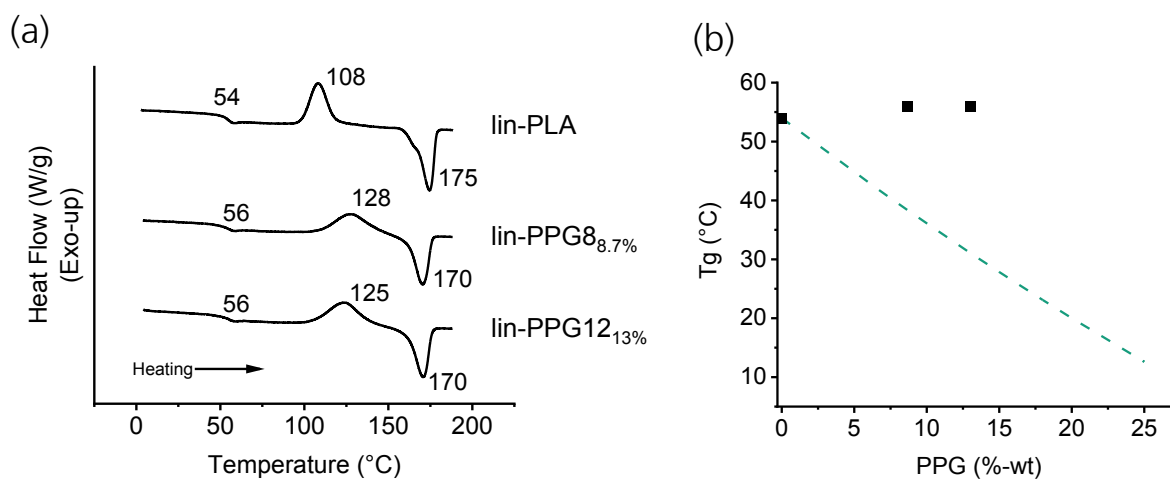
Figure 5.7: (a) Non-isothermal DSC thermograms (second heating cycle) of the lin-PLA reference and the synthesized PLLA-b-PPG-b-PLLA block copolymers. (b) (■) Experimental and (- - - -) theoretical Tg values for different %-wt PPG contents in the block copolymers. The theoretical block copolymer Tg values were calculated using the Fox equation (Equation 2.9) and the measured Tg_{PPG} = - 66 °C.

The mechanical properties of the PLLA-b-PPG-b-PLLA block copolymers are shown below in Figure 5.8. Significant changes of the mechanical behavior in comparison to the lin-PLA homopolymer were detected for the PPG initiated copolymers. A slight reduction of the elastic modulus is observed as

the PPG block content in the copolymers is increased. The elongation at break of the lin-PPG8$_{8.7\%}$ copolymer is significantly higher to the elongation at break of the lin-PLA homopolymer. Further increase of the PPG block content as in the case of the lin-PPG12$_{13\%}$ copolymer, however, did not lead to an increase of its elongation at break. Because Tg of the PPG initiated copolymers did not change as the concentration of the PPG block was increased, it is likely that the observed toughening mechanism is connected to the formation of a well dispersed PPG phase in the PLA matrix with an improved interfacial adhesion caused by the copolymerization [185]. These dispersed particles can act as stress concentration points that can terminate the growth of crazes during failure of the material [185]. The type and content of the dispersed flexible polymer phase, the particle size, interparticle distance, and the interfacial adhesion of the dispersed polymer phase with the polymer matrix are known to play an important role in defining the final properties of the polymer blend [185]. Due to the low toughness of the PPG liquid phase, the toughening potential of the PPG initiated block copolymers is likely limited at room temperature. Because elongation at break values of around 300 % are desired for the final materials, further testing with the PPG initiated copolymers to verify the mentioned toughening mechanism hypothesis was not pursued.
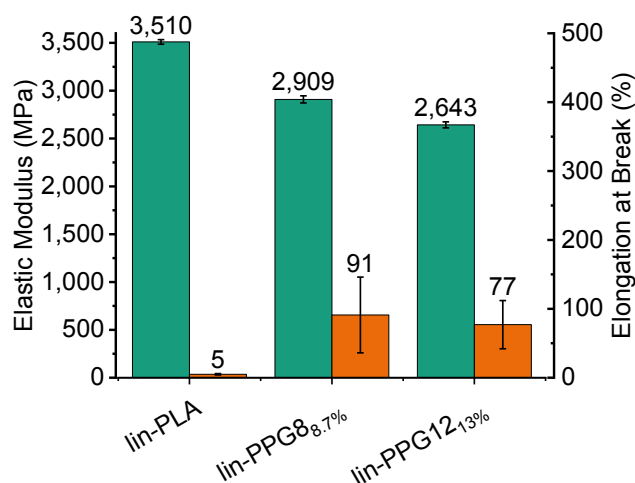
Figure 5.8: (■) Elastic modulus and (■) elongation at break of the PLLA-b-PPG-b-PLLA block copolymer injection molded samples with different PPG block length and %-wt content.
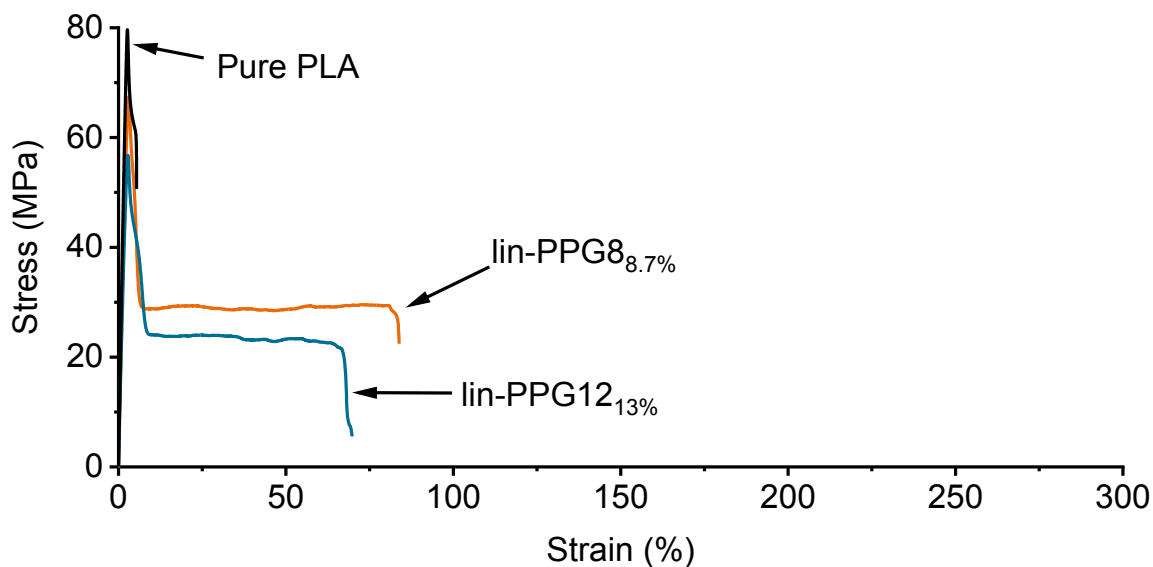
Figure 5.9: Stress strain curves of the performed PLLA-b-PPG-b-PLLA block copolymer tensile tests.

5.1.3 Linear PEPG–initiated triblock copolymers

Two linear PLLA-b-PEPG-b-PLLA block copolymers with the structure shown below in Figure 5.10 were synthesized at the laboratory scale using PEPG5.6 and PEPG12 as macromolecular initiators (Table 3.1). Again, the monomer to macroinitiator ratio was adjusted in such a way that the total copolymer Mn could be maintained fairly constant taking into consideration the difference in Mn between the PEPG5.6 and the PEPG12 initiators. The catalyst concentration used for both of the PEPG initiated copolymers was $1 \cdot 10^{-4}$ $mol_{Sn(Oct)2}/mol_{Lactide}$. The obtained Mn values as measured by ^{1}H-NMR for the block copolymers are detailed below in Table 5.3.
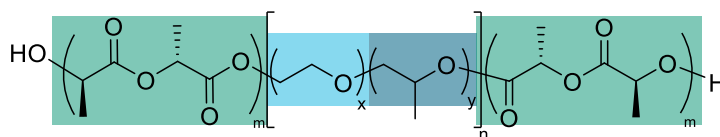
Figure 5.10: Expected chemical structure for the linear PLLA-b-PEPG-b-PLLA block copolymers.

Table 5.3: Measured Mn values of the synthesized linear PLLA-b-PEPG-b-PLLA block copolymers with different PEPG block lengths and %-wt PEPG block contents.

Initiator	Expected block copolymer structure	PEPG block content [a] [%-wt]	Copolymer name	Theoretical Mn [kDa]	Mn (^{1}H-NMR) [kDa]
PEPG5.6	PLLA-b-PEPG5.6-b-PLLA	6.5	lin-PEPG5.6$_{6.5\%}$	86	68
PEPG12	PLLA-b-PEPG12-b-PLLA	13	lin-PEPG12$_{13\%}$	92	71

[a] Confirmed by ^{1}H-NMR measurement.

As in the case of the well miscible PEG-initiated block copolymers, the measured non-isothermal DSC curves of the PLLA-b-PEPG-b-PLLA block copolymers [Figure 5.11 (a)] show a decrease of Tg as the PEPG block content in the copolymers was increased. The experimental Tg values of the block copolymers are 4 - 5 °C above the expected Tg values predicted using the Fox equation [Figure 5.11 (b)]. Although the agreement is not as close as with the PEG-initiated copolymers, the observed trend suggests miscibility of the PEPG blocks with the PLA blocks. The Tg of 35 °C of the lin-PEPG12$_{13\%}$ triblock copolymer is very similar to the Tg of 32 °C for the lin-PEG12$_{13\%}$ triblock copolymer.
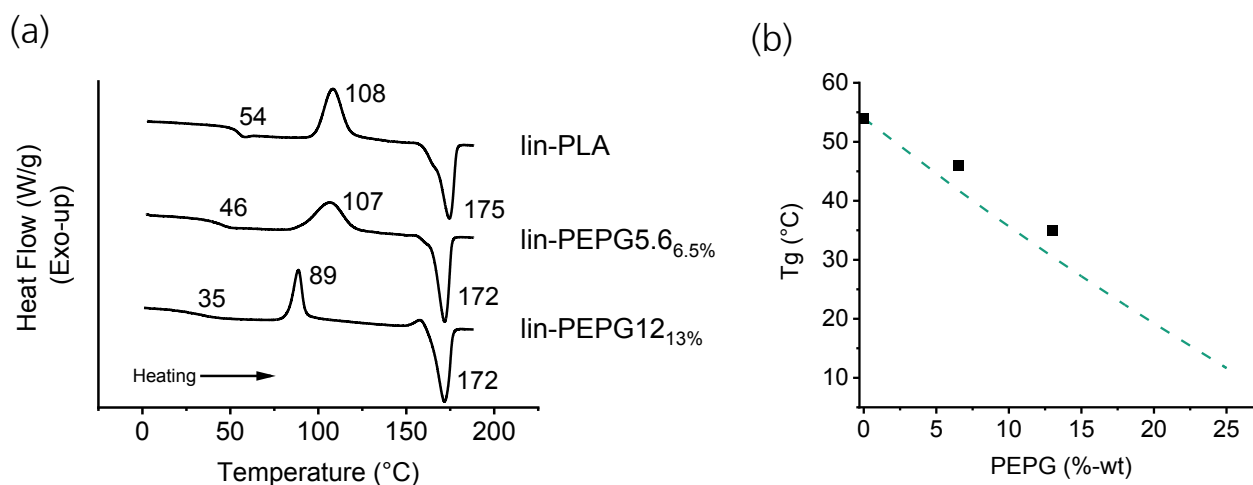
Figure 5.11: (a) Non-isothermal DSC thermograms (second heating cycle) of the lin-PLA reference and the synthesized linear PLLA-b-PEPG-b-PLLA block copolymers. (b) (■) Experimental and (-----) theoretical Tg values for different %-wt PEPG contents in the block copolymers. The theoretical Tg values were calculated using the Fox equation (Equation 2.9) and the measured Tg$_{PEPG}$ = - 70 °C.

As in the case of the PLLA-b-PEG-b-PLLA block copolymers shown in Section 5.1.1, the introduction of PEPG into the triblock copolymers seems to cause changes to the crystallization peaks of the block copolymers [Figure 5.2 (a) and Figure 5.11 (a)]. In both cases, the 6.5%-wt polyether content did not markedly reduce the peak Tc, however the crystallization peak became a bit broader suggesting that the crystallization onset is located at lower temperatures. The copolymers containing 13 %-wt content of PEPG and PEG blocks show a significantly reduced peak Tc on the non-isothermal DSC

measurements down to 89 °C and 85 °C, respectively. This contrasts with the lin-PLA homopolymer peak Tc of 108 °C. This increase of the crystallization rate can be better visualized through the isothermal crystallization kinetic experiments performed with the PEPG-initiated copolymers shown in Figure 5.12 (a).
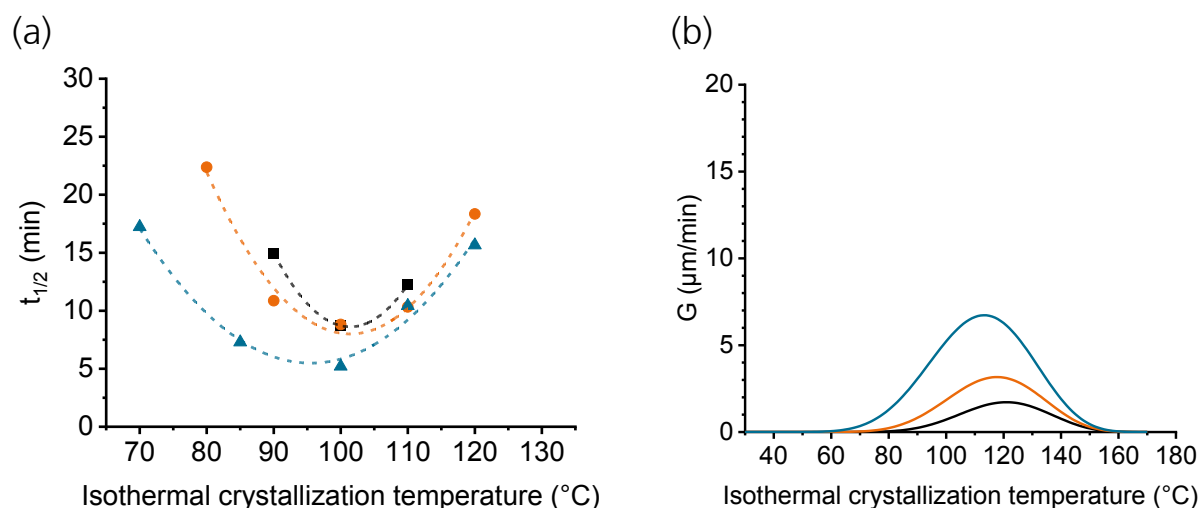
Figure 5.12: (a) Isothermal crystallization half-times ($t_{1/2}$) of the (■) lin-PLA homopolymer, (●) lin-PEPG5.6$_{6.5\%}$, (▲) and lin-PEPG12$_{13\%}$ block copolymers (left) and (b) the theoretical effect of the lower Tg on the spherulite radius growth rate (G) of the (——) lin-PLA homopolymer, (——) lin-PEPG5.6$_{6.5\%}$, (——) and lin-PEPG12$_{13\%}$ block copolymers at different isothermal crystallization temperatures using the empirical values obtained by Vasanthakumari et al. [112].

The isothermal crystallization DSC experiments show lower crystallization half time ($t_{1/2}$) values over most isothermal crystallization temperatures when comparing the lin-PEPG12$_{13\%}$ copolymer and the lin-PLA homopolymer especially at lower temperatures. The temperature of maximum crystallization rate (Tcr_{max}) of the lin-PEPG12$_{13\%}$ copolymer seems to be located at a slightly lower temperature than that of the lin-PLA homopolymer. However, more experiments are necessary to locate this temperature with more accuracy. At the Tcr_{max} of the lin-PLA homopolymer and the lin-PEPG5.6$_{6.5\%}$ triblock copolymer, the $t_{1/2}$ of both materials were very similar. At 90 °C however, the $t_{1/2}$ of the lin-PEPG5.6$_{6.5\%}$ triblock copolymer is close to 4 min lower suggesting a significantly faster crystallization rate. At 80 °C, the lin-PLA homopolymer did not show any exothermic crystallization signal within the 30 min allowed for isothermal crystallization. For this reason, the $t_{1/2}$ for this sample at 80 °C is expected to be significantly above 30 min and thus, much higher than the measured 23 min for the lin-PEPG5.6$_{6.5\%}$ copolymer sample crystallized at 80 °C.

Although more experimental data is needed for determining the parameters that describe how the PEPG blocks affect nucleation in the material using the Hoffman-Lauritzen equation (Equation 2.16), the theoretical effect of the lower Tg brought by the PEPG blocks is qualitatively analyzed in Figure 5.12 (b). Keeping all other parameters of the equation the same, the reduction of Tg in the Hoffman-Lauritzen equation caused the crystal radial growth rate to increase over the complete temperature

range. Additionally, a slight shift of the temperature of maximum crystal growth rate to lower temperatures can be observed. Taking these results into consideration, the faster crystallization kinetics of the PEPG-initiated triblock copolymers can be attributed to the improvement of chain transport brought about by the lower Tg caused by the presence of the PEPG plasticizing blocks. The relatively low Mn of the PLA blocks could also be the cause for the observed increase of crystallization kinetics. However, the increase of the crystallization rate was also observed in the blends prepared by Jia et al. using high molar mass PLA and PEPG12 [24].

The small exothermic peak observed at temperatures around 158 °C and 154 °C for both the lin-PEPG12$_{13\%}$ and the lin-PEG12$_{13\%}$ triblock copolymers, respectively, seems to be due to the lower temperature at which the crystals are formed. According to a series of studies [49; 186; 187], slightly different crystalline structures are obtained depending on the temperature at which PLA crystallizes. At temperatures below 100 °C, an α' metastable crystalline structure with conformational disorder and a loose-packing manner is believed to occur [186]. The more stable α crystalline structure with a slightly smaller crystal lattice structure is thought to occur when PLA crystallizes at temperatures above 120 °C [186]. If crystallization takes place between 100 °C and 120 °C, a mixture of both types of crystals is obtained [186]. To elucidate the cause for the observed exothermic peak in Figure 5.12 (a), a lin-PEPG12$_{13\%}$ triblock copolymer was isothermally crystallized at different temperatures, allowed to cool down to -20 °C, and heated again at 10 °C/min on DSC. The resulting changes of the endothermic melting peak are analyzed in Figure 5.13.
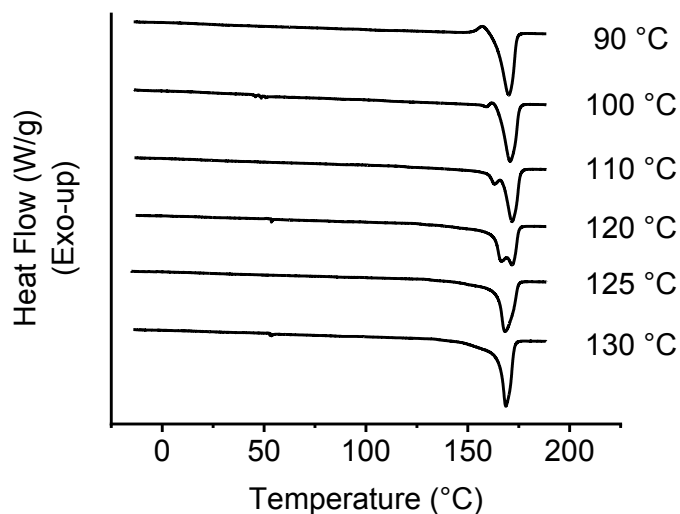
Figure 5.13: Non-isothermal heating ramp of a lin-PEPG12$_{13\%}$ triblock copolymer after isothermal crystallization at the given temperatures.

The shoulder to the left of the endothermic melting peak in the thermograms of the lin-PEPG12$_{13\%}$ triblock copolymer isothermally crystallized at 110 °C (Figure 5.13) has a similar shape as the melting peak of the lin-PLA homopolymer in Figure 5.11 (a), which exhibits crystallization during heating at a temperature close to 108 °C. This shoulder is explained by the α' to α transition in which some of the metastable α' crystals rearrange into the more stable α crystal lattice. Depending on the heating rate,

some of the α' fraction will directly melt while another fraction will directly undergo α' to α transition and subsequently melt as α crystals [186]. The fact that a lin-PEPG12$_{13\%}$ copolymer exhibits a similar melting behavior as the lin-PLA homopolymer, suggests that the exothermic peaks found before the melting peaks of both the lin-PEG12$_{13\%}$ and the lin-PEPG12$_{13\%}$ block copolymers are not directly caused by the triblock copolymer structure. Rather, the faster crystallization rate of the block copolymers with low Tg makes crystallization at T ≤ 110 °C possible even when heating at 10 °C/min in non-isothermal DSC measurements. Crystallization at this temperature preferentially produces the α' crystals that subsequently undergo the α' to α transition (exothermic shoulder peaks at T ~ 158 °C).

The changes in the crystallization (ΔHc) and melting enthalpies (ΔHm) of the block copolymers with increasing PEPG %-wt block content are summarized in Table 5.4. A reduction of the ΔHm is observed as the PEPG %-wt block content increases due to the reduced %-wt content of the crystallizing PLLA blocks. When looking at the ΔHm per gram of PLLA %-wt block content in the block copolymers (ΔHm$_{PLLA\ Blocks}$) however, a constant value of around 50.5 (± 0.7) J/g$_{PLLA\ Blocks}$ is observed. This suggests that the lower ΔHm values are due to only the lower PLLA content in the block copolymers and not to the PEPG blocks interfering with crystallite formation.

Table 5.4: Melt and cold crystallization enthalpies (during cooling and during heating) and melting enthalpies of the stereoregular lin-PLA homopolymer, lin-PEPG5.6$_{6.5\%}$, and lin-PEPG12$_{13\%}$ block copolymers. Used heating and cooling rates: 10 °C/min.

Block copolymer	ΔHc$_{Cooling}$ [J/g]	ΔHc$_{Heating}$ [J/g]	ΔHc$_{Total}$ [J/g]	ΔHm [J/g]	ΔHm$_{PLLA\ Blocks}$[6] [J/g$_{PLLA\ Blocks}$]
lin-PLA	1.4	47.6	49.0	49.8	49.8
lin-PEPG5.6$_{6.5\%}$	2.3	45.1	47.4	47.6	50.9
lin-PEPG12$_{13\%}$	8.0	34.2[7]	43.5	44.1[8]	50.7

As the PEPG block %-wt content in the copolymers was increased, a minor crystallization event could be detected during cooling at 10 °C/min (ΔHc$_{Cooling}$ in Table 5.4). This crystallization event likely results from the improved PLLA block transport promoted by the higher free volume in the block copolymers with higher PEPG content. As the PEPG content was increased, the ΔHc$_{Cooling}$ value also increased accordingly. The resulting sum of the ΔHc values during cooling and during heating (ΔHc$_{Total}$) roughly adds up to the measured ΔHm.

The observed mechanical properties (Figure 5.14 and Figure 5.15) of the PEPG-initiated copolymers followed a similar trend to the PEG-initiated ones suggesting an equally effective plasticizing effect of PEPG. As Tg of the block copolymers was reduced, the elastic modulus was reduced and the

---

[6] ΔHm$_{PLLA\ Blocks}$ refers to the melting enthalpy considering only the PLLA block %-wt content. ΔHm$_{PLLA\ Blocks}$ = ΔHm/(1 - X$_{PEPG}$)

[7] Peak integration limits chosen from a temperature below the exothermic crystallization peak with a stable baseline up to a temperature close to the α' to α transition exothermic peak where the heat flow value is close to the baseline heat flow value chosen before the exothermic crystallization peak.

[8] Substracted exothermic enthalpy of the α' to α transition peak (see Figure 5.13) to the endothermic melting peak.

elongation at break was increased up to a value of around 231 % for the lin-PEPG12$_{13\%}$. Yielding behavior and a strain hardening effect was observed for the lin-PEPG12$_{13\%}$ block copolymer.
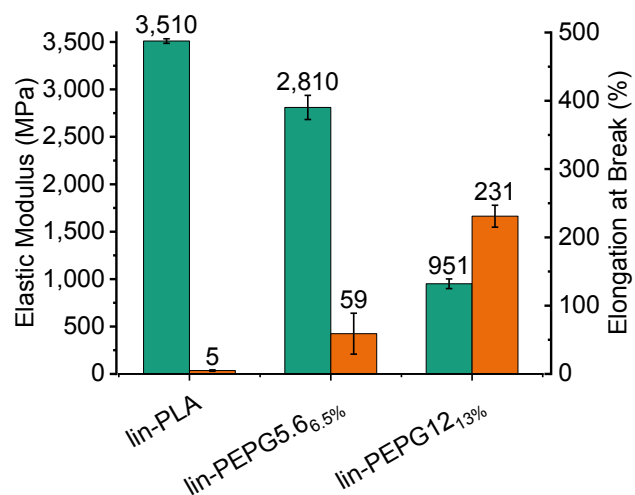
Figure 5.14: (■) Elastic modulus and (■) elongation at break of the PLLA-b-PEPG-b-PLLA block copolymer injection molded samples with different PEPG block length and %-wt content.
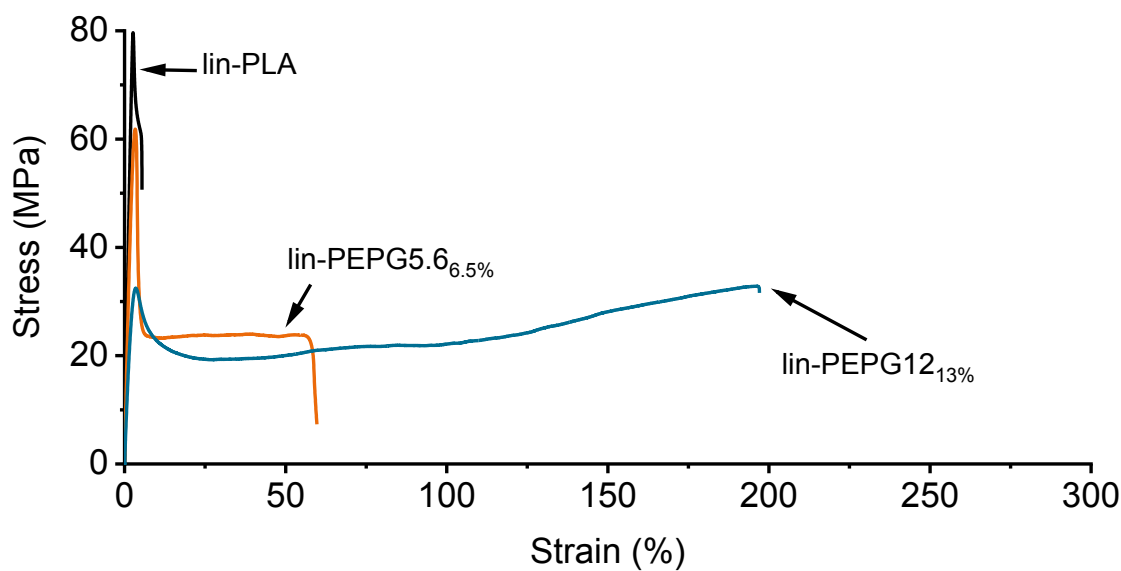
Figure 5.15: Stress strain curves of the performed PLLA-b-PEPG-b-PLLA block copolymer tensile tests.

5.1.4 Star PEPG20–initiated triblock copolymers

Until this point, all block copolymers were synthesized at the laboratory scale through initiation with polyethers containing two terminal –OH groups. This produced linear triblock copolymer structures with two outer PLLA blocks and a central polyether block. As shown on Table 3.1, PEPG20 is a tetrafunctional poly(ethylene glycol-co-propylene glycol) with a 4:1 EO to PO monomer ratio and Mn of 20 kDa. The higher molar mass of the PEPG20 initiator allows a significantly higher PEPG20 content to be introduced into the copolymers while maintaining a relatively high Mn, as discussed in Section 3. The tetrafunctionality of PEPG20 should theoretically yield block copolymers with a four arm symmetric star topology as shown in Figure 5.16 due to the chain growth mechanism of the ROP of lactide.
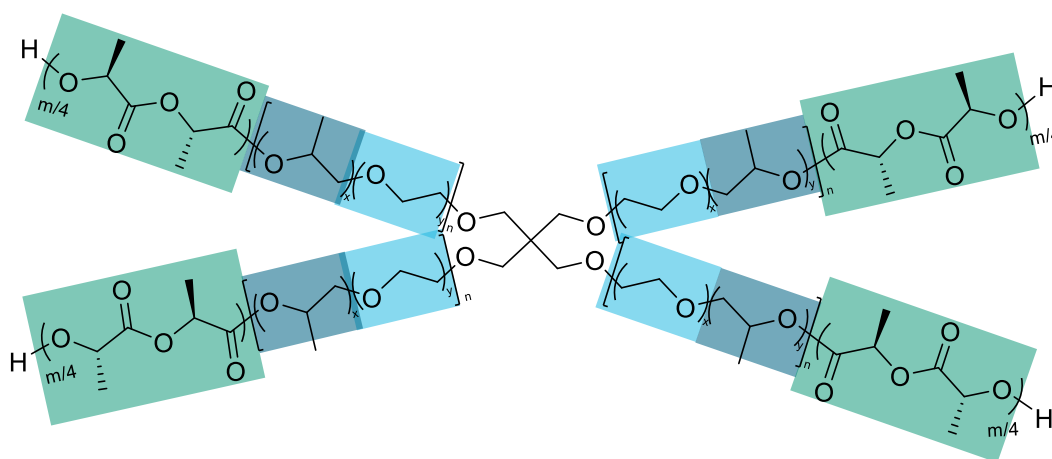
Figure 5.16: Expected chemical structure for the synthesized star PLLA>b-PEPG20-b<PLLA block copolymers.

Three different PEPG20-initiated block copolymers with varying PEPG20 content were produced using a $1 \cdot 10^{-4}$ mol_{Cat}/mol_{Lac} catalyst concentration as previously described in Section 4.2.1. Because the same PEPG20 initiator was used for all three synthesis, the total Mn of the different copolymers was expected to vary as shown on Table 5.5 below. The star topology was confirmed through oscillatory rheology measurements (Figure 5.30) and will be discussed in more detail in Section 5.2. As expected, the measured Mn_{H-NMR} of the star-PEPG20 copolymers decreased as the PEPG20 content was increased. The copolymer containing 18 %-wt PEPG20 had a Mn of 68 kDa, which is comparable to the Mn of the previously discussed linear copolymers (Sections 5.1.1 – 5.1.3). The copolymer containing a 13 %-wt PEPG20 block content, had a significantly higher Mn than its homologous lin-PEPG12$_{13\%}$ block copolymer at the same plasticizing polyether block %-wt content.

Table 5.5: Measured Mn values of the star PLLA-b-PEPG20-b-PLLA block copolymers synthesized at laboratory scale with varying PEPG20 block content.

Initiator	Expected block copolymer structure	PEPG block content [%-wt]	Copolymer name	Theoretical Mn [kDa]	Mn (^{1}H-NMR) [kDa]
PEPG12	PLLA-b-PEPG12-b-PLLA	13	lin-PEPG12$_{13\%}$	92	71
PEPG20	PLLA>b-PEPG20-b<PLLA	13	star-PEPG20$_{13\%}$	154	108
PEPG20	PLLA>b-PEPG20-b<PLLA	15	star-PEPG20$_{15\%}$	133	87
PEPG20	PLLA>b-PEPG20-b<PLLA	18	star-PEPG20$_{18\%}$	111	68

As the PEPG20 content was increased, the Tg was reduced from 34 °C for the star-PEPG20$_{13\%}$ block copolymer to 24 °C for the star-PEPG20$_{18\%}$ copolymer [Figure 5.17 (a)]. Good miscibility of the PEPG20 plasticizing blocks in the PLLA matrix can be implied (in spite of the relatively high Mn of the PEPG20 blocks) due to the agreement of the experimentally measured Tg and the calculated Tg (using the Fox equation) for the different PEPG20 %-wt block contents in the copolymers [Figure 5.17 (b)]. The lower measured Tg values led to lower Tc values as shown in Figure 5.17 (a). In all cases, the exothermic α' to α transition peak (Section 5.1.3) prior to melting was observed due to the low Tc values below 100 °C.
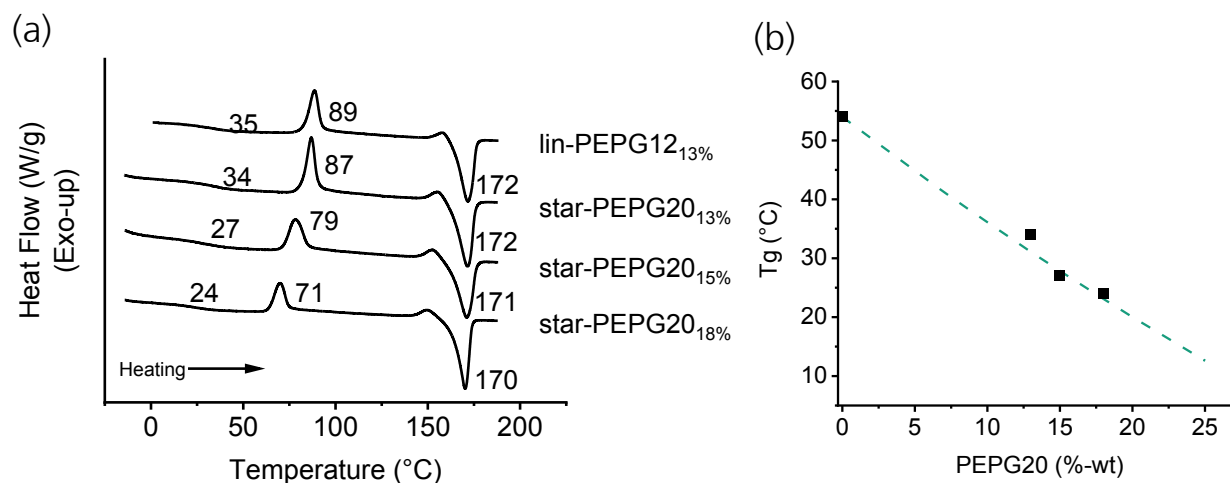
Figure 5.17: (a) Non-isothermal DSC thermograms (second heating cycle) of the lin-PLA reference and the synthesized star PLLA-b-PEPG20-b-PLLA block copolymers. (b) (■) Experimental and (-----) theoretical Tg values for different %-wt PEPG20 contents in the block copolymers. The theoretical Tg values were calculated using the Fox equation (Equation 2.9) and the measured Tg$_{PEPG20}$ = - 66 °C.

Interestingly, no major changes of the non-isothermal DSC curve were detected when comparing the star-PEPG20$_{13\%}$ and the lin-PEPG12$_{13\%}$ block copolymers, even with the star topology and significantly higher Mn of the star-PEPG20$_{13\%}$ block copolymer. This suggests that the PEPG20 macroinitiator had a similar plasticizing effect to the PEPG12 even with its slightly different chemical structure, its higher molar mass, and its tetrafunctional structure. The crystallization kinetics seem to be more strongly

defined by the plasticizer content and the Mn of the PLLA blocks which in the case of star-PEPG20$_{13\%}$ and lin-PEPG12$_{13\%}$ are both practically the same (13 %-wt plasticizer and around 30 kDa PLLA blocks).

The measured reduction of Tg by increasing the PEPG20 block content, resulted in the further decrease of the elastic modulus and increase of the elongation at break of the materials. The star-PEPG20$_{18\%}$ copolymer with a Tg practically at the testing temperature of 23 °C, shows a very smooth transition from the yield point into the strain hardening portion of the stress strain curve. This suggests that a relatively low energy barrier must be overcome for the polymer chains to begin to "flow" under the applied stress. Through the introduction of an 18 %-wt PEPG20 block content, the elongation at break could be increased to a value of 283 % (Figure 5.18) which is significantly higher to the values of around 220 - 236 % measured for the block copolymers with a 13 %-wt content of miscible polyether blocks (i.e. lin-PEG12$_{13\%}$, lin-PEPG12$_{13\%}$, lin-PEPG12$_{13\%}$DLac$_{4\%}$ and star-PEPG20$_{13\%}$). Consequently, the elastic modulus was reduced to a value of around 506 MPa.
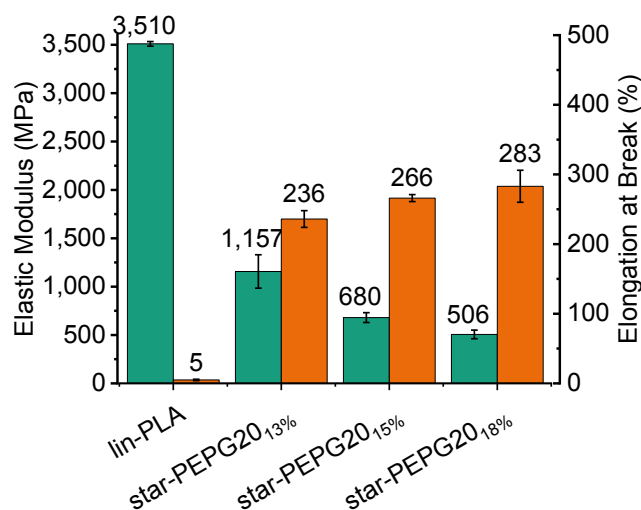
Figure 5.18: (■) Elastic modulus and (■) elongation at break of the star PLLA>b-PEPG20-b<PLLA block copolymer injection molded samples with equal PEPG20 block length, but different %-wt PEPG20 block content and different total block copolymer Mn.
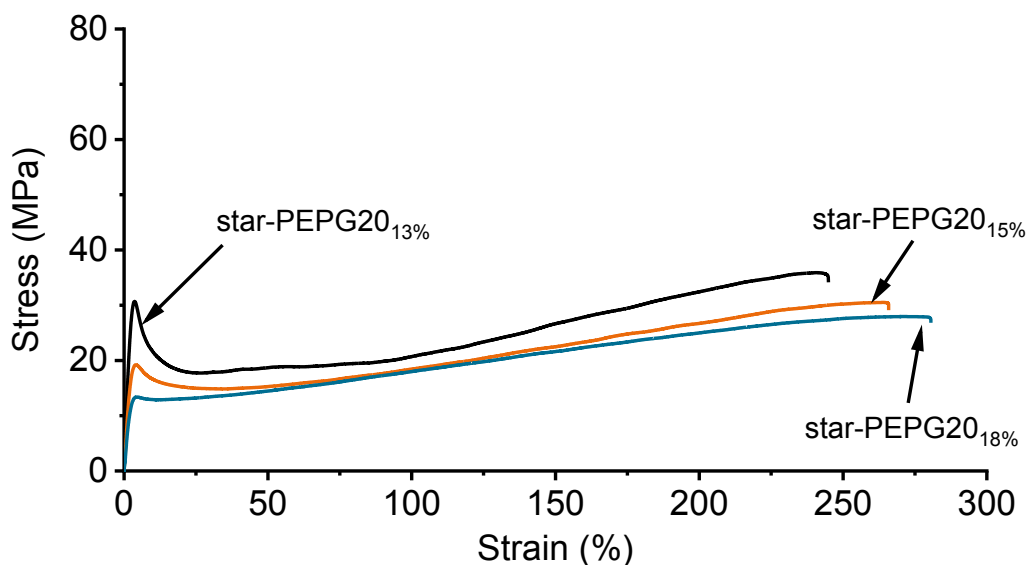
Figure 5.19: Stress strain curves of the performed star PLLA-b-PEPG20-b-PLLA block copolymer tensile tests

5.1.5 PEPG–initiated triblock copolymers modified with D-lactide comonomer

Three block copolymers with increasing D-lactide repeat unit contents, a constant 13 %-wt PEPG12 polyether block content, and a $1 \cdot 10^{-4}$ $mol_{Sn(Oct)2}/mol_{Lactide}$ catalyst concentration were synthesized at the laboratory scale (Table 5.6). The D-lactide %-mol contents (X_D) listed in Table 5.6, refer to the D-lactide moles introduced into the reaction mixture with respect to the total number of lactide moles (L- and D- lactide together). The number of D-lactide units that are actually present in the PLLA blocks of the copolymers may differ to the values given on Table 5.6 due to racemization during the ROP. However, in the ROP of lactide in the presence of $Sn(Oct)_2$ catalyst racemization is expected to be below 1 % [27] and a similar degree of racemization is expected for all block copolymers. For these reasons, no further analytical tests were done to monitor the exact content of D-lactide repeat units in the PLLA blocks.
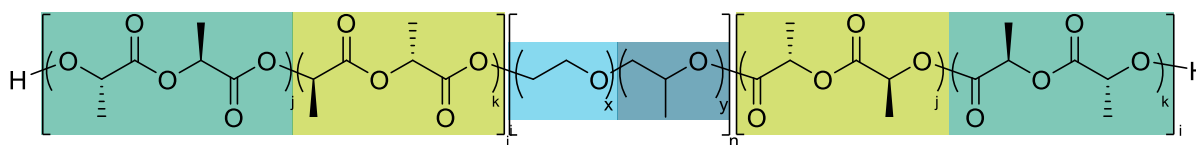
Figure 5.20: Expected chemical structure for the synthesized linear PLLA(co-DLac)-b-PEPG-b-PLLA(co-DLac) block copolymers.

Table 5.6: Theoretical Mn of the synthesized (in laboratory scale) PLLA(co-DLac)-b-PEPG12-b-PLLA(co-DLac) block copolymers with varying D-lactide content.

Initiator	Expected block copolymer structure	PEPG block content [a]	D-lactide content[b]	Copolymer name	Mn_{Theo}
		[%-wt]	[%-mol]		[kDa]
PEPG12	PLLA(co-DLac)-b-PEPG12-b-PLLA(co-DLac)	13	2.5	lin-PEPG12$_{13\%}$DLac$_{2.5\%}$	91
PEPG12	PLLA(co-DLac)-b-PEPG12-b-PLLA(co-DLac)	13	4	lin-PEPG12$_{13\%}$DLac$_{4\%}$	91
PEPG12	PLLA(co-DLac)-b-PEPG12-b-PLLA(co-DLac)	13	5	lin-PEPG12$_{13\%}$DLac$_{5\%}$	91

[a] Confirmed by ^{1}H-NMR measurement. [b] D-lactide content introduced into the reaction mixture (%-mol of total lactide content).

Non-isothermal DSC measurements (Figure 5.21) of the block copolymers containing D-lactide repeat units do not show a clear reduction of the Tg as X_D was increased from 0 to 5 %-mol. At first glance, this seems to contradict the findings of Saeidlou et al. [188], who found a relatively weak dependence between X_D and Tg in PLLA polymers (Equations 5.1 – 5.3).

$$T_g(Mn) = T_g(M \rightarrow \infty) - \frac{A}{Mn}$$

Eq. 5.1

$$T_g(M \rightarrow \infty) = \frac{13.36 + 1371.68 \cdot X_D}{0.22 + 24.3 \cdot X_D + 0.42 \cdot X_D{}^2}$$

Eq. 5.2

$$A = 52.23 + 791 \cdot X_D$$

Eq. 5.3

According to Equation 5.1 from [188], a Tg reduction from 58.5 °C to 56.3 °C is expected when increasing X_D from 0 to 30 %-mol in a PLLA polymer of Mn = 100 kDa. For a PLLA polymer (Mn = 100 kDa) and with an X_D of 5 %-mol, Tg would reduce by 1.4 °C when compared to a stereopure PLLA polymer (X_D = 0 %-mol) according to Equation 5.1. Such a small difference could have been missed in the DSC measurements performed on the PLLA(co-DLac)-b-PEPG12-b-PLLA(co-DLac) copolymers (Figure 5.21) due to the limited precision of the instrument. This could explain why the measured Tg of the synthesized block copolymers stayed practically constant with increasing X_D. To detect such small changes of Tg by DSC, a more elaborate measurement scheme would likely be necessary to ensure that the synthesized block copolymers are completely amorphous before the DSC heating ramp and a statistical approach comparing obtained data from several measurements could prove to be necessary. In any case, for the present study, such a small variation of Tg was considered to have negligible effects on the mechanical or rheological properties, which are the focus of this thesis. For this reason, no further experimental steps were taken to clarify the changes in Tg caused by increasing X_D.
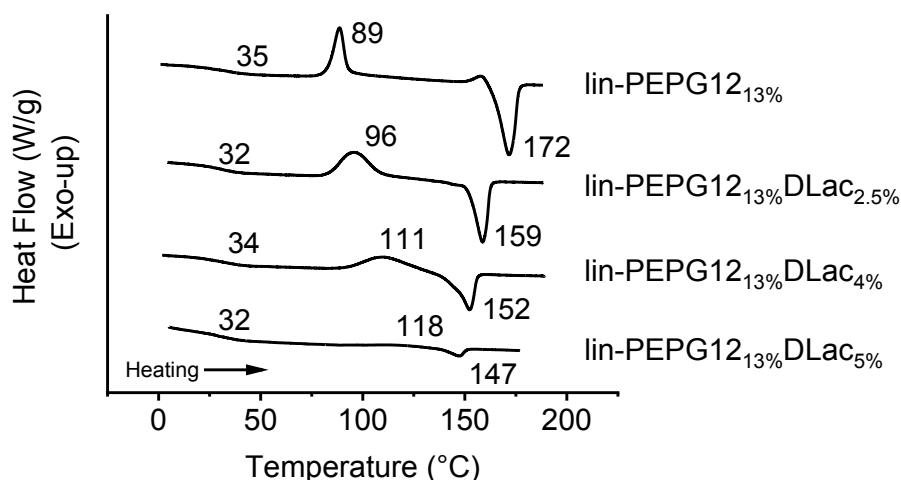
Figure 5.21: DSC thermograms (second heating cycle) showing the effect of the D-lactide content on the thermal properties of the lin-PEPG12$_{13\%}$ block copolymers.

When analyzing the effect of X_D on the peak Tm of the block copolymers (Figure 5.21), a reduction of almost 5 °C for each 1 %-mol of D-lactide comonomer used for the ROP synthesis was measured. This follows the behavior expected by the Flory equation (Equation 2.14). It is in agreement to the 5 °C reduction of the peak Tm per 1 %-mol D-lactide content reported for PLA polymers with varying X_D [105–107]. Additionally, a reduction of the melting enthalpy (ΔHm) of the synthesized block copolymers was observed as X_D was increased (Table 5.7). This suggests that that the maximum degree of crystallinity that can be obtained in such block copolymers decreases as X_D is increased.

The non-isothermal DSC measurements in Figure 5.21 show that higher X_D in the block copolymers increases the peak Tc of the block copolymers at a rate of 5.9 °C per 1 %-mol of D-lactide introduced into the reaction mixture. This increase in Tc can be attributed to the higher energy barrier required to form stable nuclei due to the presence of the D-lactide repeat units in the PLLA blocks, which interrupt crystal formation. Further crystallization kinetic experiments done on similar block copolymers are presented in more detail on Section 5.3.2. They revealed a significant decrease of the crystallization rate of the block copolymer with an X_D of 4 %-mol when compared to a similar one with an X_D of 0 %-mol.

Table 5.7: Crystallization (ΔHc) and melting (ΔHm) enthalpies of lin-PEPG12$_{13\%}$ block copolymers with increasing D-lactide content. The block copolymers were cooled from the molten state at 10 °C/min.

Block copolymer	ΔHc$_{Cooling}$ [J/g]	ΔHc$_{Heating}$ [J/g]	ΔHc$_{Total}$ [J/g]	ΔHm [J/g]
lin-PEPG12$_{13\%}$	8.0	34.2	43.5	44.1[9]
lin-PEPG12$_{13\%}$DLac$_{2.5\%}$	-	35.8	35.8	35.9
lin-PEPG12$_{13\%}$DLac$_{4\%}$	-	25.3	25.3	26.3
lin-PEPG12$_{13\%}$DLac$_{5\%}$	-	4.0	4.0	4.2

Table 5.7 summarizes the effects of increasing X_D in the PLLA blocks of the PLLA(DLac)-b-PEPG12-b-PLLA(DLac) block copolymers on ΔHc and ΔHm. As expected, increasing X_D reduced ΔHm to a value of 4.2 J/g for the lin-PEPG12$_{13\%}$DLac$_{5\%}$ block copolymer, even with the improved transport caused by a 13 %-wt PEPG12 block content. The relatively drastic reduction of ΔHm from 26.3 J/g for the lin-PEPG12$_{13\%}$DLac$_{4\%}$ block copolymer to only 4.2 J/g for the lin-PEPG12$_{13\%}$DLac$_{5\%}$ block copolymer, suggests that the crystallization rate of the lin-PEPG12$_{13\%}$DLac$_{5\%}$ block copolymer is much slower. Industrially, PLA pellets are usually pre-crystallized to allow drying of the pellets at temperatures above the Tg of PLA [189]. Drying of amorphous pellets above Tg is not possible due to sticking and agglomeration of the pellets in the rubbery state. Lower crystallization times are desired to reduce residence time or equipment size required for industrial operations. For this reason, the 5 %-wt D-lactide comonomer content could be industrially unfeasible.

The mechanical properties measured on injection molded tensile test samples of the lin-PEPG12$_{13\%}$ and the lin-PEPG12$_{13\%}$DLac$_{4\%}$ block copolymers are shown in Figure 5.18. The measured elongation at break values for both block copolymers were found to be virtually the same (~ 230 %), while the measured elastic moduli varied slightly. The similar elongation at break values were expected due to the similar Tg measured for both block copolymers. The slightly lower elastic modulus measured for the lin-PEPG12$_{13\%}$DLac$_{4\%}$ block copolymer is likely caused by the slightly lower degree of crystallinity present in its injection molded tensile test samples. As both block copolymers were injected as a melt (T = 185 °C) into a mold at a temperature of 20 °C, the cooling rate experienced by both samples can be considered equal. As shown in Table 5.7, however, the lin-PEPG12$_{13\%}$ block copolymer seems to show significant amounts of crystallization at a cooling rate of 10 °C/min, while lin-PEPG12$_{13\%}$DLac$_{4\%}$ practically does not crystallize at these conditions.

The cooling rate during the injection molding process varies significantly depending on the location in the sample. At the surface of the test sample, the cooling rate is significantly higher than 10 °C/min. In the nucleus of the sample, however, the cooling rate is quite slow due to the thermal resistance posed by the outer layer of the polymer itself. The slower cooling rate at the center of the sample could lead to some crystallization of the lin-PEPG12$_{13\%}$ block copolymer during the injection molding procedure. This crystallization during cooling could be absent during the cooling of the lin-PEPG12$_{13\%}$DLac$_{4\%}$ block copolymer due to its slower crystallization rate. The lower degree of

---

[9] Substracted enthalpy of the α′ to α transition peak (described in Section 5.1.3) to the melting peak.

crystallinity of the lin-PEPG12$_{13\%}$DLac$_{4\%}$ tensile test sample could explain its slightly lower elastic modulus. A more detailed DSC and X-ray analysis of the tensile test samples would be required to confirm this.
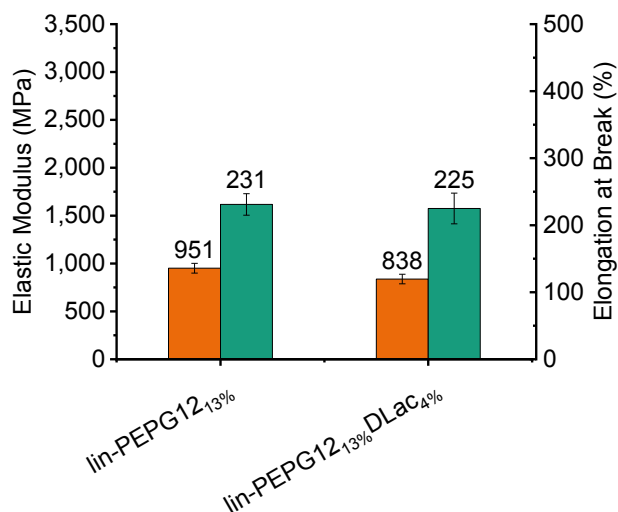
Figure 5.22: Effect of the %-wt D-lactide comonomer content on the (■) elastic modulus and (■) elongation at break of the linear PLLA(DLac)-b-PEPG-b-PLLA(DLac) block copolymers.

5.1.6 PEPG–initiated triblock copolymers modified with ε-caprolactone comonomer

Three linear copolymers with a constant PEPG12 macroinitiator content of 13 %-wt and varying %-mol ε-caprolactone (CL) comonomer content (X_{CL}) were synthesized at the laboratory scale in the presence of $1 \cdot 10^{-4}$ mol$_{Sn(Oct)2}$/mol$_{Lactide}$ as described in Section 4.2.1. The CL comonomer was added directly with the L-lactide monomer and the PEPG12 macronitiator into the reactor before the start of the ROP. The expected block copolymer structure (Figure 5.23 consists) of a central PEPG12 block and two outer PLLA blocks with different X_{CL} embedded in the PLLA blocks.
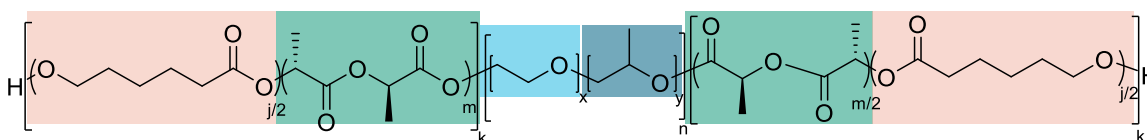
Figure 5.23: Expected chemical structure of the synthesized linear PLLA(co-CL)-b-PEPG12-b-PLLA(co-CL) block copolymers.

Table 5.8: Measured Mn values and ROP reaction times for the linear PLLA(co-CL)-b-PEPG12-b-PLLA(co-CL) block copolymers with constant PEPG12 block content and varying CL comonomer content in the PLLA blocks.

Block copolymer name	X_{CL} in rxn. mixture	Reaction time	Mn (^{1}H-NMR)	PEPG12 block content [a]	X_{CL} in copolymer (^{1}H-NMR)
	[%-mol]	[min]	[kDa]	[%-wt]	[%-mol]
lin-PEPG12$_{13\%}$CL$_{2\%}$	3	22	143	13	1.6
lin-PEPG12$_{13\%}$CL$_{4\%}$	8	25	114	13	4.0
lin-PEPG12$_{13\%}$CL$_{13\%}$	17	56	111	13	13.1

[a] Confirmed by ^{1}H-NMR.

The non-isothermal DSC curves measured for each of the block copolymers [Figure 5.24 (a)] show a similar effect of increasing X_{CL} in the PLLA blocks as when increasing X_D (Section 5.1.4). A reduction of the peak Tm was observed in accordance to the discussion in Section 2.2.1 with a corresponding increase of the peak Tc as X_{CL} was increased. The increase of the peak Tc in the PLLA(co-CL)-b-PEPG12-b-PLLA(co-CL) block copolymers, however, is significantly less pronounced than for the PLLA(co-DLac)-b-PEPG12-b-PLLA(co-DLac) block copolymers. When comparing the peak Tc of the lin-PEPG12$_{13\%}$DLac$_{4\%}$ (Tc = 111 °C) and the lin-PEPG12$_{13\%}$CL$_{4\%}$ (Tc = 96 °C) block copolymers, a lower peak Tc for the lin-PEPG12$_{13\%}$CL$_{4\%}$ copolymer is observed. This is likely due to the increased free volume and improved chain transport to the crystallization sites in the lin-PEPG12$_{13\%}$CL$_{4\%}$ block copolymer. This can be inferred by considering the significantly lower Tg of 23 °C of the lin-PEPG12$_{13\%}$CL$_{4\%}$ block copolymer than that of the lin-PEPG12$_{13\%}$DLac$_{4\%}$ copolymer (34 °C).

The reduction of Tg with increasing X_{CL} in the block copolymers can be explained by the high bond flexibility and mobility of the CL comonomer repeating units as discussed in section 2.2.1. The Tg of high molar mass PCL (-72 °C) is similar to the Tg of the used PEPG12 polyether macroinitiator (-70 °C). When these values are introduced into the Fox equation (Equation 2.9), a similar reduction of the Tg can be expected per %-wt content of CL comonomer as per %-wt of PEPG12 block content. The theoretical reduction of the Tg as a function of X_{CL} while keeping a constant PEPG12 block content of 13 %-wt as calculated with the Fox equation, is shown by the dashed line in Figure 5.24 (b).
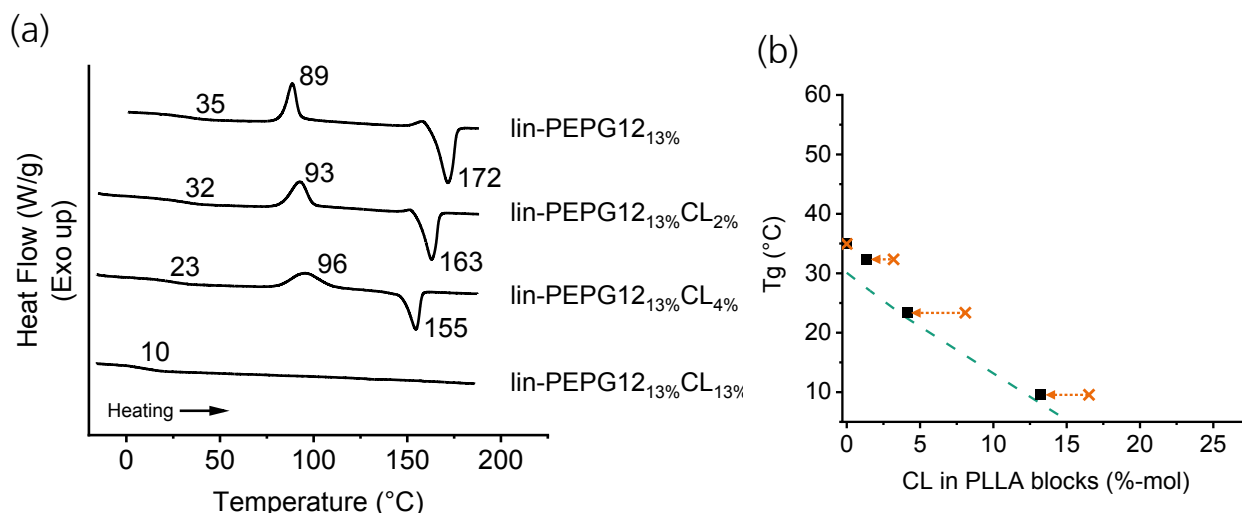
Figure 5.24: (a) Non-isothermal DSC thermograms (second heating cycle) of the lin-PLA reference and the star PLLA(co-CL)-b-PEPG12-b-PLLA(co-CL) block copolymers. (b) (■) Experimental, (✕) expected according to the CL content in the reaction mixture, and (-----) theoretical Tg values for block copolymers of varying X_{CL}. The theoretical Tg values were calculated using the Fox equation (Equation 2.9) and the measured Tg_{PEPG12} = -70 °C and Tg_{CL} = -70 °C.

When plotting the measured Tg values in Figure 5.24 (b) using the X_{CL} contents as added into the reaction mixture (✕ symbols), a significant deviation from the values expected from the Fox equation (dashed line) can be observed. Further ^{1}H-NMR analysis showed that there had been incomplete conversion of the CL comonomer units and that significantly lower CL units were covalently bonded into the PLA blocks than the X_{CL} that was introduced into the reaction mixture. The unreacted CL comonomer that remained in the block copolymer after the reaction was removed during the demonomerization procedure in the vacuum oven, and thus, the Tg of the lin-PEPG12$_{13\%}$CL copolymers were significantly higher than what was predicted by the Fox equation.

As an example, 8 %-mol CL content was introduced into the reaction mixture for the synthesis of the lin-PEPG12$_{13\%}$CL$_{4\%}$ copolymer. For such an X_{CL} of 8 %-mol (introduced into the reaction mixture), a Tg of 15.5 °C would be expected according to the Fox equation. The experimental Tg for the synthesized block copolymer, however, had a value of 23 °C. This would actually correspond to a X_{CL} of around 3.8 %-mol in the copolymer. ^{1}H-NMR analysis shows that the lin-PEPG12$_{13\%}$CL$_{4\%}$ copolymer actually had an X_{CL} of 4 %-mol covalently bonded to the PLLA blocks, which is much closer to the predicted value by the Fox equation. When adjusting the correct covalently bonded X_{CL} to the PLLA blocks as measured by ^{1}H-NMR (Table 5.8), a closer agreement with the Fox equation predictions is observed with the (■) symbols in Figure 5.24 (b).

The incomplete conversion of the CL comonomer was caused by the significantly slower reaction rate of the CL comonomer when compared to that of the L-lactide monomer, as also observed in many studies [166; 167; 170; 171]. The block copolymers synthesized initially with only a 4 and 10 %-wt CL comonomer content in the respective reaction mixtures only achieved around a 50 % conversion of the CL monomer in 22 and 25 min, respectively. When the reaction time was increased to 56 min for the synthesis of the lin-PEPG12$_{13\%}$CL$_{13\%}$ block copolymer, CL conversion was increased to around 80 %. For these syntheses, the ROP reaction times were determined by monitoring the torque

measured at the motor coupled to the mechanical stirrer used for mixing the reaction mixture. As mentioned in Section 4.2.1, reaching a stable plateau of the torque was the criteria for ending the ROP reaction and releasing the synthesized block copolymers. The lin-PEPG12$_{13\%}$CL$_{13\%}$ block copolymer required 56 min to reach a stable plateau, and thus, the copolymerization reached a much higher CL conversion than copolymers lin-PEPG12$_{13\%}$CL$_{2\%}$ and lin-PEPG12$_{13\%}$CL$_{4\%}$. This could be due to the higher contribution that the X_{CL} of 13 %-mol had on the Mn (and thus the viscosity) of the lin-PEPG12$_{13\%}$CL$_{13\%}$ block copolymer when compared to the smaller contribution of the X_{CL} in the lin-PEPG12$_{13\%}$CL$_{2\%}$ and lin-PEPG12$_{13\%}$CL$_{4\%}$ block copolymers. In the latter cases, such low X_{CL} values could have a negligible effect on the viscosity of the block copolymers considering the amount of free volume that they simultaneously introduce into the block copolymer melt (considering the VFTH equation - Equation 2.6).

To investigate the different reactivities of the L-lactide and the ε-caprolactone comonomers, a mixture containing 13 %-wt PEPG20 macronitiator and 8.1 %-mol CL comonomer content was polymerized according to the procedure in Section 4.2.1. Samples were taken 26, 56, and 82 min after the start of the reaction to monitor the CL conversion over time via ^{1}H-NMR measurements. The torque measurements and the X_{CL} covalently bonded to the PLLA blocks are shown in Figure 5.25 (a). The conversions of the monomers during the same reaction are shown in Figure 5.25 (b).
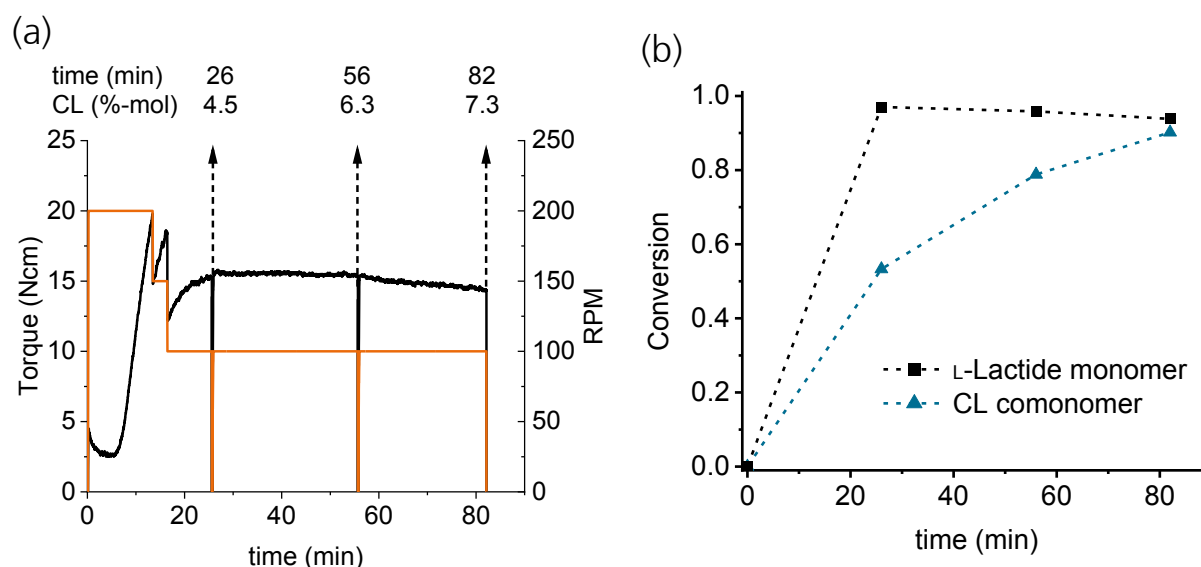
Figure 5.25: (a) covalently bonded %-mol CL comonomer content in the PLLA blocks of star-PEPG20$_{13\%}$CL$_{7\%}$ block copolymer at different times during the ROP synthesis. An X_{CL} of 8.1 %-mol was introduced into the ROP reaction mixture. The measured (——) torque (N·cm) and (——) Stirrer speed (RPM) are shown as reference. (b) L-lactide monomer and CL comonomer conversion during the ROP of the star-PEPG20$_{13\%}$CL$_{7\%}$ block copolymer as measured by ^{1}H-NMR.

The reactants were stirred at 200 RPM at the beginning of the reaction to ensure good mixing of the PEPG20 macroinitiator, Sn(Oct)$_2$ catalyst, L-lactide monomer, and CL comonomer. Initially a strong torque increase is observed, indirectly indicating an increase of the copolymer molar mass. At around t = 26 min, a first sample was extracted from the reactor to simulate the reaction time used for the synthesis of the lin-PEPG12$_{13\%}$CL$_{4\%}$ copolymer. The ^{1}H-NMR spectrum of the collected sample showed a 4.5 %-mol content of covalently bonded CL comonomer in the PLLA blocks, similarly to what was

observed in the lin-PEPG12$_{13\%}$CL$_{4\%}$ block copolymer synthesis. A second sample collected at t = 56 min, showed further integration of the CL monomer (up to an X$_{CL}$ of 6.3 %-mol) into the PLLA blocks, while after 82 min the reaction product had a total X$_{CL}$ of 7 %-mol bonded to the PLLA blocks. As shown on the conversion graph in Figure 5.25 (b), the maximum L-lactide monomer conversion (up to the equilibrium lactide concentration ~ 94 %) was achieved already after only 26 min of reaction, while the CL comonomer showed a similar conversion (~ 90 %) after 82 min.

The observed differences in reaction rates of L-lactide and CL are expected to lead to a given degree of "blockiness" within the PLLA blocks of the synthesized PLLA(co-CL)-b-PEPG12-b-PLLA(co-CL) copolymers [168; 169]. This can be observed when comparing the peak Tm of the lin-PEPG12$_{13\%}$CL$_{4\%}$ and of the lin-PEPG12$_{13\%}$DLac$_{4\%}$ block copolymers. Both block copolymers contain a 4 %-mol comonomer (CL and D-Lactide) content that interrupts crystallization. According to Equation 2.14, both of these block copolymers should reduce the peak Tm to a similar value of 152 °C. The peak Tm of the lin-PEPG12$_{13\%}$CL$_{4\%}$ block copolymer, however, is significantly higher (Tm = 163 °C) than that of the lin-PEPG12$_{13\%}$DLac$_{4\%}$ one (Tm = 152 °C). This could be due to relatively long sequences of uninterrupted CL repeat units (blockiness) in the lin-PEPG12$_{13\%}$CL$_{4\%}$ block copolymer caused by the difference in reactivity of the two monomers used, which does not occur for the lin-PEPG12$_{13\%}$Dlac$_{4\%}$ block copolymer. The blockiness gives the CL comonomer fewer chances to interrupt the growing crystals, thus reducing the Tm to a lesser degree than the D-lactide comonomer. The D-lactide comonomer is statistically distributed along the PLLA blocks and is more likely to interrupt the crystal growth, leading to a bigger reduction of the Tm.

The DSC thermograms of the lin-PEPG12$_{13\%}$CL$_{4\%}$ and the star-PEPG20$_{13\%}$CL$_{7\%}$ block copolymers (Figure 5.26) show a significantly lower peak Tm and a higher peak Tc for the copolymer with a higher X$_{CL}$. These changes in the thermal properties are the expected effects of increasing X$_{CL}$, which confirms the X$_{CL}$ values obtained by ^{1}H-NMR analysis.
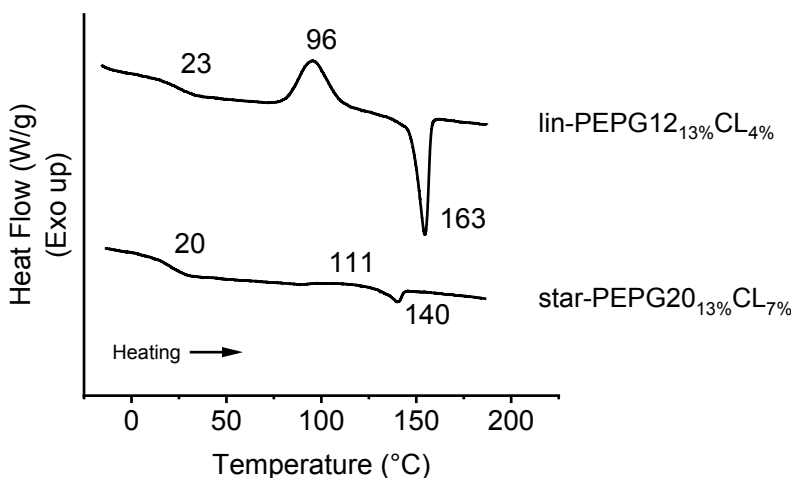
Figure 5.26: DSC thermograms of block copolymers synthesized from a reaction mixture containing 13 %-wt polyether macroinitiator and an X$_{CL}$ of 8.1 %-mol with different CL conversions.

The different block copolymers shown in this section with varying X$_{CL}$, allowed their Tg to be varied from 35 °C to 10 °C (Figure 5.24). Thus, the synthesized block copolymers make it possible to analyze the change in the tensile behavior of the materials with Tg values above, at, and below the T$_{Meas}$

(23 °C). As discussed in Section 2.2.1, this should cause the tensile behavior of the copolymers to go from a relatively stiff and tough material (Table 2.3, graph B) at Tg > T_{Meas} to a soft and flexible material (Table 2.3, graph C) at Tg < T_{Meas}. This change in behavior can be observed when looking at the stress-strain tensile test curves of the block copolymers containing CL as a comonomer (Figure 5.27). As Tg of the block copolymers approaches the measurement temperature of 23 °C, the peak at the yield point becomes less pronounced. The "yield" peak practically disappears in the tensile test stress-strain curves of the block copolymers with Tg values below the measurement temperature of 23 °C. This reflects the reduced energy barrier required to cause the polymer chains to begin to exhibit viscous behavior or "flow" as the free volume available in the materials with lower Tg values is increased.
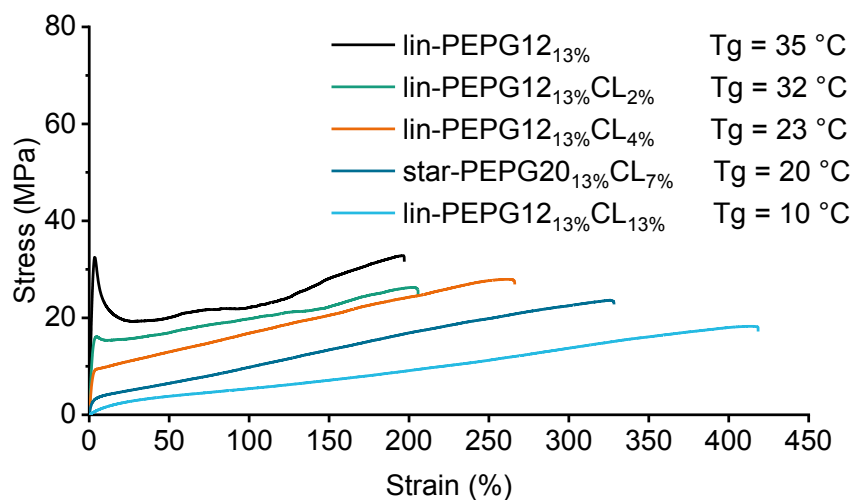
Figure 5.27: Stress-strain tensile test curves (injection-molded samples) of the block copolymers containing PEPG blocks and CL comonomer embedded in the PLLA chains.

The increase of the free volume in the block copolymers allowed the elastic modulus to be reduced from 951 MPa for the lin-PEPG12$_{13\%}$ block copolymer to 17 MPa for the lin-PEPG12$_{13\%}$CL$_{13\%}$ copolymer (Figure 5.28). This reduction in elastic modulus came with an increase of the elongation at break from 231 % for the lin-PEPG12$_{13\%}$ block copolymer to 404 % for the lin-PEPG12$_{13\%}$CL$_{13\%}$ copolymer.

The degree of polymerization of the block copolymers with X_{CL} is theoretically defined by the monomer (in this case L-lactide and CL) divided by the –OH initiator group concentration as defined by Equation 2.2. This means that higher X_{CL} values in the copolymers do not heavily affect the Mn of the block copolymer (given that a high CL comonomer conversion is achieved). Only a slight reduction of the PLLA block Mn is expected due to the different molar masses of L-lactide (144 g/mol) and CL (114 g/mol). For a DP of 550 for example, the difference in Mn of a PLLA block caused by an X_{CL} of 8 %-mol compared to using only L-lactide in the ROP would be of only around -1.7 kDa. Thus, different from using higher PEPG contents as a plasticizing agent in the block copolymers, introduction of CL as a comonomer plasticizes the copolymer without significantly changing its degree of polymerization. This is relevant for the rheological properties, as will be further discussed in Section 2.3.5.
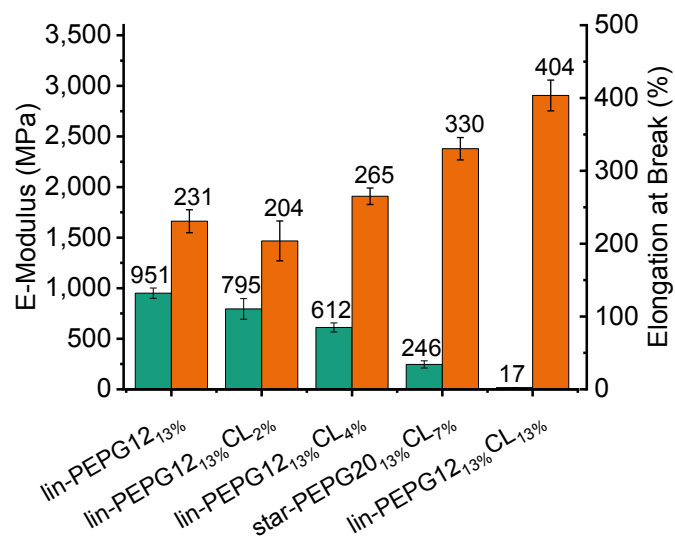
Figure 5.28: (■) Elastic modulus and (■) elongation at break of the PLLA(co-CL)-b-PEPG-b-PLLA(co-CL) block copolymers (injection molded samples) with equal %-wt PEPG block content and varying %-mol CL content.

5.2   Rheological property matrix at the laboratory scale

The previous section shows the wide range of mechanical properties that could be accessed with the different types of PLA/polyether block copolymer structures. Plasticizing agents in the form of miscible polyether blocks (i.e. PEG, PEPG) or as CL comonomer could be introduced into the block copolymer structures to increase the free volume in the materials. The increased free volume and the reduced Tg values of the block copolymers led to an increase of the elongation at break and a reduction of the elastic modulus values of the block copolymers. The obtained materials were relatively soft and flexible materials, which would make them promising for their use in flexible film applications. Still, such applications require a high viscosity (low MFI values[10]) and a high melt strength to allow stable processing in blown film or cast film extrusion operations.

As described in Section 2.2.1, typical commercial materials intended for blown film processing have relatively low MFI values of around 2 g/10min [113]. Heuristic MFI values required for stable blown film processing in semi-technical blown film extrusion lines [191] are preferably between 2 and 10 g/10min. Materials with MFI values above this are expected to present bubble instability during processing.

In this context, it is important to remember that the synthesized block copolymers with the most promising properties for flexible film applications (high elongation at break and low elastic modulus) shown on Section 5.1 have relative low Tg values of 10 – 25 °C. When considering the effects of Tg on the viscosity of polymers stipulated by the VFTH equation (Equation 2.6), an important challenge is recognized: As the block copolymers become softer and more flexible, the viscosity is also reduced due to the higher free volume in the block copolymer melt due to the plasticizing agents (lower Tg).

To gain an initial perspective, the MFI values (190 °C, 2.16 kg load) of the previously described lin-$PEPG12_{13\%}$ and star-$PEPG20_{18\%}$ block copolymers of equal Mn values (~ 70 kDa) and different chain topologies are compared to the MFI value of a linear commercial Ingeo® PLA homopolymer (Mn_{1H-NMR}) = 109 kDa) designed for film applications (Figure 5.29). The obtained results show that the MFI values of the synthesized block copolymers are significantly higher than the MFI value of the commercial film-grade Ingeo® PLA homopolymer and far away from the MFI values below 10 g/10min recommended [191] for blown film processing.

---

[10] Although the MFI is not always inversely proportional to the zero-shear viscosity due to the possibility of shear-thinning effects occurring during the MFI measurement (specially at higher MFI values), in most cases the zero-shear viscosity can be correlated to the inverse of the MFI [190].
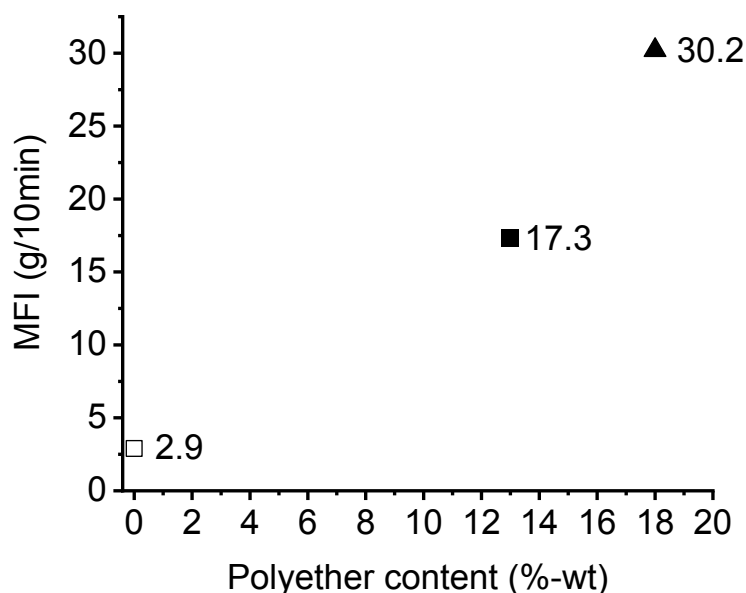
Figure 5.29: MFI values of the (□) Ingeo® 4043D PLA homopolymer, Mn = 109 kDa, Tg = 57 °C, T_{MFI} = 190 °C, the (■) lin-PEPG12$_{13\%}$ block copolymer, Mn = 71 kDa, Tg = 35 °C, T_{MFI} = 190 °C, and the (▲) star-PEPG20$_{18\%}$ block copolymer, Mn = 68 kDa, Tg = 24 °C, T_{MFI} = 190 °C.

The Ingeo® 4043D PLA homopolymer with its relatively high Mn of 109 kDa and Tg of 57 °C had the lowest measured MFI of 2.9 g/10min of the materials shown in Figure 5.29. In agreement with the η ~ Mw$^{3.4}$ dependency (Equation 2.31), the two block copolymers with lower Mn values of ~ 70 kDa than that of the Ingeo® 4043D PLA homopolymer (109 kDa), had higher MFI values (i.e. lower η). Added to this, the lower Tg values of the lin-PEPG12$_{13\%}$ (Tg = 35 °C) and the star-PEPG20$_{18\%}$ block copolymers are expected to cause a further increase of the MFI (i.e. reduction of the η) according to the VFTH equation (Equation 2.6). In the following sections, the chemical and molecular structure of the block copolymers will be adapted to reduce the MFI values of the block copolymers below 10 g/10min while maintaining a low elastic modulus and a high elongation at break for the block copolymers. The different options in the block copolymer synthesis presented in Section 5.1 will be used for this purpose.

5.2.1 Increasing molar mass of the block copolymers

Modifying the lactide monomer to –OH initiator ratio

The experiments presented in Section 5.1 showed that the Mn of the block copolymers could be well controlled by modifying the lactide monomer to –OH initiator ratio as expressed by Equation 2.2. The results of the oscillatory rheology measurements performed with the lin-PEPG12$_{13\%}$, star-PEPG20$_{13\%}$, and star-PEPG20$_{18\%}$ block copolymers described in Section 5.1 as well as with the commercially available Ingeo® 4043D PLA homopolymer are shown in Figure 5.30.

		Mn	Tg	Tm	T_{Rheo}	η_0	T_{MFI}	MFI
		[kDa]	[°C]	[°C]	[°C]	[Pa·s]	[°C]	[g/10min]
□	Ingeo® 4043D	109	57	150	185	6,900	190	2.9
■	lin-PEPG12$_{13\%}$	71	35	172	185	1,500	190	17.3
▲	star-PEPG20$_{18\%}$	68	24	170	185	900	190	30.2
▲	star-PEPG20$_{13\%}$	108	34	172	185	2,960	190	10.3
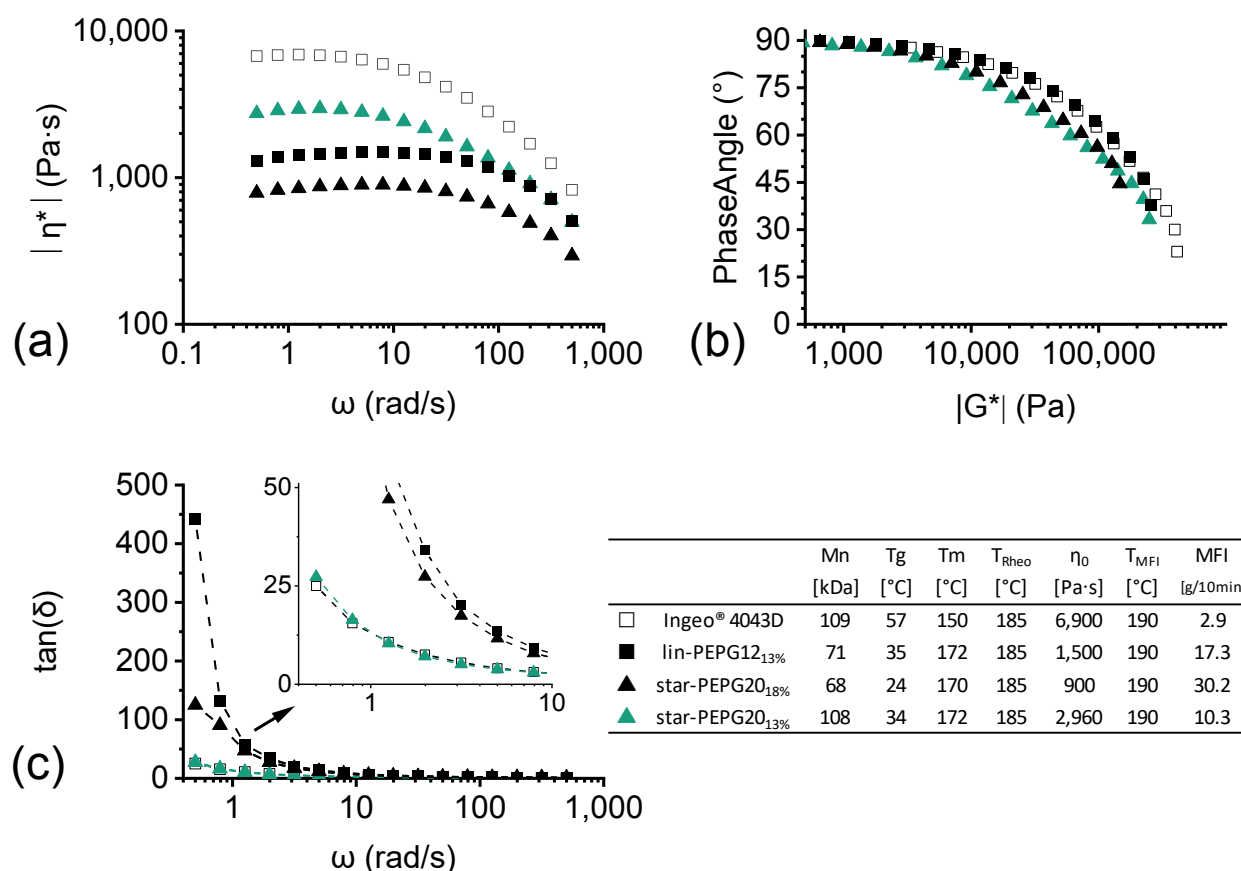
Figure 5.30: Frequency sweep, oscillatory rheology measurements (measured at the given T_{meas}) of block copolymers with different Mn values and different %-wt polyether block contents. (a) Complex viscosity vs. frequency, (b) phase angle (δ) vs |G*| plot, and (c) loss tangent vs. frequency plots. The Mn value shown is measured by ^{1}H-NMR.

The approximate η_0 values shown in the table in Figure 5.30 follow the inverse trend of the MFI measurements suggesting the general validity of the frequency sweep experiments. The slight reduction of |η*| observed at lower frequencies within the Newtonian plateau region [Figure 5.30 a)]

suggest the possible occurrence of degradation side reactions (discussed in Section 2.1.4) causing the molar mass (and consequently $|\eta^*|$) of the block copolymers to be reduced. The occurrence of degradation during measurement and the stabilization of the block copolymer melts will be discussed in more detail in the following section.

As shown in Figure 5.30, the lin-PEPG12$_{13\%}$ and the star-PEPG20$_{18\%}$ block copolymers have roughly the same Mn (~ 70 kDa) but a different topology and plasticizing polyether block content. When comparing their $|\eta^*|$ curves [Figure 5.30 (a)], lower $|\eta^*|$ values are found for the star-PEPG20$_{18\%}$ block copolymer at all frequencies. The higher free volume in the star-PEPG20$_{18\%}$ block copolymer due to the higher PEPG20 content of 18 %-wt, could be one reason behind its lower $|\eta^*|$ values. Interestingly however, Figure 5.30 (c) shows that the star-PEPG20$_{18\%}$ block copolymer has lower tan(δ) values in the low frequency range than the lin-PEPG12$_{13\%}$ block copolymer, despite the latter having a higher η_0. As discussed in Section 2.2.1, the value of tan(δ) describes the ratio of the viscous and elastic components of the viscoelastic response of a polymer melt [87]. Additionally the value of tan(δ) has been linked to the melt strength of polymer melts in some studies (Section 2.2.1). The star topology of the star-PEPG20$_{18\%}$ block copolymer could play an important role in the reduction of the tan(δ) value in the low frequency range and could help improve the processability of the copolymer in a blown film extrusion line.

Similar trends to the ones observed for the lin-PEPG12$_{13\%}$ and the star-PEPG20$_{18\%}$ block copolymers are observed when comparing the Ingeo® 4043D PLA homopolymer and the star-PEPG20$_{13\%}$ block copolymer. The Ingeo ® 4043D PLA and the star-PEPG20$_{13\%}$ block copolymers have roughly the same Mn (~ 110 kDa) but different topologies and plasticizing polyether block contents. In this case also, $|\eta^*|$ at all frequencies of the star-PEPG20$_{13\%}$ block copolymer (higher free volume) is lower than the $|\eta^*|$ of the Ingeo® 4043D PLA homopolymer. In this case, the tan(δ) of both the star-PEPG20$_{13\%}$ and the Ingeo® 4043D PLA homopolymer are roughly equal at lower frequencies in spite of the fact the viscosity of the Ingeo® homopolymer is significantly higher.

The δ vs $|G^*|$ plot shown in Figure 5.30 (b) shows that differently to both the linear Ingeo® 4043D PLA homopolymer and the lin-PEPG12$_{13\%}$ copolymer, the phase angles of the star-PEPG20$_{13\%}$ and star-PEPG20$_{18\%}$ have lower values after $|G^*|$ values of around 10,000 Pa. This could be attributed to a difference in molar mass, polydispersity, or the 4-arm star topology. Although a difference in polydispersity cannot be ruled out as the reason behind the different δ vs $|G^*|$ plot curve shapes, a big difference in polydispersity is unlikely because all copolymers were synthesized under the same conditions (temperature, catalyst content, stirring). Regarding the possibility of the different Mn causing the observed shift in the δ vs $|G^*|$ plot, attention can be directed to the star-PEPG20$_{18\%}$ and Ingeo® 4043D δ vs $|G^*|$ plots. In these cases, the δ vs $|G^*|$ plot of the lower Mn star-PEPG20$_{18\%}$ block copolymer is shifted towards lower $|G^*|$ values while the δ vs $|G^*|$ plot of the higher Mn Ingeo® 4043D is at higher $|G^*|$ values. If the shift was caused merely by the difference in Mn, the δ vs $|G^*|$ plot of the higher Mn Ingeo® 4043D should appear at lower $|G^*|$ values as shown in Section 2.2.1 [Figure 2.31 (a)]. Additionally, since both the lin-PEPG12$_{13\%}$ and the star-PEPG20$_{18\%}$ have a similar Mn, it is likely that the difference in their δ vs $|G^*|$ plots is not due to polydispersity or molar mass differences, but to the star topology of the star-PEPG20$_{18\%}$ copolymer.

The performed oscillatory rheology and MFI experiments show that the viscoelastic properties of the copolymers can be modified significantly by controlling the Mn of the copolymers. The changes in Mn of the copolymers does not seem to have a significant effect on the mechanical properties. As shown in Figure 5.14 and Figure 5.21, both the lin-PEPG12$_{13\%}$ and the star-PEPG20$_{13\%}$ showed similar mechanical properties (elastic modulus ~ 1,000 MPa, elongation at break ~ 230 %) regardless of their significantly different Mn values (lin-PEPG12$_{13\%}$: 68 kDa, star-PEPG20$_{13\%}$: 108 kDa) and chain topologies. At the same time, the experiments show that the η_0 and MFI values obtained with the copolymers are still far away from the values obtained by the commercial Ingeo® 4043D PLA homopolymer. The potentially important tan(δ) parameter of the star-PEPG20$_{13\%}$ copolymer however, was similar to the commercial Ingeo® 4043D PLA homopolymer tan(δ) which could suggest that the melt strength of both materials at 185 °C is similar.

Avoiding Mn degradation

The synthesized block copolymers presented in Section 5.1.1 through Section 5.1.5 had significantly lower Mn values of 60 – 70 kDa (measured by ^{1}H-NMR) compared to the theoretical Mn values of 90 kDa according to the used lactide monomer to –OH initiator molar ratio. As discussed in Section 3.2, several technical challenges related with the synthesis of such block copolymers can explain the low Mn values obtained quite accurately. The moisture content in the hydrophilic polyethers (even after drying), the presence of hydrolyzed lactide in the used monomer, and the incomplete reaction of lactide due to the equilibrium concentration are considered the main reasons behind the low experimental Mn values.

At the same time, additional molar mass reduction in the block copolymers can be indirectly observed through the reduction of the zero-shear viscosity during the rheological measurements as shown in Figure 5.30 (a). This Mn reduction can be caused by hydrolysis, depolymerization, and/or thermal molar mass degradation reactions as discussed in Section 2.1.4. Several additives have been presented in the literature that specifically aim to reduce the effects of each of these molar mass degradation reactions in PLA. A complete additive screening however, was considered to be out of the scope of this work. Due to the relatively large amount of literature available on the stabilization of PLA and other polyesters with tris(nonylphenyl) phosphite (TNPP), stabilization experiments on the synthesized PLA-polyether block copolymers were done exclusively with this compound. The related literature and reaction mechanisms are described in more detail in Section 2.1.4.

Additionally, due to the important role of the catalyst concentration on the reaction rates of the hydrolysis, the depolymerization, and thermal degradation side reactions (see Table 2.1), the reduction of the catalyst concentration was also studied as a way to improve the melt stability of the block copolymers during processing.

Tris(nonylphenyl) phosphite (TNPP) process stabilizer

As detailed in Section 2.1.4, the addition of (TNPP) into PLA reduces Mn degradation when PLA is exposed to high temperatures. Contents of 0.35 %-wt have been found keep viscosity of the PLA melt at a constant value, while 0.5 %-wt contents have been shown to lead to an increase of the melt viscosity [77; 79; 82]. Although in most of the literature the TNPP is blended into the viscous PLA melt (after the ROP) [77; 79; 82], other works [74; 75] suggest the addition of the TNPP into the low viscosity reaction mixture before the start of the ROP. To compare these different approaches, three star-PEPG20$_{13\%}$ block copolymers were synthesized with a $1 \cdot 10^{-4}$ mol$_{Sn(Oct)2}$/mol$_{Lactide}$ catalyst content. To the reference star-PEPG20$_{13\%}$DLac$_{4\%}$ block copolymer, no TNPP was added at any point before the measurement of the Mn by ^{1}H-NMR. To the second star-PEPG20$_{13\%}$DLac$_{4\%}$ block copolymer, a 0.35 %-wt TNPP content was added into the viscous melt in the reactor after the ROP was finished. To the third star-PEPG20$_{13\%}$DLac$_{4\%}$ block copolymer, 0.35 %-wt TNPP was added into the low viscosity reaction mixture before the start of the ROP. The results of these experiments are shown below in Figure 5.31.

Figure 5.31: Changes in the copolymer Mn depending on the moment of TNPP addition. All copolymers had a 13 %-wt PEPG20 content, a 4%-wt D-lactide content and 0.35 %-wt TNPP content with a theoretical Mn of 154 kDa according to the given [lactide] / [-OH] ratio.

As observed in the experiments in Section 5.1, both of the star-PEPG20$_{13\%}$DLac$_{4\%}$ block copolymer synthesis performed in the absence of TNPP had significantly lower measured Mn values than the maximum theoretical Mn (according to the used lactide monomer to −OH initiator molar ratio). An important observation however, is that the Mn of the star-PEPG20$_{13\%}$DLac$_{4\%}$ block copolymer into which TNPP was added *after* the ROP did not show a reduction of the block copolymer Mn even with the additional 10 min at T = 190 °C required for the TNPP to mix into the viscous star-PEPG20$_{13\%}$DLac$_{4\%}$ block copolymer melt.

Interestingly, when 0.35 %-wt TNPP was introduced into the reaction mixture *before* the start of the ROP, a Mn value close to the theoretical maximum defined by the lactide monomer to −OH initiator

ratio was measured for the resulting star-PEPG20$_{13\%}$DLac$_{4\%}$ block copolymer. The higher measured Mn came at no reduction of the ROP reaction rate as suggested by the similar reaction stirrer torque measurements recorded during the reactions with and without the presence of the TNPP (Figure A 13). This suggests that the higher Mn values achieved in the presence of TNPP are due to a chain extension mechanism and not to a catalyst deactivation mechanism. These chain extension mechanisms are also suggested by the works of Cicero et al. [78] and Jacques et al. [83], and further discussed in Section 2.1.4.

Further experiments with TNPP contents of up to 1 %-wt added before the start of the ROP of several star-PEPG20$_{18\%}$DLac$_{4\%}$ block copolymers were done to analyze whether the chain-extension mechanism occurs to a larger degree. The catalyst concentration used for these experiments was of $1 \cdot 10^{-4}$ mol$_{Sn(Oct)2}$/mol$_{Lactide}$, and the results are shown in Figure 5.32
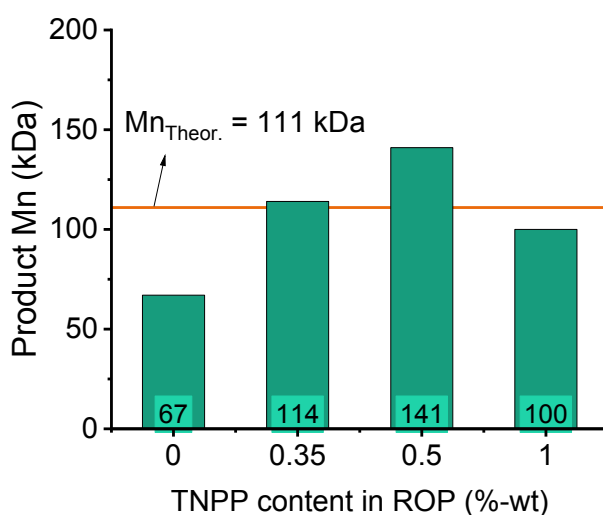
Figure 5.32: Effect of the presence of varying amounts on TNPP during the ROP synthesis of star-PEPG20$_{18\%}$DLac $_{4\%}$ block copolymers. Theoretical Mn is of 111 kDa according to the lactide monomer to –OH initiator ratio.

Similar results were obtained when comparing the star-PEPG20$_{18\%}$DLac$_{4\%}$ block copolymers synthesized in the absence and in the presence of 0.35 %-wt TNPP content. The addition of 0.35 %-wt TNPP before the start of the ROP again caused the Mn of the star-PEPG20$_{18\%}$DLac$_{4\%}$ block copolymer to be increased roughly to the expected theoretical Mn for the given lactide monomer to –OH initiator ratio. Interestingly, the further increase of the TNPP content to a value of 0.5 %-wt, resulted in a Mn significantly above the theoretical value, suggesting that even a higher degree of chain extension was obtained. A further increase of the TNPP content to 1 %-wt, however, did not lead to further chain extension, as the obtained Mn value is close to the theoretical one defined by the lactide monomer to –OH initiator ratio.

Similar behavior was observed by Jacques et al. [83] when adding increasing amounts of the similar triphenyl phosphite (TPP) stabilizer into PET/PBT blends. As explained in Section 2.1.4, the chain extension mechanism of TNPP in PLA was explained by Cicero et al. [78] through initial incorporation

of phosphorous to the polymer chain ends and subsequent transesterification of the phosphite chain-ends in the presence of –COOH end-groups. Because these –COOH end-groups can be formed through hydrolysis reactions with water and ester bonds, the transesterification of –COOH with phosphite chain-ends could explain the higher molar masses obtained when the ROP occurs in the presence of TNPP. The reduction of the molar mass back to the theoretical value when introducing 1 %-wt of TNPP (Figure 5.32), was explained by Jacques et al. [83] through a combination of hydrolysis caused by equilibrium displacement due to end-group capping and the presence of reactive degradation byproducts as explained in Section 2.1.4.

Regardless of the mechanism, the addition of 0.5 %-wt TNPP increases Mn. The MFI value of the star-PEPG20$_{18\%}$DLac$_{4\%}$ block copolymer synthesized in the presence of 0.5 %-wt TNPP (Figure 5.32) was 6.9 g/10min at 160 °C with a 2.16 kg load. This value is significantly lower than the MFI of 10.5 g/10min measured at 160 °C with a 2.16 kg load for the star-PEPG20$_{18\%}$DLac$_{4\%}$ block copolymer synthesized in the presence of only 0.35 %-wt TNPP. Thus, TNPP was identified as a viable option to obtain block copolymers with slightly higher Mn values resulting in reduced MFI values.

Lower catalyst content and TNPP process stabilizer

The previous experiments show that the Mn achieved during the ROP synthesis can be increased by adding TNPP into the reaction mixture before the start of the ROP. The higher Mn obtained for these block copolymers led to lower MFI values, however their thermal stability was not significantly improved by the presence of TNPP. For example, the MFI of a star-PEPG20$_{13\%}$DLac$_{4\%}$ block copolymer ($1 \cdot 10^{-4}$ mol$_{Sn(Oct)2}$/mol$_{Lactide}$, 0.5 %-wt TNPP added before the ROP) increased from 7.2 g/10min to 8.6 g/10min when the material was maintained at a temperature of 160 °C for 100 s and 300 s, respectively.

To obtain more information about the degradation behavior of the block copolymers when exposed to higher temperatures, a series of star-PEPG20$_{10\%}$DLac$_{4\%}$ block copolymers with varying TNPP and catalyst concentrations were synthesized. Samples of these block copolymers were dried for 4 h at 80 °C under vacuum, sealed in a dry glass ampoule, and exposed to 210 °C for 1 h in an oil bath. The Mn and lactide content of the block copolymers were monitored via ^{1}H-NMR measurements before and after exposure to 210 °C for 1 h and are compared to commercial Ingeo® 4043D PLA homopolymer (reference) in Figure 5.33.

(a)
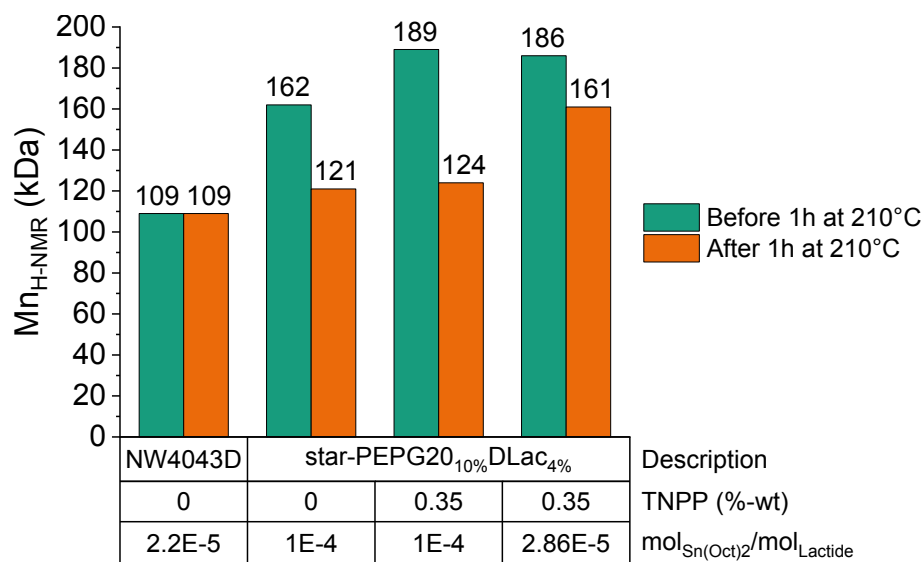
(b)
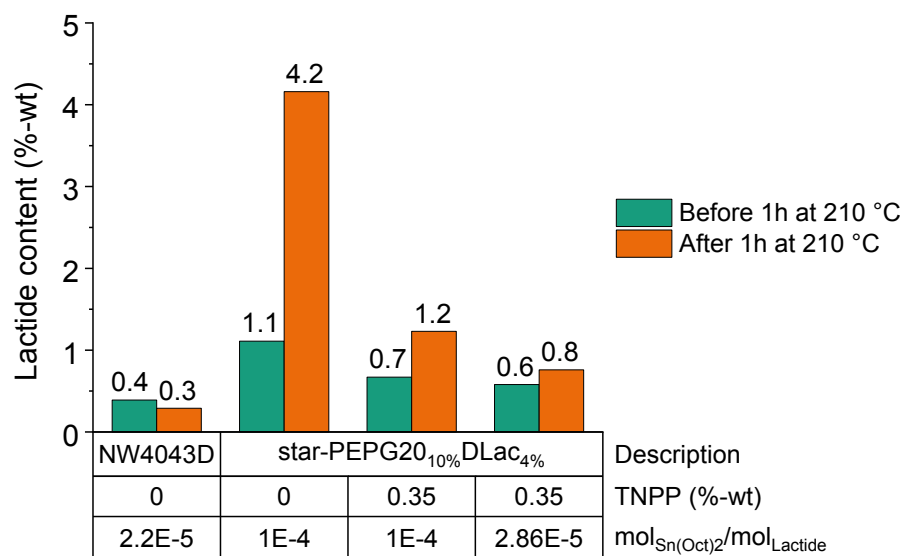
Figure 5.33: Changes in (a) Mn (kDa) and (b) lactide content (%-wt) before and after exposure of star-PEPG20$_{10\%}$DLac$_{4\%}$ block copolymers synthesized with varying catalyst and TNPP concentrations to 210 °C for 1 h in a glass ampoule. Commercial Ingeo® 4043D PLA homopolymer from NatureWorks (NW 4043D) is added as a reference.

The results in Figure 5.33 reveal that the commercial Ingeo® 4043D PLA homopolymer showed no signs of Mn degradation and produced no additional lactide after being exposed to 210 °C for 1 h. These results contrast significantly to the changes observed on the star-PEPG20$_{10\%}$DLac$_{4\%}$ copolymer with a $1 \cdot 10^{-4}$ mol$_{Sn(oct)2}$/mol$_{Lactide}$ catalyst content and no TNPP after the same thermal exposure. In

the latter case, a Mn reduction of 40 kDa was observed together with an increase in the lactide concentration from 1.1 %-wt after demonomerization to 4.2 %-wt after 1h at 210 °C.

As also discussed in the previous section, synthesis of the star-PEPG20$_{10\%}$DLac$_{4\%}$ block copolymers with and without TNPP [Figure 5.33 (a)] shows that a higher Mn (189 kDa) is obtained when TNPP is added before the ROP synthesis than when no TNPP is added (162 kDa). The Mn reduction of 65 kDa observed after exposing the star-PEPG20$_{10\%}$DLac$_{4\%}$ block copolymer (synthesized in the presence of TNPP) to 210 °C for 1 h suggests that TNPP does not stop Mn degradation. This could be caused by the formation of labile phosphorous bonds (Figure 2.11, Figure 2.12) that increase the Mn of the block copolymers, but that when exposed to high temperatures accelerate the molar mass degradation as discussed in Section 2.1.4.

When analyzing the formation of lactide after thermal stress [Figure 5.33 (b)], the depolymerization rate was found to be significantly reduced by the 0.35 %-wt TNPP content in the block copolymer. This could be due to a lower number of –OH end-groups caused by their reaction with TNPP (see Figure 2.10) to create phosphite chain ends. Assuming that the depolymerization molar equilibrium constant is defined by $K_{Depoly} = [- OH] / [lactide]$, a reduction of the $[- OH]$ concentration would require a corresponding reduction of the [lactide] molar concentration to satisfy the equilibrium constant. This hypothesis, however, remains to be confirmed.

Inductively coupled plasma – optical emission spectroscopy (ICP-OES) measurements of the reference Ingeo® 4043D PLA homopolymer revealed a tin content of only 18 ppm which translates to a catalyst concentration of around $2.2 \cdot 10^{-5}$ mol$_{Sn(oct)2}$/mol$_{Lactide}$ (Figure 5.33). This catalyst concentration is around 4.5 times lower than the catalyst concentration of $1 \cdot 10^{-4}$ mol$_{Sn(oct)2}$/mol$_{Lactide}$ that had been used for the synthesis of the block copolymers in Section 5.1. To analyze the effects of a lower catalyst content, a star-PEPG20$_{10\%}$DLac$_{4\%}$ block copolymer was synthesized in the presence of 0.35 %-wt TNPP stabilizer and a reduced $2.86 \cdot 10^{-5}$ mol$_{Sn(oct)2}$/mol$_{Lactide}$ catalyst concentration (about 1/3.5 of $1 \cdot 10^{-4}$). This block copolymer showed a lower Mn degradation rate (25 kDa in 1hr at 210 °C) than the two block copolymers with the higher $1 \cdot 10^{-4}$ mol$_{Sn(oct)2}$/mol$_{Lactide}$ catalyst concentrations. At the same time, the copolymer with the reduced catalyst content showed a lower depolymerization reaction rate as the lactide content increased by only 0.2 %-wt after exposure to 210 °C for 1h. It is important to mention however, that the ROP synthesis of the star-PEPG20$_{10\%}$DLac$_{4\%}$ block copolymer with a $2.86 \cdot 10^{-5}$ mol$_{Sn(oct)2}$/mol$_{Lactide}$ catalyst content took around 3 times longer (80 min vs. 27 min) than the synthesis of a similar copolymer with a $1 \cdot 10^{-4}$ mol$_{Sn(oct)2}$/mol$_{Lactide}$ catalyst concentration. In the case of industrial application of this technology, the benefits of an improved copolymer melt stability must be balanced against the increased production costs that come together with the longer reaction time. This was not further analyzed in the present study.

The obtained data suggests that TNPP added into the reaction mixture before the start of the ROP can help reach higher Mn values than the theoretical values determined by the lactide monomer to – OH initiator ratio due to the chain extension mechanisms explained in Section 2.1.4. The presence of TNPP in the block copolymers seems to reduce the depolymerization rate when they are exposed to high temperatures. However, molar mass degradation remains a problem. The reduction of the catalyst concentration to a value of $2.86 \cdot 10^{-5}$ mol$_{Sn(oct)2}$/mol$_{Lactide}$ seems to be a more effective option to reduce molar mass degradation of the block copolymers at high temperatures.

5.2.2 Lowering processing temperature

According to the VFTH equation (Equation 2.6) measurement of the viscosity at temperatures closer to Tg result in higher viscosity values. Additionally, the study by Kim et al. [134] found a higher temperature dependency of the viscosity in star PLA polymers when compared to linear polymers. The experiments described in Section 5.1.4 and Section 5.1.6, show that the crystal melting temperature (Tm) of the block copolymers could be well controlled by introducing a non-crystallizable comonomer such as D-lactide or ε-caprolactone into the PLA blocks as predicted by Equation 2.14. Such a reduction of the peak Tm of the block copolymers could allow them to be processed at lower temperatures closer to their Tg.

As shown in figure 5.20 (a), the block copolymers have Tg values of 35 °C and 24 °C when a 13 %-wt and 18 %-wt of PEPG block content, respectively, is introduced. Processing these polymers at 190 °C (above the Tm of 170 °C for the stereo-pure PLLA blocks) gives values of $T_{Processing}$-Tg of around 155 and 166 °C for the block copolymers containing 13 %-wt and 18 %-wt blocks, respectively. If the pure Ingeo® 4043D PLA homopolymer is processed at 190 °C, its $T_{Processing}$ - Tg value is of only 133 °C (due to its higher Tg value of 57 °C) and thus shows a significantly lower MFI value. A reduction of the peak Tm of the PLA-polyether block copolymers to 150 °C by introducing 4 %-wt D-lactide, and processing these copolymers at 160 °C would reduce the $T_{Processing}$ - Tg value to 125 and 136 °C for the copolymers containing 13 %-wt and 18 %-wt PEPG20 blocks, respectively.

The effects of reducing the peak Tm and, with it, the MFI measurement temperature was observed when synthesizing similar star-PEPG20$_{13\%}$ and star-PEPG20$_{13\%}$DLac$_{4\%}$ block copolymers. The Tm of 170 °C for the star-PEPG20$_{13\%}$ allowed a measurement temperature of 190 °C (where a complete melting of the pellets could be observed) while the star-PEPG20$_{13\%}$DLac$_{4\%}$ peak Tm value of 150 °C allowed MFI measurements[11] to be performed at a temperature of 160 °C. The resulting MFI value of the star-PEPG20$_{13\%}$ block copolymer at 190 °C was 10.3 g/10min while the MFI value for the star-PEPG20$_{13\%}$DLac$_{4\%}$ at 160 °C was 5.8 g/10min. As will be demonstrated in the following section, this experiment shows that the control over the Tm can be a valuable tool within the synthetic possibilities of the polyether/PLA block copolymers for controlling the rheology of the copolymer melt.

5.2.3 Combining strategies with the ε-caprolactone comonomer: higher molar mass and lower processing temperature

As shown in Section 5.1.6, an alternative way to reduce the Tm of the block copolymers (other than introducing D-lactide as a comonomer), is by introducing ε-caprolactone (CL) as a comonomer. This has the added advantage, that the X_{CL} simultaneously introduces free volume into the copolymer, thus reducing Tg and increasing the elongation at break. Additionally, the introduction of CL

---

[11] Measured under a 2.16 kg load

theoretically does not entail a reduction in the total copolymer Mn. Of course, the same cannot be said when introducing a higher amount of any polyether macroinitiator of constant Mn. The latter case invariably results in a copolymer of lower Mn and, consequently, leads to an increase of the MFI value.

Taking the before-mentioned arguments into consideration, several PLLA(co-CL)-b-PEPG-b-PLLA(co-CL) block copolymers were synthesized with the goal of obtaining a high degree of plasticiziation (i.e. a low Tg) while keeping the Mn of the block copolymer high enough to keep the MFI value as low as possible. The thermal properties and MFI values of some of the produced copolymers are summarized in Table 5.9.

Table 5.9: MFI of selected PEPG-initiated copolymers containing ε-caprolactone as a comonomer

Copolymer	Theoretical Mn [kDa]	Mn (^{1}H-NMR) [kDa]	Tg [°C]	Tm [°C]	T_{MFI}[a] [°C]	MFI[b] [g/10min]
star-PEPG20$_{13\%}$	154	105	34	172	190	10.3
star-PEPG20$_{10\%}$CL$_{2\%}$	200	222	31	154	170	3.8
star-PEPG20$_{13\%}$CL$_{7\%}$	154	[c]	20	141	160	15.0
star-PEPG20$_{9\%}$CL$_{6\%}$	222	[c]	25	146	160	7.2

[a] MFI measurement temperature; [b] Measured under 2.16kg load; [c] no end-group signal found

The MFI value for the star-PEPG20$_{10\%}$CL$_{2\%}$ block copolymer in Table 5.9 can be used to illustrate the advantages of using CL as a comonomer. In this case, the theoretical Mn of the block copolymer was increased by reducing the PEPG20 macroinitiator content to 10 %-wt. As discussed in Section 5.1.6, the Mn values of the block copolymers containing CL as a comonomer should be taken with caution. Given that the reaction rate of the CL comonomer is much slower than the reaction rate of the lactide monomer (Section 5.1.6), a high amount of CL is expected to be integrated into the PLA blocks at or near the end-groups. For this reason, the end-group signal at 4.3 ppm in the ^{1}H-NMR spectrum used for the Mn calculations can be misleadingly small due to the preferential presence of CL monomer units. The free volume that was not introduced through the addition of PEPG20 block content was substituted by X_{CL}. In total, the star-PEPG20$_{10\%}$CL$_{2\%}$ block copolymer had a 13 %-wt "equivalent" plasticizing agent content[12] in its chemical structure and thus, had a similar Tg (~ 34 °C) to the star-PEPG20$_{13\%}$ block copolymer. Additionally, the X_{CL} in the star-PEPG20$_{10\%}$CL$_{2\%}$ block copolymer significantly reduced the peak Tm to 154 °C, allowing the MFI value to be measured at 170 °C. This initial experiment shows that the flow behavior of the block copolymer can be adjusted by reducing the T_{MFI} while simultaneously increasing the copolymer Mn. Combining these strategies, the MFI value could be modified from 10.3 g/10min measured at 190 °C for the star-PEPG20$_{13\%}$ copolymer to 3.8 g/10min at 160 °C for star-PEPG20$_{10\%}$CL$_{2\%}$.

---

[12] A 2 %-mol CL content is roughly equal to a 3 %-wt CL content

A similar effect can be detected when analyzing the experimental results from the star-PEPG20$_{13\%}$CL$_{7\%}$ and the star-PEPG20$_{9\%}$CL$_{6\%}$ block copolymers (Table 5.8). Both copolymers have a significantly higher "equivalent" plasticizing agent content than that of the star-PEPG20$_{13\%}$ block copolymer. In the case of the star-PEPG20$_{13\%}$CL$_{7\%}$ block copolymer, however, the theoretical Mn is the same as for the star-PEPG20$_{13\%}$ copolymer. Even though the T$_{MFI}$ of the star-PEPG20$_{13\%}$CL$_{7\%}$ block copolymer was lowered to 160 °C, its MFI is still higher than that of the star-PEPG20$_{13\%}$ block copolymer. When increasing the copolymer theoretical Mn as done with the star-PEPG20$_{9\%}$CL$_{6\%}$ block copolymer and simultaneously reducing the MFI measurement temperature to 160 °C, the MFI is reduced to 7.2 g/10min while keeping a relatively high "equivalent" plasticizing agent content of ~ 17 %-wt. This results in a material with a Tg of 25 °C and an MFI below 10 g/10min (as desired for blown film processing).

	Mn$_{Theo}$	Tg	Tm	T$_{Rheo}$	η$_0$	T$_{MFI}$	MFI
	[kDa]	[°C]	[°C]	[°C]	[Pa·s]	[°C]	[g/10min]
□ Ingeo® 4043D	-	57	150	185	6,900	190	2.9
▲ star-PEPG20$_{10\%}$CL$_{2\%}$	200	31	154	170	4,800	170	3.8
△ star-PEPG20$_{9\%}$CL$_{6\%}$	222	25	146	160	2,700	160	7.2
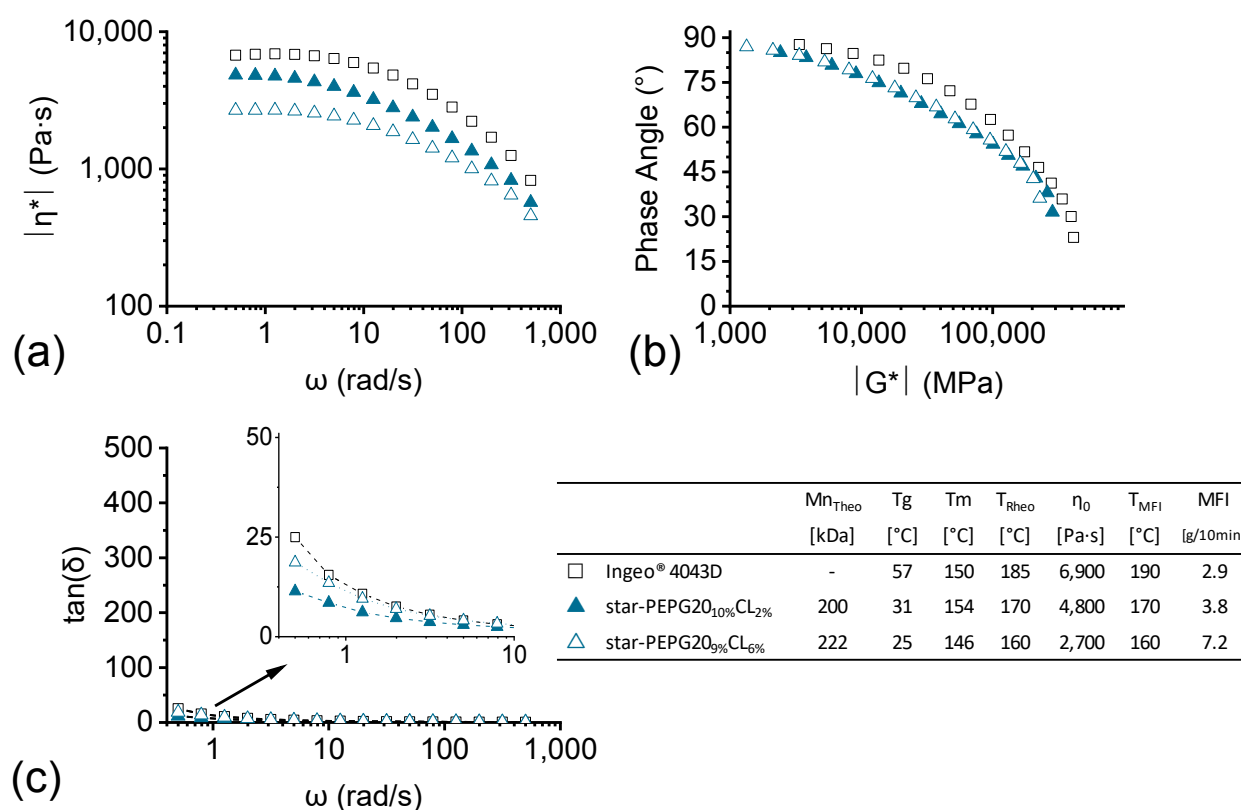
Figure 5.34: Frequency sweep, oscillatory rheology measurements of block copolymers with different Mn$_{Theo}$ and different %-wt polyether block contents. (a) complex viscosity vs. frequency, (b) δ vs |G*| plot, and (c) loss tangent vs. frequency plots. Mn$_{Theo}$ is the theoretical Mn calculated from the [Lactide] / [-OH].

The approximate η$_0$ values shown in the table in Figure 5.34 follow the inverse trend of the MFI measurements suggesting the general validity of the frequency sweep experiments. Similarly to the star-PEPG20$_{13\%}$ block copolymer in Figure 5.30, the star-PEPG20$_{9\%}$CL$_{6\%}$ block copolymer has a significantly lower η$_0$ value than the commercial Ingeo® 4043D PLA homopolymer [Figure 5.34 (a)] but shows slightly lower tan(δ) values [Figure 5.34 (c)] in the lower frequency range. The star topology of the CL-containing block copolymers can be implied when analyzing the δ vs |G*| plot in Figure 5.34 (b).

5.2.4 Polyether macroinitiator of higher molar mass

The previous experiments in Section 5.2.2 showed that an acceptable MFI value could be obtained for a copolymer containing 18 %-wt plasticizing agent content if its Mn was sufficiently high and the processing temperature reduced to 160 °C. Although this could be achieved using relatively high X_{CL} of up to 6 %-mol, an alternative using only a polyether macrointiator and lactide monomers was desired to simplify the synthesis process. Additionally, a lower D-lactide content in the block copolymers could be advantageous due to the faster crystallization rate expected when compared to block copolymers with higher 6 %-mol CL comonomer contents (as in the case of the star-PEPG20$_{9\%}$CL$_{6\%}$ block copolymer).

A polyether macroinitiator (mix-PEPG20/PEG35) containing a mixture of 30 %-wt of the PEG35 and 70 %-wt of the PEPG20 polyethers described in Table 3.1 was obtained. As PEG35 has a Mn of 35 kDa and PEPG20 has a Mn of 20 kDa, the average Mn of the polyether mixture is 24.5 kDa and the average functionality is 3.4. According to Equation 2.2, the increased Mn of the polyether mixture (mix-PEPG20/PEPG35) should allow a theoretical Mn of 127 kDa to be obtained with an 18 %-wt mix-PEPG20/PEPG35 block content. The topology of this copolymer should theoretically be a mixture of linear and star block copolymer chains according to the chain growth ROP mechanism.

To analyze the effects of using the mix-PEPG20/PEG35 polyether macroinitiator with higher Mn$_{avg}$, a mix-PEPG20/PEG35$_{18\%}$DLac$_{4\%}$ and a mixPEPG20/PEG35$_{20\%}$DLac$_{4\%}$ block copolymer were synthesized at the laboratory scale with a catalyst concentration of $1 \cdot 10^{-4}$ mol$_{Sn(Oct)2}$/mol$_{Lactide}$ and a 0.35 %-wt TNPP content added before the start of the ROP. The obtained characterization results are summarized in Table 5.10.

Table 5.10: MFI and thermal properties of the block copolymers initiated with the mixPEPG20/PEG35 polyether mixture.

Copolymer	TNPP	Mn$_{Theor.}$	Mn$_{H-NMR}$	Tg	Tm	T$_{MFI}$[a]	MFI[b]
	[%-wt]	[kDa]	[kDa]	[°C]	[°C]	[°C]	[g/10min]
star-PEPG20$_{13\%}$	0.35	154	111	34	172	190	10.3
mix-PEPG20/PEG35$_{18\%}$DLac$_{4\%}$	0.35	127	120	26	150	160	4.6
mix-PEPG20/PEG35$_{20\%}$DLac$_{4\%}$	0.35	115	111	22	150	160	8.6

[a] T$_{MFI}$ = MFI measurement temperature, [b] MFI measurement performed under a 2.16 kg load

Table 5.10 shows that the higher molar mass mix-PEPG20/PEG35 polyether macroinitiator allows the introduction of up to 20 %-wt polyether block content in the copolymers while keeping MFI within the ideal processible range (at T = 160 °C). Although the mechanical properties of the mix-PEPG20/PEG35$_{20\%}$DLac$_{4\%}$ block copolymer were not measured, a relatively high elongation at break value is expected considering its low Tg of 22 °C.

The approximate η_0 values shown in the table in Figure 5.35 follow the inverse trend of the MFI measurements suggesting the general validity of the frequency sweep experiments. The measured $|\eta^*|$ of the mix-PEPG20/PEG35$_{18\%}$DLac$_{4\%}$ copolymer [Figure 5.35 (a)] reached similar values to those

of the Ingeo® 4043D PLA homopolymer. The tan(δ) values in the low frequency range of the mix-PEPG20/PEG35$_{18\%}$DLac$_{4\%}$ block copolymer [Figure 5.35 (c)] are lower than those of the Ingeo® 4043D PLA homopolymer suggesting a higher melt strength.

Increasing the polyether block content to 20 %-wt, as in the case of the mix-PEPG20/PEG35$_{20\%}$DLac$_{4\%}$ block copolymer, led to a reduction of |η*| as seen in Figure 5.35 (a). Interestingly, the tan(δ) values of this block copolymer still remained at a similar level to those of the Ingeo® 4043D PLA homopolymer, suggesting that the mix-PEPG20/PEG35$_{20\%}$DLac$_{4\%}$ block copolymer has an acceptable melt strength for blown film processing. Considering its low Tg of 22 °C, the argument could be made that the necessary balance between rheological and mechanical properties could have been achieved with the mix-PEPG20/PEG35$_{20\%}$DLac$_{4\%}$ block copolymer.

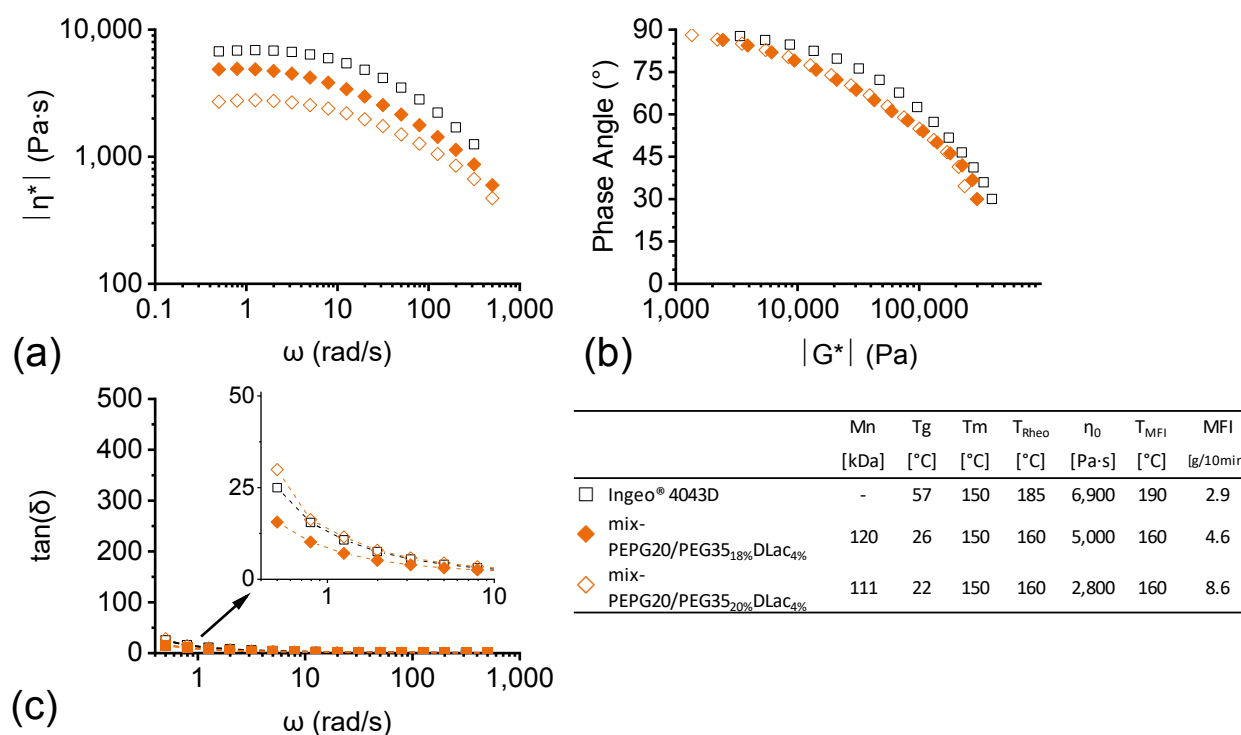|	Mn	Tg	Tm	T_{Rheo}	η_0	T_{MFI}	MFI
	[kDa]	[°C]	[°C]	[°C]	[Pa·s]	[°C]	[g/10min]
□ Ingeo® 4043D	-	57	150	185	6,900	190	2.9
◆ mix-PEPG20/PEG35$_{18\%}$DLac$_{4\%}$	120	26	150	160	5,000	160	4.6
◇ mix-PEPG20/PEG35$_{20\%}$DLac$_{4\%}$	111	22	150	160	2,800	160	8.6

Figure 5.35: Oscillatory rheology measurements of block copolymers with different mix-PEPG20/PEG35 macroinitiator contents measured at the given T_{Rheo}.

MFI measurements of the block copolymers described in Table 5.10 with a catalyst content of $1 \cdot 10^{-4}$ mol$_{Sn(Oct)2}$/mol$_{Lactide}$ exhibited significant Mn degradation during MFI measurement, especially when held at 160 °C for 200 or 300 s as shown in Figure 5.37. One possible reason for this could be its higher hydrophilic PEPG20 and PEG35 %-wt block content as suggested by the water uptake experiments shown in Figure 5.36.
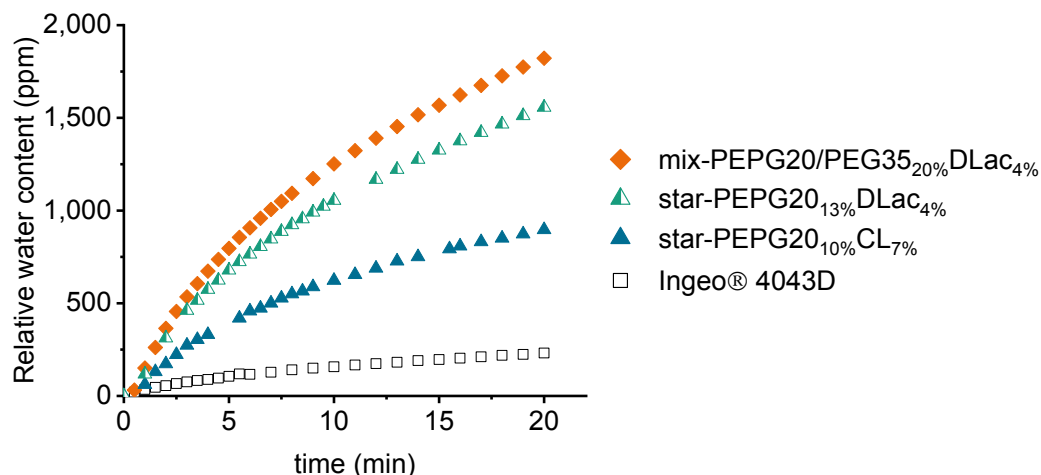
Figure 5.36: Measured relative water uptake of dried pellets over time at $T_{environment}$ = 23 °C and R.H. = 50 % of various samples. The relative water uptake was determined as the ratio between the mass of the pellets at time = t and the mass of the pellets at time = 0 (directly after drying).

The significantly lower water uptake rate of the Ingeo® 4043D PLA homopolymer (Figure 5.36) is partially explained by its significantly lower surface area to volume ratio (pellet diameter of Ingeo® 4043D was 3 mm, of block copolymers 1.5 mm). Additionally, the lack of the hydrophilic polyether block in its structure likely plays a role in its lower water uptake rate. This effect is more clear when comparing the block copolymers with similar pellet geometries but different chemical composition. In these experiments, the water uptake rate increases as the hydrophilic plasticizing polyether block content in the copolymers is higher. Figure 5.36 reveals that in 60 seconds, the Ingeo® 4043D PLA homopolymer takes up 35 ppm of water, while the mix-PEPG20/PEG35$_{20\%}$DLac$_{4\%}$ block copolymer takes up 150 ppm. Considering the case in which all the adsorbed water were to cause Mn degradation by hydrolysis, the Mn of a 90 kDa PLA polymer would be reduced by 15 % and 43 % for the 35 ppm and 150 ppm water contents, respectively. This highlights the importance of reducing the hydrolysis reaction rate in the block copolymers to maintain the required rheological properties during blown film extrusion processing.

Considering the data discussed in Section 5.2.1, the stability of a mix-PEPG20/PEG35$_{20\%}$DLac$_{4\%}$ block copolymer during MFI measurement was improved by reducing the catalyst concentration to a value of $2.86 \cdot 10^{-5}$ mol$_{Sn(Oct)2}$/mol$_{Lactide}$ (Figure 5.37). The MFI value was maintained at a value of around 6 g/10min even after keeping it at 160 °C for 300 s.

The block copolymers are exposed to environmental humidity during the MFI measurement (during weighing and introducing the pellets into the MFI reservoir), and likely adsorb significant amounts of water (Figure 5.36). The more stable MFI value (Figure 5.37) of the copolymer synthesized with the lower catalyst concentration is likely due to the reduction of the hydrolysis reaction rate. Even with the presence of water during the MFI measurement, the Mn degradation caused by hydrolysis is not enough to cause a significant increase in the MFI value at the processing temperature (160 °C).
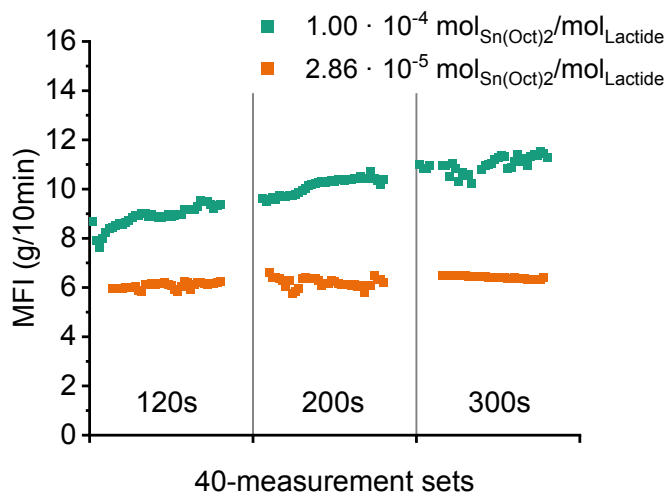
Figure 5.37: 40-measurement sets of the MFI value of two mix-PEPG20/PEG35$_{20\%}$DLac$_{4\%}$ block copolymers with different catalyst contents measured at 160 °C after holding the samples for 120, 200, and 300s at 160 °C to simulate extruder residence time. Both materials were kept dry before measurement. Ambient temperature during measurement was 27 °C and Relative humidity 66 %.

5.3 Blown film extrusion grade copolymers at the semi-technical scale

The high elastic modulus, low elongation at break, and low melt strength of pure PLA homopolymers commercially available have not allowed PLA to be used in flexible film applications. These material properties make PLA difficult to process and only allows the production of relatively stiff and brittle films [11; 71; 72; 153; 154]. In this section, the structure-property relationships established in Section 5.1 and Section 5.2 are used develop a soft and flexible material that can be processed in a conventional, semi-technical blown film processing extrusion line. The first insights into the processing behavior of the block copolymers and the properties of the obtained blown films are also presented.

5.3.1 Synthesis in semi-technical scale reactor

To obtain enough material for processing in a semi-technical blown film extrusion line (Section 4.3.1) the block copolymer synthesis was upscaled to a 7.5 L Büchi stainless steel reactor. Around 3 kg of block copolymer pellets were obtained per batch. This was enough material to allow continuous blown film extrusion processing for 1 – 2 h. The block copolymers synthesized in the semi-technical scale for blown film extrusion experiments are listed in Table 5.11.

Table 5.11: Reaction details and Mn measurement calculated from ^{1}H-NMR measurements

Copolymer	Mn (^{1}H-NMR) [kDa]	Catalyst content [mol/mol]	Reac. Time [min]	TNPP Content [%-wt]	TNPP added
star-PEPG20$_{13\%}$	111	$1 \cdot 10^{-4}$	44	0.35	After ROP
star-PEPG20$_{13\%}$DLac$_{4\%}$	122	$1 \cdot 10^{-4}$	49	0.35	After ROP
star-PEPG20$_{10\%}$CL$_{7\%}$	a)	$1 \cdot 10^{-4}$	72	0.35	After ROP
mix-PEPG20/PEG35$_{20\%}$DLac$_{4\%}$	114	$2.86 \cdot 10^{-5}$	141	0.50	Before ROP

a) No end-group signal found.

The star-PEPG20$_{13\%}$ and the star-PEPG20$_{13\%}$DLac$_{4\%}$ block copolymers were both synthesized with an equal $1 \cdot 10^{-4}$ mol$_{Sn(Oct)2}$/mol$_{Lactide}$ catalyst concentration. Roughly the same reaction time of 45 -50 min was given for each reaction to finish. TNPP process stabilizer was added into the viscous reaction melt (after the ROP), stirred for 10 min, and the reactor was drained. Similar Mn values to the ones obtained for the same formulations at the laboratory scale were measured from the products of the reaction in the semi-technical scale ($\sim$ 110 kDa).

After blown processing of the synthesized star-PEPG20$_{13\%}$ and the star-PEPG20$_{13\%}$DLac$_{4\%}$ block copolymers, it was found that even lower elastic moduli and higher elongation at break values were necessary for flexible film applications (further detailed in Section 5.3.5). To reduce the stiffness and brittleness of the blown films, the Tg of the block copolymers had to be further reduced (Section 5.1). To achieve this while maintaining a good processability of the block copolymer melt (Section 5.2.3), the star-PEPG20$_{10\%}$CL$_{7\%}$ block copolymer was synthesized (based on the laboratory experimental data detailed in Section 5.1.6). A $1 \cdot 10^{-4}$ mol$_{Sn(Oct)2}$/mol$_{Lactide}$ catalyst concentration was used and the reaction time was increased to 72 min to achieve a CL comonomer conversion of 85 % (Section 5.1.6). After the ROP, a 0.35 %-wt TNPP content was introduced into the viscous reaction melt and stirred for 10 min before draining the reactor. As mentioned in Section 5.1.6, the absence of the ^{1}H-NMR end-group signal (Table 5.11) is likely due to the presence of the CL comonomer at the chain-ends of the block copolymer; however, a higher Mn value than that of the star-PEPG20$_{13\%}$ and the star-PEPG$_{13\%}$DLac$_{4\%}$ block copolymers is expected due to the lower PEPG20 concentration of 10 %-wt (Equation 2.2).

The processing experiments of the star-PEPG20$_{10\%}$CL$_{7\%}$ block copolymer showed that adherence between the film layers, or "blocking" occurred (further explained in Section 5.3.4). To avoid this problem, anti-blocking additives had to be pre-blended into the copolymer before blown film extrusion in a twin-screw extrusion blending step at a temperature above the block copolymer Tm. To reduce Mn degradation during this pre-blending step, the mix-PEPG20/PEG35$_{20\%}$DLac$_{4\%}$ block copolymer (Table 5.11) was synthesized with a reduced catalyst concentration of $2.86 \cdot 10^{-5}$ mol$_{Sn(Oct)2}$/mol$_{Lactide}$ and in the presence of a 0.5 %-wt TNPP content added before the ROP (based on Section 5.2.1). A significantly longer reaction time of 141 min was necessary to complete the ROP due to the low catalyst concentration.

5.3.2 Thermal properties

The thermal properties of the synthesized blown film extrusion grade block copolymers shown in Figure 5.38, are close to the expected values from the data collected in the laboratory experiments (Section 5.1). The Tg values shown in the non-isothermal DSC curves in Figure 5.38 are mainly influenced by the free volume introduced into the material by the plasticizing PEPG blocks and/or the CL comonomer. The Tg of the materials (Figure 5.38) decreased from 37 °C for the star-PEPG20$_{13\%}$ and star-PEPG20$_{13\%}$DLac$_{4\%}$ copolymers (13 %-wt plasticizing agent) to 27 °C for the star-PEPG20$_{10\%}$CL$_{7\%}$ copolymer (17.7 %-wt plasticizing agent) and further to 22 °C for the mix-PEPG20/PEG35$_{20\%}$DLac$_{4\%}$ copolymer (20 %-wt plasticizing agent).

The peak Tm of the block copolymers (Figure 5.38) was mainly influenced by the X$_D$ and X$_{CL}$ in the PLLA blocks (as described in Section 5.1.4 and Section 5.1.6). Similarly to the laboratory experiments, the star-PEPG20$_{13\%}$ block copolymer (X$_D$ = 0 %-mol) had a peak Tm of 170 °C, the star-PEPG20$_{13\%}$DLac$_{4\%}$ and the mix-PEPG20/PEG35$_{20\%}$DLac$_{4\%}$ copolymers (X$_D$ = 4 %-mol) had a Tm of 152 °C, and the star-PEPG20$_{10\%}$CL$_{7\%}$ (X$_{CL}$ = 7 %-mol) had a Tm of 141 °C.
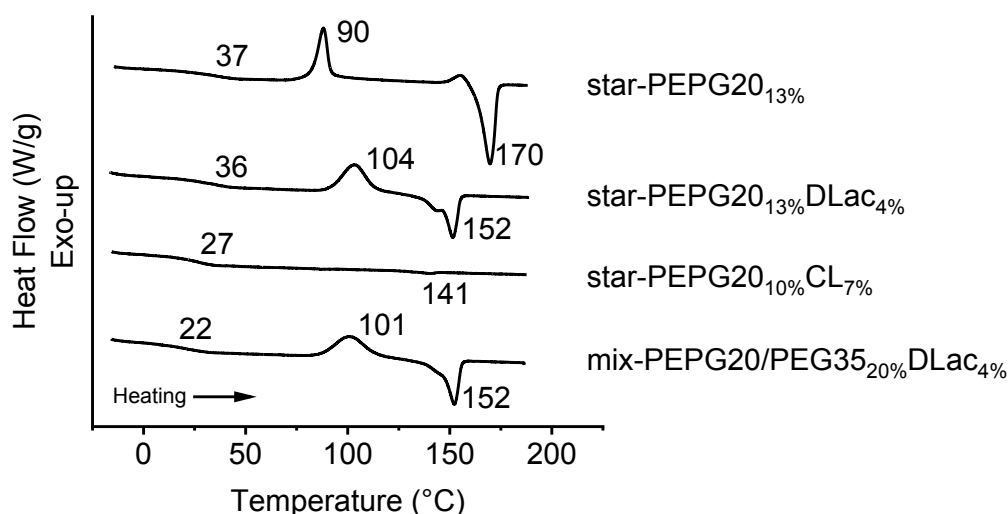

Figure 5.38: Non-isothermal DSC thermograms of the block copolymers produced in the 7.5 L stainless steel reactor.

The crystallization rate of the block copolymers under isothermal conditions was strongly influenced by their Tg and peak Tm (Figure 5.38). The crystallization half-times (t$_{1/2}$) of the block copolymers at several isothermal crystallization temperatures are presented in Figure 5.39. The temperatures at which the maximum crystallization rates were observed (Tcr$_{Max}$) for each block copolymer are listed in Table 5.11. The Tcr$_{Max}$ values obtained experimentally are close to the theoretical Tcr$_{Max}$ (Tcr$_{Max}$ = (Tg + Tm)/2) suggested by Rudin et al. [102]. This follows what is expected by the Hoffmann-Lauritzen theory (Section 2.2.1) where both the viscous transport and the nucleation energy terms in Equation 2.16 have their highest combined contribution to the spherulite radius growth-rate.
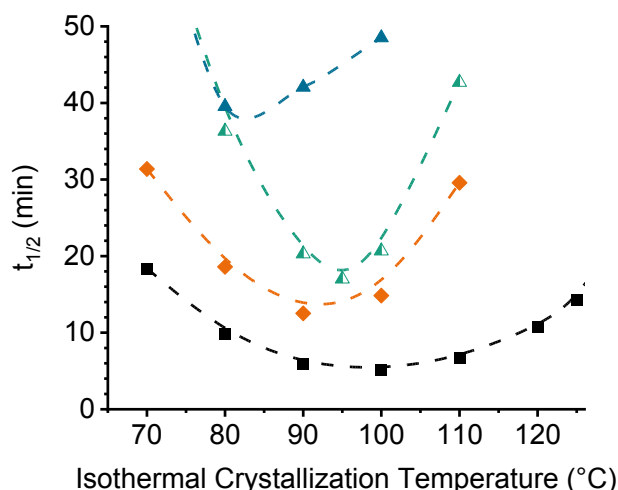
Figure 5.39: Crystallization half-time ($t_{1/2}$ - min) from DSC isothermal measurements of the virgin pellets of the (■) star-PEPG20$_{13\%}$, (△) star-PEPG20$_{13\%}$DLac$_{4\%}$, (▲) star-PEPG20$_{10\%}$CL$_{7\%}$ and (◆)mix-PEPG20/PEG35$_{20\%}$DLac$_{4\%}$ block copolymers.

Table 5.12: Theoretical and experimental isothermal crystallization temperatures of maximum crystallization rate (Tcr$_{Max}$)

Block Copolymer	Theoretical[a] Tcr$_{Max}$ [°C]	Experimental Tcr$_{Max}$ [°C]	$t_{1/2}$ at Tcr$_{Max}$ [min]
star-PEPG20$_{13\%}$	103.5	100	5.1
star-PEPG20$_{13\%}$DLac$_{4\%}$	94	95	17
star-PEPG20$_{10\%}$CL$_{7\%}$	81.5	80	39.5
mix-PEPG20/PEG35$_{20\%}$DLac$_{4\%}$	87	90	12.5

a) The theoretical isothermal crystallization temperature of maximum crystallization rate is calculated using the Tg and peak Tm measured in non-isothermal DSC through the following relation: Tcr$_{Max}$ = (Tg + Tm) / 2 – from Rudin et al. [102].

b) The experimental Tcr$_{Max}$ is the isothermal crystallization temperature shown in Figure 5.39 at which the lowest crystallization half-time was measured for each block copolymer.

The effect of the nucleation energy barrier can be seen when comparing the $t_{1/2}$ the star-PEPG20$_{13\%}$ and the star-PEPG20$_{13\%}$DLac$_{4\%}$ block copolymers. Both of these block copolymers have practically the same Mn and Tg, but a significantly different peak Tm. The $t_{1/2}$ at the Tcr$_{Max}$ (100 °C) of the star-PEPG20$_{13\%}$ block copolymer is only of 5.12 min while the $t_{1/2}$ at the Tcr$_{Max}$ (95 °C) of the star-PEPG20$_{13\%}$DLac$_{4\%}$ is 17 min. This 332 % increase of $t_{1/2}$ at Tcr$_{Max}$ is likely due to the increased nucleation energy barrier caused by the X_D of 4 %-mol in the star-PEPG20$_{13\%}$DLac$_{4\%}$ copolymer. When analyzing the mix-PEPG20/PEG35$_{20\%}$DLac$_{4\%}$ block copolymer with a similar peak Tm but lower Tg than the star-PEPG20$_{13\%}$DLac$_{4\%}$ copolymer, a general reduction of $t_{1/2}$ is observed at all isothermal crystallization temperatures. This reduction is observed even though the Mn of the mix-PEPG20/PEG35$_{20\%}$DLac$_{4\%}$ copolymer is expected to be slightly higher than that of the star-PEPG20$_{13\%}$DLac$_{4\%}$ copolymer (which is expected to increase $t_{1/2}$ – Section 2.2.1). The $t_{1/2}$ reduction is likely due to the improved transport of the polymer chains to the nucleation sites in the mix-

PEPG20/PEG35$_{20\%}$DLac$_{4\%}$ copolymer compared to the star-PEPG20$_{13\%}$DLac$_{4\%}$ copolymer. This improved transport however, does not reduce t$_{1/2}$ of the mix-PEPG20/PEG35$_{20\%}$DLac$_{4\%}$ block copolymer to a similar value of the more stereoregular star-PEPG20$_{13\%}$ copolymer. Addition of a nucleating agent such as talc powder[13] into the mix-PEPG20/PEG35$_{20\%}$DLac$_{4\%}$ block copolymer was found to significantly increase its crystallization rate. This led to lower t$_{1/2}$ values than even those of the highly stereoregular star-PEPG20$_{13\%}$ block copolymer as shown in Figure 5.40.
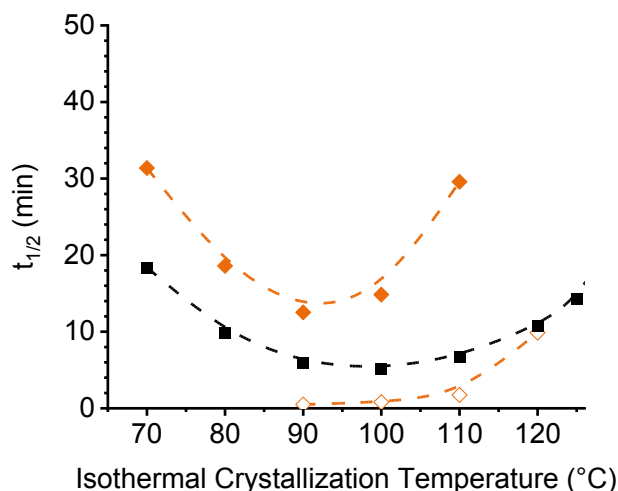

Figure 5.40: Isothermal crystallization experiments of the (■) star-PEPG20$_{13\%}$, (◆) mix-PEPG20/PEG35$_{20\%}$DLac$_{4\%}$ copolymers compared to the (◇) mix-PEPG20/PEG35$_{20\%}$DLac$_{4\%}$ block copolymer with a 2 %-wt anti-block talc additive content.

After studying the effects of the nucleation energy barrier on the crystallization rate of the block copolymers, it is no surprise that the star-PEPG20$_{10\%}$CL$_{7\%}$ block copolymer showed a significantly lower crystallization rate than the other copolymers. The t$_{1/2}$ of ~ 40 min at Tcr$_{Max}$ (80 °C) of the star-PEPG20$_{10\%}$CL$_{7\%}$ block copolymer (X$_{CL}$ = 7 %-mol) is significantly higher than the t$_{1/2}$ of 17 min at Tcr$_{Max}$ (95 °C) of the star-PEPG20$_{13\%}$DLac$_{4\%}$ copolymer with an X$_D$ of 4 %-mol. Considering that the star-PEPG20$_{10\%}$CL$_{7\%}$ copolymer has an improved chain transport caused by its low Tg, the strong effect of the increased nucleation energy barrier caused by the high X$_{CL}$ led to a net reduction of its crystallization rate.

5.3.3 Rheological properties

All the block copolymers synthesized in the 7.5 L reactor (Table 5.11) except for the star-PEPG20$_{13\%}$ block copolymer (MFI = 10.3 g/10min) had MFI values well within the 2 – 10 g/10min range required

---

[13] Added as an anti-block additive into mix-PEPG20/PEG35$_{20\%}$DLac$_{4\%}$ for processing as further discussed in Section 5.3.4

for stable blown film processing [191] at their respective processing temperatures (Table 5.13). The strategies discussed in Section 5.2 were used to reduce the MFI values of the copolymers while maintaining a high plasticizing agent content (i.e. high free volume) in the materials.

The relatively low polyether block content (13 %-wt) in the star-PEPG20$_{13\%}$ copolymer allowed a high Mn (111 kDa) to be achieved keeping the MFI value at 10.3 g/10min at 190 °C. Introduction of an X_D of 4 %-mol (star-PEPG20$_{13\%}$DLac$_{4\%}$) allowed processing at 160 °C (Section 5.2.2). At this temperature, the MFI of the star-PEPG20$_{13\%}$DLac$_{4\%}$ copolymer was of 5.8 g/10mol, which was well within the processible range [191].

Table 5.13: MFI values of the synthesized block copolymers measured at their respective processing temperatures and under a 2.16 kg load.

Material	Tm (DSC) [°C]	T_{MFI} [°C]	MFI [g/10min]
Ingeo® 4043D PLA-homopolymer	150	190	2.9
star-PEPG20$_{13\%}$	170	190	10.3
star-PEPG20$_{13\%}$DLac$_{4\%}$	152	160	5.8
star-PEPG20$_{10\%}$CL$_{7\%}$	141	160	6.7
mix-PEPG20/PEG35$_{20\%}$DLac$_{4\%}$	152	160	5.7

The plasticizing agent content was further increased in the star-PEPG20$_{10\%}$CL$_{7\%}$ copolymer while keeping its MFI in the processible range through the strategy outlined in Section 5.2.3. The Mn of this copolymer was increased by reducing the plasticizing PEPG20 block content to 10 %-wt. This reduced the lactide monomer to –OH initiator ratio (Equation 2.2). The lower PEPG20 plasticizer content (compared to copolymers with 13 %-wt PEPG20 content) was replaced (and even increased) by an X_{CL} of 7 %-mol (~ 7.7 %-wt CL in total copolymer), totaling a plasticizing agent content in the copolymer of ~ 17.7 %-wt. The X_{CL} simultaneously reduced the peak Tm of the copolymer to 141 °C, allowing processing at 160 °C. The MFI at this temperature was of 6.7 g/10min and was well within the recommended MFI range of 2 – 10 g/10min for blown film processing [191].

Finally, the mix-PEPG20/PEG35$_{20\%}$DLac$_{4\%}$ block copolymer with an MFI of 5.7 g/10min at its processing temperature of 160 °C was synthesized. This MFI value could only be achieved by the combination of using a macroinitiator of high molar mass and minimizing the Mn degradation reactions (Section 5.2.1 and Section 5.2.4). The PEPG20/PEG35 macroinitiator with its Mn$_{Avg}$ of 24.5 kDa, allows a low number of –OH initiating groups to be introduced per gram of plasticizing polyether PEPG20/PEG35 content. The used 20 %-wt PEPG20/PEG35 macroinitiator content theoretically leads to a maximum Mn of 111 kDa (under ideal conditions) as defined by Equation 2.2. This is significantly lower than the maximum theoretical Mn of the star-PEPG20$_{13\%}$ block copolymers of 154 kDa. The introduction of 0.5 %-wt TNPP before the start of the ROP reaction, however, allowed a Mn value of 114 kDa (slightly above the theoretical maximum) to be obtained by counteracting the hydrolytic Mn degradation reactions (Section 5.2.1). The reduced catalyst concentration used for the synthesis of

this copolymer additionally helped reduce degradation during the pre-blending step with anti-blocking additives.
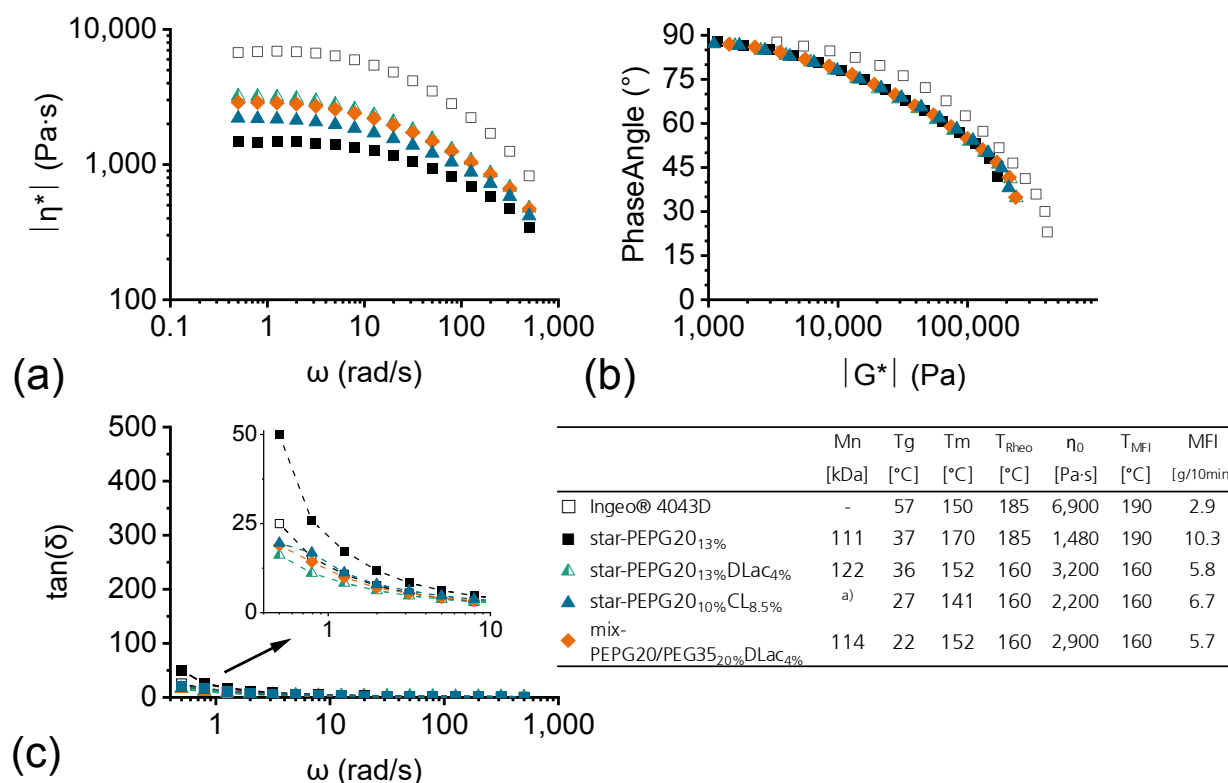

Figure 5.41: Frequency sweep, oscillatory rheometry measurements (measured at the given T_{meas} of the blown film extrusion grade polymers (Table 5.11). (a) Complex viscosity vs frequency, (b) δ vs |G*| plot, and (c) loss tangent vs frequency plot. Measurements were performed on injection molded disks of the block copolymers (as synthesized). Shown Mn values were measured by ^{1}H-NMR, [a] no end-group signal found in ^{1}H-NMR spectrum. The Ingeo® 4043D PLA homopolymer was not injection molded into a disk.

	Mn	Tg	Tm	T_{Rheo}	η_0	T_{MFI}	MFI
	[kDa]	[°C]	[°C]	[°C]	[Pa·s]	[°C]	[g/10min]
□ Ingeo® 4043D	-	57	150	185	6,900	190	2.9
■ star-PEPG20$_{13\%}$	111	37	170	185	1,480	190	10.3
△ star-PEPG20$_{13\%}$DLac$_{4\%}$	122	36	152	160	3,200	160	5.8
▲ star-PEPG20$_{10\%}$CL$_{8.5\%}$	[a]	27	141	160	2,200	160	6.7
◆ mix-PEPG20/PEG35$_{20\%}$DLac$_{4\%}$	114	22	152	160	2,900	160	5.7

In general, the oscillatory rheology measurements shown in Figure 5.41 follow the expected inverse relationship to the measured MFI values. Although none of the block copolymers has an η_o value close to that of the commercial Ingeo® 4043D PLA homopolymer, the tan(δ) values of most of the block copolymers (except for the star-PEPG20$_{13\%}$ copolymer) were below those of the Ingeo® 4043D PLA material. This suggests that the melt strength of most of the block copolymers could be high enough to maintain bubble stability during blown film processing. The δ vs |G*| plot suggests a star-topology for the block copolymers and a linear topology for the Ingeo® 4043D PLA homopolymer.

5.3.4 Processing

The block copolymers (Table 5.11) were processed in a semi-technical blown film extrusion line (Section 4.3.1) to study the performance of their respective rheological properties during processing and their mechanical properties for flexible film applications. Due to the relatively small amounts of material that could be synthesized (3 kg), an in-depth study of the processability of the block copolymers was not performed. The first impressions on the processability of the materials, together with some orientation effects, however, were studied. Initial processing trials were done using the minimum process conditions at which blown film materials are expected to be processible according to [191] (screw speed [V_{Screw}] 40 RPM, nip-roll speed [V_{NR}] 4 m/min).

Effect of different MFI with a similar plasticizing polyether block content

Initial processing experiments using the star-PEPG20$_{13\%}$ block copolymer were done at a melt temperature of 190 °C, V_{Screw} = 40 RPM, and V_{NR} = 4 m/min. Blown films with a 40 μm thickness could be produced under these conditions, however instability of the blown film extrusion bubble was observed. The low melt strength [high tan(δ)] of the star-PEPG20$_{13\%}$ copolymer at 190 °C allowed the air inside the bubble to shift around and stretch the block copolymer melt at different points during solidification. The unevenly stretched areas of the film were then pressed together by the nip-rolls at the top of the bubble resulting in wrinkles on the obtained films [Figure 5.42 (a)]. Processing of the star-PEPG20$_{13\%}$ copolymer was not possible at a higher V_{NR} of 6 m/min and constant V_{Screw} of 40 RPM. At these conditions, the polymer melt bubble broke and the air inside the bubble escaped, forcing the process to be interrupted.
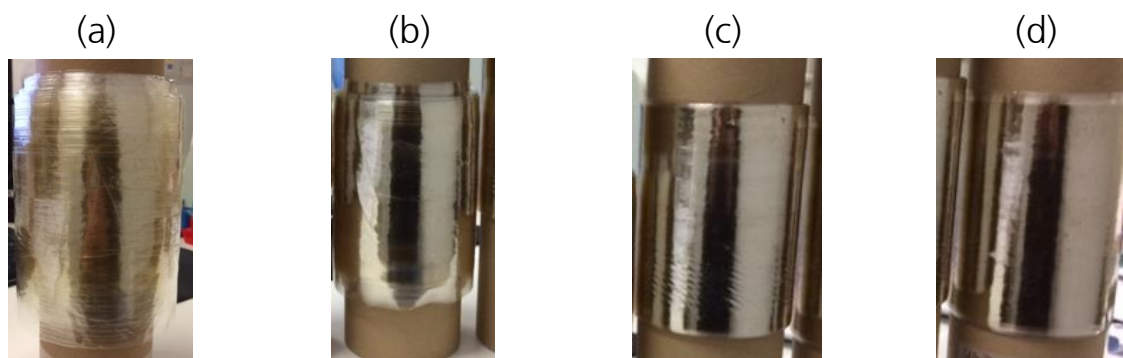
(a)　　　　　(b)　　　　　(c)　　　　　(d)

Figure 5.42: Blown film extruded films of the star-PEPG20$_{13\%}$ and star-PEPG20$_{13\%}$DLac$_{4\%}$ block copolymers at the conditions defined below in Table 5.14.

Table 5.14: Blown film-processing conditions for the samples shown in Figure 5.42.

Reference to Fig. X	Material	Melt Temp. [°C]	Screw Speed [RPM]	Nip-Roll speed [m/min]	Film Thickness [µm]	Comments
(a)	star-PEPG20$_{13\%}$	187	40	4	40 - 50	Bubble instability / wrinkles
	star-PEPG20$_{13\%}$	187	40	6	-	Not processible
(b)	star-PEPG20$_{13\%}$DLac$_{4\%}$	157	40	4	50	Stable bubble /uniform film
(c)	star-PEPG20$_{13\%}$DLac$_{4\%}$	157	40	8	20	Stable bubble /uniform film
(d)	star-PEPG20$_{13\%}$DLac$_{4\%}$	157	70	8	35	Stable bubble /uniform film

A stable bubble was observed when processing the star-PEPG20$_{13\%}$DLac$_{4\%}$ block copolymer at a temperature of 160 °C, V_{Screw} = 40 RPM, and V_{NR} = 4 m/min. Uniform blown films with a thickness of around 50 µm were obtained. The wrinkles on these films were significantly less [Figure 5.42 (b)] than the wrinkles on the star-PEPG20$_{13\%}$ films [Figure 5.42 (a)] due to the improved bubble stability. The improved processing stability is attributed to the lower MFI and tan(δ) values of the star-PEPG20$_{13\%}$DLac$_{4\%}$ copolymer compared to those of the star-PEPG20$_{13\%}$ copolymer.

Blown film processing of the star-PEPG20$_{13\%}$DLac$_{4\%}$ block copolymer remained stable even when increasing V_{NR} to 8 m/min while keeping V_{Screw} and temperature constant at 40 RPM and 160 °C, respectively. The films processed at this higher V_{NR} were equally as uniform [Figure 5.42 (c)] as the ones produced at V_{NR} = 4 m/min [Figure 5.42 (b)] but had a lower thickness of 20 µm. When the V_{Screw} was increased to 70 RPM (keeping V_{NR} at 8 m/min and $T_{Processing}$ at 160 °C), the star-PEPG20$_{13\%}$DLac$_{4\%}$ copolymer bubble remained stable. Uniform films [Figure 5.42 (d)] with a thickness of 35µm could be produced even at this higher processing rate due to the lower MFI and improved melt stability of the star-PEPG20$_{13\%}$DLac$_{4\%}$ copolymer.

Processing of low-Tg star-PEPG20$_{10\%}$CL$_{7\%}$ block copolymer

Stable processing of the star-PEPG20$_{10\%}$CL$_{7\%}$ block copolymer was observed when operating at V_{Screw} = 40 RPM and V_{NR} = 4 m/min and V_{NR} = 6 m/min. Additionally, operation at a V_{Screw} of 70 RPM and a V_{NR} of 6 m/min was found to also run under stable conditions. The extruded bubble remained stable under the before-mentioned settings and the resulting films were smooth and uniform as shown in Figure 5.43.
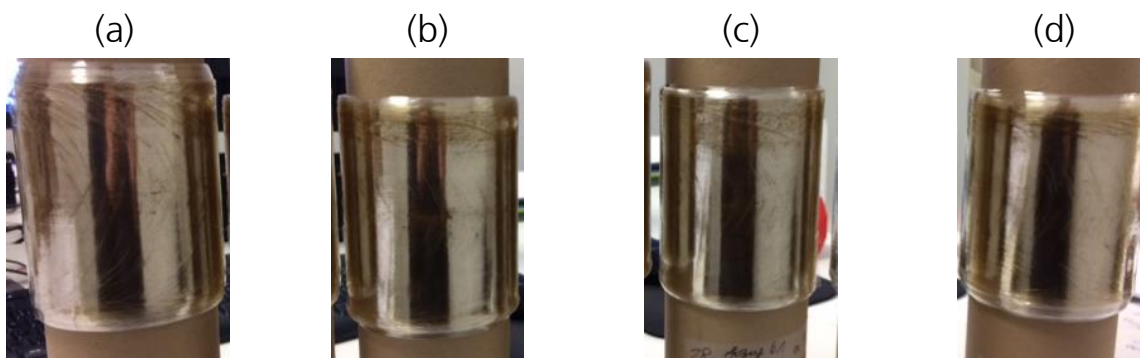
Figure 5.43: Obtained star-PEPG20$_{10\%}$CL$_{7\%}$ block copolymer blown films when operating at the following V$_{Screw}$, V$_{NR}$ and with the given film thickness (μm): (a) 40 RPM, 3 m/min, 45 μm, (b) 40 RPM, 4 m/min, 40 μm, (c) 55 RPM, 6 m/min, 30 μm, and (d) 70 RPM, 6 m/min, 30 μm.

All of the produced films were winded on cardboard cylinders directly after solidification (Figure 5.43). When separating the star-PEPG20$_{13\%}$ and the star-PEPG20$_{13\%}$DLac$_{4\%}$ copolymer film layers from each other, some adherence between the layers was evident. With sufficient force however, these film layers could be separated from each other even after several months. In contrast, the star-PEPG20$_{10\%}$CL$_{7\%}$ block copolymer blown films showed a significantly stronger adherence between the film layers than the star-PEPG20$_{13\%}$ and star-PEPG20$_{13\%}$DLac$_{4\%}$ block copolymer films. Directly after production, the star-PEPG20$_{10\%}$CL$_{7\%}$ copolymer film layers could be separated from each other if enough force was applied. After two to three days, however, the star-PEPG20$_{10\%}$CL$_{7\%}$ copolymer film layers could no longer be separated. This is a common phenomenon in blown film applications called "blocking" and is known to be caused by the temperature activated diffusion (above the Tg) of polymer chains across the layer interface [192]. Blocking can be avoided by blending finely dispersed particles with a particle diameter below 1 μm of materials like CaCO$_3$, talc, or SiO$_2$ into the films before processing [193], which reduce the surface contact between the films. Alternatively, pre-blending lubricants such as fatty amides or polysiloxanes into polymers [193], which can later migrate to the film surface, helps create a weak layer interface between the films that reduces blocking. These substances are commonly known as anti-blocking or slip additives and are commercially available. Film unwinding problems can also be minimized by efficient bubble cooling and/or reduced winding tension [192].

Processing of mix-PEPG20/PEG35$_{20\%}$DLac$_{4\%}$ block copolymer with anti-blocking additives

Anti-blocking additives were blended into the mix-PEPG20/PEG35$_{20\%}$DLac$_{4\%}$ block copolymer before blown film extrusion processing to avoid blocking (as observed with the star-PEPG20$_{10\%}$CL$_{7\%}$ copolymer). The chosen anti-blocking additives were a 2 %-wt content of Plustalc H05C® and a 0.5 %-wt content of Incromax® 100. To achieve a good dispersion of the anti-block additives in the mix-PEPG20/PEG35$_{20\%}$DLac$_{4\%}$ copolymer, an additional melt extrusion blending step in a twin screw extruder was done at 160 °C before the blown film processing. To avoid the undesired MFI increase

to above 10 g/10min during the pre-blending operation, a high melt degradation stability of the mix-PEPG20/PEG35$_{20\%}$DLac$_{4\%}$ copolymer had to be ensured.

This was achieved through the strategies presented in Section 5.2.1. The mix-PEPG20/PEG35$_{20\%}$DLac$_{4\%}$ block copolymer was synthesized in the presence of a lower catalyst content of 2.86 · 10^{-5} mol$_{Sn(oct)2}$/mol$_{Lactide}$ and a 0.5 %-wt TNPP content. The TNPP content allowed a Mn value slightly above the theoretical maximum to be obtained by avoiding hydrolysis side reactions, while the reduced catalyst reduced the hydrolysis Mn degradation rate during processing and led to a lower discoloration of the mix-PEPG20/PEG35$_{20\%}$DLac$_{4\%}$ block copolymer when compared to the previous star-PEPG20$_{13\%}$, star-PEPG20$_{13\%}$DLac$_{4\%}$, and star-PEPG20$_{10\%}$CL$_{7\%}$ block copolymers (Figure 5.44).

<div align="center">(a)   (b)</div>
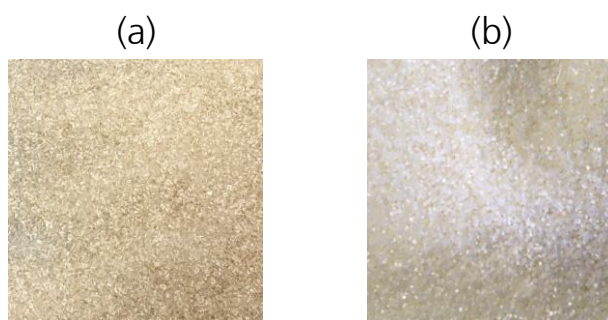
Figure 5.44: Discoloration of the pellets of the a) star-PEPG20$_{13\%}$DLac$_{4\%}$ block copolymer and b) the mix-PEPG20/PEG35$_{20\%}$DLac$_{4\%}$ block copolymer. Color of the star-PEPG20$_{13\%}$ and star-PEPG20$_{10\%}$CL$_{7\%}$ block copolymers were similar to the star-PEPG20$_{13\%}$DLac$_{4\%}$ block copolymer.

The mix-PEPG20/PEG35$_{20\%}$DLac$_{4\%}$ block copolymer and the Plustalc H05C® anti-block additive were thoroughly dried before melt blending. MFI measurements before and after blending of the anti-block additives into the mix-PEPG20/PEG35$_{20\%}$DLac$_{4\%}$ copolymer show a slight increase of the MFI value from 5.6 g/10min to 5.9 g/10min at 160 °C. The MFI value of 5.9 g/10min allowed stable blown film processing of the mix-PEPG20/PEG35$_{20\%}$DLac$_{4\%}$ block copolymer containing the anti-block additives. Smooth, uniform films with low adherence between the layers were produced. The film layers could be separated from each other even several months after production.

Orientation effects during processing

Stretching of the melt during blown film extrusion processing is known to lead to orientation of the polymer chains in the direction of stretching. The degree of orientation can have an effect on the mechanical, barrier, and thermal properties of the produced blown films. Although the effects of orientation on the material properties are out of the scope of this work, the effect of orientation on the thermal properties was investigated to obtain a general perspective of the degree of orientation that was obtained during processing of the copolymers.
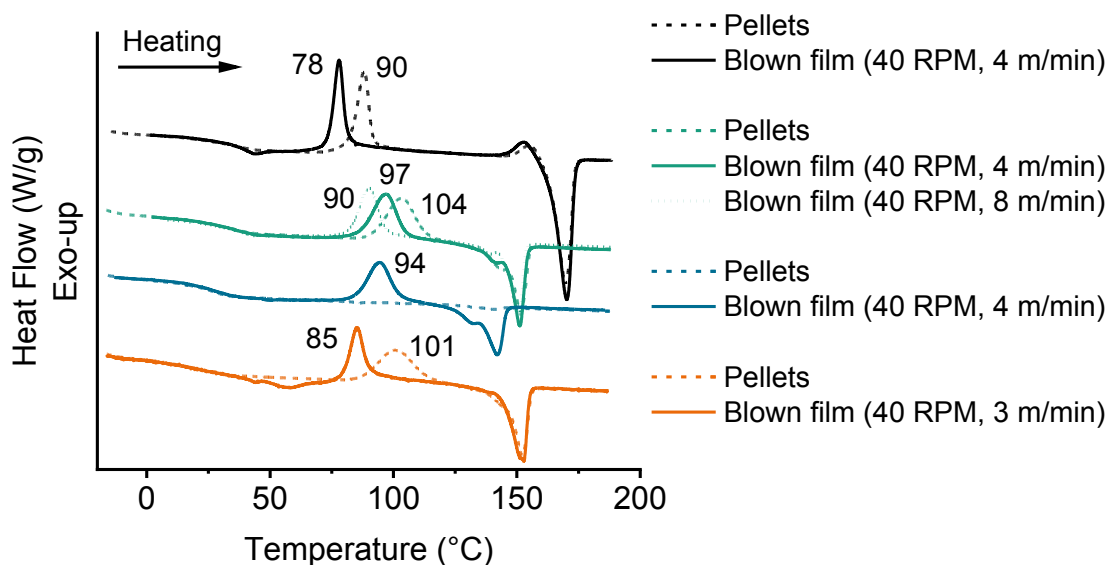
Figure 5.45: Non-isothermal DSC measurements (10 °C/min) of the second heating cycle of the (dashed lines) pellets as synthesized and first heating cycle for the (solid lines) processed blown films at the given conditions (V_{Screw}, V_{NP}). Line colors refer to: (■) star-PEPG20$_{13\%}$, (■) star-PEPG20$_{13\%}$DLac$_{4\%}$, (■) star-PEPG20$_{10\%}$CL$_{7\%}$, and (■) mix-PEPG20/PEG35$_{20\%}$DLac$_{4\%}$ block copolymers.

Figure 5.45 shows that the peak Tc of the processed blown films was below the peak Tc of the virgin pellets. When the V_{NR} was increased while keeping V_{Screw} constant, as done during blown film processing of the star-PEPG20$_{13\%}$DLac$_{4\%}$ block copolymer, a further reduction of the peak Tc of the blown films was observed. The peak Tc reduction could be caused by the molecular orientation achieved by the polymer chains when stretched during blown film processing and by the formation of crystalline nuclei that reduce the onset temperature of cold crystallization [194]. To further investigate the presence of crystalline nuclei, the degree of crystallinity (X_C) of the blown films (based on the non-isothermal DSC measurements in Figure 5.45) were calculated and are shown in Figure 5.46.
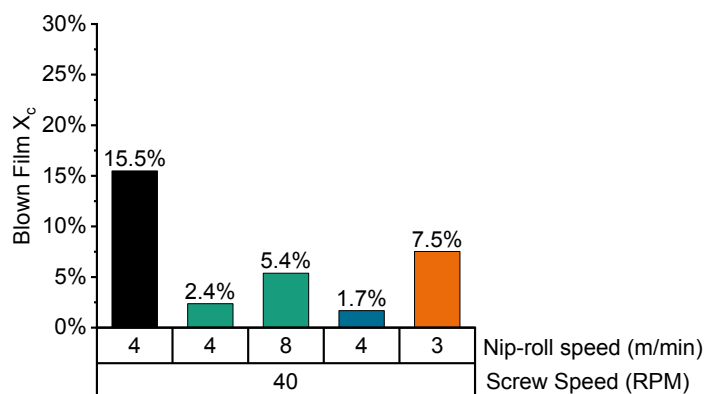

Figure 5.46: Degree of crystallinity (X_c) of the blown films directly after processing at the given nip-roll (V_{NR}) and screw speeds (V_{Screw}) for the (■) star-PEPG20$_{13\%}$, (■) star-PEPG20$_{13\%}$DLac$_{4\%}$, (■) star-PEPG20$_{10\%}$CL$_{7\%}$, and (■) mix-PEPG20/PEG35$_{20\%}$DLac$_{4\%}$ block copolymers.

X_C of almost 16 % could be observed for the star-PEPG20$_{13\%}$ copolymer blown film processed at V_{Screw} of 40 RPM and V_{NR} of 4 m/min. The other two blown films processed the same conditions show significantly lower X_C values of only 2.4 % (star-PEPG20$_{13\%}$DLac$_{4\%}$ copolymer) and 1.7 % (star-PEPG20$_{10\%}$CL$_{7\%}$ copolymer). This is likely due to their X_D and X_{CL} values reducing their crystallization rates (Figure 5.39). Although these X_C values are relatively low, they are likely able to generate the necessary crystal nuclei to cause the observed peak Tc reductions in the processed films shown in Figure 5.45. When V_{NR} was doubled from 4 to 8 m/min (while keeping V_{Screw} at 40 RPM) during processing of the star-PEPG20$_{13\%}$DLac$_{4\%}$ copolymer, the X_C increased from 2.4 % to 5.4 %. The higher X_C of the star-PEPG20$_{13\%}$DLac$_{4\%}$ copolymer film processed when the V_{NR} was further increased could explain the further peak Tc reduction from 97 °C to 90 °C (Figure 5.45).

Additionally to the lower peak Tc of the blown films directly after processing (Figure 5.45), the star-PEPG20$_{13\%}$ and the PEPG20/PEG35$_{20\%}$DLac$_{4\%}$ block copolymer blown films showed a melt crystallization peak during cooling (Figure 5.47). None of the as-synthesized virgin block copolymer pellets show any significant melt crystallization peaks during cooling at 10 °C/min.
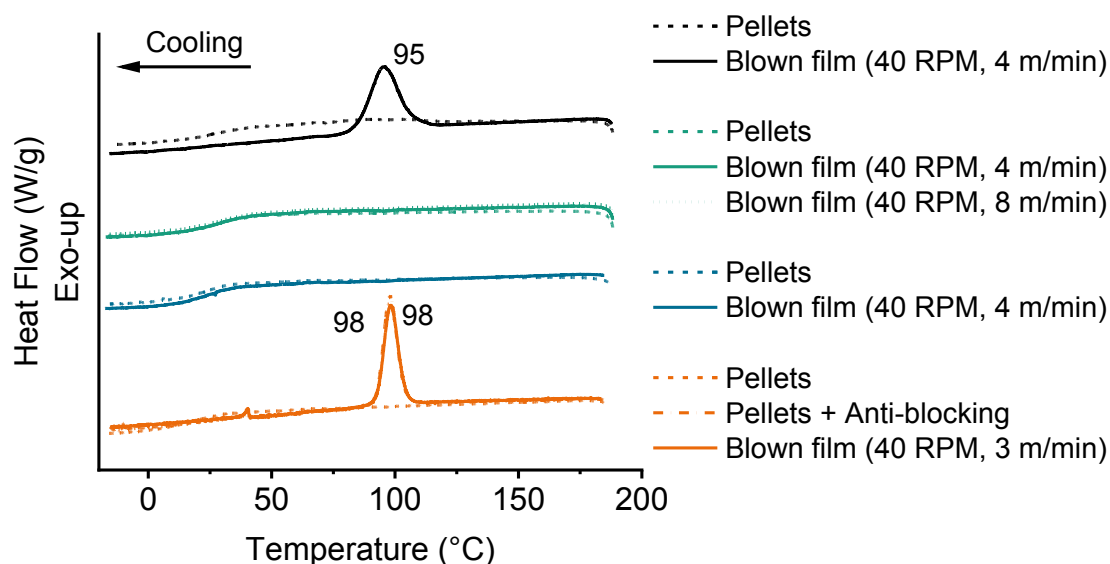

Figure 5.47: Non-isothermal DSC measurements of the second cooling cycle (10 °C/min) of the as-synthesized pellets (dashed lines) and of the first cooling cycle of the different blown films produced with the given conditions (V_{Screw}, V_{NP}) after holding them at 190 °C for 2 min. Line colors refer to: (■) star-PEPG20$_{13\%}$, (■) star-PEPG20$_{13\%}$DLac$_{4\%}$, (■) star-PEPG20$_{10\%}$CL$_{7\%}$, and (■) mix-PEPG20/PEG35$_{20\%}$DLac$_{4\%}$ block copolymers.

Interestingly, the unprocessed mix-PEPG20/PEG35$_{20\%}$DLac$_{4\%}$ block copolymer (containing anti-blocking additives) virgin pellets also exhibited a melt crystallization peak during cooling (Figure 5.47). In this case, the anti-blocking additives could be functioning as a nucleating agent that reduces the nucleation energy barrier and increases the crystallization rate of this copolymer (Figure 5.40). The crystallization rate is increased to such a level, that melt crystallization during cooling can occur with the relatively low stereoregularity of this material (X_D = 4 %-wt).

The melt crystallization peak observed during cooling of the star-PEPG20$_{13\%}$ copolymer film suggests that some of the orientation obtained during blown film processing was maintained even after subsequently melting the films. Once the star-PEPG20$_{13\%}$ block copolymer blown films had been

processed, the crystallization peak was found to only appear during cooling the molten star-PEPG20$_{13\%}$ block copolymer films (at 10 °C/min) and not anymore during heating of the films even after repeating the heating and cooling cycles four times (Figure A 25).

A similar so-called "melt memory effect" was observed in polyamide polymers by Khanna et al. and other groups [195–199]. They showed that the retained orientation memory of the polymer melt influenced the recrystallization rate and the morphology of the polymers in subsequent heating cycles, even after melting the crystals. Khanna et al. [195] proposes a hypothesis in which the virgin material has a relatively higher level of polymer chain entanglement than the oriented (processed) material. This was explained through the formation of entanglements during polymerization (as the polymer chain length is increasing) that are otherwise be highly unlikely in a pre-oriented system composed of polymer chains already of the final length (after polymerization).

Khanna et al. [196] suggested that intermolecular interactions such as the well-known hydrogen bonds in polyamide polymers retain the orientation achieved during processing even after heating the polymers above their equilibrium melting temperature for a long time. The persistence of the hydrogen bonds at such high temperatures however, seems unlikely. Alternatively, the entropic barrier that would have to be overcome to obtain the entangled conformations achieved directly after polymerization, could simply be too large for the "oriented" or processed polymer to reconfigure to this high-entropy state. In this way, the polymer would thus permanently remain in a less entangled state than the one achieved directly after polymerization.
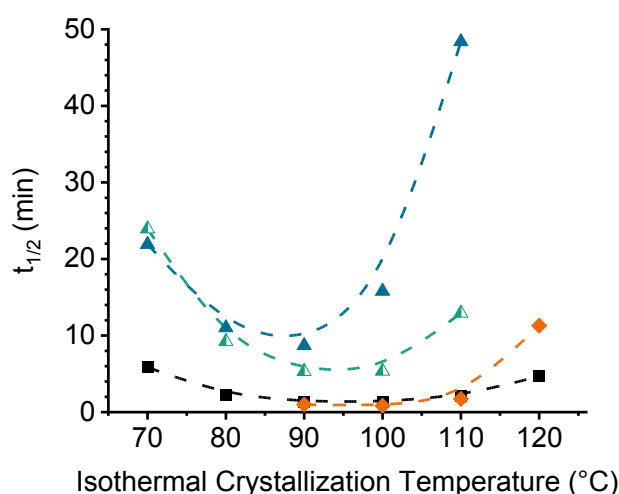

Figure 5.48: Crystallization half-time ($t_{1/2}$ - min) calculated from DSC isothermal crystallization measurements of the blown films produced with the given process parameters. (■) star-PEPG20$_{13\%}$ processed at V_{Screw} = 40 RPM and V_{NR} 4 m/min, (△) star-PEPG20$_{13\%}$DLac$_{4\%}$ processed at V_{Screw} = 40 RPM and V_{NR} = 4 m/min, (▲) star-PEPG20$_{10\%}$CL$_{7\%}$ processed at V_{Screw} = 40 RPM and V_{NR} = 4 m/min, and (◆)mix-PEPG20/PEG35$_{20\%}$DLac$_{4\%}$ with 2 %-wt anti-block talc additive processed at V_{Screw} = 40 RPM and V_{NR} = 3 m/min.

Figure 5.48 shows the $t_{1/2}$ of the processed blown films. In all cases, a significant increase in the crystallization rate (i.e. lower $t_{1/2}$) were observed even when for the block copolymers that did not show melt crystallization during cooling in the non-isothermal DSC curves (Figure 5.48). For example,

the $t_{1/2}$ at 90 °C of the star-PEPG20$_{13\%}$DLac$_{4\%}$ copolymer was reduced from 20.3 min for the virgin pellets to 5.3 min for the processed blown film (V_{screw} = 40 RPM, V_{NR} = 4 m/min). Similarly, the $t_{1/2}$ of the star-PEPG20$_{10\%}$CL$_{7\%}$ copolymer was reduced from 42 min for the virgin pellets to 11 min (at 80 °C) for the processed blown film. These experiments suggest that a higher degree of orientation (achieved after processing) that facilitates nucleation of the block copolymers, remains present even after melting of the crystals. This is true even if no crystallization during cooling (melt crystallization) is observed in the non-isothermal DSC measurements (Figure 5.47).

5.3.5 Mechanical properties

Blown film samples with comparable single-layer film thicknesses of roughly 50 µm were obtained for all the block copolymers shown in Table 5.11. Unfortunately, the star-PEPG20$_{10\%}$CL$_{7\%}$ blown films were completely blocked a couple of days after processing (Section 5.3.4) and measurement of the single-layer films was not possible. The tensile properties of the blocked star-PEPG20$_{10\%}$CL$_{7\%}$ films were anyway measured using both layers together (double-layer film thickness = 85 µm). Although the measured force in a typical tensile test is in a way "normalized" by the test sample thickness (stress = force / area), the elastic modulus and elongation at break values measured for the star-PEPG20$_{10\%}$CL$_{7\%}$ block copolymer double-layer films should be compared with some skepticism (due to the different experimental conditions). A description of the produced films is shown in Table 5.15 and their respective elastic modulus and elongation at break values in the machine (MD) and the transversal directions (TD) are shown in Figure 5.49.

Similar tendencies to those observed with the injection-molded tensile test specimens produced at the laboratory scale (Section 5.1) were observed with the processed blown films. The star-PEPG20$_{13\%}$ and star-PEPG20$_{13\%}$DLac$_{4\%}$ copolymer blown films with similar Tg values of 36 °C and 37 °C, showed similar elongation at break values (MD) of 280 % and 300 % respectively. The elastic modulus (MD) of the star-PEPG20$_{13\%}$DLac$_{4\%}$ blown film however, was found to be slightly lower than the elastic modulus of the star-PEPG20$_{13\%}$ blown film. This is likely due to the reduced X_C of the star-PEPG20$_{13\%}$DLac$_{4\%}$ copolymer films (compared to that of the star-PEPG20$_{13\%}$ films) as shown in Figure 5.46.

As Tg of the block copolymer films was reduced, their elongation at break increased and the elastic modulus decreased (Figure 5.49). The star-PEPG20$_{10\%}$CL$_{7\%}$ copolymer films (Tg = 27 °C), had a lower elastic modulus (MD) of 186 MPa and a higher elongation at break (MD) of 350 % than the copolymer films with Tg ~ 36 °C. When the Tg was reduced to 22 °C (as in the mix-PEPG20/PEG35$_{20\%}$DLac$_{4\%}$ copolymer films) an even lower elastic modulus (MD) of 139 MPa and a higher elongation at break (MD) of 410 % were obtained.

Table 5.15: Processing conditions and thickness of a single layer of the blown films (when applicable) used for mechanical testing.

Material	Screw Speed [RPM]	Nip-roll speed [m/min]	Film Thickness [μm]
star-PEPG20$_{13\%}$	40	4	54 (± 3.2)
star-PEPG20$_{13\%}$DLac$_{4\%}$	40	4	48 (± 2.3)
star-PEPG20$_{10\%}$CL$_{7\%}$	40	4	84 (± 1.7)[a]
mix-PEPG20/PEG35$_{20\%}$DLac$_{4\%}$	40	3	56 (± 1.3)

a) Blocking of the star-PEPG20$_{10\%}$CL$_{7\%}$ block copolymer blown film did not allow tensile testing of a single layer of film. The two layers stuck together were used for mechanical tensile testing.
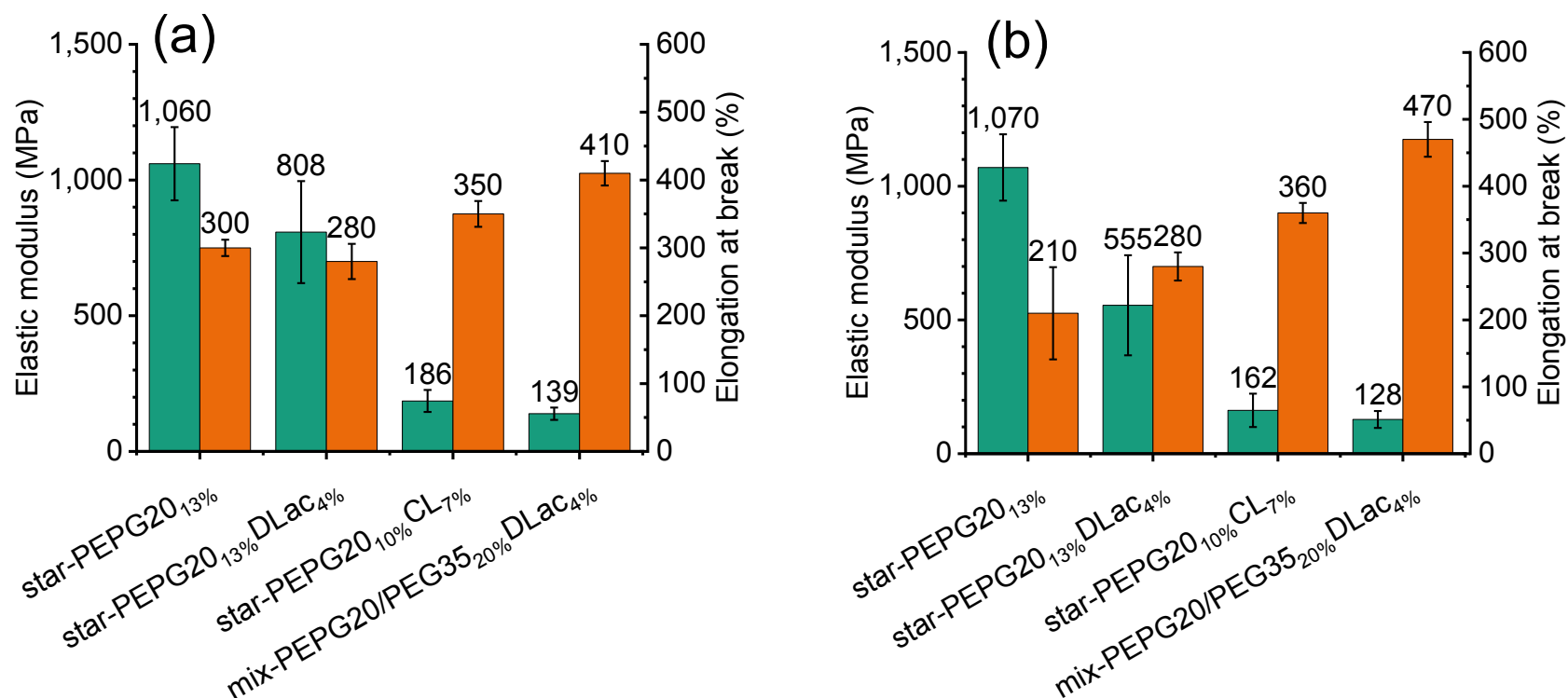
Figure 5.49: (■) Elastic modulus and (■) elongation at break of blown film type 2 test specimens elongated along (a) the machine direction (MD) and along (b) the transverse direction (TD) according to DIN EN ISO 527-3.

Although the elongation at break values of the star-PEPG20$_{13\%}$ and star-PEPG20$_{13\%}$DLac$_{4\%}$ copolymer blown films were significantly higher than those of commercial Ingeo® 4043D blown films (3 % for 25 µm Ingeo® 4043D blown film [200]), these copolymer blown films were still relatively stiff and brittle. When these films were stretched manually, the films apparently had an irregular failure behavior. In some cases, the films would break directly after an elongation force was applied, while in other cases the films would first elongate quite a bit before failure. Tensile tests at different elongation rates (Figure 5.50) of the star-PEPG20$_{13\%}$ and mix-PEPG20/PEG35$_{20\%}$DLac$_{4\%}$ block copolymer blown films, show that what was thought to be irregular behavior is actually a relatively strong dependency of the elongation at break of the star-PEPG20$_{13\%}$ films on the rate of elongation. As mentioned in Section 2.2.1, low elongation rates give the polymer chains in a material enough time to begin to "flow" under an imposed deformation. This is observed with the star-PEPG20$_{13\%}$ block copolymer blown film. At a low elongation rate of 1 mm/min, this film exhibits a relatively low elastic modulus of 708 MPa and a high elongation at break value of 470 %. When the same film is elongated at a higher rate of 1,000 mm/min, its elastic modulus increased to 1,200 MPa and its elongation at break was reduced to 13 % (exhibiting a more stiff and brittle behavior). The mix-PEPG20/PEG35$_{20\%}$DLac$_{4\%}$ copolymer film showed a more stable elongation at break value of around 480 % at elongation rates of both 1 mm/min and a 1,000 mm/min, while its elastic modulus increased from 319 MPa at an elongation rate of 1 mm/min to 780 MPa at an elongation rate of 1,000 mm/min.

Interestingly, the mechanical properties of the star-PEPG20$_{13\%}$ copolymer film tested at an elongation rate of 1 mm/min appear to be quite similar to the properties of the mix-PEPG20/PEG35$_{20\%}$DLac$_{4\%}$ copolymer film tested at 1,000 mm/min. This illustrates the similar effects that strain rate and temperature can have on the mechanical properties of these viscoelastic copolymer films. The effects of a Tg difference of 15 °C between the star-PEPG20$_{13\%}$ and the mix-PEPG20/PEG35$_{20\%}$DLac$_{4\%}$ copolymer films was roughly mimicked by elongating the mix-PEPG20/PEG35$_{20\%}$DLac$_{4\%}$ copolymer film 1,000 times faster than the star-PEPG20$_{13\%}$ copolymer film (Figure 5.50).
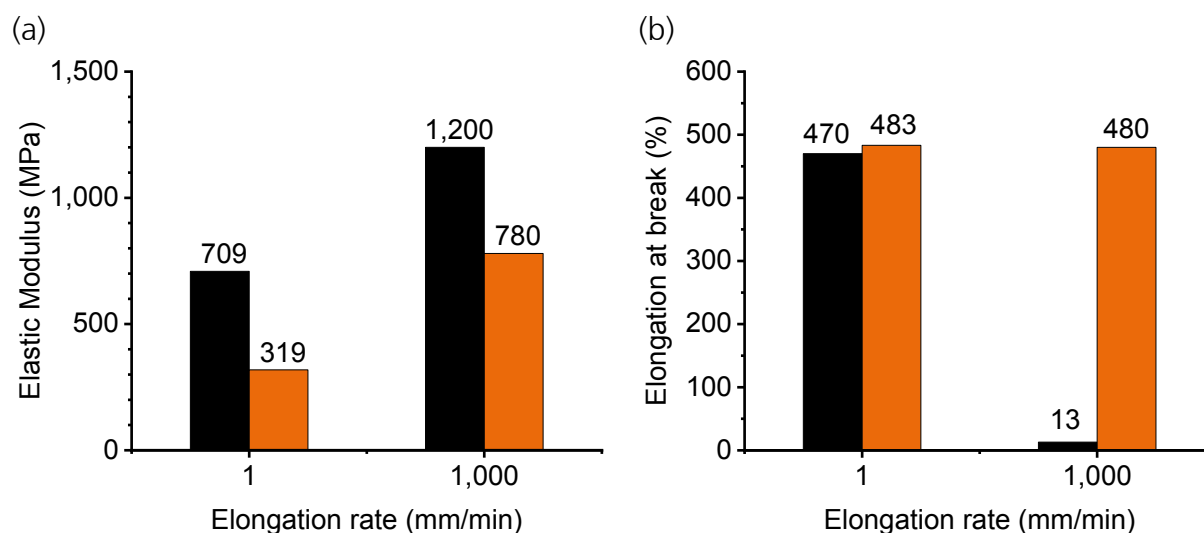

Figure 5.50: Effect of the rate of elongation (mm/min) on (a) the elastic modulus and (b) the elongation at break of the (■) star-PEPG20$_{13\%}$ block copolymer and the (■) mix-PEPG20/PEG35$_{20\%}$DLac$_{4\%}$ block copolymer blown films in the machine direction.

5.3.6 Physical ageing experiments in N$_2$ atmosphere

To study the physical ageing behavior of the mix-PEPG20/PEG35$_{20\%}$DLac$_{4\%}$ block copolymer, 40 injection-molded tensile test specimens were produced. Of these specimens, 15 were injection-molded with the virgin copolymer pellets and tested as produced (amorphous). Another 15 specimens were injection-molded with the virgin copolymer pellets and subsequently crystallized by annealing the pre-dried specimens between two glass plates at 100 °C for 30 min (semi-crystalline). Finally, 10 specimens were injection-molded using the mix-PEPG20/PEG35$_{20\%}$DLac$_{4\%}$ + anti-block additive blend used for the blown film extrusion experiments (anti-block mix). All samples were stored under a dry nitrogen atmosphere in sealed aluminum bags until 24 h before tensile testing to avoid molar mass degradation by hydrolysis during ageing. Tensile tests of the amorphous and semi-crystalline specimens (5 specimens per measurement) were done 2, 21, and 108 days after production, while tensile tests of the anti-block mix specimens were done 17 and 108 days after production. The changes in the elastic modulus and elongation at break over time for each material are shown in Figure 5.51.
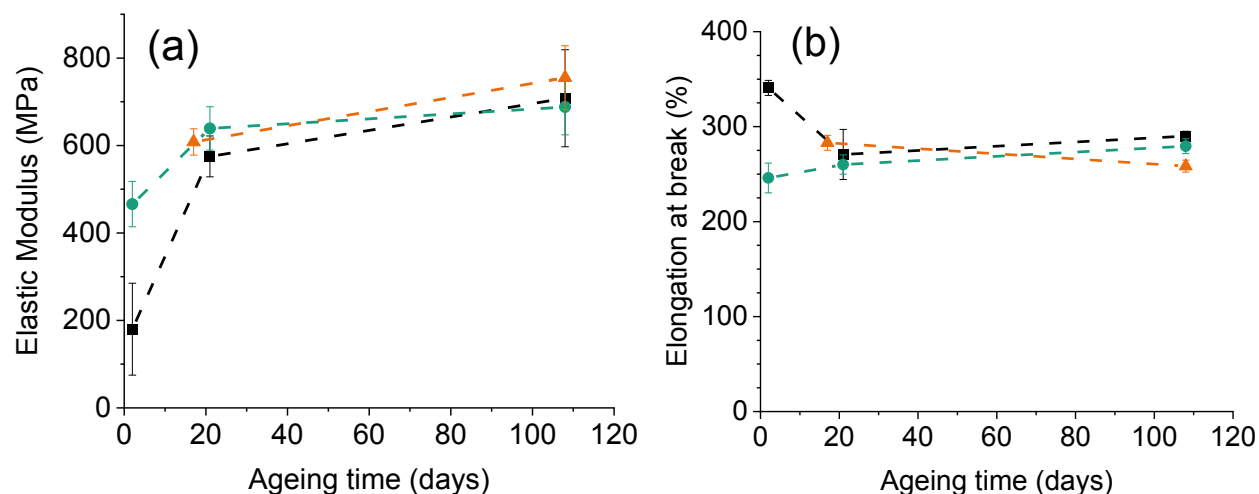

Figure 5.51: Elastic modulus (a) and elongation at break (b) of injection molded tensile test specimens of the mix-PEPG20/PEG35$_{20\%}$DLac$_{4\%}$ block copolymer in the (– ■ –) amorphous state, (– ● –) crystalline state, and in the presence of (– ▲ –) anti-blocking additives. Samples were aged under inert atmosphere to avoid hydrolysis.

Between 2 and 21 days after production of the injection-molded tensile test specimens, a significant increase of the elastic modulus was observed for the amorphous and semi-crystalline materials [Figure 5.52 (a)]. The increase of the elastic modulus in the amorphous specimens (from 180 to 575 MPa) was more pronounced than for the semi-crystalline specimens (from 466 to 639 MPa). After the initial 21 days (until the next measurement 108 days later) however, virtually no change in the elastic modulus (~ 700 MPa) of the amorphous, semi-crystalline, or anti-block mix specimens was observed.

Small and defective chain-extended fibrilar crystals are known to form after processing (causing polymer chain orientation) of polymers like i-PP [201] and PET [202; 203]. A rearrangement of these

fibrilar crystals into periodic microstructures through folding of the extended chains into lamellar crystals of higher perfection is known to occur upon heat treatment (annealing above Tg) of such oriented polymer chains [201–203]. Given the orientation achieved during blown film extrusion (Figure 5.46) or injection molding (Figure A 23) of the mix-PEPG20/PEG35$_{20\%}$DLac$_{4\%}$ copolymer chains, the formation of fibrilar crystals during processing is a possibility that could be further investigated with x-ray measurements. Because the Tg of the mix-PEPG20/PEG35$_{20\%}$DLac$_{4\%}$ copolymer (22 °C) is below room temperature, ageing of the tensile test specimens above their Tg (at room temperature) could give the copolymer chains enough mobility to allow crystal rearrangement into lamellar crystals (similar to a heat treatment for oriented i-PP or PET). It is important to note that the glass transition of this block copolymer has an onset at 10 °C and an end-point at 30 °C. Considering the glass transition range (and not a single point) a significant changes in the rate of chain rearrangement are expected depending on the storage temperature of the tensile test specimens.

Such a crystallization event could cause the increase of elastic modulus (between 2 and 21 days) observed for the amorphous tensile test specimens (Figure 5.51). The higher elastic modulus of the semi-crystalline specimens than that of the amorphous ones could be caused by an "accelerated" rearrangement of the fibrilar crystals into lamellar crystals achieved by the annealing process (30 min at 100 °C) to which the semi-crystalline specimens were exposed. The crystal rearrangement process is likely to be almost complete after storage of the tensile test specimens for 21 days, given the similar elastic modulus values of all the samples (regardless of crystallinity) after this time. Such reorientation events have been observed in melt oriented PLA films upon heat treatment above the Tg in several studies [7; 204–208].

A reduction in the elongation at break [Figure 5.51 (a)] was only registered for the amorphous material tensile test specimens between 2 and 21 days after production (from 340 to 270 %). This reduction is likely due to the before-mentioned crystal rearrangement process. Interestingly, the elongation at break of the semi-crystalline specimens measured after 2 days (250 %) was in a similar range to the elongation at break of the amorphous sample after 21 days (270 %). This could be due to the semi-crystalline sample reaching the equilibrium lamellar crystal arrangement (avoiding further reduction of the elongation at break). This is supported by the observation that the elongation at break of all the samples after the initial 21 days (until 108 days of ageing) remained stable at a value of around 270 %. It is important to note however, that the elongation at break remained relatively high even with the rigid crystal structures formed during ageing. This suggests (1) that the plasticizing polyether block content remains fairly well distributed in the amorphous regions between the crystalline structures even after crystallization events and (2) that the low X_C that can be achieved due to the X_D of 4 %-mol does not allow the creation of a rigid crystalline network that completely immobilizes the copolymer chains. The aggregation of the polyether plasticizer or its migration out of the PLA matrix during chain rearrangement is likely avoided by the covalent bonds between the polyether and PLLA blocks. Further studies with simple PLLA / polyether blends (no covalent bonds) could give further information about the role of the covalent bond during ageing of the materials.

Although the performed ageing tests were mainly done to determine the stability of the mechanical properties of the material over longer periods of time, a possible crystal rearrangement mechanism was detected. Further ageing experiments of processed blown films having a higher degree of orientation coupled with DSC and x-ray measurements could give further information about the

possible mechanism. Additionally, ageing the specimens at temperatures below the Tg of the material could give information about the influence of the temperature on the possible rearrangement mechanisms.

5.3.7   Comparison with commercial films

The mechanical properties in the machine direction (MD) of the mix-PEPG20/PEG35$_{20\%}$DLac$_{4\%}$ block copolymer blown films are compared to the reported mechanical properties (MD) of commercially available films in Figure 5.52. The LDPE 525E® film is a completely fossil based product and the Ecovio® C2224 films contains 55 %-wt of the fossil-based PBAT polyester and a 45 %-wt PLA content.
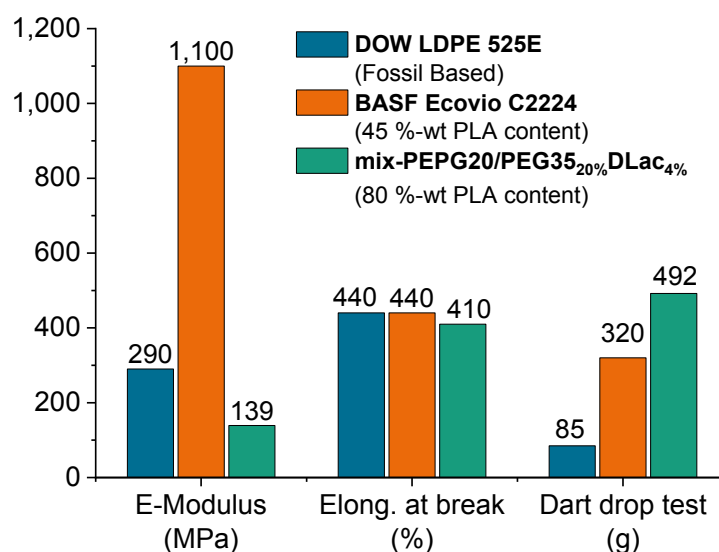
Figure 5.52: Comparison of the mechanical properties (ISO 527-3) in the machine direction (MD) of commercial LDPE 525E® from Dow (data taken from [209]), Ecovio® C2224 PLA + PBAT blend from BASF (data taken from [210]), and the measured mix-PEPG20/PEG35$_{20\%}$DLac$_{4\%}$ block copolymer blown films.

In general, the mechanical properties of the copolymer films are in a similar range to those of the commercial film-grade materials. This was done with a significantly higher PLA content of 80 %-wt (bio-based and biodegradable) when compared to the commercial materials (Figure 5.52). As previously mentioned, the possibility of using bio-based polyethers (in the future) [25; 26] as the plasticizing block in the copolymers could make these films completely bio-based. Further tests are required to determine the biodegradability of the copolymer films. If the production costs of the block copolymers were found to be sufficiently low and the copolymer films were found to be biodegradable, they would be able to compete commercially with the Ecovio® C2224 material.

The mix-PEPG20/PEG35$_{20\%}$DLac$_{4\%}$ copolymer films have practically the same elongation at break values as the commercial films (~ 400 %). The elastic modulus of the copolymer films is significantly lower than that of the BASF Ecovio C2224 PLA + PBAT blend and slightly lower than that of the LDPE

525E film. A higher elastic modulus of the copolymer films could be obtained by inducing some crystallization during processing or through a subsequent annealing process. The falling dart impact resistance of the copolymer films was higher than that of the commercial films. Figure 5.52 shows that the obtained mechanical properties of the copolymer films are comparable to those of commercial products.

6   Conclusions

In this thesis, PLLA-b-polyether-b-PLLA block copolymers with different chemical structures were synthesized. The thermal, mechanical, and rheological properties of these copolymers were systematically studied to establish structure-property relationships that can be used to design PLA-based materials for specific applications. This was demonstrated by successfully processing a PLA-based block copolymer in a conventional semi-technical blown film extrusion line and obtaining uniform films with similar properties to those made with commercial LDPE flexible film grade materials.

The block copolymers were synthesized through an industrially feasible ROP of L-lactide in the bulk, at 180 °C, and using the conventional $Sn(Oct)_2$ as catalyst. Instead of using high boiling alcohol ROP initiators like 1-undecanol (as commonly done industrially), polyether macroinitiators with –OH end-groups were used as macroinitiators. Through this synthesis method, the molar mass of the block copolymers was controlled by defining the lactide monomer to –OH initiator ratio. Different polyether block chemical structures were introduced into the copolymers by using different polyether macroinitiators (i.e. PEG, PPG, PEPG). The chemical structure of the PLLA blocks were also modified by copolymerizing L-lactide with D-lactide or ε-caprolactone (CL).

A wide range of material properties of the block copolymers were accessed through the before-mentioned modifications in their chemical structure. By introducing D-lactide or CL repeat units into the PLLA blocks, the peak Tm of the block copolymers together with their crystallization rates were reduced. By increasing the miscible PEG or PEPG polyether block content or by increasing the CL repeat units in the PLLA blocks, Tg of the block copolymers was reduced through a plasticization mechanism. As the Tg of the copolymers was reduced, the copolymer materials became softer and more flexible. Block copolymers with elastic moduli as low as 17 MPa and elongation at break values as high as 400 % were produced, which strongly contrast with the typical elastic moduli of 3,500 MPa and elongation at break values of 5 % of PLA homopolymers.

The Tg reductions required to achieve the desired mechanical properties, simultaneously reduced the melt flow index (MFI) of the copolymers. A soft and flexible block copolymer with a Tg of 24 °C had a relatively high MFI of 30 g/10min at its processing temperature. This MFI value did not match the targeted processing range (between 2 and 10 g/10min) for blown film extrusion, through which such soft and flexible materials are normally processed. To reduce the MFI into the processible range while keeping the Tg at a low value (to have soft and flexible materials), the molar mass of the block copolymers was increased. Hydrolytic molar mass degradation was counteracted by adding TNPP into the reaction mixture to promote chain extension of the hydrolyzed PLA chains during the ROP. Further, the rate of the molar mass degradation reactions during processing was reduced by lowering the catalyst concentration in the block copolymers. Moreover, tetrafunctional macroinitiators with Mn values of 20 – 25 kDa were used to synthesize block copolymers of higher Mn values and with star topologies. With these optimizations, block copolymers of high molar mass (Mn ~ 111 kDa) with an acceptable melt stability were synthesized while keeping the Tg of the copolymers at 22 °C (polyether block contents of 20 %-wt). Additionally, the Tm of the block copolymers was reduced by introducing D-lactide and CL comonomers into the PLLA blocks, which rendered their processing at

lower temperatures possible. The lower processing temperatures reduced the molar mass degradation rate and reduced the MFI values (increased melt viscosity).

Based on the mentioned changes in the molecular structure and on the optimizations of the ROP synthesis, a soft and flexible PLA-based block copolymer (~ 80 %-wt PLA content) with an MFI value of 5.7 g/10min was synthesized and successfully processed in a blown film extrusion line. Uniform blown films with a thickness of 50 μm were produced under steady processing conditions. The elastic modulus (139 MPa) and the elongation at break (410 %) of the produced blown films were similar to those of commercially available flexible film grade materials. The mechanical properties of these materials remained stable over 108 days (~ 3.5 months) without any plasticizer migration during this time.

7   Outlook

Although PLLA-b-polyether-b-PLLA block copolymer structures could enable the use of PLA-based materials in flexible film applications, further research on the end-of-life concept for such block copolymers is still necessary. Multi-component materials such as these block copolymers could pose important challenges during recycling, which is a relevant concern for such "sustainable" materials. If recycling of the block copolymers proves to be too difficult, biodegradation can be considered as an additional end-of-life option. Biodegradability tests of the block copolymers would determine if the flexible films designed in this work could be a viable option in applications like agricultural films, food packaging, or organic waste collection bags (were biodegradability is desired). Copolymerization with comonomers such as glycolide (known to improve the biodegradability of PLA) can be considered as an option to control the biodegradability of the copolymer films.

If improved barrier properties of the copolymer films are required for some food packaging applications, co-extrusion experiments with ethylene vinyl acetate (EVA) polymers to produce multi-layer films can be investigated. EVA is a biodegradable polymer that is known to improve the water and oxygen barrier properties of films.

Additionally, a more detailed rheological study of the block copolymers could help further improve the processability of the copolymers. Until now, the plateau modulus of the block copolymers has not been measured because of the low temperatures required (below the Tm of the copolymers). When considering the isothermal crystallization experiments performed in Section 5.3.2 however, it seems possible to measure a frequency sweep at temperatures well below Tm before significant crystallization occurs (~ 5 to 10 min), especially with the copolymers with a comonomer content (X_D or X_{CL}). The value of the plateau modulus could help determine the entanglement molecular mass (M_e) of the block copolymers and its dependency on the different chemical copolymer structures and their different topologies.

The use of kinetic models (available in the literature) for designing an industrial-scale synthesis process of the PLLA-b-polyether-b-PLLA block copolymers is an important area of future work. Such modelling can allow the economic viability of such triblock copolymer structures to be analyzed as well as give a strong basis on which such a process could be realized. Industrial or semi-industrial scale synthesis of the block copolymers could allow more in-depth studies on the processing behavior of the copolymers to be performed.

Finally, future work includes the development of PLLA-b-polyether-b-PLLA block copolymer structures designed for other specific applications (as done in this work for flexible blown film applications). The rheological and mechanical properties can be optimized to ensure efficient processing and adequate mechanical properties for a wide range of applications, given the wide range of mechanical properties that could be accessed with the copolymers.
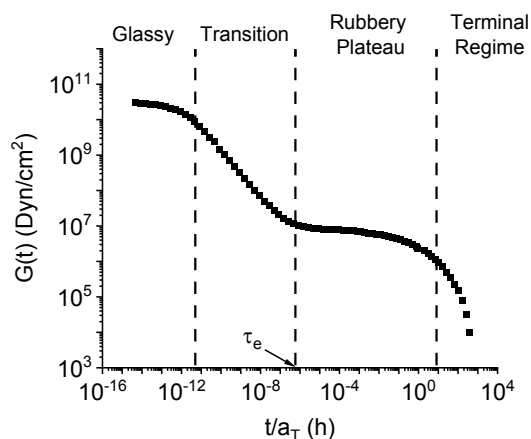
8   Appendix

Figure A 1: Master stress relaxation curve for polyisobutylene taken from [211] showing the different stress relaxation events.

At low relaxation times, a solid-like glassy plateau (no relaxation) with a high G(t) value is observed. This is followed by a reduction of the G(t) (relaxation) called the transition regime at longer times. At a time τ_e, shows a second solid-like plateau (relaxation halts) called the rubbery plateau in which the temporary molecular entanglements in the polymer melt act as physical crosslinks similar to what would be encountered in a crosslinked rubber. This plateau continues until finally at sufficiently long times, the polymer enters the terminal relaxation regime in which a final relaxation event occurs down to very low values of the G(t).
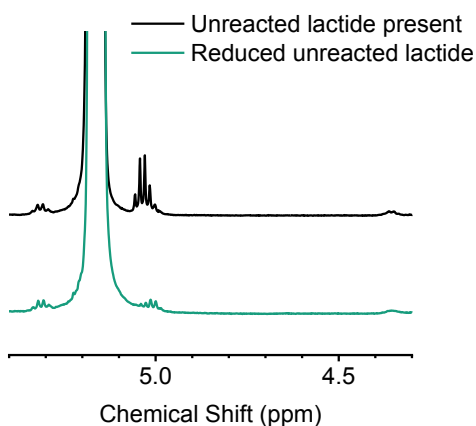
Figure A 2: Used ^{1}H-NMR signals for Mn calculations: 5.2 ppm (–CHOH proton in the PLA chains), 4.35 ppm (–CHOH proton in the PLA end-group). Used signals for lactide %-wt content calculations: at 5.2 and 5 ppm for the –CHOH proton in the PLA chains and in the unreacted lactide monomer respectively together with the satellite peak signal at 5.3 ppm.
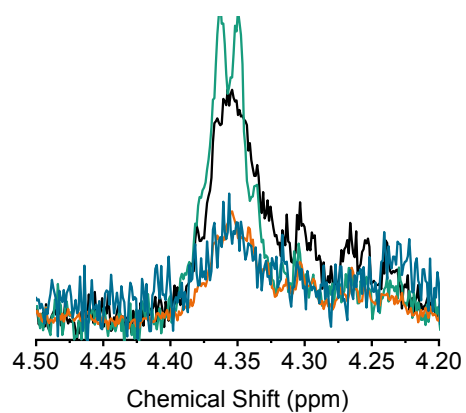
Figure A 3: Close-up of the used ^{1}H-NMR –C$\underline{H}$OH proton in the PLA end-group signal at 4.35 ppm used for the Mn calculations.
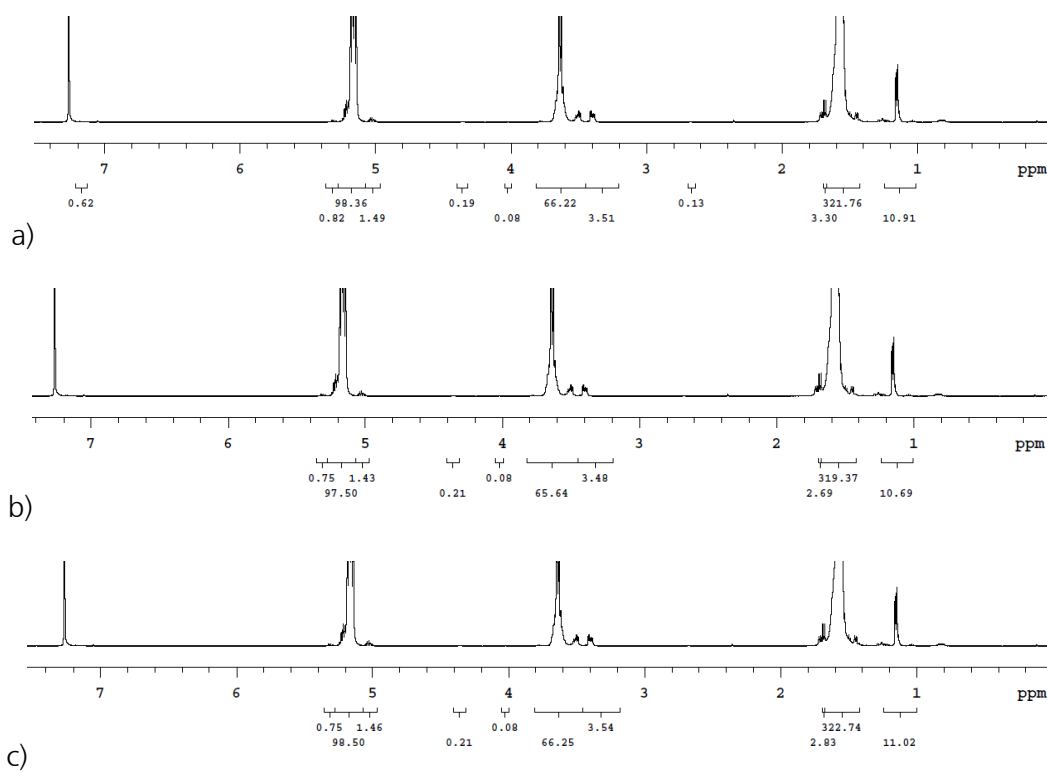
Figure A 4: Effects of changing the integration limits of the ^{1}H-NMR signals on the calculation of the Mn for a star-PEPG20$_{10\%}$DLac$_{4\%}$ block copolymer.
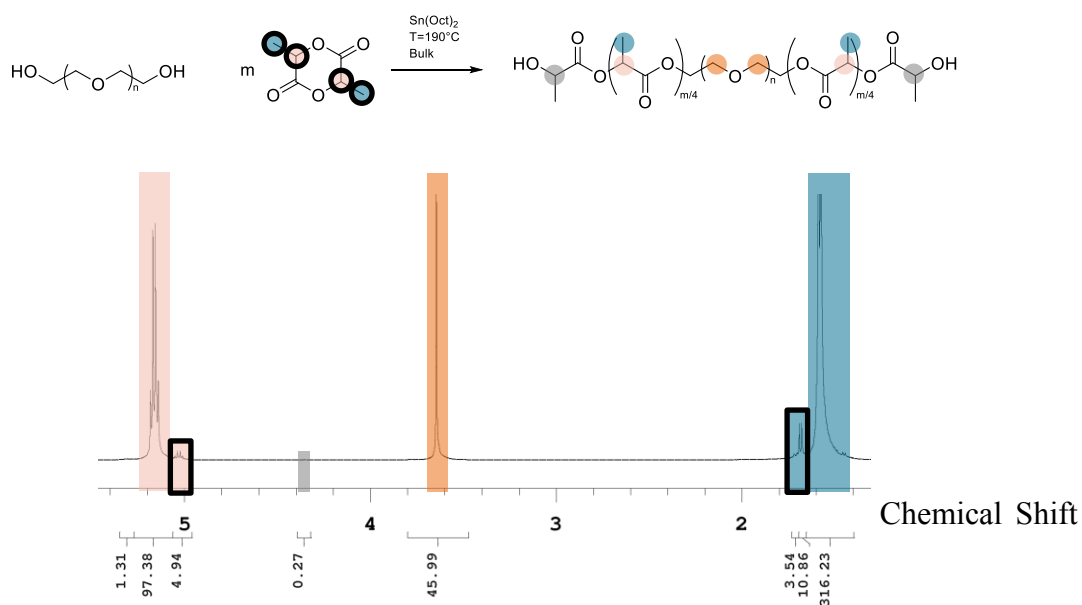
Figure A 5: ^{1}H-NMR spectrum signal designation for a linear PLLA-b-PEG-b-PLLA block copolymer. Boxes with black outline refer to the monomer signals.
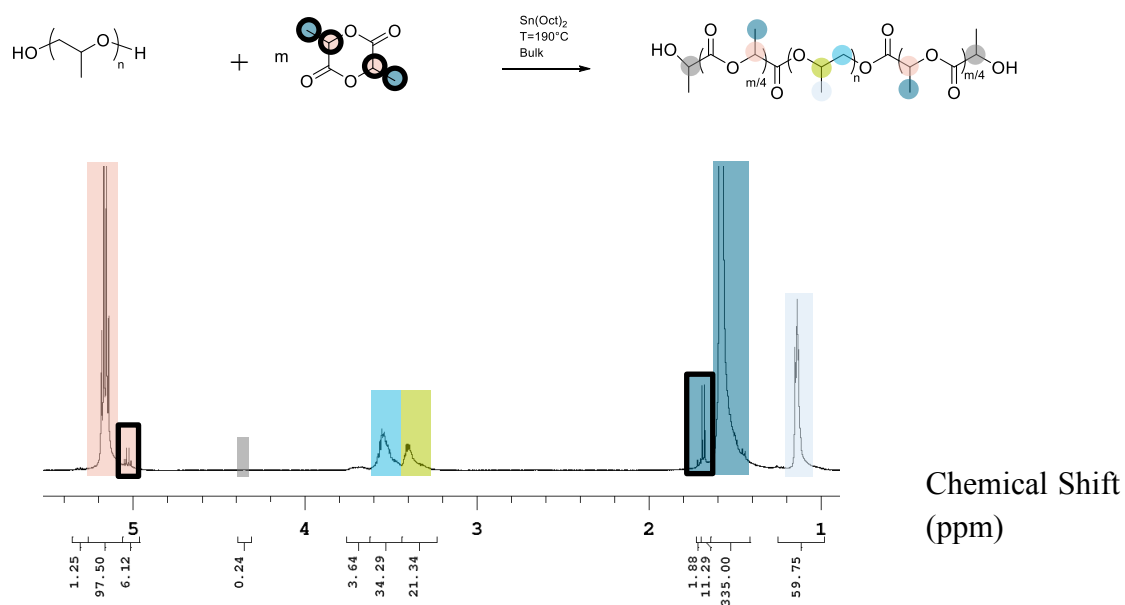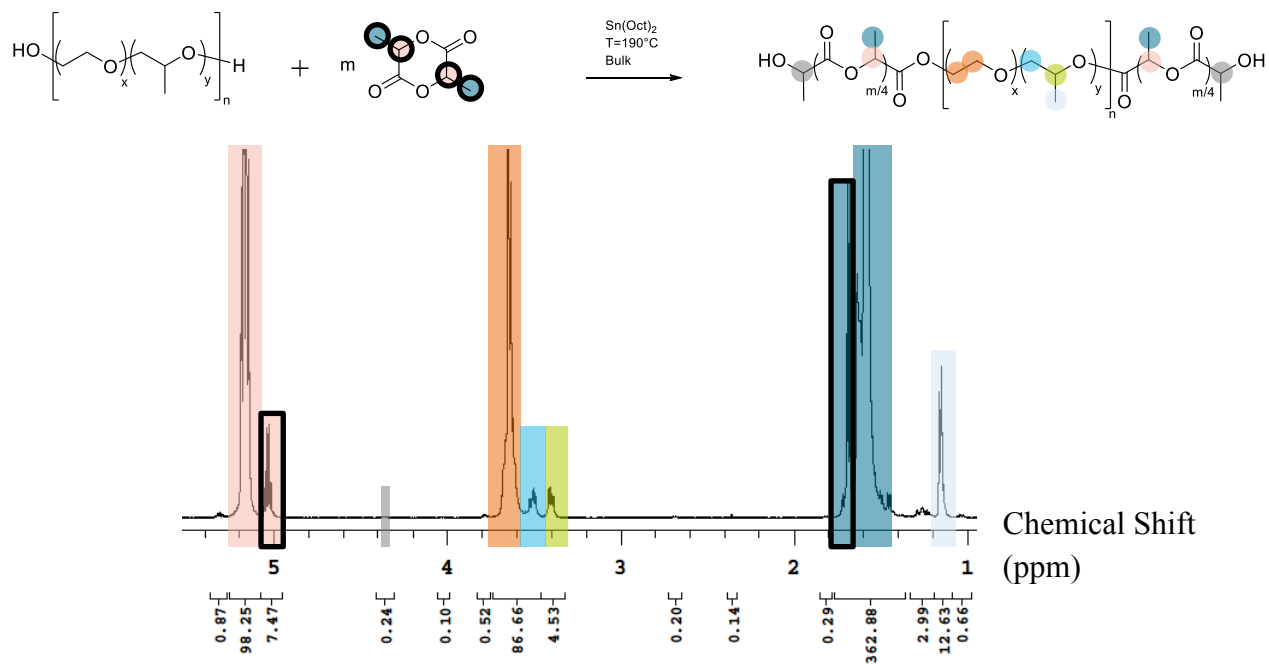

Figure A 6: 1H-NMR spectrum signal designation for a linear PLLA-b-PPG-b-PLLA block copolymer. Boxes with black outline refer to the monomer signals.
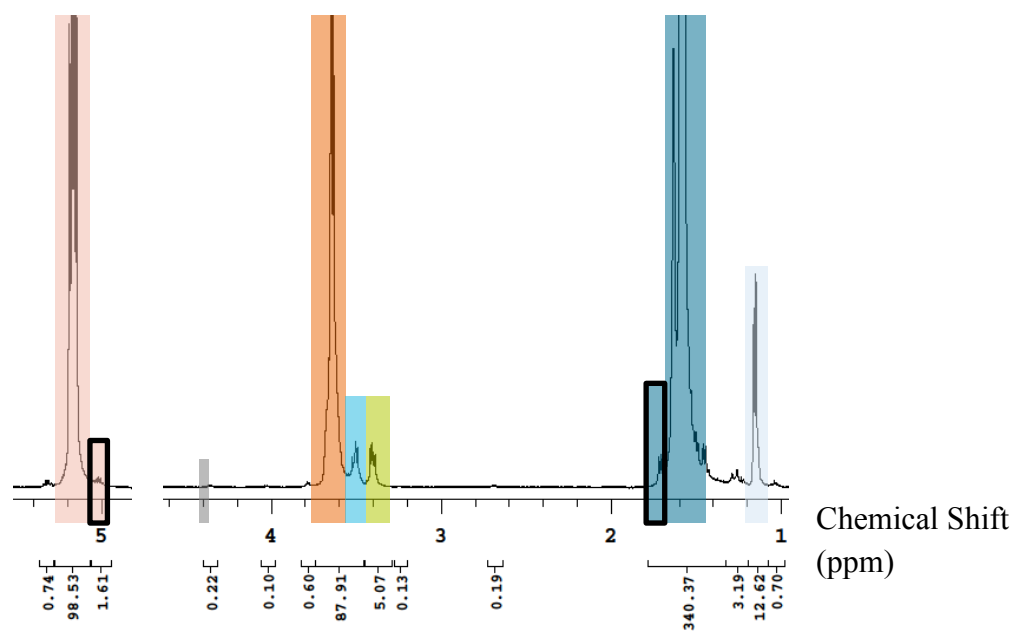
Figure A 7: ^{1}H-NMR spectrum signal designation for a linear PLLA-b-PEPG-b-PLLA block copolymer with a high unreacted lactide monomer content. Boxes with black outline refer to the monomer signals.

Figure A 8: ^{1}H-NMR spectrum signal designation for a linear PLLA-b-PEPG-b-PLLA block copolymer with a low unreacted L-lactide comonomer %-wt content. Boxes with black outline refer to the monomer signals.
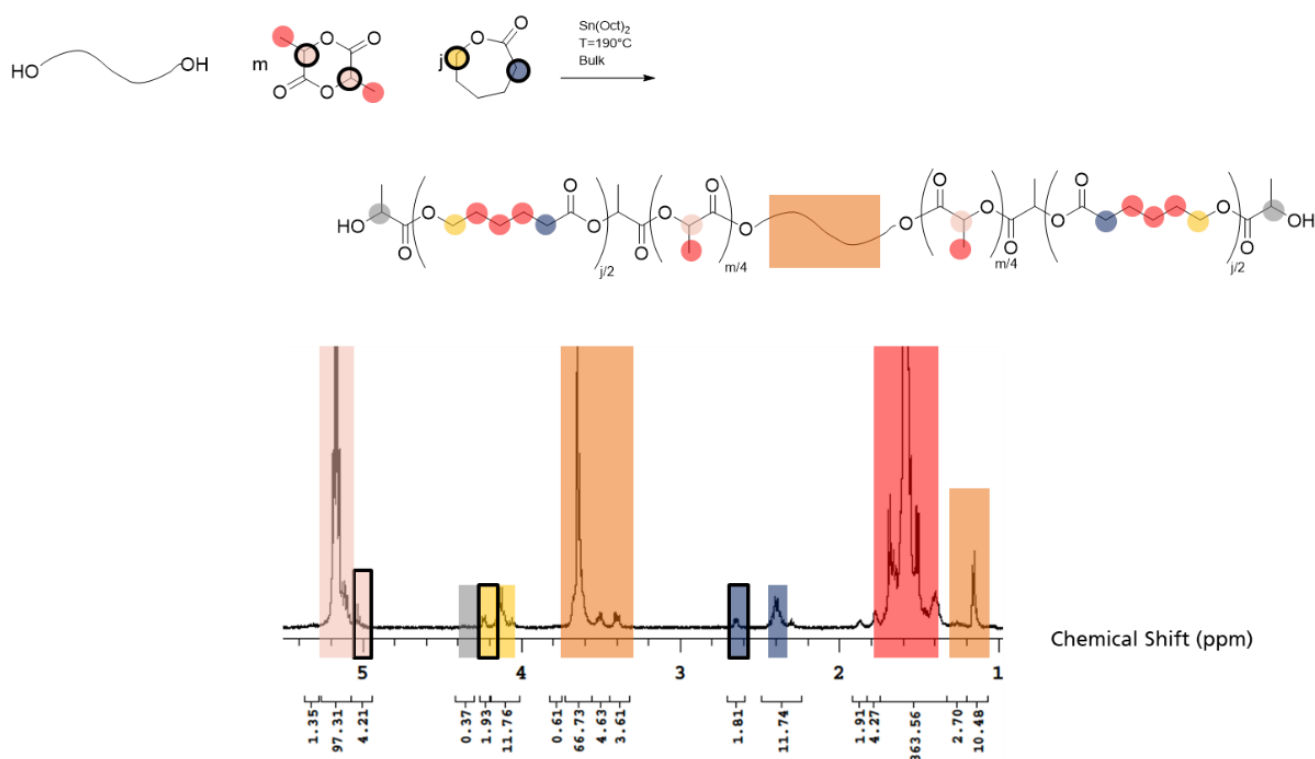
Figure A 9: ^{1}H-NMR spectrum signal designation for a linear PLLA(CL)-b-PEPG-b-PLLA(CL) block copolymer with a high unreacted CL comonomer %-wt content. Boxes with black outline refer to the monomer signals.
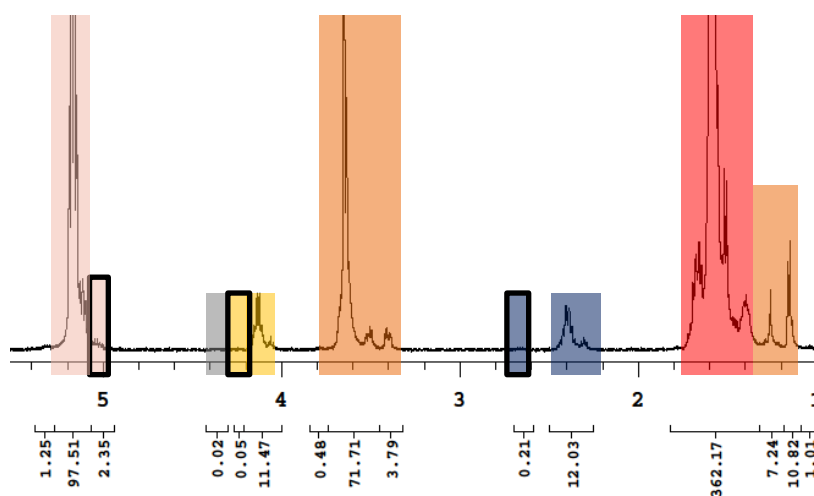

Figure A 10: ^{1}H-NMR spectrum signal designation for a linear PLLA(CL)-b-PEPG-b-PLLA(CL) block copolymer with a low unreacted CL comonomer %-wt content. Boxes with black outline refer to the monomer signals.
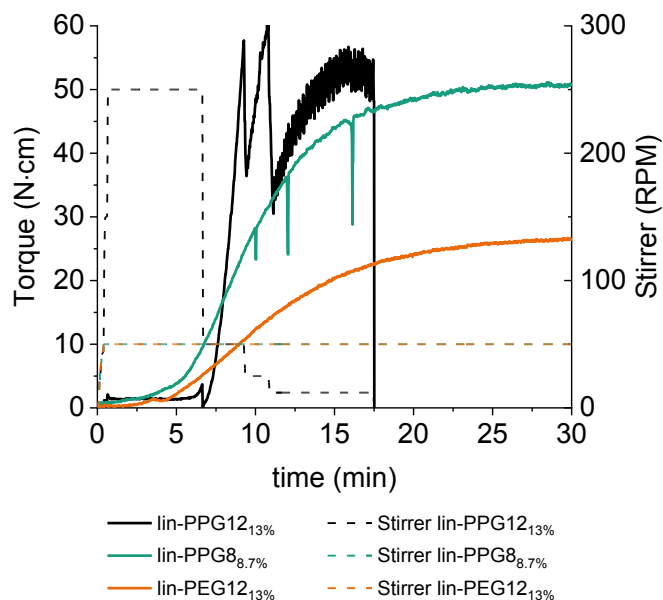
Figure A 11: Torque measurements during the synthesis of the PLLA-b-PPG-b-PLA block copolymers. The stirrer speed during the polymerization of lin-PPG12$_{13\%}$ at the beginning of the polymerization was increased to 250 RPM to ensure mixing of the PPG12 macroinitiator and then reduced to 50 RPM when a torque increase was observed. As the measured torque during this polymerization reached values higher than the technical limit of 60 N·cm, the stirrer speed had to be reduced to allow stirring to continue.
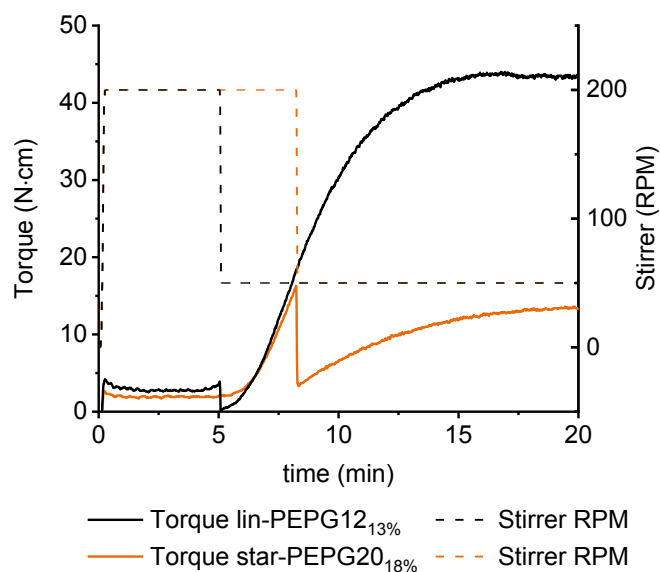

Figure A 12: Observed Measured torque difference during the synthesis of the lin-PEPG12$_{13\%}$ and the star-PEPG20$_{18\%}$.
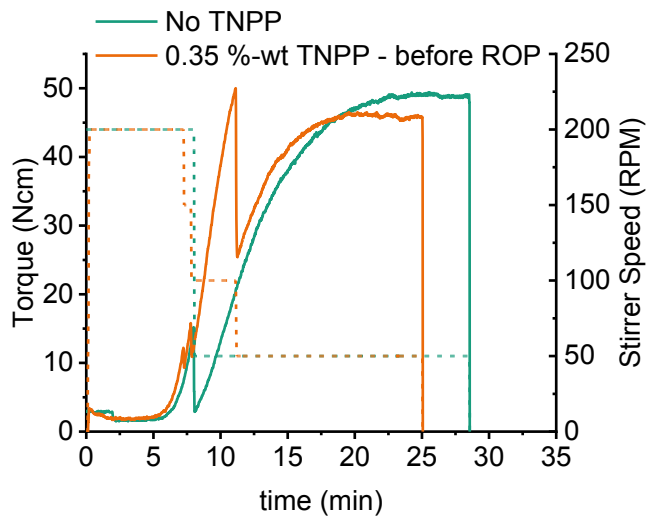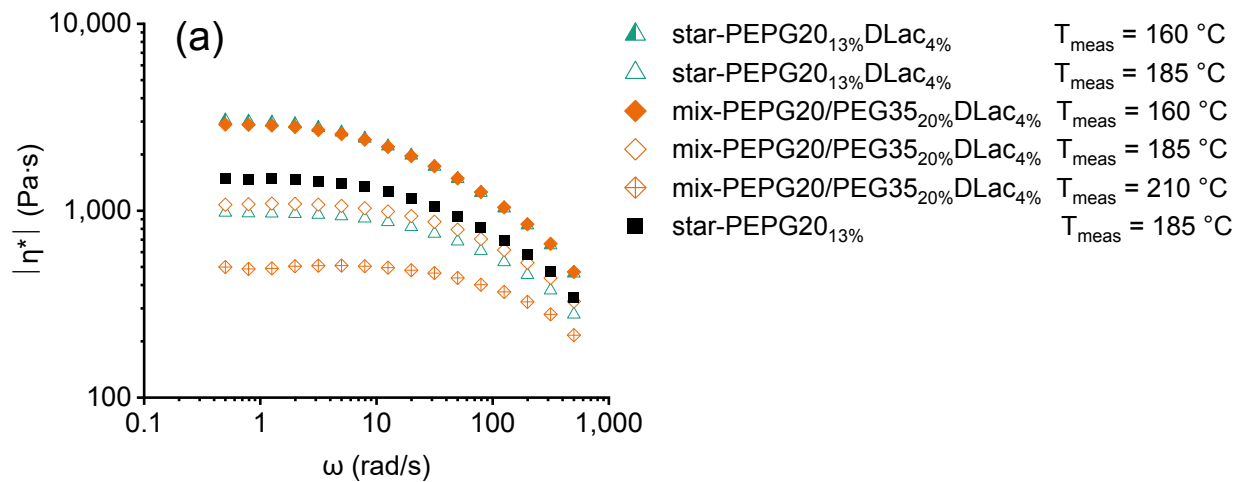
Figure A 13: Torque measurements of the ROP of star-PEPG20$_{13\%}$ synthesized with no TNPP and in the presence of 0.35 %-wt TNPP content added before the ROP. Similar reaction rates and final torque measurements at 50 RPM can be found for both polymerizations. Dashed lines refer to the stirrer speeds at the given times.
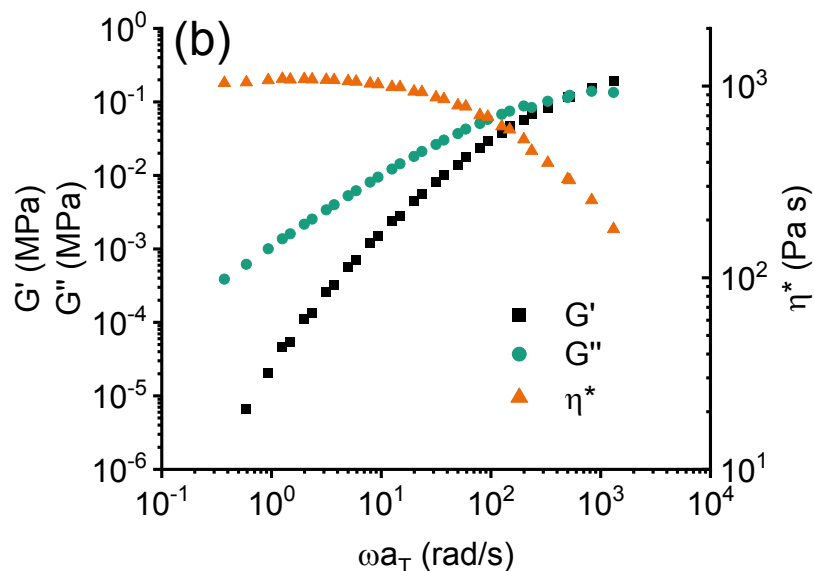
Figure A 14: (a) Effect of temperature on the complex viscosity of the mix-PEPG20/PEG35$_{20\%}$DLac$_{4\%}$ and the star-PEPG20$_{13\%}$DLac$_{4\%}$ block copolymers. The complex viscosity of the star-PEPG20$_{13\%}$ block copolymer is added as a reference. (b) Time-temperature superposition of the frequency sweeps at different temperatures for the mix-PEPG20/PEG35$_{20\%}$DLac$_{4\%}$ block copolymer.

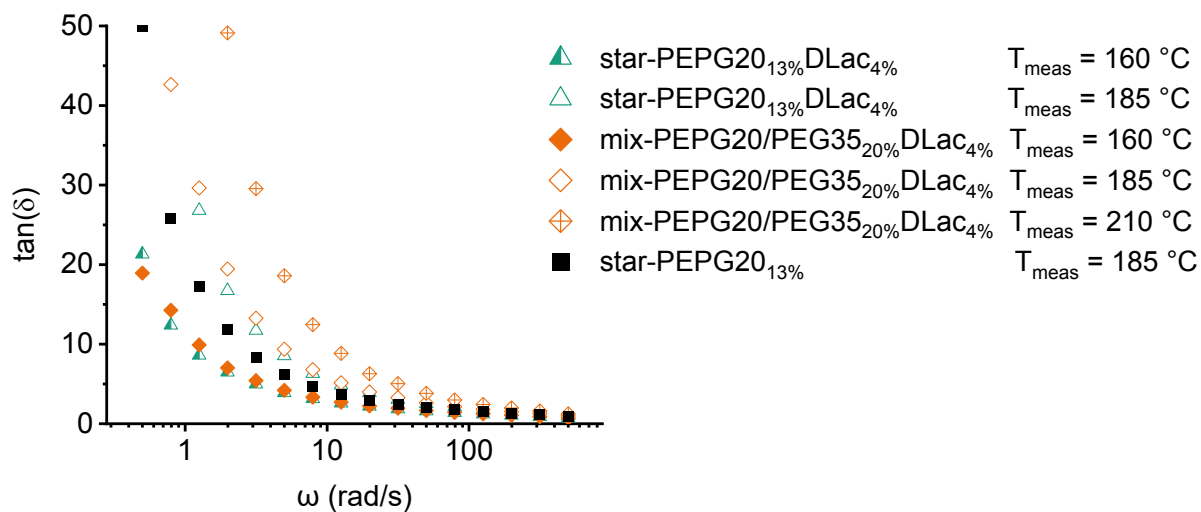Figure A 15: Effect of temperature on the tan(δ) of the mix-PEPG20/PEG35$_{20\%}$DLac$_{4\%}$ and the star-PEPG20$_{13\%}$DLac$_{4\%}$ block copolymers. The complex viscosity of the star-PEPG20$_{13\%}$ block copolymer is added as a reference.

Figure A 16: Isothermal crystallization heat flow curves and integrated degree of crystallization curves used for the crystallization half-time curve of the star-PEPG20$_{13\%}$ block copolymer pellets shown in Figure 5.40.

Figure A 17: Isothermal crystallization heat flow curves and integrated degree of crystallization curves used for the crystallization half-time curve of the star-PEPG20$_{13\%}$DLac$_{4\%}$ block copolymer pellets shown in Figure 5.40.
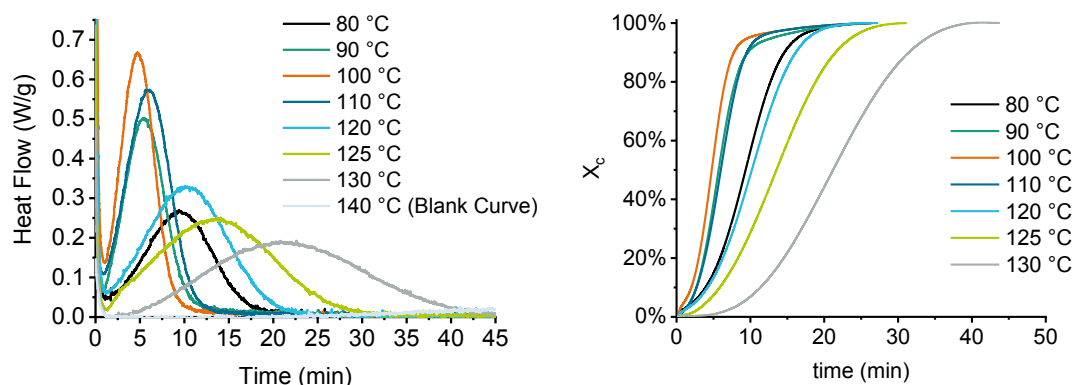
Figure A 18: Isothermal crystallization heat flow curves and integrated degree of crystallization curves used for the crystallization half-time curve of the star-PEPG20$_{10\%}$CL$_{7\%}$ block copolymer pellets shown in Figure 5.40.

Figure A 19: Isothermal crystallization heat flow curves and integrated degree of crystallization curves used for the crystallization half-time curve of the star-PEPG20$_{10\%}$CL$_{7\%}$ block copolymer blown films shown in Figure 5.49.
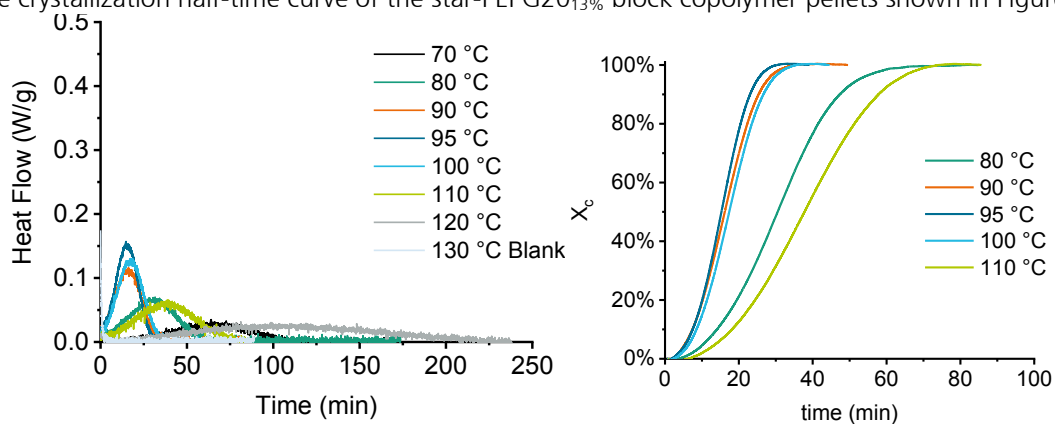

Figure A 20: Isothermal crystallization heat flow curves and integrated degree of crystallization curves used for the crystallization half-time curve of the pure mix-PEPG20$_{20\%}$DLac$_{4\%}$ block copolymer pellets shown in Figure 5.40.
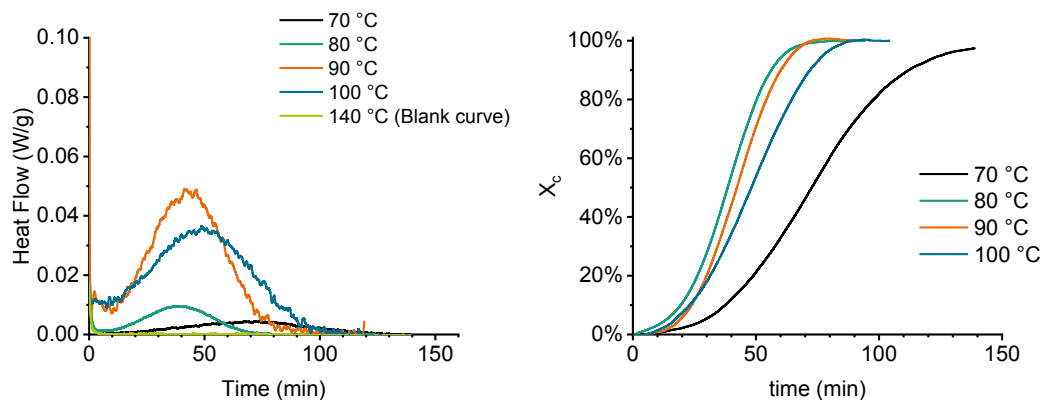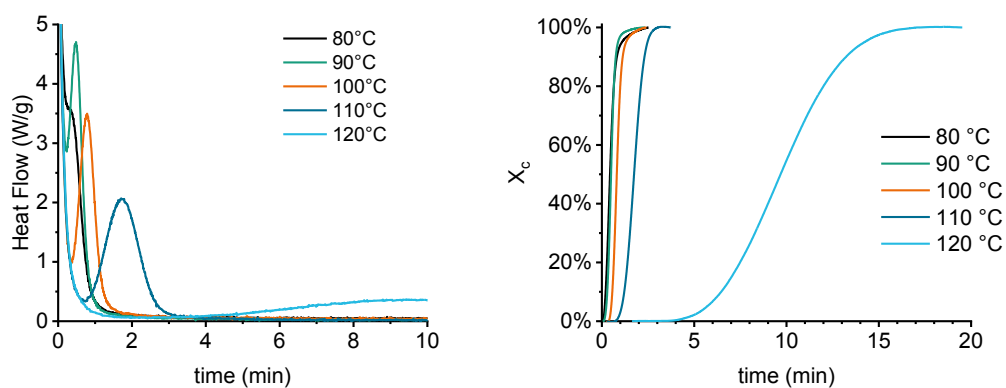

Figure A 21: Isothermal crystallization heat flow curves and integrated degree of crystallization curves used for the crystallization half-time curve of the pure mix-PEPG20$_{20\%}$DLac$_{4\%}$ block copolymer pellets after being mixed with anti-blocking additives shown in Figure 5.41.
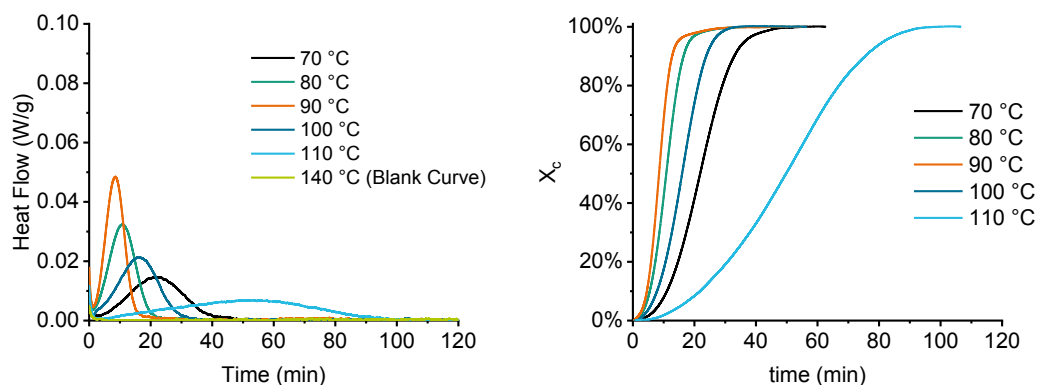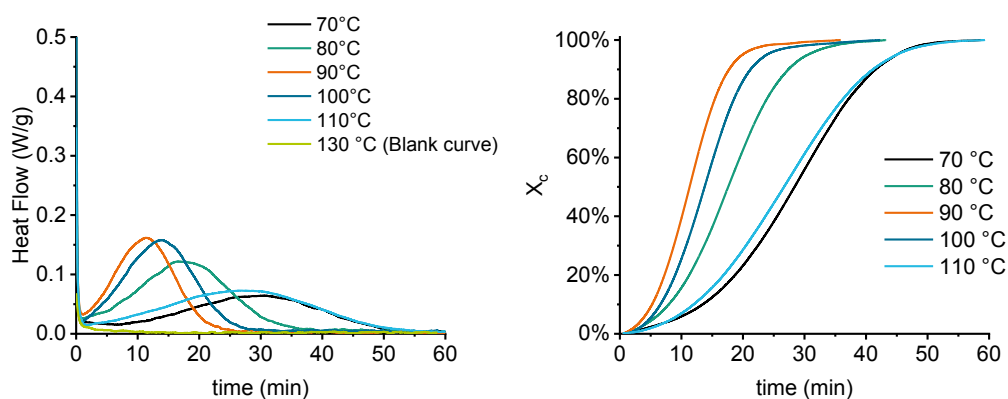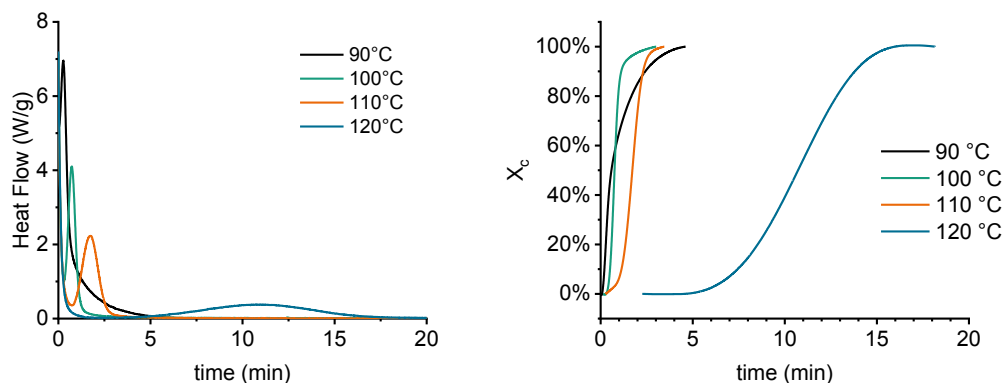
Figure A 22: Isothermal crystallization heat flow curves and integrated degree of crystallization curves used for the crystallization half-time curve of the pure mix-PEPG20$_{20\%}$DLac$_{4\%}$ block copolymer mixed with anti-blocking additives and processed into a blown film shown in Figure 5.49.
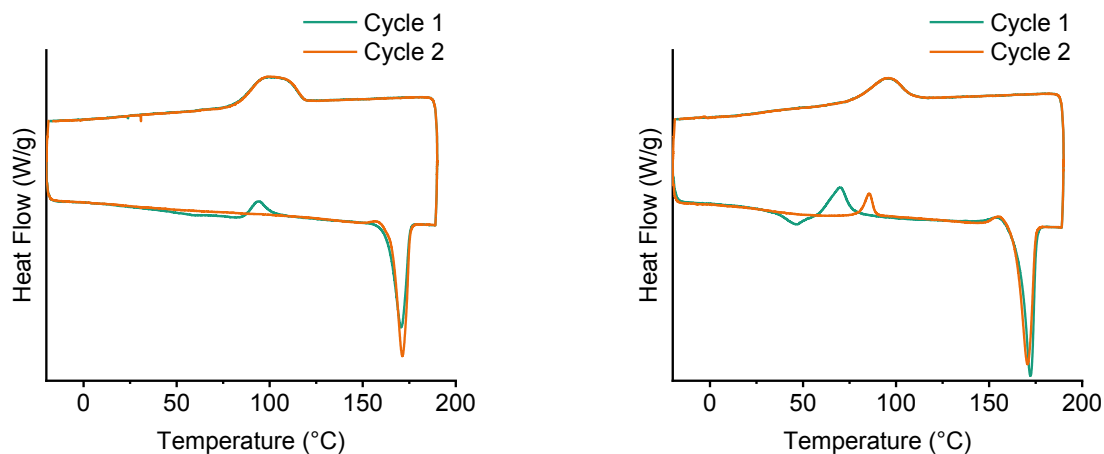
Figure A 23: Effect of reprecipitation (left) and injection molding (right) on the crystallization of the star-PEPG20$_{13\%}$ block copolymer.
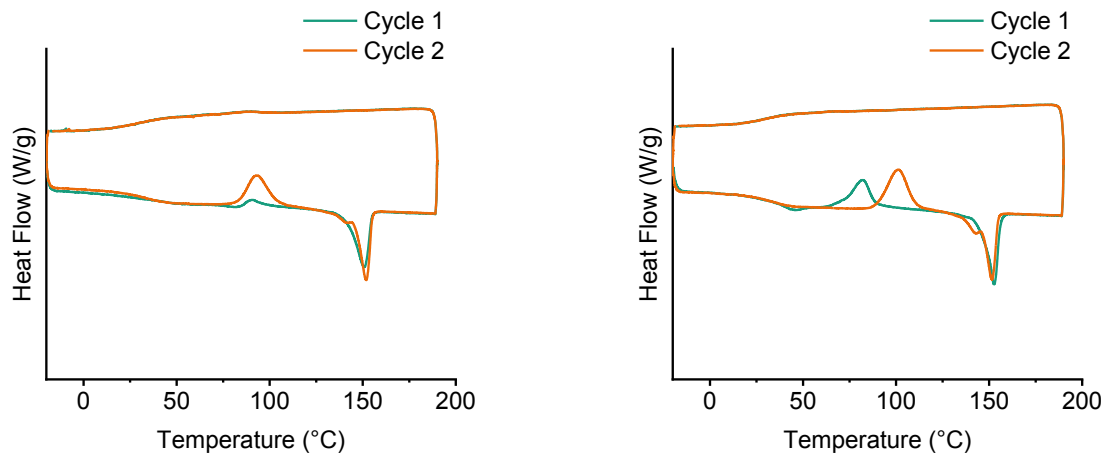
Figure A 24: Effect of reprecipitation (left) and injection molding (right) on the crystallization of the star-PEPG20$_{13\%}$DLac$_{4\%}$ block copolymer.

Figure A 25: Melt memory effect after four heating and cooling cycles of the star-PEPG20$_{13\%}$ (left) and the star-PEPG20$_{13\%}$DLac$_{4\%}$ (right) block copolymer blown films.

Figure A 26: Elastic modulus and elongatin at break of injection molded tensile test specimens type 5A according to DIN EN ISO 52 of the film grade block copolymers from Section 5.3

8.1 List of Reactions

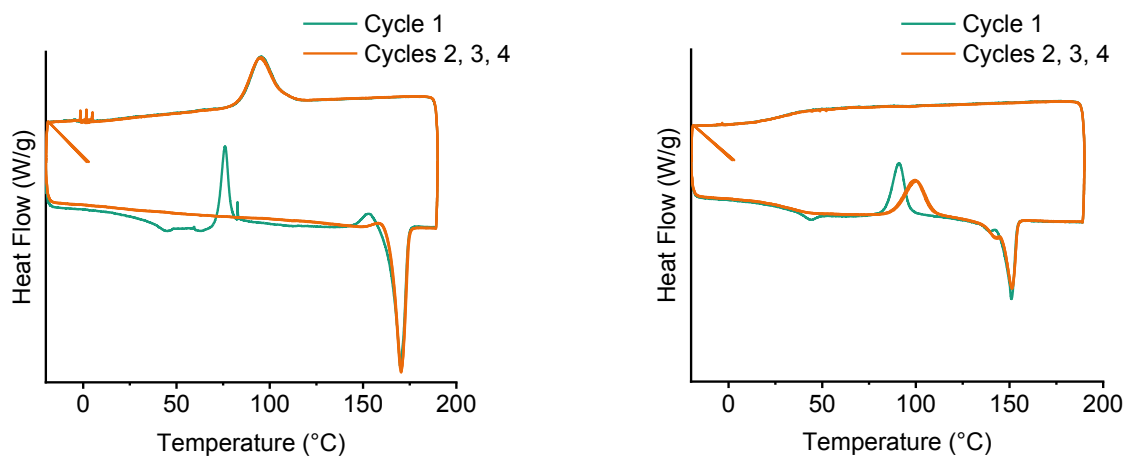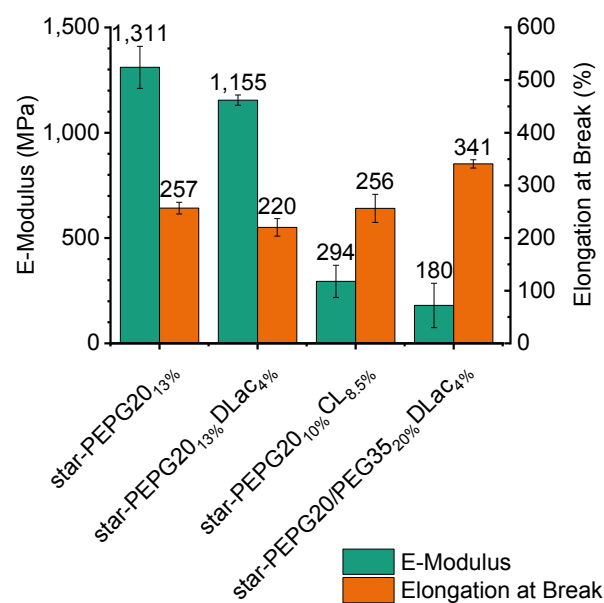| Block copolymer name	Scale	Macroinitiator used	Macroinitiator content	X_L	X_D	X_{CL}	T_{Reac}	Catalyst concentration	TNPP addition moment	TNPP content	Mn_{Theo}	Mn (^{1}H-NMR)
	[kg]		[%-wt]	[%-mol]	[%-mol]	[%-mol]	[°C]	$mol_{Sn(Oct)2}/mol_{Lactide}$		[%-wt]	kDa	kDa
lin-PLA	0.03	Undecanol	-	100.0%			180	1.00E-04	None	0.00%	91	-
lin-PEG6$_{6.6\%}$	0.03	PEG6	6.6%	100.0%			180	1.00E-04	None	0.00%	91	60
lin-PEG8$_{8.7\%}$	0.03	PEG8	8.0%	100.0%			180	1.00E-04	None	0.00%	92	65
lin-PEG12$_{13\%}$	0.03	PEG12	12.0%	100.0%			180	1.00E-04	None	0.00%	92	52
lin-PPG8$_{8.7\%}$	0.03	PPG8	8.7%	100.0%			180	1.00E-04	None	0.00%	92	81
lin-PPG12$_{13\%}$(1)	0.03	PPG12	13.0%	100.0%			180	1.00E-04	None	0.00%	92	75
lin-PPG12$_{13\%}$(2)	0.03	PPG12	13.0%	100.0%			180	1.00E-04	None	0.00%	92	64
lin-PEPG5.6$_{6.5\%}$	0.03	PEPG5.6	6.5%	100.0%			180	1.00E-04	None	0.00%	86	68
lin-PEPG12$_{13\%}$	0.03	PEPG12	13.0%	100.0%			180	1.00E-04	None	0.00%	92	71
lin-PEPG12$_{13\%}$DLac$_{2.5\%}$	0.03	PEPG12	13.0%	97.5%	2.5%		180	1.00E-04	None	0.00%	92	-
lin-PEPG12$_{13\%}$DLac$_{4\%}$	0.03	PEPG12	13.0%	96.0%	4.0%		180	1.00E-04	None	0.00%	92	-
lin-PEPG12$_{13\%}$DLac$_{5\%}$	0.03	PEPG12	13.0%	95.0%	5.0%		180	1.00E-04	None	0.00%	92	-
star-PEPG20$_{13\%}$	0.03	PEPG20	13.0%	100.0%			180	1.00E-04	None	0.00%	154	108
star-PEPG20$_{15\%}$	0.03	PEPG20	15.0%	100.0%			180	1.00E-04	None	0.00%	133	87
star-PEPG20$_{18\%}$	0.03	PEPG20	18.0%	100.0%			180	1.00E-04	None	0.00%	111	68
lin-PEPG12$_{13\%}$CL$_{2\%}$	0.03	PEPG12	13.0%	98.0%		2.0%	180	1.00E-04	None	0.00%	92	143
lin-PEPG12$_{13\%}$CL$_{4\%}$	0.03	PEPG12	13.0%	96.0%		4.0%	180	1.00E-04	None	0.00%	92	114
lin-PEPG12$_{13\%}$CL$_{13\%}$	0.03	PEPG12	13.0%	87.0%		13.0%	180	1.00E-04	None	0.00%	92	111
star-PEPG20$_{13\%}$CL$_{7\%}$	0.03	PEPG20	13.0%	93.0%		7.0%	180	1.00E-04	None	0.00%	154	-
star-PEPG20$_{13\%}$	0.03	PEPG20	13.0%	100.0%			180	1.00E-04	None	0.00%	154	105
star-PEPG20$_{13\%}$	0.03	PEPG20	13.0%	100.0%			180	1.00E-04	After ROP	0.35%	154	108
star-PEPG20$_{13\%}$	0.03	PEPG20	13.0%	100.0%			180	1.00E-04	Before ROP	0.35%	154	142
star-PEPG20$_{18\%}$	0.03	PEPG20	18.0%	100.0%			180	1.00E-04	Before ROP	0.35%	111	114

star-PEPG20$_{18\%}$	0.03	PEPG20	18.0%	100.0%			180	1.00E-04	Before ROP	0.50%	111	141
star-PEPG20$_{18\%}$	0.03	PEPG20	18.0%	100.0%			180	1.00E-04	Before ROP	1.00%	111	100
star-PEPG20$_{10\%}$DLac$_{4\%}$	0.03	PEPG20	10.0%	96.0%	4.0%		180	1.00E-04	None	0.00%	200	162
star-PEPG20$_{10\%}$DLac$_{4\%}$	0.03	PEPG20	10.0%	96.0%	4.0%		180	1.00E-04	Before ROP	0.35%	200	189
star-PEPG20$_{10\%}$DLac$_{4\%}$	0.03	PEPG20	10.0%	96.0%	4.0%		180	2.86E-05	Before ROP	0.35%	200	186
star-PEPG20$_{10\%}$CL$_{2\%}$	0.03	PEPG20	10.0%	97.6%		2.4%	180	1.00E-04	After ROP	0.35%	200	222
star-PEPG20$_{13\%}$CL$_{7\%}$	0.03	PEPG20	13.0%	92.7%		7.3%	180	1.00E-04	After ROP	0.35%	154	-
star-PEPG20$_{9\%}$CL$_{6\%}$	0.03	PEPG20	9.0%	93.6%		6.4%	180	1.00E-04	After ROP	0.35%	222	-
mix-PEPG20/PEG35$_{18\%}$DLac$_{4\%}$	0.03	mix PEPG20 + PEG35	18.0%	96.0%	4.0%		180	1.00E-04	Before ROP	0.35%	127	120
mix-PEPG20/PEG35$_{20\%}$DLac$_{4\%}$	0.03	mix PEPG20 + PEG35	20.0%	96.0%	4.0%		180	1.00E-04	Before ROP	0.35%	115	111
mix-PEPG20/PEG35$_{20\%}$DLac$_{4\%}$	0.03	mix PEPG20 + PEG35	20.0%	96.0%	4.0%		180	2.86E-05	Before ROP	0.35%	115	-
star-PEPG20$_{13\%}$	3	PEPG20	13.0%	100.0%			180	1.00E-04	After ROP	0.35%	154	111
star-PEPG20$_{13\%}$DLac$_{4\%}$	3	PEPG20	13.0%	96.0%	4.0%		180	1.00E-04	After ROP	0.35%	154	122
star-PEPG20$_{10\%}$CL$_{7\%}$	3	PEPG20	10.0%	93.0%		7.0%	180	1.00E-04	After ROP	0.35%	200	-
mix-PEPG20/PEG35$_{20\%}$DLac$_{4\%}$	3	mix PEPG20 + PEG35	20.0%	96.0%	4.0%		180	2.86E-05	Before ROP	0.50%	115	114

9   References

[1] T. P. Haider, C. Völker, J. Kramm, K. Landfester, F. R. Wurm, *Angew. Chem., Int. Ed. Engl.* **2019**, *58*, 50.

[2] D. K. Schneiderman, M. A. Hillmyer, *Macromolecules.* **2017**, *50*, 3733.

[3] J. Hopewell, R. Dvorak, E. Kosior, *Philos. Trans. R. Soc., B.* **2009**, *364*, 2115.

[4] Plastics Europe. *Plastics - the Facts 2021* **2021**.

[5] R. Geyer, J. R. Jambeck, K. L. Law, *Sci. Adv.* **2017**, *3*, 1-5.

[6] B. D. Vogt, K. K. Stokes, S. K. Kumar, *ACS Appl. Polym. Mater.* **2021**, *3*, 4325.

[7] Z. Wang, C. Zhang, Z. Zhang, X. Chen, X. Wang, M. Wen, B. Chen, W. Cao, C. Liu, *Soft Matter.* **2020**, *16*, 7018.

[8] R. Essel, L. Engel, M. Carus, R. H. Ahrens. (Federal Environmental Agency (Germany)). *Sources of microplastics relevant to marine protection in Germany,* Dessau-Roßlau **2015**.

[9] V. Bauchmüller, M. Carus, R. Chinthapalli, L. Dammer, N. Hark, A. Partanen, P. Ruiz, S. Lajewski. (nova! Institut für politische und ökologische Innovation GmbH). *BioSinn: Products for which biodegradation makes sense,* Germany **2021**.

[10] C. Wang, L. Zhao, M. K. Lim, W.-Q. Chen, J. W. Sutherland, *Resour., Conserv. Recycl.* **2020**, *153*.

[11] A. Künkel, J. Becker, L. Börger, J. Hamprecht, S. Koltzenburg, R. Loos, M. B. Schick, K. Schlegel, C. Sinkel, G. Skupin, M. Yamamoto. in *Ullmann's Encyclopedia of Industrial Chemistry,* Wiley-VCH Verlag, Weinheim, Germany **2000,** pp. 1–29.

[12] European Bioplastics e. V. *Bioplastics market development update 2021* **2021**.

[13] K. Cantor. *Blown film extrusion,* 3rd ed. Hanser Publications, Cincinnati, OH **2018**.

[14] F. Pardos. *Plastic films: Situation and outlook.* Rapra Technology Ltd, Shropshire, U.K. **2004**.

[15] N. Arbeck, J. Lehmann, N. Sporrer, U. Peintner, M. Kern, H.-J. Siepenkothen. (C.A.R.M.E.N. e.V., Witzenhausen-Institut für Abfall und Energie GmbH). *Abschlussbericht zum Modellprojekt Praxis Bio-Beutel - Kreislaufwirtschaft mit kompostierbaren Obst- und Gemüsebeuteln* **2022**.

[16] FKuR Kunststoff GmbH. *Technisches Datenblatt: Bio-Flex(R) F 1814,* 2nd ed., Willich, Nordrhein-Westfalen. **2020**.

[17] S. Su, R. Kopitzky, S. Tolga, S. Kabasci, *Polymers.* **2019**, *11*.

[18] Y. Hu, Y. S. Hu, V. Topolkaraev, A. Hiltner, E. Baer, *Polymer.* **2003**, *44*, 5711.

[19] Y. Hu, Y. S. Hu, V. Topolkaraev, A. Hiltner, E. Baer, *Polymer.* **2003**, *44*, 5681.

[20] Y. Hu, M. Rogunova, V. Topolkaraev, A. Hiltner, E. Baer, *Polymer.* **2003**, *44*, 5701.

[21] Z. Kulinski, E. Piorkowska, *Polymer.* **2005**, *46*, 10290.

[22] Z. Kulinski, E. Piorkowska, K. Gadzinowska, M. Stasiak, *Biomacromolecules.* **2006**, *7*, 2128.

[23] Z. Jia, C. Han, L. Dong, Y. Yang, *Acta Polym. Sin.* **2009**, *9*.

[24] Z. Jia, J. Tan, C. Han, Y. Yang, L. Dong, *J. Appl. Polym. Sci.* **2009**, *114*, 1105.

[25] S. Kliem, M. Kreutzbruck, C. Bonten, *Materials.* **2020**, *13*.

[26] A. Thielen, *Bioplastics Magazine.* **02.2022**, *17*, 24.

[27] D. E. Henton, P. Gruber, J. Lunt, J. Randall. in *Natural fibers, biopolymers, and biocomposites*, (Eds: A. K. Mohanty, M. Misra, L. T. Drzal), CRC Press, Boca Raton, FL **2005,** pp. 527–578.

[28] R. Auras, L. Loong-Tak, S. E.M. Selke, H. Tsuji. *Poly(lactic acid): Synthesis, structures, properties, processing, and application.* John Wiley & Sons, Inc., Hoboken, NJ **2010**

[29] K. J. Jem, B. Tan, *Adv. Ind. Eng. Polym. Res.* **2020**, *3*, 60.

[30] M. Thielen, *Bioplastics Magazine.* **01.2019**, *14*, 5.

[31] M. Thielen, *Bioplastics Magazine.* **05.2020**, *15*, 14.

[32] M. Thielen, *Bioplastics Magazine.* **01.2022**, *17*, 5.

[33] J. Ren. *Biodegradable Poly(Lactic Acid): Synthesis, Modification, Processing and Applications.* Tschinghua University Press; Springer-Verlag, Beijing, Heidelberg, New York **2010**.

[34] P. J. Flory. *Principles of Polymer Chemistry,* 1st ed. Cornell University Press, Ithaca, NY **1953**.

[35] Purac. *Product Data Sheet - PURAC® HiPure 90: Puralact D* **2020**.

[36] Y. J. Du, P. J. Lemstra, A. J. Nijenhuis, H. A. M. van Aert, C. Bastianseen, *Macromolecules.* **1995**, *28*, 2124.

[37] H. R. Kricheldorf, I. Kreiser-Saunders, C. Boettcher, *Polymer.* **1995**, *36*, 1253.

[38] P. Gruber, D. E. Henton, J. Starr. in *Biorefineries - industrial processes and products*, (Eds: B. Kamm, P. Gruber, M. Kamm), Wiley-VCH Verlag, Weinheim, Germany **2010,** pp. 381–407.

[39] P. Degée, P. Dubois, R. Jérome, S. Jacobsen, H.-G. Fritz, *Macromol. Symp.* **1999**, *144*, 289.

[40] X. Zhang, D. A. Macdonald, M. F. A. Goosen, K. B. Mcauley, *J. Polym. Sci.* **1994**, *32*, 1965.

[41] J. Dahlmann, G. Rafler, *Acta Polym.* **1993**, *44*, 103.

[42] D. K. Gilding, A. M. Reed, *Polymer.* **1979**, *20*, 1459.

[43] H. R. Kricheldorf, M. Sumbél, *Eur. Polym. J.* **1989**, *25*, 585.

[44] A. J. Nijenhuis, D. W. Grijpma, A. J. Pennings, *Polym. Bull.* **1991**, *26*, 71.

[45] A. J. Nijenhuis, D. W. Grijpma, A. J. Pennings, *Macromolecules.* **1992**, *25*, 6419.

[46] J. Dahlmann, G. Rafler, *Acta Polym. Sin.* **1993**, *44*, 103.

[47] T. M. Ford. (E. I. Du Pont de Nemours and Company), *US 5,310,599* **1994**.

[48] D. R. Witzke, *PhD Thesis,* Michigan State University, **1997**.

[49] P. Pan, W. Kai, B. Zhu, T. Dong, Y. Inoue, *Macromolecules.* **2007**, *40*, 6898.

[50] C. Shih, *J. Controlled Release.* **1995**, *34*, 9.

[51] W. Limsukon, R. Auras, S. Selke, *Polym. Test.* **2019**, *80*.

[52] A. K. Mohanty, M. Misra, L. T. Drzal. *Natural fibers, biopolymers, and biocomposites.* CRC Press, Boca Raton, FL **2005**.

[53] H. Nishida, T. Mori, S. Hoshihara, Y. Fan, Y. Shirai, T. Endo, *Polym. Degrad. Stab.* **2003**, *81*, 515.

[54] Y. Fan, H. Nishida, Y. Shirai, T. Endo, *Polym. Degrad. Stab.* **2004**, *84*, 143.

[55] I. C. McNeill, H. A. Leiper, *Polym. Degrad. Stab.* **1985**, *11*, 309.

[56] I. C. McNeill, H. A. Leiper, *Polym. Degrad. Stab.* **1985**, *11*, 267.

[57] I. C. McNeill, H. A. Leiper, *Polym. Degrad. Stab.* **1985**, *12*, 373.

[58] Y. Yu, G. Storti, M. Morbidelli, *Ind. Eng. Chem. Res.* **2011**, *50*, 7927.

[59] D. H. S. Ramkumar, M. Bhattacharya, *Polym. Eng. Sci.* **1998**, *38*, 1426.

[60] U. Mühlbauer, R. Hagen. (UHDE inventa-fischer GmbH), *US 2018/0118882 A1* **2018**.

[61] J. J. Kolstad, D. R. Witzke, M. H. Hartmann, E. S. Hall, J. Nangeroni. (Cargill, Incorporated), *EP 1070097 B1* **2016**.

[62] U. Mühlbauer, R. Hagen. (UHDE inventa-fischer GmbH), *US 2019/0352457 A1* **2019**.

[63] L. I. Costa, F. Tancini, S. Hofmann, F. Codari, U. Trommsdorff, *Macromol. Symp.* **2016**, *360*, 40.

[64] P. Gruber, J. J. Kolstad, C. M. Ryan. (Cargill, Incorporated), *EP 0615529 B1* **1994**.

[65] A. Södergård. in *Hydrogels and Biodegradable Polymers for Bioapplications*, (Eds: R. M. Ottenbrite, S. J. Huang, K. Park), American Chemical Society, Washington, DC **1996,** pp. 103–117.

[66] L. Babcock, J. D. Schroeder. (Natureworks LLC), *WO 2008/141265 AI* **2008**.

[67] O. Wachsen, K. Platkowski, K.-H. Reichert, *Polym. Degrad. Stab.* **1997**, *57*, 87.

[68] J. Schneider, X. Shi, S. Manjure, D. Gravier, R. Narayan, *J. Appl. Polym. Sci.* **2015**, *132*, 42243-42250.

[69] Y.-M. Corre, J. Duchet, J. Reignier, A. Maazouz, *Rheol. Acta.* **2011**, *50*, 613.

[70] M. Mihai, M. A. Huneault, B. D. Favis, *Polym. Eng. Sci.* **2010**, *50*, 629.

[71] B. Mallet, K. Lamnawar, A. Maazouz, *Polym. Eng. Sci.* **2014**, *54*, 840.

[72] P. Gruber, J. J. Kolstad, D. R. Witzke, M. H. Hartmann, A. L. Brosch. (Cargill, Incorporated), *US 5,549,095* **1997**.

[73] C. Fu, B. Zhang, C. Ruan, C. Hu, Y. Fu, Y. Wang, *Polym. Degrad. Stab.* **2010**, *95*, 485.

[74] J. J. Kolstad, D. R. Witzke, M. H. Hartmann, E. S. Hall, J. Nangeroni. (Cargill, Incorporated), *US 6,353,086* **2002**.

[75] P. Gruber, J. J. Kolstad, E. S. Hall, R. S. Eichen, C. M. Ryan. (Cargill, Incorporated), *US 5,338,822* **1994**.

[76] X. Zhang, U. P. Wyss, D. Pichora, M. F. A. Goosen, *Polym. Bull.* **1992**, *27*, 623.

[77] H. J. Lehermeier, J. R. Dorgan, *Polym. Eng. Sci.* **2001**, *41*, 2172.

[78] J. A. Cicero, J. R. Dorgan, S. F. Dec, D. M. Knauss, *Polym. Degrad. Stab.* **2002**, *78*, 95.

[79] J. Burlet, M.-C. Heuzey, C. Dubois, P. Wood-Adams, J. Brisson. *Thermal Stabilization of High Molecular Weight L-Polylactide.* Society of Plastics Engineers **2005**.

[80] a) X. Meng, G. Shi, W. Chen, C. Wu, Z. Xin, T. Han, Y. Shi, *Polym. Degrad. Stab.* **2015**, *120*, 283; b) L.-I. Palade, H. J. Lehermeier, J. R. Dorgan, *Macromolecules.* **2001**, *34*, 1384;

[81] X. Meng, G. Shi, C. Wu, W. Chen, Z. Xin, Y. Shi, Y. Sheng, *Polym. Degrad. Stab.* **2016**, *124*, 112.

[82] K. Sirisinha, K. Samana, *J. Appl. Polym. Sci.* **2021**, *138*, 49951.

[83] B. Jacques, J. Devaux, R. Legras, E. Nield, *Polymer.* **1997**, *38*, 5367.

[84] N. Najafi, M. C. Heuzey, P. J. Carreau, P. M. Wood-Adams, *Polym. Degrad. Stab.* **2012**, *97*, 554.

[85] J. E. Mark. *Polymer Data Handbook.* Oxford University Press, New York, NY **1998**.

[86] J. D. Menczel, R. B. Prime. *Thermal analysis of polymers: Fundamentals and applications.* John Wiley & Sons, Inc., Oxford, U. K. **2009**.

[87] P. C. Hiemenz, T. P. Lodge. *Polymer Chemistry,* 2nd ed. CRC Press, Boca Raton, FL **2007**.

[88] G. Erhard. in *Designing with plastics*, (Ed: G. Erhard), Elsevier Ltd., Munich, Germany **2014,** pp. 101–173.

[89] G. M. Swallowe. in *Mechanical Properties and Testing of Polymers*, (Ed: G. M. Swallowe), Springer Science + Business Media Dordrecht, Dordrecht, Netherlands **1999,** pp. 214–218.

[90] A. K. Doolittle, *J. Appl. Phys.* **1952**, *23*, 236.

[91] M. Ionescu. *Chemistry and technology of polyols for polyurethanes,* 1st ed. Rapra Technology, Shropshire, U.K. **2005**.

[92] V. L. Simril, *J. Polym. Sci.* **1946**, 142.

[93] C. F. Hammer. in *Polymer blends*, (Ed: T. Alfrey), Academic Press, Inc., New York, NY **1978**.

[94] E. H. Immergut, H. F. Mark. in *Plasticization and Plasticizer Processes*, (Ed: N. A. J. Platzer), American Chemical Society, Washington D. C. **1965,** pp. 1–26.

[95] M. C. Shen, A. V. Tobolski. in *Plasticization and Plasticizer Processes*, (Ed: N. A. J. Platzer), American Chemical Society, Washington D. C. **1965,** pp. 27–34.

[96] T. G. Fox, P. J. Flory, *J. Appl. Phys.* **1950**, *21*, 581.

[97] G. W. Ehrenstein. in *Polymeric materials*, (Ed: G. W. Ehrenstein), Hanser Publications, Munich, Germany **2001**.

[98] S. Manjure, M. Annan, *Bioplastics Magazine.* **2016**, *11*, 16.

[99] Y. Srithep, P. Nealey, L.-S. Turng, *Polym. Eng. Sci.* **2013**, *53*, 580.

[100] N. V. Pogodina, H. H. Winter, *Macromolecules.* **1998**, *31*, 8164.

[101] C. Schwittay, M. Mours, H. H. Winter, *Faraday Discuss.* **1995**, *101*, 93.

[102] A. Rudin, P. Choi. in *The Elements of Polymer Science & Engineering,* Elsevier Ltd. **2013,** pp. 149–229.

[103] H. Tsuji, *Macromol. Biosci.* **2005**, *5*, 569.

[104] P. J. Flory, *Trans. Faraday Soc.* **1955**, *51*, 848.

[105] E. W. Fischer, H. J. Sterzel, G. Wegner, *Kolloid-Z.u.Z.Polymere.* **1973**, *251*, 980.

[106] J. J. Kolstad, *J. Appl. Polym. Sci.* **1996**, *62*, 1079.

[107] D. M. Bigg, *Adv. Polym. Technol.* **2005**, *24*, 69.

[108] Y. He, Z. Fan, Y. Hu, T. Wu, J. Wei, S. Li, *Eur. Polym. J.* **2007**, *43*, 4431.

[109] A. J. Müller, M. Ávila, G. Saenz, J. Salazar. in *Poly(lactic acid) Science and Technology*, (Eds: A. Jiménez, M. Peltzer, R. Ruseckaite), Royal Society of Chemistry, Cambridge, U. K. **2014,** pp. 66–98.

[110] J. D. Hoffman, J. I. Lauritzen, *J. Res. Natl. Inst. Stand. Technol.* **1961**, *65A*, 297.

[111] P. C. Painter, M. M. Coleman. *Fundamentals of Polymer Science: An introductory text,* 2nd ed. CRC Press, Boca Raton, FL **1997**.

[112] R. Vasanthakumari, A. J. Pennings, *Polymer.* **1983**, *24*, 175.

[113] Natureworks LLC. *Ingeo resin product guide: Naturally Advanced Materials,* United States **2014**.

[114] T. G. Heggs. in *Ullmann's Encyclopedia of Industrial Chemistry,* Wiley-VCH Verlag, Weinheim, Germany **2000**.

[115] C. W. Macosko. *Rheology: Principles, measurements, and applications,* 1st ed. Wiley-VCH Verlag, New York, NY **1994**.

[116] M. Kruse, *PhD Thesis,* Technsche Universität Berlin (Berlin), **2017**.

[117] T. Mezger. *Applied Rheology: With Joe Flow on Rheology Road,* 4th ed. Anton Paar GmbH, Graz, Austria **2017**.

[118] D. Auhl, J. Ramirez, A. E. Likhtman, P. Chambon, C. Fernyhough, *J. Rheol.* **2008**, *52*, 801.

[119] P. - G. de Gennes, *Phys. Today.* **1983**, *36*, 33.

[120] P.-G. de Gennes. *Scaling Concepts in Polymer Physics,* 1st ed. Cornell University Press, Ithaca, NY **1979**.

[121] V. A. H. Boudara, D. J. Read, J. Ramírez, *J. Rheol.* **2020**, *64*, 709.

[122] J. M. Dealy, D. J. Read, R. G. Larson. *Structure and Rheology of Molten Polymers: From Structure to Flow Behavior and Back Again,* 2nd ed. Carl Hanser Verlag, Munich, Germany **2018**.

[123] L. J. Fetters, D. J. Lohse, D. Richter, T. A. Witten, A. Zirkel, *Macromolecules.* **1994**, *27*, 4639.

[124] J. R. Dorgan, J. Janzen, M. P. Clayton, S. B. Hait, D. M. Knauss, *J. Rheol.* **2005**, *49*, 607.

[125] J. R. Dorgan, J. S. Williams, D. N. Lewis, *J. Rheol.* **1999**, *43*, 1141.

[126] F. A. Morrison. *Understanding Rheology,* 1st ed. Oxford University Press, New York, NY **2001**.

[127] H. Xu, H. Fang, J. Bai, Y. Zhang, Z. Wang, *Ind. Eng. Chem. Res.* **2014**, *53*, 1150.

[128] S. Trinkle, P. Walter, C. Friedrich, *Rheol. Acta.* **2002**, *41*, 103.

[129] D. Auhl, F. J. Stadler, H. Münstedt, *Macromolecules.* **2012**, *45*, 2057.

[130] M. Chellamuthu, *PhD Thesis,* University of Massachusetts Amherst, **2010**.

[131] S. Trinkle, C. Friedrich, *Rheol. Acta.* **2001**, *40*, 322.

[132] S. Li, M. Xiao, D. Wei, H. Xiao, F. Hu, A. Zheng, *Polymer.* **2009**, *50*, 6121.

[133] D. Graebling, *Macromolecules.* **2002**, *35*, 4602.

[134] E. S. Kim, B. C. Kim, S. H. Kim, *J. Polym. Sci., Part B: Polym. Phys.* **2004**, *42*, 939.

[135] S. H. Kim, Y.-K. Han, Y. H. Kim, S. I. Hong, *Makromol. Chem.* **1992**, *193*, 1623.

[136] P. J. Flory, *J. Am. Chem. Soc.* **1945**, *67*, 2048.

[137] T. Ogawa, *J. Appl. Polym. Sci.* **1992**, *44*, 1869.

[138] P. J. Flory, *J. Chem. Phys.* **1942**, *10*, 51.

[139] M. L. Huggins, *J. Am. Chem. Soc.* **1942**, *64*, 1712.

[140] F. S. Bates, *Science.* **1990**, *251*, 898.

[141] O. Olabisi, L. M. Robeson, M. T. Shaw. *Polymer–Polymer Miscibility,* 1st ed. Academic Press, Inc., New York, NY **1979**.

[142] S. Krause, *Macromolecules.* **1970**, *3*, 84.

[143] D. J. Meier, *J. Polym. Sci., Part C: Polym. Symp.* **1969**, *26*, 81.

[144] M. T. Martello, D. K. Schneiderman, M. A. Hillmyer, *ACS Sustainable Chem. Eng.* **2014**, *2*, 2519.

[145] A. M. Mannion, F. S. Bates, C. W. Macosko, *Macromolecules.* **2016**, *49*, 4587.

[146] L. Jiang, M. P. Wolcott, J. Zhang, *Biomacromolecules.* **2006**, *7*, 199.

[147] E. Fortunati, D. Puglia, A. Iannoni, A. Terenzi, J. M. Kenny, L. Torre, *Materials.* **2017**, *10*.

[148] Jun Wuk Park, Seung Soon Im, *J. Appl. Polym. Sci.* **2002**, *86*, 647.

[149] M. Shibata, Y. Inoue, M. Miyoshi, *Polymer.* **2006**, *47*, 3557.

[150] I. Fortelny, A. Ujcic, L. Fambri, M. Slouf, *Front. Mater.* **2019**, *6*.

[151] G. Maglio, M. Malinconico, A. Migliozzi, G. Groeninckx, *Macromol. Chem. Phys.* **2004**, *205*, 946.

[152] O. Martin, L. Avérous, *Polymer.* **2001**, *42*, 6209.

[153] G. L. Loomis, G. J. Ostapchenko. (E. I. Du Pont de Nemours and Company), *US 5,076,983* **1991**.

[154] R. Sinclair. (L. BioPak Technology), *US 5,180,765* **1993**.

[155] N. Ljungberg, B. Wesslén, *Biomacromolecules.* **2005**, *6*, 1789.

[156] N. Ljungberg, B. Wesslén, *Polymer.* **2003**, *44*, 7679.

[157] Mihir Sheth, R. Ananda Kumar, Vipul Davé, Richard A. Gross, Stephen P. McCarthy, *J. Appl. Polym. Sci.* **1997**, *66*, 14095-1505.

[158] A. J. Nijenhuis, E. Colstee, D. W. Grijpma, A. J. Pennings, *Polymer.* **1996**, *37*, 5849.

[159] X. Ran, Z. Jia, C. Han, Y. Yang, L. Dong, *e-Polym.* **2010**, *62*.

[160] X. Ran, Z. Jia, C. Han, Y. Yang, L. Dong, *J. Appl. Polym. Sci.* **2010**, 2050-2058.

[161] Le Li, Z.-Q. Cao, R.-Y. Bao, B.-H. Xie, M.-B. Yang, W. Yang, *Eur. Polym. J.* **2017**, *97*, 272.

[162] S. S. Venkatraman, P. Jie, F. Min, B. Y. C. Freddy, G. Leong-Huat, *Int. J. Pharm.* **2005**, *298*, 219.

[163] Y. Ding, W. Feng, B. Lu, P. Wang, G. Wang, J. Ji, *Polymer.* **2018**, *146*, 179.

[164] Y. Baimark, Y. Srisuwan, *J. Elastomers Plast.* **2020**, *52*, 142.

[165] X. Yun, X. Li, Y. Jin, W. Sun, T. Dong, *Polym. Sci., Ser. A.* **2018**, *60*, 141.

[166]   D. W. Grijpma, A. J. Pennings, *Polym. Bull.* **1991**, *25*, 335.

[167]   D. W. Grijpma, G. J. Zondervan, A. J. Pennings, *Polym. Bull.* **1991**, *25*, 327.

[168]   H. Tsuji, A. Mizuno, Y. Ikada, *J. Appl. Polym. Sci.* **2000**, *76*, 947.

[169]   M. Hiljanen-Vainio, T. Karjalainen, J. Seppälä, *J. Appl. Polym. Sci.* **1996**, *59*, 1281.

[170]   J. Fernández, E. Meaurio, A. Chaos, A. Etxeberria, A. Alonso-Varona, J. R. Sarasua, *Polymer.* **2013**, *54*, 2621.

[171]   J. Fernández, A. Etxeberria, J.-R. Sarasua, *J. Mech. Behav. Biomed. Mater.* **2012**, *9*, 100.

[172]   J. Fernández, A. Etxeberria, J. M. Ugartemendia, S. Petisco, J.-R. Sarasua, *J. Mech. Behav. Biomed. Mater.* **2012**, *12*, 29.

[173]   E.-J. Choi, J.-K. Park, Chang Ho-Nam, *J. Polym. Sci., Part B: Polym. Phys.* **1994**, *32*, 2481.

[174]   H. R. Kricheldorf, K. Bornhorst, H. Hachmann-Thiessen, *Macromolecules.* **2005**, *38*, 5017.

[175]   a) E. Deenadayalan, A. K. Lele, M. Balasubramanian, *J. Appl. Polym. Sci.* **2009**, *112*, 1391; b) L. M. Pitet, S. B. Hait, T. J. Lanyk, D. M. Knauss, *Macromolecules.* **2007**, *40*, 2327;

[176]   F. Tasaka, Y. Ohya, T. Ouchi, *Macromol. Rapid Commun.* **2001**, *22*, 820.

[177]   S. Corneillie, M. Smet, *Polym. Chem.* **2015**, *6*, 850.

[178]   E. Saldívar-Guerra, E. Vivaldo-Lima. *Handbook of polymer synthesis, characterization, and processing.* John Wiley & Sons, Inc., Hoboken, NJ **2013**.

[179]   G. J. Field, P. Micic, S. N. Bhattacharya, *Polym. Int.* **1999**, *48*, 461.

[180]   Clariant International AG. *Your uniersally applicable polymer Polyglykol,* Muttenz, Schweiz **2013**.

[181]   Clariant International AG. *Components and additives for adhesives & Sealants,* Muttenz, Schweiz **2016**.

[182]   A. de Almeida, M. Nébouy, G. P. Baeza, *Macromolecules.* **2019**, *52*, 1227.

[183]   S. Vyazovkin, K. Chrissafis, M. L. Di Lorenzo, N. Koga, M. Pijolat, B. Roduit, N. Sbirrazzuoli, J. J. Suñol, *Thermochim. Acta.* **2014**, *590*, 1.

[184]   M. C. Righetti, M. L. Di Lorenzo, M. Angiuli, E. Tombari, P. La Pietra, *Eur. Polym. J.* **2007**, *43*, 4726.

[185]   X. Zhao, H. Hu, X. Wang, X. Yu, W. Zhou, S. Peng, *RSC Adv.* **2020**, *10*, 13316.

[186]   M. L. Di Lorenzo, R. Androsch, *Polym. Int.* **2019**, *68*, 320.

[187]   J. Zhang, Y. Duan, H. Sato, H. Tsuji, I. Noda, S. Yan, Y. Ozaki, *Macromolecules.* **2005**, *38*, 8012.

[188]   S. Saeidlou, M. A. Huneault, H. Li, C. B. Park, *Prog. Polym. Sci.* **2012**, *37*, 1657.

[189]   Natureworks LLC. *Processing Guide Ingeo Crystallizing and Drying* **2016**.

[190]   T. Bremner, A. Rudin, *J. Appl. Polym. Sci.* **1990**, *41*, 1617.

[191]   T. Buesse, Fraunhofer IAP Biopolymer Processing Technical Center. **2020**.

[192]   O. Vincent, E. Osmont, F. Sommer, *J. Plast. Film Sheeting.* **2004**, *20*, 247.

[193]   P. Schmitz, S. Janocha. in *Ullmann's Encyclopedia of Industrial Chemistry,* Wiley-VCH Verlag, Weinheim, Germany **2000**.

[194]   R. Xu, J. Xie, C. Lei, *RSC Adv.* **2017**, *7*, 39914.

[195]   Y. P. Khanna, R. Kumar, A. C. Reimschuessel, *J. Appl. Polym. Sci.* **1988**, *28*, 1607.

[196]   Y. P. Khanna, A. C. Reimschuessel, *J. Appl. Polym. Sci.* **1988**, *35*, 2259.

[197]   Y. P. Khanna, A. C. Reimschuessel, A. Banerjie, C. Altman, *J. Appl. Polym. Sci.* **1988**, *28*, 1600.

[198]   L. Penel-Pierron, C. Depecker, R. Seguela, J. M. Lefebvre, *J. Polym. Sci.* **2001**, *39*, 484.

[199]   L. Penel-Pierron, R. Seguela, J. M. Lefebvre, V. Miri, C. Depecker, M. Jutigny, J. Pabiot, *J. Polym. Sci.* **2001**, *39*, 1224.

[200]   J. Offers, N. Lack. (Fachagentur Nachwachsende Rohstoffe e.V.). *Processing of Bioplastics: a guideline,* 1st ed. **2016**.

[201]   J. M. Schultz, J. Petermann, *Colloid Polym. Sci.* **1984**, 294.

[202]   R. M. Gohil, *J. Appl. Polym. Sci.* **1993**, *48*, 1635.

[203]   R. M. Gohil, *J. Appl. Polym. Sci.* **1994**, *52*, 920.

[204]   G. Stoclet, R. Seguela, J.-M. Lefebvre, C. Rochas, *Macromolecules.* **2010**, *43*, 7228.

[205]   G. Stoclet, R. Seguela, J. M. Lefebvre, S. Elkoun, C. Vanmansart, *Macromolecules.* **2010**, *43*, 1488.

[206]   J. Zhang, K. Tashiro, H. Tsuji, A. J. Domb, *Macromolecules.* **2008**, *41*, 1352.

[207]   Y. Wang, M. Li, K. Wang, C. Shao, Q. Li, C. Shen, *Soft Matter.* **2014**, *10*, 1512.

[208]   J. Hu, T. Zhang, M. Gu, X. Chen, J. Zhang, *Polymer.* **2012**, *53*, 4922.

[209]   The Dow Chemical Company. *Technical Information DOW LDPE 525E: Low Density Polyethylene Resin,* Midland, Michigan **2011**.

[210]   BASF. *Brochure: Ecovio® – Biologically degradable solutions for extrusion application,* Ludwigshafen am Rhein, Germany **2017**.

[211]   E. Catsiff, A. V. Tobolsky, *J. Colloid Sci.* **1955**, *10*, 375.

Nomenclature

Latin Symbols

A	empirical parameter Flory equation for Tg as a function of Mn
A_R	empirical Ahrrenius prefactor
A'	empirical constant Doolittle equation
A_{VFTH}	empirical constant VFTH equation
B'	empirical constant Doolittle equation
E_a	activation energy
f	functionality
f_F	heat of fusion factor $[2 \cdot Tc / (T_m° + Tc)]$
f_g	fractional free volume at temperatures below the Tg
G''	loss modulus
$|G*|$	absolute value complex modulus
G'	storage modulus
$G°_N$	plateau modulus
G_0	pre-exponential empirical factor with units of length over time
$<h^2>$	mean square end-to-end distance
k_B	Boltzmann constant
K_{Depoly}	depolymerization equilibrium constant
K_g	nucleation constant
M	torque
M_{arm}	molar mass of the arm in a symmetric star molecule
M_B	molar mass of the branches
M_{bond}	molar mass per backbone bond
M_c	critical molar mass
M_e	entanglement molar mass
Mn	number average molar mass
Mv	viscosity average molar mass
Mw	weight average molar mass
N_{av}	average number of bonds on the polymer backbone
N	number of segments per polymer chain molecule
$p*$	packing length
R	ideal gas constant
r_0	radius at the die exit
r_f	radius of the final film
R_g	radius of gyration
sS	symmetric star

T^*_m	equilibrium melting point in the absence of non-crystallizable comonomer
T_0	Vogel temperature
$t_{1/2}$	crystallization half-time
T_∞	hypothetical temperature below Tg at which viscous flow ceases
Tc	peak crystallization temperature
Tcr_{Max}	isothermal crystallization temperature of maximum crystallization rate
Tg	glass transition temperature
Tm	peak melting temperature
T_m^0	equilibrium melting temperature
T_{MFI}	MFI measurement temperature
$T_{processing}$	processing temperature
Tr	Trouton ratio ($\eta E / 3 \cdot \eta S$)
U*	activation energy for transport of chain segments to the crystallization site
V_0	extrusion throughput velocity
V_f	free volume
V_{NR}	nip-roll velocity
V_{occ}	volume occupied by the polymer chains
V_{Screw}	Extruder screw rotating speed
W_n	weight fraction component "n"
X_A	mole fraction of the crystallizable monomer
X_C	degree of crystallinity
X_{CL}	ε-caprolactone molar fraction (%-mol)
X_D	D-lactide molar fraction (%-mol)

Greek Symbols

α	ordered PLA crystal structure
α'	metastable PLA crystalline structure (loosely packed)
α_f	coefficient of expansion of the free volume only
γ	strain
δ	phase angle
$\Delta E_{Cohesive}$	difference of cohesive energies
ΔG_M	Gibbs free energy change of the melting process
ΔG_{Mix}	Gibbs free energy change of mixing
ΔH_M	enthalpy change during melting
ΔH_{Mix}	enthalpy change during mixing
$\Delta H_{m100\%}$	extrapolated enthalpy of melting of PLA crystals with infinite thickness
ΔH_u	heat of melting per mole of repeating unit
$\Delta L/t$	elongation rate
ΔS_M	entropy change during melting

ΔS_{Mmix}	entropy change during mixing
ε	strain
ϵ	contact energy between segments
η	viscosity
η_0	zero-shear viscosity
η_E	elongational viscosity
η_S	shear viscosity
θ	top disk rotating angle (rheometry)
σ	stress
$\sigma'(t)$	stress response of a completely elastic solid to the oscillating strain input
$\sigma''(t)$	stress response of a completely viscous liquid to the oscillating strain input
ϕ	volume fraction of a component in a polymer blend
ϕ_C	critical volume fraction
χ	Flory-Huggins segment-segment interaction parameter
χ_C	Flory-Huggins parameter at the critical point
Ω	angular velocity
ω	frequency

Abbreviations

^{1}H-NMR	proton nuclear magnetic resonance
AN	acid number
BUR	blow-up ratio
CL	ε-caprolactone
-COO-	ester bond
-COOH	carbonyl functional group
DBM	diethyl bishydroxymethyl malonate
DBMATA	diethyl bishydroxymethyl malonate with amide functionality
DP	degree of polymerization
DR	draw ratio
DSC	differential scanning calorimetry
EO	ethylene oxide
FTIR	Fourier-transform infrared spectroscopy
GPC	gel permeation chromatography
HFIP	hexafluoroisopropanol
ICP-OES	inductively coupled plasma – optical emission spectroscopy
i-PP	isotactic polypropylene
K_{eq}	polycondensation equilibrium constant
Kevlar®	poly(p-phenylene terephthalamide)

LDPE	low-density polyethylene
MD	machine direction
MFI	melt flow index
-OH	hydroxyl functional group
OLA	oligomeric lactic acid
PA 6	polycaprolactam
PAA	polyacrylic acid
PBAT	poly(butylene adipate-co-terephthalate)
PBS	polybutylene succinate
PBT	polybutylene terephthalate
PCL	polycaprolactone
PE	polyethylene
PEG	polyethylene glycol
PEPG	poly(ethylene glycol-co-propylene glycol) (statistical copolymer)
PET	polyethylene terephthalate
PHA	polyhydroxyalkanoates
PHBV	poly(3-hydroxybutyrate-co-3-hydroxyvalerate)
PI	polyisoprene
PLA	polylactic acid
PLLA	isotactic polylactic acid (only l-lactide units)
PLOM	polarized light optical microscopy
PMMA	poly(methyl methacrylate)
PO	propylene oxide
poly(THF)	polytetrahydrofuran
PPG	polypropylene glycol
PS	polystyrene
PTFE	poly(tetrafluoroethylene)
PVA	poly(vinyl alcohol)
PVC	polyvinyl chloride
RH	relative humidity
RI	refractive index
ROP	ring-opening polymerization
RPM	revolutions per minute
RT	room temperature
sc-PLA	stereocomplex pla
$Sn(Oct)_2$	tin(II) 2-ethylhexanoate
TD	transverse direction
TDBP	tris(2,4-di-tert-butylphenyl)
TNPP	tris(nonyl phenyl) phosphite
TPE-E	thermoplastic elastomer (copolyester)

TPP	triphenyl phosphite
TPU	thermoplastic elastomer (polyuerthane)
TUR	take-up ratio
VFTH	Vogel-Fulcher-Tammann-Hesse
vGP-plot	van Gurp - Palmen plot

Acknowledgements